The emergence of pelagic calcification and its influence on seawater chemistry in the Upper Triassic.

Demangel, Isaline

2022

Document Version:
Publisher's PDF, also known as Version of record

The emergence of pelagic calcification and its influence on seawater chemistry in the Upper Triassic

Dissertation

Zur Erlangung des akademischen Grades einer

Doktorin der Naturwissenschaften

an der Karl-Franzens-Universität Graz

Vorgelegt von

Isaline Demangel

Am Institut für Erdwissenschaften

Esrtbegutachter: Sylvain Richoz

Zweibegutachterin: Silvia Gardin

Drittbegutachter: Jeremy Young

2022

TABLE OF CONTENTS

PREFACE

The origin of pelagic calcification and its influence on seawater chemistry is a project, which started in January 2017 with the funding of the Austrian Science Fund (FWF). This project was designed for three years using a multi-proxies approach combining micropalaeontology and geochemistry. The Mesozoic account major events in the biomineralisation evolution with the appearance of the calcifying dinoflagellates, the coccolithophorids, the planktonic foraminifera and the diatoms (Ridgwell, 2005). The evolution of the planktonic calcifiers suggested having shifted the carbonate deposition from continental shelves to deep-ocean and therefore affecting considerably the chemistry of the ocean (Ridgwell, 2005). With the occurrence of the planktonic calcifiers in the late Triassic, this shift could have happened during this period. The Triassic (251.9 – 201.36 Ma; Ogg et al., 2020) is a key period between the end-Permian and the end-Triassic mass extinction. The late Triassic (237.0 – 201.36 Ma; Ogg et al., 2020), is the focus of the project since the early form of coccoliths were found in Austria around the Norian/Rhaetian boundary (Gardin et al., 2012). The first aim was a detailed investigation of Norian sediments of different palaeo-settings and palaeo-latitudes to verify the first occurrence of the coccolithophorids and to follow their evolution during the Rhaetian. The second, a quantitative estimation of the volume and palaeo-fluxes produced by the calcareous nannofossils during the late Triassic to additionally compare with the quantification made in two Italian sections showing a rock-forming abundance in the late Rhaetian (Preto et al., 2013). In parallel to those micropalaeontological analyses, the second PhD student, Zsofia Kovacs, measured strontium (see co-authored paper Kovács et al., 2020), calcium (see chapter 6) and carbon isotopes (co-authored paper Kovács et al., submitted) with a high biostratigraphical resolution, at differents palaeolatitudes (25°N, equator, 20°S) and along two shallow-to-depth transects. The strontium isotope curve help to constrain the weathering flux and major tectonics process. The calcium isotope results bring details on changes in calcium palaeo-fluxes and shifts between calcite and aragonite sea. The carbon isotope evolution provides information on productivity changes. This multiproxy approach aims to evaluate possible changes in seawater chemistry due to the early emergence of the calcareous nannoplankton.

Reference

Gardin, S., Krystyn, L., Richoz, S., Bartolini, A., Galbrun, B., 2012: Where and when the earliest coccolithophores? Lethaia, 45, 507 – 523.

Kovács, Z., Demangel, I., Richoz, S., Hippler, D., Baldermann, A., Krystyn, L., 2020: New constraints on the evolution of $^{87}Sr/^{86}Sr$ of seawater during the Upper Triassic. Global and Planetary Change, 192, 103255.

Kovács, Z., Demangel, I., Urban, I., Krystyn, L., Galbrun, B., Boulila, S., Bartolini, A., Gardin, S., Adatte, T., Richoz, S., submitted: Carbon isotope stratigraphy of the Late Triassic.

Ogg, J.G., Chen, Z.-Q., Orchard, M.J., Jiang, H.S., 2020: The Triassic Period. Geologic Time Scale *2020*, 903 – 953.

Preto, N., Agnini, C., Rigo, M., Sprovieri, M., Westphal, H., 2013: The calcareous nannofossil *Prinsiosphaera* achieved rock-forming abundances in the latest Triassic of western Tethys: Consequences for the $\delta^{13}C$ of bulk carbonate. Biogeosciences, 10, 6053 – 6068.

Ridgwell, A., 2005: A Mid Mesozoic Revolution in the regulation of ocean chemistry. Marine Geology, 217, 339 – 357.

ACKNOWLEDGEMENTS

I am grateful to the **Austrian Science Fund (FWF)**, the **Royal Physiographic Society of Lund** and « **RESPECT** » (A major evolutive **R**evolution: the **E**mergence and **S**preading of **PE**lagic **C**alcifiers in the late **T**riassic) PICS-CNRS project for the funding of this PhD.

I acknowledge the **Doctoral School of Earth Sciences, the University of Graz** through Prof. **Steffen Birk** for the financial help attributed to attempt scientific congresses. **The Department of Geology of Lund University** for providing me with a positive and stimulating work environment with quality laboratory equipment.

I strongly thank my supervisor **Sylvain Richoz** for giving me the chance to live this amazing experience since 2017. This project taught me much, thanks to your knowledge, your expertise in the field, your detailed corrections of all versions of my different manuscripts. Your trust and confidence in my work, helped me to develop as a young scientist. Your patience, comprehension and true kindness during those difficult times I had, was a real human balance of great value to me. I would never thank you enough for being able to discover new cultures, languages, travel to so many beautiful places, your trust in my candidature brought me on a wonderful life adventure ending (for now) in Sweden with lovely twins.

Zsófia, I am so glad to work in pairs with you. Besides your great knowledge, you were always so helpful with the German, the administrative paper. It was wonderful to share the same office and be able to talk about everything when we needed breaks, to share nice hikes during the weekend together, go to yoga or brunch, discover Austria and Sweden. You were a colleague and friend presents when I felt far from my family.

I especially express my gratitude to **Silvia Gardin** for her expertise, her help during all those years and a warm welcome in Paris to introduce me the Late Triassic calcareous nannofossils species.

I am thankful to **Werner E. Piller** for providing me with a favourable working place at the University of Graz with great SEM, new high magnification ocular. I am grateful for your help to improve our manuscripts as well as your expertise in terminology and English.

I thank **all my co-authors** for their precious help and patience to improve our manuscript(s) during all the versions. **Andre Baldermann** for your help during the ICP-OES analyses, your

quick feedback and critical comments. **Leopold Krystyn** for your helpful knowledge of the studied sections. **Richard Howe** for our sudden collaboration to improve the description of the *Eoconusphaera* species in the Late Triassic. **Eugene Gradinaru** for your consideration ending with great collaboration and good discovery. **Nicolas Thibault** for your trust and our collaboration on this project I am enthusiastic to continue soon.

My **colleagues in Graz, Zsófia, Angie, Jenny, Magda, Juliane**, for your welcome to the institute of Geology, the nice lunchtime under the sun, the adventures on weekends visiting Lurgrotte, cross country skiing, eating cakes and the nice parties with Angie. **Gerald Auer** for taking the time to share your excellent quantification methodology.

My **colleagues in Lund**, all the PhD students for the nice times (lunch, Fika, Ariman, monthly restaurants). **Florian** for all the nice moments on the roof from the simple fika to the snowball fight but I do not thank you for trying to bring me in your dark side of the procrastination. You and **Guillaume** for all the great last-minute parties and after-work. **Ingrid** for all the nice activities during the weekends and swimming pool evenings with **Rosine**. **Carl Alwmark** for your help related to the scanning electron microscope.

Christian, this thesis leads us on the same path for a while and I do not know how I can thank you for everything you offer me. You gave me your passion for living at 110%! I am so thankful for your warm welcome in your country, the sweet home you offered me, your care when I was sick, all our movie nights, our great discussions, the amazing hikes and sport sessions with FocusGuide!

To **all my family**, but especially my parents and sister. J'exprime ma reconnaissance à ma **maman** qui m'a donné la motivation de toujours faire mieux. Je te remercie ainsi que **Jean-Paul** et **Coraly** d'être toujours là pour moi, pendant toutes nos heures d'appels pour être un peu plus proche les uns des autres, et pour vos visites rafraichissantes en Autriche et en Suède ! Ett stort tack till **Nils, Agneta** for being so motivating and proud of my work. A thunder of applause for the one able to support me every day, stay patient and understanding, my partner **Johan**. Finally, they say "all the good things must come to an end", **my sweet twins** made this great PhD last for one more year so should probably be thankful for that…

ABSTRACT

After the early biomineralisation event in the early Paleozoic (Cambrian – Ordovician; 541 – 443.8 Ma), the Late Triassic (237 – 201.3 Ma) represents another key period of biomineralisation with the onset of the Mesozoic plankton radiation. In the Carnian (237 – 227 Ma), the first calcifying dinoflagellates are recorded followed by the nannoliths in the middle Norian (Alaunian) and the coccolithophorids dated until this study at the Norian/Rhaetian boundary. Those marine primary producers are influencing the concentration of oceanic and atmospheric CO_2 via their photosynthesis and calcification processes. Timing and quantification of their early evolution would help to understand their impact on the ocean chemistry during the Late Triassic. The Austrian Northern Calcareous Alps, Romanian North Dobrogea and North West Australia record several good potential sediments from the Upper Triassic. This project aims to investigate Norian to Rhaetian outcrops from widespread localities around the poorly studied Paleo-Tethys as well as the Neo-Tethys Ocean in the Upper Triassic. The calcareous nannofossils contents were observed by light and scanning electron microscope and quantified (if present) in six Austrian and Romanian sections (25°N), one section from Turkey (palaeo-equator), and six sections from Oman (20°S). In parallel, geochemical analyses were performed first with trace elements concentration to evaluate the impact of diagenesis on the preservation of the sediments and calcareous nannofossils but also to trace changes in weathering rate during the Late Triassic. Second, isotopic measurements were performed for strontium, calcium and carbon to better constrain the environmental conditions during the early evolution of the calcareous nannofossils.

The first coccoliths, not identified at a species level, occurred in the middle Norian (Alaunian 3). The oldest coccolith species identified is *Crucirhabdus minutus*, observed in the upper Norian (Sevatian), followed by *Archaeozygodiscus koessenensis*. *Crucirhabdus primulus* first occurred in the lower Rhaetian. These occurrences suggest *C. minutus* as the ancestor of the coccolithophorids and a slow temporal evolution. *C. primulus* occurred ~ 4.2 million years after the ancestor *C. minutus*, and the evolution of the new genus *A. koessenensis* takes around 0.35 Myr. The incertae sedis, *Prinsiosphaera triassica* dominates the assemblage throughout the Upper Triassic. Its abundance increases slightly in the lower and middle Rhaetian and reaches its maximum abundance in the upper Rhaetian. Detailed microscopic investigations detected two different significant structures of the conical Rhaetian forms

belonging to *Eoconusphaera*. Based on this, a new species, *E. hallstattensis* was described and *E. zlambachensis* was emended. Those two species represent new biostratigraphic markers for the Rhaetian with short and specific occurrence intervals. *Eoconusphaera hallstattensis* is constrained to the upper *Paracochloceras suessi* Zone (lower Rhaetian) and disappeared during the lower *Vandaites stuerzenbaumi* Zone (middle Rhaetian), wherein it is progressively replaced by the second Eoconusphaeraceae species *E. zlambachensis*. Throughout the Rhaetian, *P. triassica* is affected by biological and environmental stress conditions. First, with the occurrence of Eoconusphaeraceae introducing competition between the *P. triassica* and the Eoconusphaeraceae and, second palaeo-environmental changes alter its calcification potential, leading to a size decrease from the lower Rhaetian. These two species, *P. triassica* and *E. zlambachensis* were observed for the first time in Romanian sections (North Dobrogea) located in the Palaeo-Tethys Ocean during the Late Triassic and are common (if present).

During the Upper Triassic, the calcareous nannofossils are observed in both hemispheres and show increasing abundance through the Rhaetian and are described as rock-forming during the upper Rhaetian. The comparison between quantification data and calcium isotope measurements does not show any evidence for a significant influence of those calcifiers on the geochemical composition of the Western Neo-Tethys Ocean.

ZUSAMMENFASSUNG

Nach dem frühen Biomineralisierungsereignis im frühen Paläozoikum (Kambrium - Ordovizium; 541 – 443.8 Ma) stellt die Späte Trias (237 – 201.3 Ma) eine andere Schlüsselperiode für Biomineralisierung mit der Verbreitung von kalkigem Nannoplankton dar. Im Karnuim (237 – 227 Ma) werden die ersten kalzifizierenden Dinoflagellaten nachgewiesen, gefolgt von den Nannolithen im mittleren Norium (Alaunium) und von den Coccolithophoriden, deren erstes Auftreten bis zu diesen Untersuchungen an der Norium-Rhaetium Grenze bekannt war. Diese marinen Primärproduzenten beeinflussen über den Photosynthese- und Verkalkungsprozess die Konzentration von ozeanischem und atmosphärischem CO_2. Die Datierung und die Quantifizierung ihrer frühen Entwicklung würden helfen, ihren Einfluss auf die Ozeanchemie während der Späten Trias zu verstehen. Die österreichischen Nördlichen Kalkalpen, die rumänische Norddobrudscha und Nordwestaustralien weisen mehrere potenziell geeignete Sedimente aus der Obertrias auf. Ziel dieses Projektes war es, Aufschlüsse im Norium und im Rhaetium von weit entfernten Fundorten rund um die wenig untersuchte Palaeo-Tethys sowie den Neo-Tethys-Ozean (in der Obertrias) zu untersuchen. In sechs österreichischen und rumänischen Profilen (25°N), in einem Profil aus der Türkei (Paläo-Äquator) und in sechs Aufschlüssen aus dem Oman (20°S) wurden kalkige Nannofossilien beobachtet (Licht- und Rasterelektronenmikroskop) und, soweit möglich, quantifiziert. Parallel dazu wurden zunächst geochemische Analysen mit Spurenelementkonzentrationen durchgeführt, um den Einfluss der Diagenese auf den Erhalt der Sedimente und kalkhaltigen Nannofossilien zu bewerten, aber auch um Veränderungen der Verwitterungsrate während der Späten Trias zu verfolgen. Zweitens wurden Isotopenmessungen an Strontium, Kalzium und Kohlenstoff durchgeführt, um die Umweltbedingungen während der frühen Entwicklung der kalkigen Nannofossilien besser zu verstehen.

Die ersten Coccolithen, die nicht auf Artebene identifiziert wurden, kamen im mittleren Norium (Alaunium 3) vor. Die älteste identifizierte Coccolithen-Art ist *Crucirhabdus minutus*, der im oberen Norium (Sevatium) beobachtet wurde, gefolgt von *Archaeozygodiscus koessenensis*. *Crucirhabdus primulus* kam erstmals im unteren Rhaetium vor. Diese Vorkommen lassen *C. minutus* als Vorfahren der Coccolithophoriden und eine langsame zeitliche Entwicklung vermuten. *C. primulus* trat ~ 4,2 Millionen Jahre nach dem Vorfahren

C. minutus auf, und die Entwicklung der neuen Gattung *Archaeozygodiscus* dauert etwa 0,35 Myr. Die Art *Prinsiosphaera triassica,* deren taxonomisch-systematische Zuordnung nicht geklärt ist, dominiert die Vergesellschaftungen in der gesamten Obertrias. Ihre Häufigkeit nimmt im unteren und mittleren Rhaetium leicht zu und erreicht ihre maximale Häufigkeit im Oberrhaetium. Detaillierte mikroskopische Untersuchungen zeigten zwei unterschiedliche signifikante Strukturen der kegelförmigen rhaetischen Formen der Gattung *Eoconusphaera*. Eine neue Art, *E. hallstattensis*, wurde beschrieben und die Beschreibung von *E. zlambachensis* wurde emendiert. Diese beiden Arten liefern neue biostratigraphische Marker für das Rhaetium mit kurzen und spezifischen Vorkommensintervallen. *Eoconusphaera hallstattensis* ist auf die obere *Paracochloceras suessi*-Zone (unteres Rhaetium) beschränkt und verschwand während der unteren *Vandaites stuerzenbaumi*-Zone (mittleres Rhaetium), wo sie durch die zweite *Eoconusphaera*-Art *E. zlambachensis* ersetzt wurde. Im ganzen Rhaetium ist *P. triassica* von Stresszuständen betroffen. Erstens führt das Auftreten von Eoconusphaeraceae zu einer Konkurrenz zwischen den *P. triassica* und den Eoconusphaeraceae und zweitens beinflussen paläo-ökologische Veränderungen sein Verkalkungspotential, was zu einer Größenabnahme gegenüber dem unteren Rhaetium führte. Diese beiden Arten, *P. triassica* und *E. zlambachensis*, wurden zum ersten Mal in rumänischen Aufschlüssen (Norddobrudscha) im Paläo-Tethys-Ozean während der Späten Trias beobachtet und sind, wenn vorhanden, häufig.

Während der Obertrias werden die kalkigen Nannofossilien in beiden Hemisphären beobachtet und zeigen eine zunehmende Häufigkeit durch das Rhaetium und werden im Oberrhaetium als gesteinsbildend beschrieben. Der Vergleich zwischen Quantifizierungsdaten und Kalziumisotopenmessungen gibt allerdings keinen Hinweis auf einen signifikanten Einfluss dieser kalkproduzierenden Organismen auf die geochemische Zusammensetzung des westlichen Neo-Tethys-Ozeans.

CHAPTER 1 – INTRODUCTION TO THE BIOMINERALISATION, THE CALCAREOUS NANNOFOSSILS AND THE LATE TRIASSIC PERIOD (ENVIRONMENTAL CONDITIONS AND STUDIED AREA)

1. Biocalcification thought time

1.1 *The avent of the biocalcification*

Biomineralisation is a process used by organisms to form biogenic minerals most commonly including silicates, carbonates (mainly calcite, aragonite) and phosphates (Knoll, 2003). Before the advent of biologically controlled mineralization, organomineralisation were induced by the metabolism of some organisms (e.g. stromatolites; Porter, 2011). The molecular clock analyses suggest the beginning of biologically controlled mineralization around the Cryogenian (Sperling et al., 2010). The first possible evidence of biomineralization is dated in the Neoproterozoic around 760 ±1 million years ago (Tonian) into Namibian rocks (Otavi group). *Otavia antiqua* is a sponge-like fossil with an external wall made of calcium phosphate and a small amount of dolomite (Bob'Brain et al., 2012). Later on, calcified fossils of sponges were found in the Trezona Formation (South Australia) around 630 million years ago (Cryogenian; Maloof et al., 2010a). The first attempt of expansion by organisms biomineralising occurs during the Ediacaran diversification (~600 million years ago) (Germs, 1972; Bengtson, 1992; Grotzinger et al., 2000) with for example the appearance of the first reef builder *Cloudina* (Penny et al., 2014) or the development of the early sponges of the phylum Porifera (Love et al., 2009). However, the increase in diversity and large multicellular fossils of biologically controlled mineralization occurred during the "Cambrian explosion" (~ 542 to 515 million years ago) (Porter, 2007; Maloof et al., 2010b; Kouchinsky et al., 2011). This major event records the appearance of 18 animals clades using biomineralisation to form aragonites, calcites, phosphates and siliceous skeletons (Porter, 2007). During the Cambrian, some biomineralized microfossils are recorded including the conodonts (Ginot and Goudemand, 2020), benthic foraminifera (Scott et al., 2003), and radiolarians (Braun et al., 2007). The ostracods appear later in the early Ordovician (~ 450 million years ago; Martens et al., 2008). The Mesozoic is a key era in the advent of biomineralization in the main extent phytoplanktonic groups. Indeed, from the Triassic (Carnian), the oldest dinocysts from calcifying

dinoflagellates are recorded (Janofske, 1992) (see chapter 1, sub-chapter 2.2). Nannoliths and coccolithophorids are reported from the Late Triassic (see chapter 1, sub-chapter 2.1). The planktonic foraminifera occurs in the Jurassic (Oxford et al., 2002), however, Kucera and Morard (2019) suggest their possible evolution after the Permian/Triassic crisis. The calpionellids appears in the Late Jurassic (Lorenz, 1902), and the diatoms in the early Cretaceous (Sims et al., 2006) but the molecular clock suggest an occurrence in the Upper Triassic (Nakov et al., 2018).

The triggers of those biomineralisation initiations are unclear, but this process is probably necessary for the survival of those clades regarding the cost of it. Ocean geochemistry has played a major role in the biomineralisation initiation (Bengtson, 1994, 2004). Indeed, changes in seawater Mg/Ca ratios during the Ediacaran-Early Cambrian period could have facilitated widespread aragonite and high-Mg calcite precipitation (Wood, 2018). The Ca^{2+} availability seems crucial as the Cambrian was characterized by supersaturation in a shallow environment (Grotzinger and James, 2000; Brennan et al., 2004) and the highest level of Ca supersaturation was recorded during the Late Cretaceous (Stanley and Hardie, 1998; Stanley, 2006) known as the golden age of the coccolithophorids. Additionally, researchers have shown that biomineralisation in modern calcifying photosynthetic organisms is strongly dependent on calcium carbonate supersaturation (Gattuso et al., 1999). And culture experimentations report an increased rate of calcification linked to an increasing amount of Ca^{2+} in the medium (Blackwelder et al., 1976). The rising levels of oxygen during the Cambrian and/or the stability of oxygen available must have been another important factor (Canfield et al., 2007; Wood, 2018), probably among others still to be defined.

1.2 *Pelagic calcifiers and seawater chemistry*

The phytoplankton corresponds to less than 1% of Earth's photosynthetic biomass (Falkowski, 2012), however, they are a key component of the oceanic carbon cycle. They regulate ocean-atmospheric CO_2 levels and participate largely in atmospheric oxygen production. These photosynthetic organisms constitute 45% of the carbon annual net primary production (Field et al., 1998). For their development, they use dissolved carbon dioxide from the upper layer; after the death of the organism, these organic matters (in form of single particles or fecal pellets) start to sink into deeper water (100 – 1000 m) causing a net decrease

in CO_2 at the surface layer. However, grazing by zooplankton and bacterial consumption remineralized back some carbon dioxide. The remaining organic carbon continues to sink to the bottom of the ocean for burial and long-term sequestration, causing the net drawdown of the CO_2 from the atmosphere into the ocean (Rost and Riebesell, 2004). With this process called biological carbon pump, the oceans stores about 50 times more carbon than the atmosphere and have uptakes of about 30% of the greenhouse gases emitted by humans so far (Hannah, 2022). However, the formation of a hard skeleton by nannoplankton leads to the opposite effect (Rost and Riesbesell, 2004). The biocalcification use Ca^{2+} and 2 HCO_3^- to form $CaCO_3$ and release H_2O and CO_2 (Rost and Riebesell, 2004). This process called the carbonate counter pump cause the net release of CO_2 in the atmosphere on a shorter time scale. On the other hand, the sink of the calcium carbonate skeleton after the death of the organisms leads to the burial of the carbonate in sediments for a long term (Rost and Riebesell, 2004).

During the Late Triassic, coccolithophorids, nannoliths and calcareous dinoflagellates were the first planktonic calcifiers playing a role in the biological carbonate pump and carbonate counter pump. Before the appearance of the pelagic calcifiers, the biological precipitation of $CaCO_3$ was restricted to the neritic environment (the first ~200 m depth of the ocean still on the continental shelf). In those conditions, the equilibrium state was possible if the neritic carbonate production equals the riverine flux. This so-called Neritan Ocean was characterised by infinite saturation with variations from supersaturation to low saturation (Zeebe and Westbroek, 2003). Then, with the onset of the pelagic biocalcification from the early Mesozoic onward, the carbonate deposition was shifted from shallow to open-ocean allowing a better regulation of the calcium carbonate saturation state. This so-called Cretan Ocean presents biogenic precipitation of calcium carbonate dominating the pelagic environment (Zeebe and Westbroek, 2003), leading to a sustained saturation state regulation by the accumulation and dissolution of deep-sea sediments (Ridgwell et al., 2003).

Biological and inorganic calcification controls the Ca removal from the ocean which is balanced mostly by riverine and hydrothermal Ca input (Schmitt et al., 2003). The most abundant and stable calcium isotopes, ^{40}Ca, is preferentially incorporated into the solid phase, leaving seawater enriched in ^{44}Ca at a steady-state relative to the delivery and burial fluxes. Due to the long residence time of Ca in seawater ($\tau Ca \approx 1$ to 2 Ma) relative to the short mixing time of the global ocean (around 1000 years), the Ca isotope composition of modern (DePaolo

2004) and past seawater (Hippler et al., 2003) is globally homogeneous. Consequently, scenarios that require imbalances between the delivery (weathering and hydrothermal influx) and burial fluxes of calcium in the oceans should impact changes in the calcium isotope composition in the oceans and associated sediments. It was suggested that large-scale changes in the Ca record of the seawater during the Paleozoic, possibly due to change from a calcitic to aragonitic sea, were no more possible after the Jurassic and the apparition of a stabilizing deep-sea sink through coccoliths and foraminifers (Blätter et al., 2012). The apparition of calcifying organisms in the Triassic aragonitic seas should have decreased the Ca isotope values and mainly have a buffering effect on the highly variable shallow-water Ca sink (Blätter et al., 2012). This assumption has until now, nowhere stratigraphically been tested. During this project, quantification of the early evolution of the calcareous nannofossils and comparison with calcium isotopic data aims to verify the theoretical model and thus the influence of the calcareous nannofossils on seawater chemistry.

1.3 *Calcareous nannofossils carbonate deposition through time*

Since their appeared in the Late Triassic, calcareous nannofossils started to contribute to calcium carbonate accumulation. During the Norian – Rhaetian, the main producer is the nannoliths *Prinsiosphaera triassica*. Point counting in Italian sections from proximal basinal settings reports rock-forming abundance reaching up to 60 % of the rock in the upper Rhaetian (Preto et al., 2013a). After the end-Triassic mass extinction, the calcareous nannoplankton started to recover with an accelerated rate of origination at the Hettangian/Sinemurian boundary. During the Early Jurassic, the accumulation rate is around 10^9 nannofossils m^{-2} yr^{-1} (Suchéras-Marx et al., 2019) with the contribution of the abundant and massive incertae sedis *Schizosphaerella punctulata* (Mattioli and Pittet, 2002; Suan et al., 2008; Clémence et al., 2015). The Middle Jurassic is characterized by the occurrence of *Watznaueria* (coccolithophorids) which until the end-Cretaceous mass extinction dominated the assemblages with abundant deposition in all marine settings (Erba, 2006). From the Late Jurassic (~150 Ma) onward, calcareous nannofossils produce a noticeable accumulation of $CaCO_3$ (Morse and Mackensie, 1990), average accumulation rate plot slightly above 10^{10} nannofossil m^{-2} yr^{-1} (Suchéras-Marx et al., 2019). At the Jurassic/Cretaceous boundary, the accumulation of calcium carbonates deposited increases with the appearance of three new nannoliths, including especially the massive nannoconids considered as the first effective

carbonate-producers during the Mesozoic (Erba, 1989; Bornemann et al., 2003; Bown et al., 2004). The golden period of the calcareous nannofossils is recorded in the Late Cretaceous and is visible with the massive chalk deposition present over the world (Roth, 1989; Hay, 2004). From the Cretaceous to nowadays average accumulation rate fluctuates slightly around 10^{11} nannofossil m^{-2} yr^{-1} (Suchéras-Marx et al., 2019). To evaluate the calcareous nannofossils accumulation in the Upper Triassic, and compare with other localities or younger periods, quantification was performed on every species of calcareous nannofossil present in the sample.

2. The calcareous nannofossils: An overview of the groups and their main characteristic

The calcareous nannofossil is a group of calcareous fossils smaller than 30 µm, including 1) the coccolith corresponding to calcite plate (Ehrenberg, 1896) produce by the haptophyte algae called coccolithophorids, 2) the nannoliths from unknown phylogenetic affinity and presenting a broad variety of shape, 3) the calcareous remains often produces by single-cell protist dinoflagellate (Dale 1983, 1992; Head, 1996).

2.1 *The coccolithophorids*

Coccolithophorids are unicellular, planktonic, protozoa belonging to the class Prymnesiophyceae (Hibbert, 1976). Those circular to sub-circular algae are classified in a distinct phylum called Haptophyta, due to the specific inner structure of their flagellum-like, multi-functional, organelle haptomena (Fig.1.1) (Bown, 1998; Billard and Inouye, 2004). The coccoliths are circular to elliptical calcium carbonate plate (low Mg-$CaCO_3$) composed of a rim with an outer and inner cycle and a central area bearing a structure (Figs.1.1; 1.2) (Bown, 1998). Two different types of coccoliths can be produced: 1) holococcolith with submicroscopic calcite crystals of similar shape and size formed during a motile stage in current species (Tyrrell and Young, 2009), 2) heterococcolith with large calcite crystals of different shape and size (Bown, 1998; Armstrong and Brasier, 2005) produce during a non-motile stage of the life cycle (Fig.1.1) (Tyrrell and Young, 2009). Among the heterococcolith, three types of rims can be observed: 1) the most common is murolith, corresponding to a wall-like structure made of sub-vertical, imbricating elements. Those elements composing the rim can be vertically-oriented in the protolith or imbricated (tilted) in the case of a loxolith rim

structure (Fig.1.1.11); 2) placolith made of two or more sub-horizontal shields separated by a tube (Fig.1.1.12); 3) planolith corresponding to a disc shape shield (Fig.1.1.13) (Flores and Sierro, 2007).

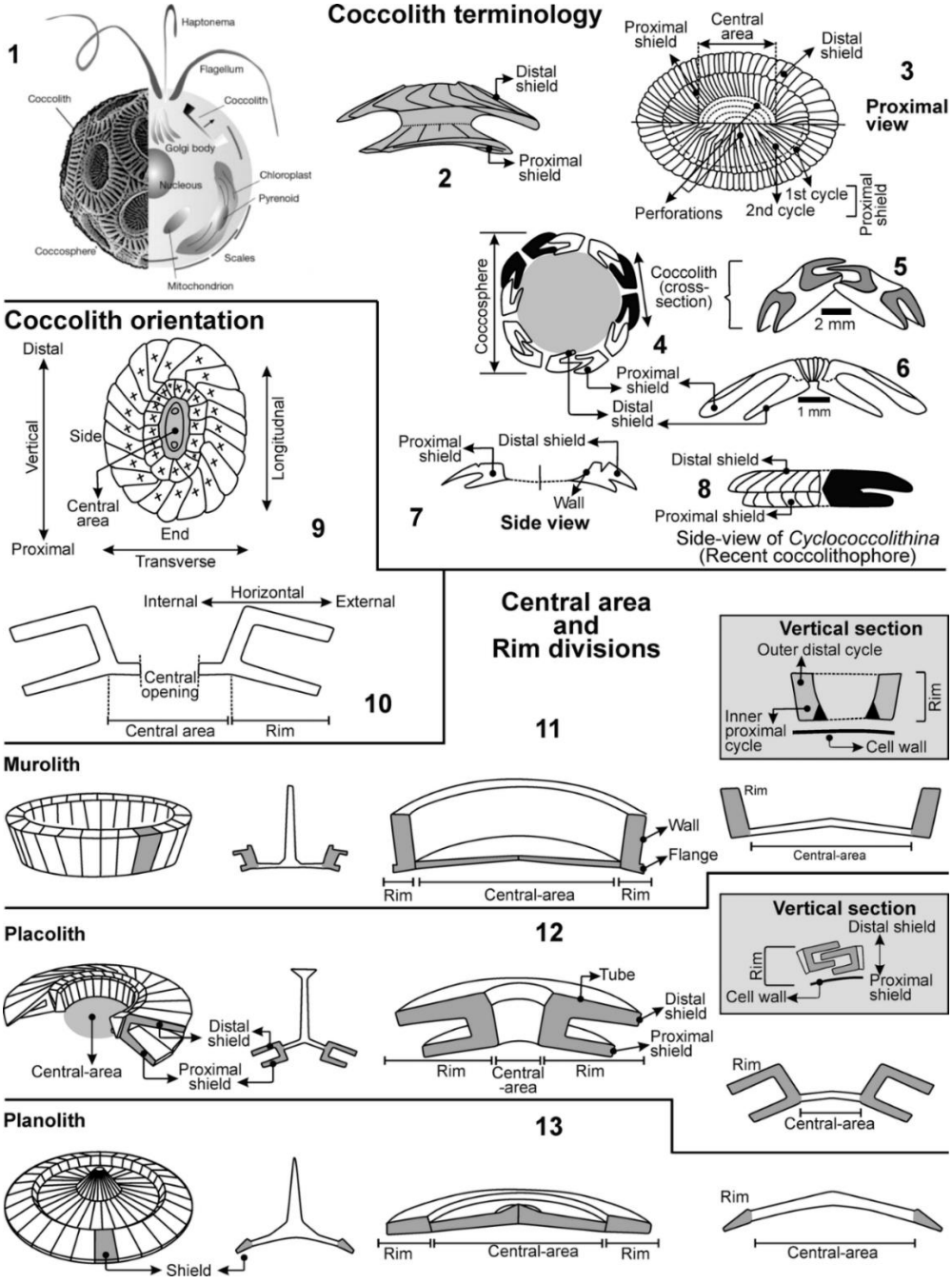

Fig.1.1 – Terminology and schematic representation of the coccolith with 1: View of a coccolithophorid with the left-hand side showing the coccosphere composed of several coccoliths and the right-hand side the inner cell with the haptonema and the Golgi body forming the calcite plate (After Flores and Sierro, 2007). 2: Coccolith with the distal shield facing out the coccosphere and the proximal shield facing in the coccosphere. 3: Proximal view of a

coccolith and the terminology of the different elements. 4 – 6: Representation of the coccoliths arrangement on the coccosphere. 7 – 8: Side view of coccoliths. 9 – 10: Terminology of the coccoliths orientation. 11 – 13: Representation of the three types of rims occurring among the heterococcoliths, including the murolith (11), the placolith (12) and planolith (13). 2 – 13 modified after Jain (2020a).

The coccoliths are produced under light stimulation by the Golgi body (Fig. 1.1) (Winter and Siesser, 1994) with around one coccolith per hour in the case of *Emiliania huxleyi* (Jakob et al., 2018), the current most abundant species. The coccoliths formation start with an organic baseplate, followed by the nucleation with a proto-coccolith ring of simple crystals around the margin of the organic baseplate (Fig.1.2) (Young et al., 1992; Bown, 1998). From this proto-coccolith ring, originate two types of crystals units alternating. This growth process is called the V/R model due to the alternation of V-unit with sub-vertical crystallographic c-axes appearing dark in cross-polarized light (XPL) and R-unit with sub-radial c-axes appearing bright in XPL (Fig.1.2) (Young et al., 1992; Bown, 1998).

The V/R model seems stable thought time and is presents among the different genera (Young et al., 1992). This feature can be used to reconstruct phylogenetic relationships between forms. Recent technology can provide additional information concerning the evolution of the coccolithophorids. A calculation of the mutation rate of biomolecule presents in the current coccolithophorids can be used to trace back speciation and/or radiation. The molecular clock has been applied to the Calcihaptophycidae (calcifying haptophytes) and suggests their earliest origin between 270 and 240 Myr for SSU rDNA (Small SubUnit ribosomal DeoxyriboNucleic Acid) and at 200 Ma for LSU rDNA (Large SubUnit ribosomal DeoxyriboNucleic Acid) (De Vargas et al., 2007).

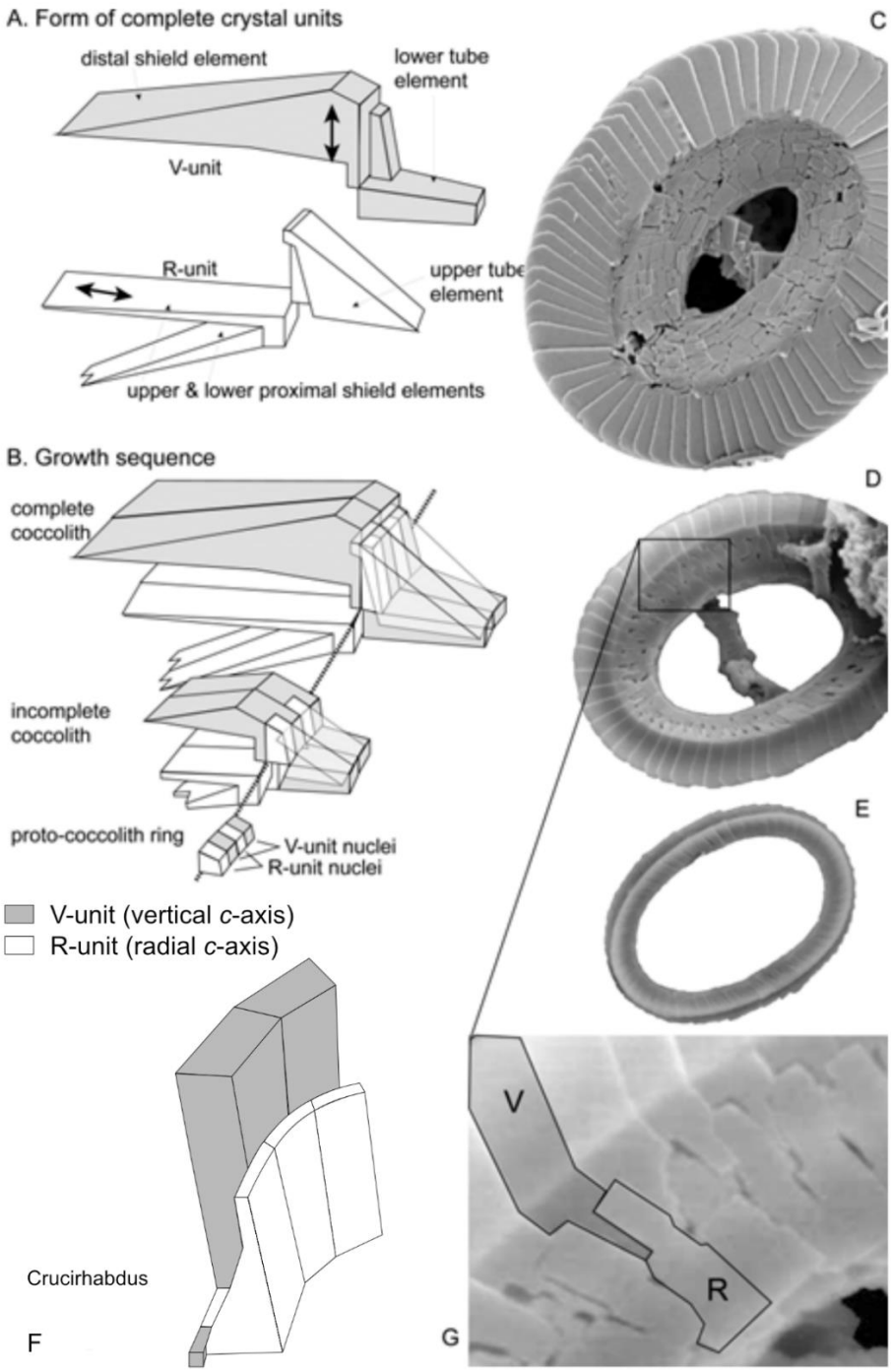

Fig.1.2 – Representation of the coccoliths growth (example of *Coccolithus pelagicus*) with A: Schematic view of the V- and R-unit and the c-axis represented by the black arrow. B: Schematic representation of the step of the coccoliths formation. C – E: Scanning Electron Microscope image showing a different stage of growth of *Coccolithus pelagicus*. F: Representation of the structure of *Crucirhabdus* genera. G: SEM image of *Coccolithus pelagicus* rim showing the V and R-units imbricated. From Young and Henriksen, 2003.

In practice, the observation falls in the range of time suggested by the molecular clock calculations. During this study, the oldest coccolithophorid was observed and identified as *Crucirhabdus sp.*, during the middle Norian (Alaunian) (Demangel et al., 2020; ~ 212 – 220 Myr; Kent et al., 2017). *C. minutus* is first described by Jafar (1983) and corresponds to a tiny elliptical coccolith with a size range between 1.6 and 2.4 µm. The protolith rim is holding a spine in the central area which appears as two small knobs under the light microscope (LM) (Bown, 1985). Above the first observed specimen of *C. minutus, C. primulus* is observed in the Rhaetian (Gardin et al., 2012). First described by Prins (1969), this elliptical coccolith presents a size between 3 and 5 µm and a loxolith rim imbricated in a clockwise direction. The central area is spanned by crossbars holding a spine. *Archaeozygodiscus koessenensis* is the third and last Triassic species, described by Bown (1985). It corresponds to elliptical coccolith with a size between 1.9 and 3.2 µm and loxolith rim structure imbricating in an anticlockwise direction. The central area is crossed by a width bar. This species was recorded, until this study, only from the late Rhaetian (*Choristoceras marshi* Zone) (Gardin et al., 2012). In the study of an Austrian section (Steinbergkogel), Gardin et al. (2012) report coccolith forms not identified at the species level already from the latest Norian. The origin of coccolithophorids in the Norian were the focuses of several studies but after revision of the stratigraphy, all oldest forms were observed (until this study) in Rhaetian sediments (Gardin et al., 2012). Those observations brought the interest of investigating in detail Norian sediment of the Northern Calcareous Alps showing good preservation to study the coccolithophorids.

From the simple murolith, protolith, rim of *C. minutus* proposed as the ancestor of *C. primulus* (Thierstein, 1976; Jafar, 1983; Bown, 1987; Gardin et al., 2012) and the slightly more complex structure of *A. koessenensis* presenting a loxolith (anticlockwise) rim, a broad diversity of complex structure occurred after several biomineralisation innovations (Monteiro et al., 2016) (Fig.1.3). After the end-Triassic mass extinction, only *C. primulus* survived (Bown et al., 2004). The first speciation event occurred at the Hettangian/Sinemurian boundary with the appearance of 5 new genera and 6 new species. The first placolith occurs in the lower Jurassic followed slightly after by the first holococcoliths (Erba, 2006). The Middle Jurassic is characterised by the evolution of the genus *Watznaueria* which colonised all the marine habitats and produce a large number of coccoliths until the end-Cretaceous. The Cretaceous is marked by a major turnover with maximum species richness in the Campanian with 65 genera and 200

species (Bown et al., 2004; Monteiro et al., 2016) (Fig.1.3). From the Jurassic onward the coccolithophorids are relatively well studied with detailed information on their evolution (diversity, abundance, extinction, size variation), however pre-Jurassic species were studied only for the first occurrence of the coccolithophorids and details on their evolution are rare. This study is focusing on the characterisation of the coccoliths diversification, size evolution and abundance variation from their first occurrence until the late Rhaetian.

Upper Triassic coccolithophorids were observed until now only in two different areas, in the Western and Southern Tethys Ocean. The Austrian Alps in the Western Tethys and the Wombat Plateau (North-West Australia) in the Southern Tethys were located in low latitudes, respectively, at 25°N (Gallet et al., 1996) and 17°S (Bralower et al., 1991). The Austrian sites cover the toe-of-slope to the deep-shelf and basinal environment (Richoz et al., 2012). The Australian sites correspond to shallower water, often under influence of the continent, covering lagoonal, deltaic, swamp, paralic, open-shelf and deep-shelf environments (Bralower et al., 1991). Only from the late Jurassic, coccolithophorids start to occupy oligotrophic, open oceans (De Vargas et al., 2007). Nowadays, they live in all the latitudes (except very high polar ones) from brackish to saline water and most of the current species are found in subtropical oceanic gyres associated with oligotrophic conditions (Tyrrell and Young, 2009). To better constrain the palaeo-geographic and environmental evolution of the early coccolithophorids, differents palaeo-latitudes and palaeo-settings were studied from sections not investigated so far for their coccolithophorids content, i.e. Romania, Turkey and Oman.

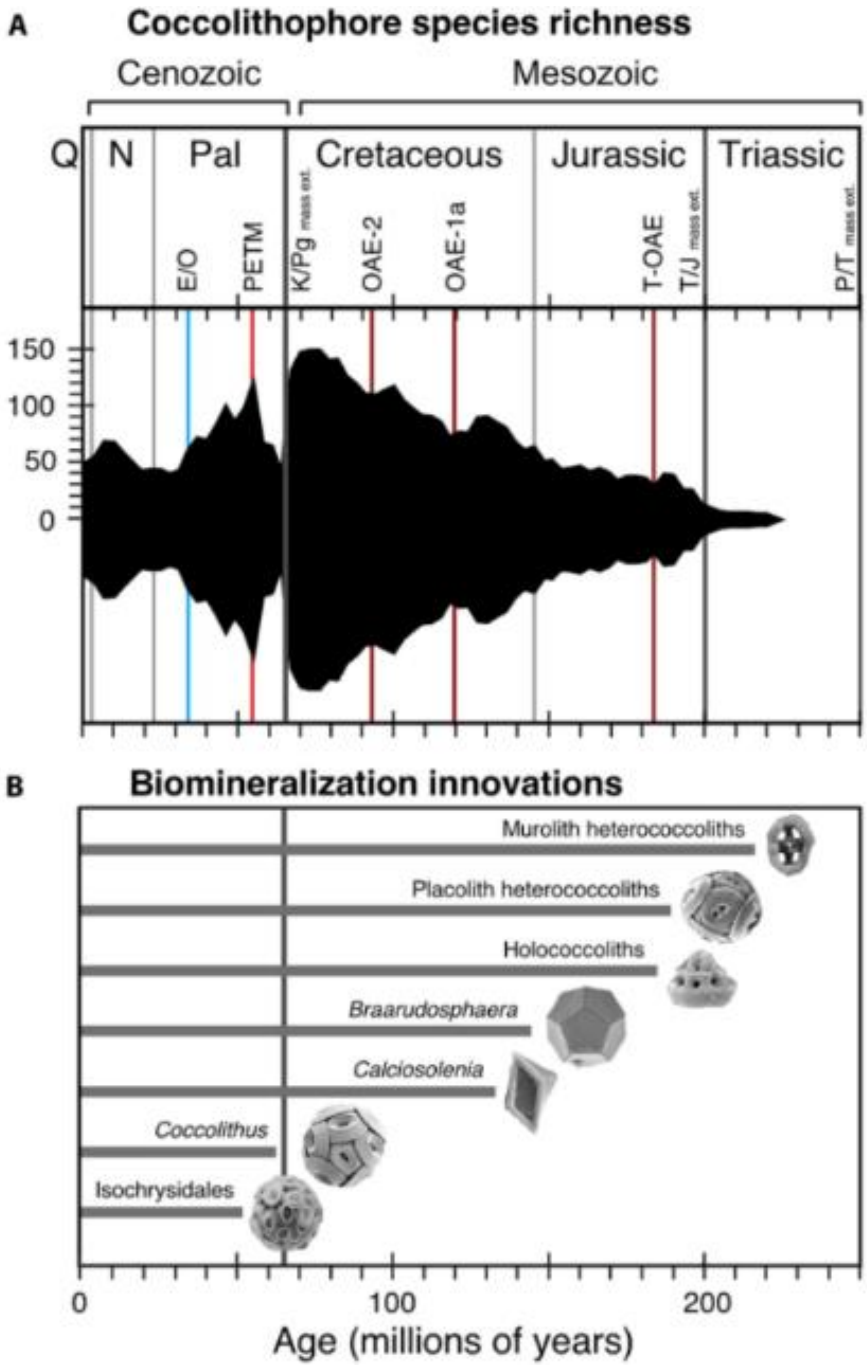

Fig.1.3 – Diagrams representing the evolution of the coccolithophorids through time with A: Coccolithophorids and nannoliths species richness over time (data from Bown et al., 2004). Q = Quaternary; N = Neogene; Pal = Paleogene; E/O = Eocene/Oligocene glacial onset event; PETM = Paleocene/Eocene thermal maximum warming event; K/Pg = Cretaceous/Paleogene; OAE = oceanic anoxic event; T-OAE = Toarcian OAE; T/J = Triassic/Jurassic; P/T = Permian/Triassic; mass ext. = mass extinction. B: Major coccolithophorids biomineralisation innovations and morphogroups with the vertical line marking the K/Pg mass extinction (from Monteiro et al., 2016).

2.2 *The calcareous dinoflagellates remaining*

The dinoflagellates are ubiquitous, unicellular, eukaryotes forming the phylum Dinoflagellata, division Pyrrhophyta and class Dinophyceae. This taxon presents species living with autotrophic mode (e.g. Tangen et al., 1982) like the plants and others being mixotrophic using autotrophism and heterotrophism through the ingestion of prey (Stoecker, 2007). Dinoflagellate presents a life cycle including motile and non-motile cells. Their mode of reproduction can be asexual (by binary fission, desmoschisis, eleutheroschisis, sporogenesis) or sexual.

The motile cell possesses two flagella (longitudinal and transversal). The cell can be armoured (=thecate) with vesicle containing cellulosic plates (=thecal plates) beneath the cell membrane or unarmoured (=athecate, naked) with vesicle lacking thecal plates (Fensome et al., 1993). The cell can be extended by horns, crests, ridges, flanges or spines (Fensome et al., 1993).

Nonmotile cells with a cell wall are called cysts, they can be fossilizable if made of dinosporin, calcium carbonate or rarely silica (Fensome et al., 1993). Four types of cysts are recognised regarding their mode of production. First, the most common in the fossil remains is a resting cyst which represents a dormant stage, resistant to adverse conditions (Pfiester and Anderson, 1987). They present a thick wall of one to three layers (Bravo and Figueroa, 2014). The resting cysts that are produced after sexual reproduction are called hypnozygote or zygotic resting cysts (Fensome et al., 1993). This mode of reproduction is present in a small amount of dinoflagellate species and is triggered by changes in temperature, nutrients and/or light availability (Pfiester and Anderson, 1987). Second, a pellicle cyst (previously temporary or ecdysal cyst) is formed by some thecate species which present a pelliculate layer internal to the theca. In response to adverse conditions, the cell shed its theca, cell membrane and flagella and, the pelliculate layer become the wall of the pellicle cyst. This form is called after its origin (ecdysis cell) and is characterised by the absence of dormancy (temporary) and thin-wall (pellicle; see text-figure 3 in Fensome et al., 1993) (Bravo and Figueroa, 2014). This type of cyst is produced by both sexual and asexual reproduction by eleutheroschisis (see text figure 6 in Fensome et al., 1993) and play an important role in the dynamic of dinoflagellate blooms (Garcés et al., 2002). The third type is a vegetative cyst, a dividing non-motile cell surrounded by a continuous wall probably similar to the pellicle (Bravo and Figueroa, 2014). For the genera

Thoracosphaera (see below), this cyst wall is made of calcium carbonate (see sub-chapter 2.2.2). Forth, the digestion cysts are thin-wall cysts formed after phagocytosis observed among mixotrophs species (Sarjeant et al., 1987). The encystment in dinoflagellate occurs to survive the adverse climatic condition, for nutrition, as a strategy to avoid predation, in the reproductive process and for dispersion (Sarjeant et al., 1987). Studies on Cretaceous material suggested an influence of the change in temperature, salinity and distance to the shore on the ornamentation, shape and wall thickness of the cyst and diversity of species (Keupp, 1981, 1982, 1992a, 1992b, 1995a, 1995b; Keupp and Mutterlose, 1984; Keupp and Versteegh, 1989; Zügel, 1994).

2.2.1 Calcareous dinoflagellates cysts

The calcareous dinocysts are produced by calcifying dinoflagellates from the order Peridiniales (Jain, 2020b), which are marine, planktonic, autotrophic species (Tangen et al., 1982; Vink, 2004). They were very abundant in the Cretaceous reaching 80% of the sediment volume (Willems, 1988, 1992, 1996) and nowadays around 30 species are described from neritic to oceanic water (Vink, 2004). Most dinoflagellates have a haplontic life cycle. The species belonging to the Peridiniales presents six stages (Evitt, 1985) including 1) Vegetative fission resulting in motile haploid schizonts favouring rapid growth and population expansion. 2) Fusion of the schizonts to form diploid zygote. 3) Formation of a new theca resulting in a planozygote. 4) The zygote theca is thicker and larger than the vegetative theca. The cell activity decreases and the flagella are lost, the cell becomes an hypnozygote. The protoplast shrinks and cyst forms within the theca. 5). The thecal plates are gone and the hypnozygote besomes a resting cyst in the sediment. 6). After a dormancy period the cell excyst, form a theca and become motile again. The hypnozygote or resting cyst made of calcium carbonate represents the calcareous dinoflagellates cyst formed after the sexual phase.

The characterization of the calcareous dinoflagellate cysts is based on their wall ultrastructure corresponding to the crystallographic orientation of the crystals forming the wall. Four types of wall exist: tangential, pithonelloid, oblique (= obliquipithonelloid) and radial (= orthopithonelloid) (Fig.1.4)(Young et al., 1997; Streng et al., 2004). The tabulation (number and position of articulated plates composing the wall) is another characteristic used for their classification (Fensome et al., 1993). Four types of tabulation are present including holotabulate, intratabulate, cingulotabulate and cryptotabulate (= no tabulation patterns, except

the ones reflected by the archaeopyle) (Fig.1.4) (Fensome et al., 1993; Young et al., 1997; Streng et al., 2004). A classification based on the archaeopyle (opening serving for excystment) was introduced by Streng et al. (2004), who described monoplacoid, apical archeopyle among the Late Triassic species. But this classification is difficult to apply on Triassic calcareous dinoflagellates cysts when the preservation is poor and the sutures or opening not visible. The calcareous cysts length average between 16 to 26 µm (Höll et al., 1999).

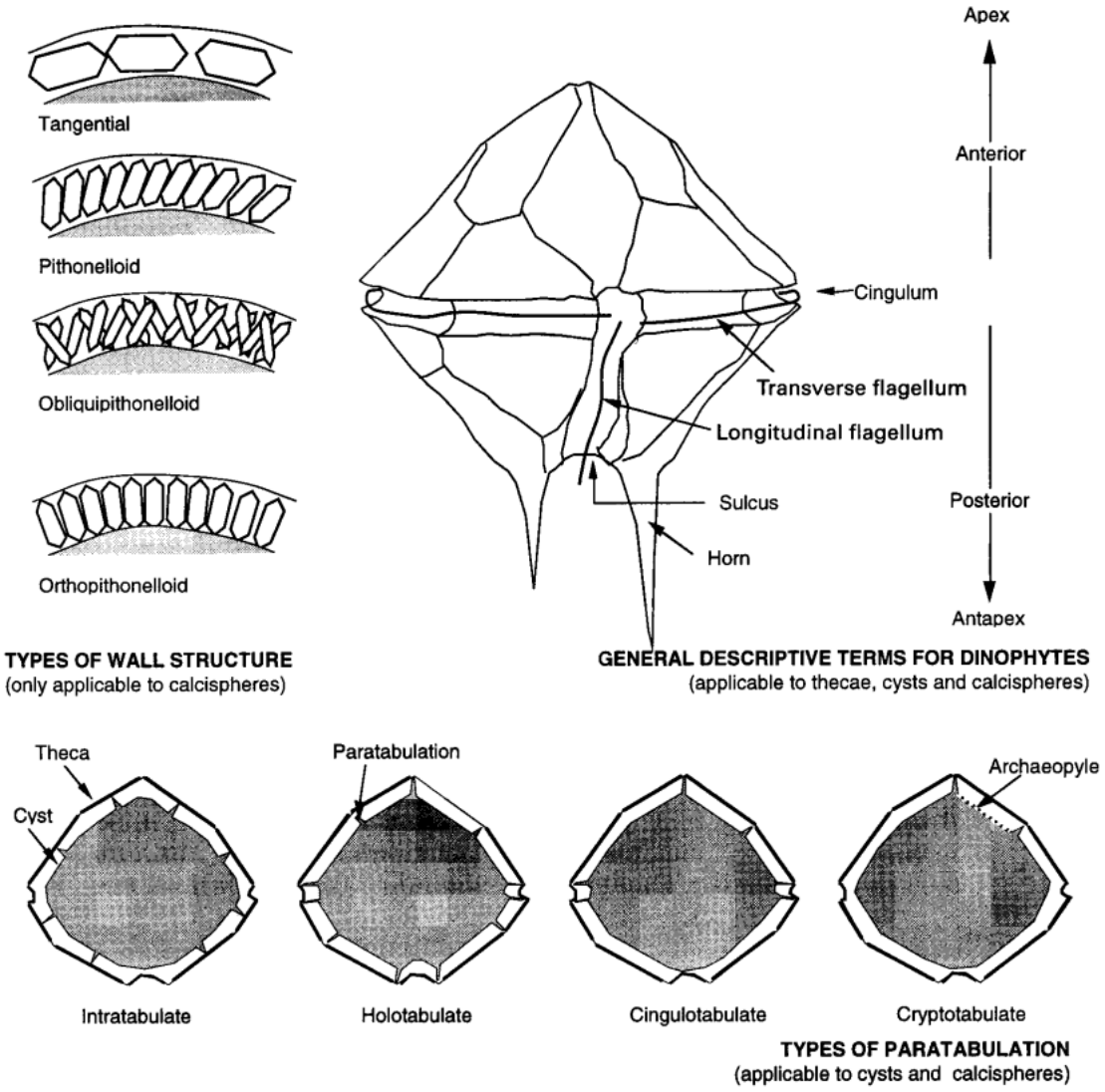

Fig.1.4. – Schematic representation of the four wall structures (upper left corner) and types of paratabulation (bottom) existing among the calcareous dinoflagellates and representation of a dinophytes (upper right corner). After Young et al., 1997.

Calcareous dinoflagellates cysts are found in a broad range of latitudes from tropical to sub-arctic zones (Zonneveld et al., 1999) but present higher abundance in tropical and

subtropical zones (Vink et al., 2002; Vink, 2004). Calcareous dinoflagellates as autotrophic species are thought to produce numerous cysts in subsurface water mass between 50 and 100 m (Janofske and Karwath, 2000; Vink et al., 2000). Their abundance is influenced by subsurface water conditions including, salinity, temperature, nutrient and stratification (Vink, 2004). However, they seem to tolerate a wide range of temperatures, salinities (Zonneveld et al., 1999, 2000), nutrient level (Höll et al., 1998, 1999; Esper et al., 2000; Vink et al., 2000; Zonneveld et al., 2000; Vink et al., 2002; Wendler et al., 2002), water stratification (Höll et al., 1998, 1999; Vink et al., 2000, 2002; Wendler et al., 2002). Previous studies show different conclusions concerning the optimal trophic conditions as these preferences seem species-specific (Vink, 2004).

The oldest calcareous dinoflagellate cyst described are *Obliquipithonella prasina* and *Orthopithonella misurinae* in the Cordevolian (Early Carnian) sediments of the Western Tethys (Janofske, 1992; Dal Corso et al., 2020) but are not observed further in the Late Carnian. *Orthopithonella geometrica* (Jafar, 1983) and *Obliquipithonella rhombica* (Janofske, 1987) evolved during the Rhaetian. *Orthopithonella geometrica* corresponds to an empty sphere with a mean diameter of 9 µm, made of perpendicular calcite elements forming the wall. Under LM, *Orthopithonella geometrica* appears circular with a bright centre composed of a black square whose corners extend to the inner part of the wall. The wall is bright, thin and well defined. *Obliquipithonella rhombica* is nearly similar to the previous species but possesses elements oblique to the wall and a smaller size with a mean diameter of around 6 µm. Under LM, this species appears circular with a full black centre and a thick wall formed of overlapping elements. However, specimens from the Upper Triassic are rare and their preservation is often slightly altered, study on these species are thus rare and the phylogenic relation to the dinophyceae is still under debate.

2.2.2 Thoracosphaeroideae (Kamptner) calcareous sphere

The *Thoracosphaera* species produce cysts during a coccoid, vegetative phase with a calcareous wall. The extant species *Thoracosphaera heimii* is well studied and the production of its calcareous shell is well understood. After asexual division, the calcification starts from different points of the organic membrane of the new cell. Early grown crystals are rhombic or irregular polygons. After growing the crystals join and then fuse completely forming the

spherical shell (Tangen et al., 1982). Those immobile, small-size cells are produced in high numbers, i.e. up to one division per day, for *Thoracosphaera heimii* (Tangen et al., 1982).

The calcareous cell is spheric and most often present an aperture with distinct edges, used for the release of the cell content (Tangen et al., 1982). The size of the calcareous cell range between 9 µm (Fütterer, 1977) to 30 µm (Kamptner, 1967). The oldest *Thoracosphaera* species described *T. wombatensis* dated back to the Norian from the Wombat Plateau (Australia) in the Sourthern Tethys (Bralower et al., 1991). *Thoracosphaera* species are described in the Western Tethys from the Rhaetian (Jafar, 1979). *Thoracosphaera wombatensis* is a bowl-shaped fossil, been included in the Dinophyceae, but its affinity to calcareous dinoflagellates is questionned due to a lack of characteristics structures such as an archeopyle and tabulation (Gottschling et al., 2008). Another study suggests a relation to the Jurassic nannolith family Schizosphaerellaceae (Fig.1.5; Streng et al., 2004). The main species *Schizosphaerella punctulata* first described by Deflandre and Dangeard (1938) is occurring from the Hettangian until the end-Kimmeridgian. It corresponds to a globular shell made of two interlocking, dissimilar, sub-hemispherical valves (Fig.1.5 B).

2.3 *The nannoliths*

The nannolith is a term used to classify calcareous nannofossils from an unknown origin. However, studies have shown that many were produced by haptophyte algae (Young et al., 1999) during a haploid stage of their life cycle (Young and Henriksen, 2003; De Vargas et al., 2007). They present a broad diversity of shapes from compact (e.g. conical, cubical, and cylindrical) to dibrachiate and radiate (Young et al., 1997) (Fig.1.5).

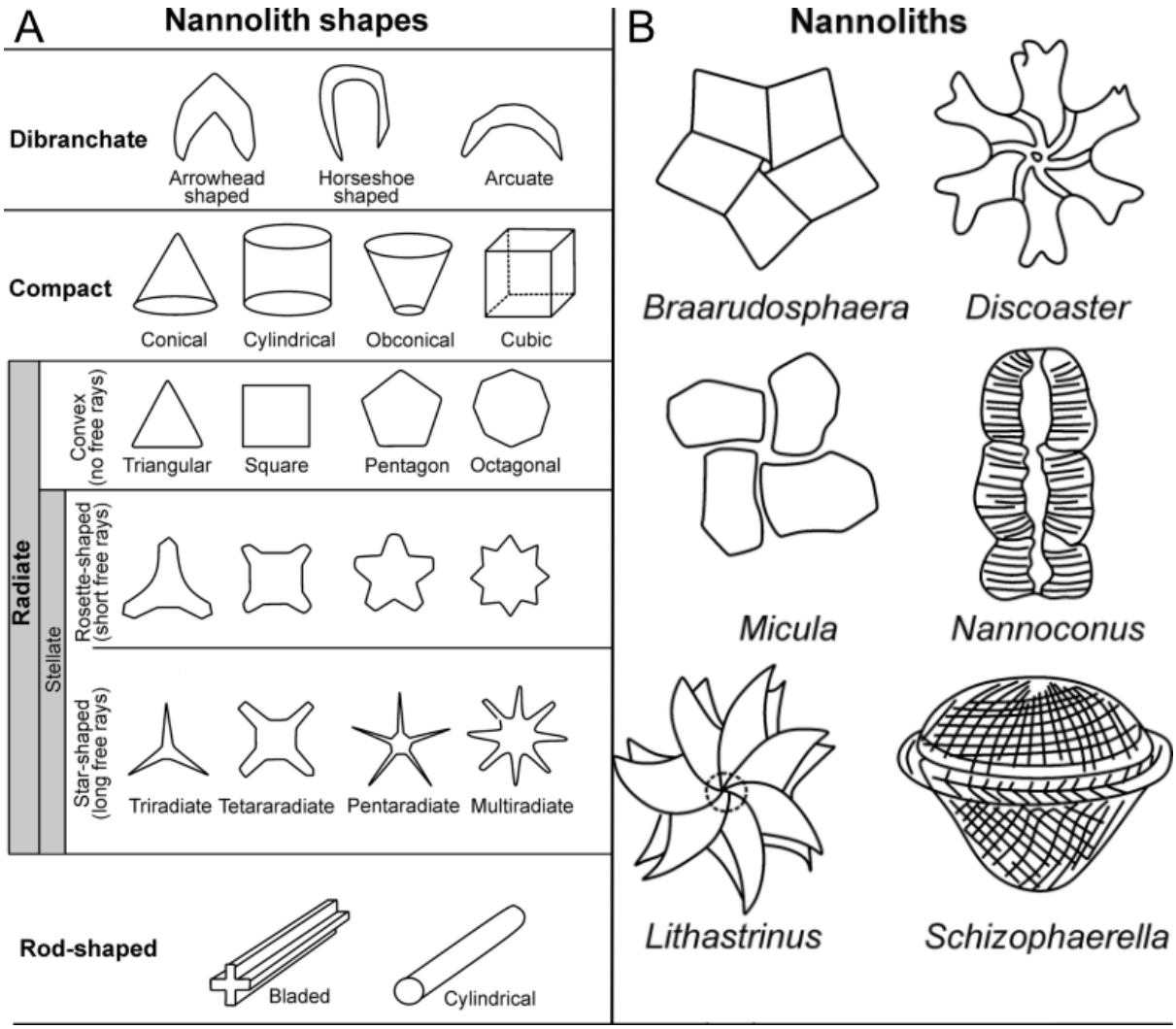

Fig.1.5 – Schematic representation of nannolith with A: the broad variety of shapes occurring among the nannolith group. B: Representation of the most abundant groups of nannoliths. Modified after Young et al., 1997; Jain, 2020a.

2.3.1 Upper Triassic calcispheres incertae sedis

The Upper Triassic records various calcispheres from unknown origin (Figs.1.6, 1.7)(e.g. Jafar, 1983; Janofske, 1987, 1990; Bellanca et al., 1993; Onoue and Yoshida, 2010; Gardin et al., 2012; Preto et al., 2012, 2013a, 2013b; Bottini et al., 2016).

The main Upper Triassic calcisphere with unknown affinities is *Prinsiosphaera triassica*, which occurs from the middle Norian (Fischer et al., 1967) to the Upper Rhaetian (Clémence et al., 2010). First described by Jafar (1983), as a spherical to hemispherical calcite solid with one depression and composed of thin, tabular, calcite rhombohedra arranged in parallel in

groups randomly placed together to form the sphere. The spheres have a mean diameter of 9 µm but present a broad variation of size from 5 to 13 µm (Clémence et al., 2010; Bottini et al., 2016; this study). Jafar (1983) described 5 sub-species regarding the aspects of their outlayers. However, Bralower et al. (1991) ruled out those 5 sub-species explaining the different aspects by degrees of diagenetic alterations. Four etching stages were described from well preserved *P. triassica* with the entire outer layer (Fig.1.6) to badly preserved specimen without outer layer remaining and the etched inner layer (Fig.1.6).

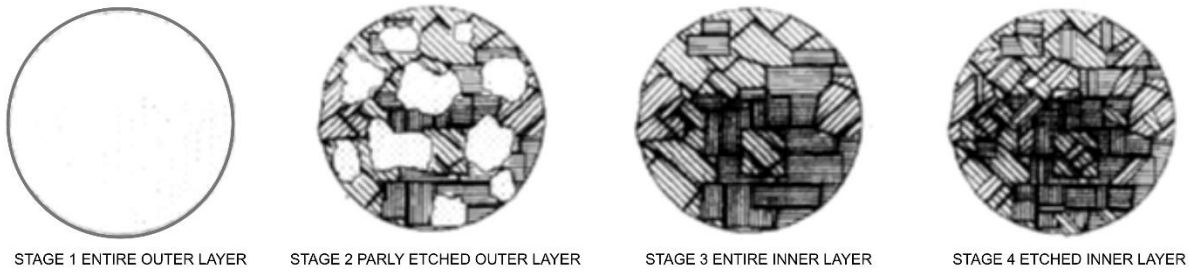

Fig.1.6. – Schematic representation of the four etching stages affecting *Prinsiosphaera triassica*. From Bralower et al., 1991.

P. triassica is described as common to abundant through the late Triassic but until this work only one quantification was performed in two basins of southern Italy (Preto et al., 2013a). In hemipelagic lime mudstones, *P. triassica* builds from 10 % of the rock during the Norian up to 60 % in the upper Rhaetian (Preto et al., 2013a). When considered as rock-forming, *P. triassica* fullfill the condition to trigger the "mid-Mesozoic revolution" leading to stabilisation of the long-term oceanic carbon cycle (Ridgwell, 2005). In order to investigate this hypothesis, we perform a quantitative estimation of the volume and palaeo-fluxes of *P. triassica* during the Upper Triassic in Northern Calcareous Alps sections. This second set of abundance values allow comparison with Italian abundance. Additionally, as *P. triassica* is the most important calcifier, its abundance will be compared with calcium isotope values to evaluate its influence.

Additionnally, one type of calcisphere (Fig.1.7 C) is often observed and described from several localities with different palaeo-environments (shallow to deep-water). The specimens are circular calcite structures with radially, arranged, elongated calcite crystals and a void centre or filled with blocky calcite crystals (Di Nocera and Scandone, 1997; Bellanca et al., 1993; Preto et al., 2012, 2013a, 2013b). The study of Upper Triassic calcispheres is

complicated by the poor preservation of the sediments at many localities. This study aims to complement the few descriptions and pictures on the Upper Triassic calcisphere with scanning electron microscopy (SEM) and LM analyses.

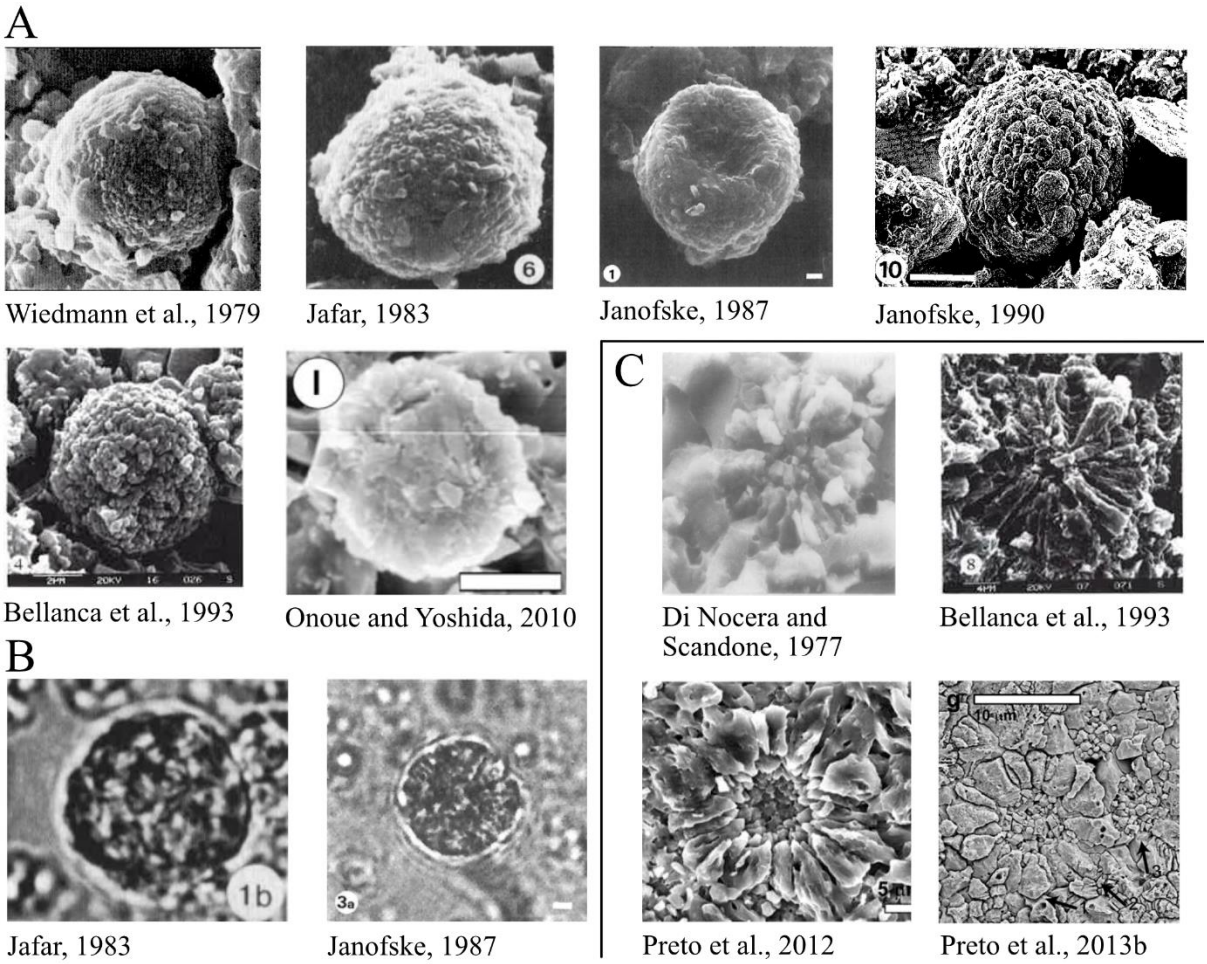

Fig.1.7 – Pictures representing Triassic calcispheres diversity with A: Scanning Electron Microscope. B: Light Microscope. C: Calcisphere form with radially, arranged, elongated calcite crystals frequently observed at different localities.

2.3.2 Upper Triassic conical calcareous nannofossils

In addition to the calcisphere, the second group of nannoliths occurring in the Upper Triassic corresponds to conical calcareous structures. From the Rhaetian, *Conusphaera zlambachensis* was first described by Moshkovitz (1982) as an elongated cone, truncated at both ends, composed in the inner part of 35 – 40 radial, inclined calcitic lamellae sinistrally turning and in the outer part of long smooth plates. From the same deposition environment, i.e.

lower Rhaetian sediments of Zlambach Formation, Jafar (1983), described a new genus and species *Eoconusphaera tollmanniae*. Jafar (1983) characterised this new genus by the presence of a dome at the broader end and the lack of axial "canal". However, the two species descriptions and illustrations are similar and *Conusphaera* species (e.g. *Conusphaera mexicana*) does not present any axial "canal" neither. These last criteria can not be used to separate the two genera. Janofske (1987) regarded the species *C. zlambachensis* and *C. tollmanniae* as differing in the orientation of the inner laths, vertical in *C. tollmanniae* and inclined in C. *zlambachensis*. Although, the poor quality of the illustrations does not allow clear observations of those differences in the inner lamellae orientation, so the two species *zlambachensis* and *tollmanniae* were considered as a synonym. In this study, observation of sediments dated from the Norian to the middle Rhaetian aimed to revolve taxonomic confusion around the conical form and help to describe their evolution and diversity in the Upper Triassic (see Chapter 2, 3 and 5).

3. The Late Triassic, studied localities and samples

3.1 *The Late Triassic period*

The Late Triassic expands from ~ 237.0 until 201.4 Ma (Ogg and Chen, 2020). The supercontinent Pangea is centred on the equator, surrounded by the Panthalassa Ocean on the western coast and the Tethys Ocean on the Eastern one (Ziegler et al., 2003). The Tethys Ocean is enclosed in the C-shape supercontinent limited to the tropical and subtropical zones (Ziegler et al., 2003). During Permian and then the Triassic, the Cimmerian archipelago drifted away north from the northern margin of Gondwana, splitting the Tethys Ocean (Stampfli and Borel, 2002). The Paleo-Tethys is enclosed in the northern part between Laurasia and Cimmeria and the Neo-Tethys Ocean is opening in the southern part between Cimmeria and Gondwana (Golonka et al., 2018). The Triassic period is described as a warm, ice-free world (Preto et al., 2010), but the mega-monsoon system was at the maximum during the Late Triassic (Robinson, 1973), modulated by Milankovitch cycles (Ogg, 2012). Such a climatic system must lead to an alternate dry and monsoonal climate in the Western Tethys (Preto et al., 2010).

3.2 *The studied areas*

The studied area covered the Paleo-Tethys Ocean (Romania) and the Neo-Tethys Ocean (Austria, Turkey, Oman, Australia) and three different latitudes: 25°N with the Austrian and Romanian sections (Gallet et al., 1996), equator with the section from Turkey (Gallet et al., 2007) and 20°S with sections from Oman (Richoz et al., 2014). The samples from the Romanian sections were not initially included in the sampling of the project but added lately thanks to a collaboration with Pr. Eugen Gradinaru. The samples from N-W Australia were analysed by Richard Howe and included in the study of the Eoconusphaeraceae.

3.2.1 The Northern Calcareous Alps (Austria)

During the Late Triassic, Austria was located in the western Neo-Tethys margin around 25° N (Gallet et al. 1996). The Northern Calcareous Alps recorded the expansion of large-carbonate platforms during the Middle and Late Triassic (Mandl, 2000; Kenter and Schlager, 2009; Richoz and Krystyn, 2015). From the late Carnian (237–227 Ma), the Dachstein Platform started to spread. It is composed of large lagoons and intra-platform basins such as the Eiberg basin with alternated limestone and marl (Eiberg and Kuhjoch sections). The Dachstein platform extends toward the South with fringing reefs and then open-ocean where Hallstatt facies pelagic limestones developed (Richoz and Krystyn, 2015). The deeper margin area was subject to diapirism of the Permian evaporates, creating a hemipelagic high environment where the sediment from Leislingkogel, Sommeraukogel and Steinbergkogel sections were deposited. This environment, around 300 m to 500 m deep, shows lateral differences between massive light limestone and red condensed limestone (Krystyn, 1980). In the early Rhaetian, with an increase in terrigenous input, marls were deposited in a toe-of-slope to open-marine basin environment covering slowly the Hallstatt-type facies. This corresponds to the studied section of Zlambach.

3.2.2 North Dobrogea (Romania)

North Dobrogea in Romania is an alpine orogenic chain located in the south of the Danube delta and northwest of the marginal black sea. This orogenic belt corresponds to a Late Permian-Early Triassic rifted basin, inverted during the Late Triassic phase of the Cimmerian orogeny and Early Cretaceous phases of the Alpine orogeny (Dinu et al., 2005). During the Triassic, this region was located in the Paleo-Tethys Ocean. The North Dobrogea is composed

of three tectonic units: Macin, Niculitel and Tulcea Nappes, which consists of Triassic to Jurassic sediments (Grădinaru, 1984; Seghedi, 2001). Three of the studied sections, i.e. Frecătei, Răndunica and Izvoarele, belong to the Tulcea nappes. Frecătei and Izvoarele correspond to deep-water, basinal palaeo-environment, while Răndunica corresponds to shallow-water carbonate platform facies (Grădinaru, 2000). The two other studied cores, i.e. 817 Lebăda Vest (LV) and 816 LV belong to the offshore histria depression and correspond to the deep-sea palaeo-environment (Forel and Grădinaru, 2020). Finally, the Vaşcău section part of the Vaşcău nappe is located in the west of Romania, at the southwestern end of the Codru-Moma Mountains. It corresponds to a deep-sea palaeo-environment (Bucur, 2001).

3.2.3 Central Taurides (Turkey)

Oyuklu section (36.835, 32.939) is located in the central Taurides in the southwest of Turkey. It corresponds to a succession of cherty, fossil-poor hemipelagic limestone deposited in a deep-water environment around the paleo-equator in the Neo-Tethys Ocean (Gallet et al., 2007). The section is condensed without a sedimentation gap between the upper Norian to the upper Rhaetian. The datation is based on conodonts, providing five biozones: *Epigondolella bidentata – Misikella hernsteini*, *E. bidentata – M. posthernsteini*, *M. hernsteini – M. posthernsteini*, *M. rhaetica* and *M. ultima* zones (Gallet et al., 2007). No calcareous nannofossils were observed in the seven samples analysed.

3.2.4 Arabian platform (Oman and the United Arab Emirates)

On the southern margin of the Neo-Tethys, around 20°S, the Arabian platform was deposited from the Permian onward (Richoz et al., 2014). The Triassic carbonates were deposited in shallow water. Six sections (= twenty-two analysed samples) including Wadi Alva, Sumeini, Wadi Suwayh, Wadi Milaha, Aqil, Wadi Mayan were analysed for their calcareous nannofossil contents but none were observed. Wadi Milaha and Wadi Suwayh represent shallow platform environment, Sumeini toe-of-slope deposits and Wadi Mayan proximal basin sedimentation. Wadi Alwa and Aquil were deposited close to the platform ridge on isolated platforms developed on top of tilted blocks and volcanic islands. Aqil section (22.787, 57.855) corresponds to a block of platform sediments in a 500 to 600 m long breccia redeposited in the adjacent Hawasina Basin. The studied samples correspond to Hallstatt-type

limestone, mainly wackestones (brown/red). The lower (Lacian 3) to middle Norian presents thin-shelled bivalves and upper Norian to middle Rhaetian sediments present crinoids and shell debris. One grainstone bed with ammonoids is recorded in upper Norian suggesting a storm event (Baud et al., 2001). Wadi Alwa (23.172, 58.393) belong to a mega-block of several kilometres in length and width (Béchennec, 1988; Pillevuit et al., 1993). Deposited in the deep-water palaeo-environment, the studied samples correspond to red limestone rich in ammonoids (Pillevuit et al., 1993; Baud et al., 2001; Richoz, 2006). The studied section is 20 m thick covering the lower Norian (Lacian 3) to uppermost Rhaetian (*M. ultima* Zone).

3.2.5 Northern Carnarvon Basin (Australia)

The analysed samples from Pluto-3 and 4 (petroleum exploration wells) belong to the Northern Carnarvon Basin (Northwestern Australia) located in the southern margin of the Neo-Tethys Ocean around 30 °S (Woodside, 2007a, 2007b). The samples from the Brigadier Formation (Rhaetian) corresponds to offshore marine marl deposited in a wide and shallow epicontinental sea (Marshall and Lang, 2013).

4. Methodology

4.1 *Evaluation of the diagenetic alterations*

The diagenetic impact on the calcareous nannofossils preservation was estimate using scanning electron microscopy description of the matrix and cements (see chapters 2 and 5). Moreover, to evaluate the diagenesis and for the accuracy of the isotopic measurement performed by Zsofia Kovacs, the major, minor and traces elements were measured by inductively coupled plasma optical emission spectroscopy (ICP-OES) at Graz University of Technology (Graz) with the help of Andre Baldermann.. Results and detail of the method are developped in Chapter 2 and 5. Additionally, the Li/Ca ratio was useful to trace the continental influx variation (Kovacs et al., 2020). Local variations in $\delta^{44/40}Ca$ gave also details on the early diagenesis in the studied sections (Chapter 6).

4.2 *Calcareous nannofossils samples preparation*

To trace the oldest coccoliths, the Norian samples from the Sommeraukogel section were prepared following the standard methods of smear slide described in Bown (1998). However, no calcareous nannofossils were found, despite the abundant *Prinsiosphera triassica*, already present in the Norian, should have been found. Thus, alternative solutions were tried. The smear slide (without the slide) were analysed under the SEM but without better success. Finally, the methods described by Preto et al. (2013a, b) was tested. Small blocks of sediment of 1 cm^2 were polished and rapidly etched in HCl before being analysed under SEM providing good results. For Steinbergkogel, this last method was applied on samples with hard lithology and smear slides were produced for marly samples. Those two different methods, adapted to each lithology, were performed on all the others sections and provided satisfactory results (see Chapter 2 for a precise description of the methods).

References

Armstrong, H., Brasier, M.D., 2005: Microfossils. Malden: Blackwell Publishing, Second Edition. ISBN: 0-632-05279-1.

Baud, A., Béchennec, F., Krystyn, L., Le Métour, J., Marcoux, J., Maury, R., Richoz, S., 2001: Permo-Triassic deposits: from the Platform to the Basin and Seamounts. Conference on the Geology of Oman, Fields guidebook, Excursion A01, 1 – 54.

Béchennec, F., 1988: Géologie des nappes d'Hawasina dans la partie orientale et centrales des montagnes d'Oman: Documents du Bureau de Recherches Géologiques et Minières, 127, 1 – 474.

Bellanca, A., Di Stefano, E., Di Stefano, P., Erba, E., Neri, R., Pirini Radrizzani, C., 1993: Ritrovamento di ''Calcisfere'' e nannofossili calcarei in terreni carnici della Sicilia. Paleopelagos, 3, 91 – 96.

Bengtson, S., 1992: Proterozoic and earliest Cambrian skeletal metazoans, *in* Schopf, J.W., Klein, C., (Eds.), The Proterozoic Biosphere: A multidisciplinary study: Cambridge, UK, Cambridge University Press, 397 – 411.

Bengtson, S., 1994: The advent of animal skeletons. In: Bengtson, S., (Ed.), Early Life on Earth. Nobel Symposium, 84, New York: Columbia University Press, 412 – 425.

Bengtson, S., 2004: Early skeletal fossils. In: Lipps, J.H., Waggoner, B:M. (Eds.), Neoproterozoic–Cambrian Biological Revolutions. The Paleontological Society Papers, 10, 67 – 77.

Billard, C., Inouye, I., 2004: What is new in coccolithophores biology? In: Thierstein, H.R., Young, J.R. (Eds)., Coccolithophores: From molecular processes to Global Impact. Springer-Verlag, Berlin, 1 – 29.

Blackwelder, P.L., Weiss, R.E., Wilbur, K.M., 1976: Effects of calcium, strontium, and magnesium on the coccolithophorids *Cricosphaera* (*Hymenomonas*) *carterae*. I. Calcification. Marine Biology, 34 (1), 11 – 16. 10.1007/BF00390781.

Blätter, C.L., Henderson, G.M., Jenkyns, H.C., 2012: Explaining the Phanerozoic Ca isotope history of seawater. Geology 40, 843 – 846.

Bornemann, A., Aschwer, U., Mutterlose, J., 2003: The impact of calcareous nannofossils on the pelagic carbonate accumulation across the Jurassic–Cretaceous boundary. Palaeogeography, Palaeoclimatology, Palaeoecology. 199, 187 – 228.

Bottini, C., Jadoul, F., Rigo, M., Zaffani, M., Artoni, C., Erba, E., 2016: Calcareous nannofossils at the Triassic/Jurassic boundary: Stratigraphic and paleoceanographic characterization. *Rivista Italiana di Paleontologia e Stratigrafia (Research in Paleontology and Stratigraphy)* 122, 141 – 164.

Bown, P.R., 1985. *Archaeozygodiscus* gen. nov. and other Triassic coccoliths. INA Newsletter. 7, 32 – 35.

Bown, P.R., 1987: The structural Development of Early Mesozoic Coccoliths and its Evolutionary and Taxonomic Significance. Abhandlungen der Geologischen Bundesanstalt. 39, 33 – 49.

Bown, P.R., 1998: Calcareous Nannofossil Biostratigraphy. London: Chapman & Hall, First Edition. ISBN: 0-412-78970-1.

Bown, P.R., Lees, J.A., Young, J.R., 2004. Calcareous nannoplankton evolution and diversity through time. In: Thierstein, H.J.R. (Eds.), Coccolithophores. From Molecular Processes al Impact. Springer-Verlag, Berlin, 481 – 508.

Bob‘ Brain, C.K., Prave, A.R., Hoffmann, K.H., Fallick, A.E., Botha, A., Herd, D.A., Sturrock, C., Young, I., Condon, D.J., Allison, S.G., 2012: The first animals: ca. 760-million-year-old sponge-like fossils from Namibia. South African Journal of Science, 108 (1/2), 1 – 8. 10.4102/sajs.v108i1/2.658.

Bralower, T.J., Bown, P.R., Siesser, W.G., 1991. Significance of Upper Triassic nannofossils from the Southern Hemisphere (ODP Leg 122, Wombat Plateau, N.W. Australia) – Marine Micropaleontology, 17, 119 – 154. 10.1016/0377-8398(91)90025-2.

Braun, A., Chen, J., Waloszek, D., Maas, A., 2007: "First Early Cambrian Radiolaria". In Vickers-Rich, P., Komarower, P., (eds.): The Rise and Fall of the Ediacaran Biota, Geological Society, Special publications, London, 286, 143 – 149, 10.1144/SP286.10.

Bravo, I., Figueroa, R.I., 2014: Towards and Ecological Understanding of Dinoflagellate Cyst Functions. Microorganisms, 2 (1), 11 – 32.

Brennan, S.T., Lowenstein, T.K., Horita, J., 2004: Seawater chemistry and the advent of biocalcification. Geology, 32 (6), 473 – 476. 10.1130/G20251.1.

Bucur, I.I., 2001: Upper Triassic deposits of Vaşcău plateau. In: Bucur, I:I., Filipescu, S., Sasaran, E., (Eds.): Algae and carbonate platforms in the western part of Romania. 4th Regional Meeting of IFAA, Cluj-Napoca, Romania, Field Trip Guidebook, 18 – 28.

Canfield, D.E., Poulton, S.W. and Narbonne, G.M., 2007: Late-Neoproterozoic deep-ocean oxygenation and the rise of animal life. Science, 315, 92 – 95. 10.1126/science.1135013.

Clémence, M.E., Gardin, S., Bartolini, A., Paris, G., Beaumont, V., Guex, J. 2010: Bentho-planktonic evidence from the Austrian Alps for a decline in sea-surface carbonate production at the end of the Triassic. *Swiss Journal of Geosciences* 103, 293 – 315.

Clémence, M.E., Gardin, S., Bartolini, A., 2015: New insights in the patterns and timing of the Early Jurassic calcareous nannofossils crisis. Palaeogeography, Palaeoclimatology, Palaeoecology, 427, 100 – 108. 10.1016/j.palaeo.2015.03.024.

Dal Corso, J., Preto, N., Agnini, C., Hohn, S., Merico, A., Willems, H., Gianolla, P., 2020: Rise of calcispheres during the Carnian Pluvial Episode (Late Triassic). Global and Planetary Change, 200, 103453. 10.1016/j.gloplacha.2021.103453.

Dale, B., 1983: Dinoflagellate resting cysts: benthic plankton. In: Survival strategies of the algae. Edited by G. A. Fryxell. Cambridge University Press, U.K. 69 – 136.

Dale, B., 1992: Chapter 1. Dinoflagellate contributions to the open ocean sediment flux. In: Dinoflagellate contributions to the deep sea. Edited by B. Dale and A.L. Dale: Ocean Biocoenosis, 5. Woods Hole Oceanographic Institution, Woods Hole, Mass. 1 – 32.

Deflandre, G., Dangeard, L., 1938: *Schizosphaerella*, un nouveau microfossile méconnu du Jurassique moyen et supérieur. *Comptes Rendus Hebdomadaires des Séances de l'Académie des Sciences, Paris.* 207, 1115 – 1117.

Demangel, I., Kovacs, Z., Richoz, S., Gardin, S., Krystyn, L., Baldermann, A., Piller, W. E., 2020: Development of early calcareous nannoplankton in the Northern Calcareous Alps (Austria) in the Late Triassic. Global and Planetary Change, 193, 103254, 10.1016/j.gloplacha.2020.103254.

DePaolo D.J., 2004: Calcium isotopic variations produced by biological, kinetic, radiogenic and nucleosynthetic processes, in: C.M. Johnson, B.L. Beard, F. Albarede (Eds.), Geochemistry of Nontraditional Stable Isotopes. Review in Mineralogy and Geochemistry 55, 255 – 288.

De Vargas, C., Aubry, M.P., Probert, I., Young, J., 2007. Origin and evolution of coccolithophores: from coastal hunters to oceanic farmers. In: Falkowski, P.G., Knoll, A.H. (Eds), Evolution of Aquatic Photoautotrophs, Boston, Elsevier. 251 – 285.

Di Nocera S., Scandone P., 1977. Triassic nannoplankton limestones of deep basin origin in the central Mediterranean region. Palaeogeography, Palaeoclimatology, Palaeoecology. 21, 101 – 111. 10.1016/0031-0182(77)90008-6.

Dinu, C., Wong, H.C., Țambrea, D., Mațenco, L., 2005: Stratigraphic and structural characteristics of the Romanian Black Sea shelf. Tectonophysics, 410: 417 – 435. 10.1016/j.tecto.2005.04.012.

Ehrenberg, C. G., 1836. Bemerkungen über feste mikroskopische anorganische Formen in den erdigen und derben Mineralien. – Abhandlungen der Königlich Preussischen Akademie der Wissenschaften Berlin. 1836, 84 – 85.

Erba, E., 1989: Upper Jurassic to Lower Cretaceous Nannoconus distribution in some sections from northern and central Italy. Memorie di Scienze Geologiche, 41, 255 – 261.

Erba, E., 2006: The first 150 million years history of calcareous nannoplankton: Biosphere-geosphere interactions; Palaeogeography, Palaeoclimatology, Palaeoecology, 232, 23 – 250.

Esper, O., Zonneveld, K.A.F., Höll, C., Karwath, B., Kuhlmann, H., Schneider, R.R., Vink, A., Weise-Ihlo, I., Willems, H., 2000: Reconstruction of palaeoceanographic conditions in the South Atlantic Ocean at the last two Terminations based on calcareous dinoflagellate cysts. International Journal of Earth Sciences, 88, 680 – 693.

Evitt, W.R., 1985: Sporopollenin Dinoflagellate Cysts: Their morphology and Interpretation. Dallas, Texas, American Association of Stratigraphic Palynologists Foundation.

Falkowski, P., 2012: The power of plankton. Nature, 483, 17 – 20.

Fensome, R. A., Taylor, F. J. R., Norris, G., Sarjeant, W. A. S., Wharton, D. I., Williams, G.L., 1993: A classification of living and fossil dinoflagellates. Micropaleontology, special publication, 7, 351 p.

Field, C.B., Behrenfeld, M.J., Randerson, J.T., Falkowski, P., 1998: Primary Production of the Biosphere: Integrating Terrestial and Oceanic Components. Science, 281 (5374), 237 – 240. 10.1126/science.281.5374.237.

Fischer, A.G., Honjo, S., Garrison, R.A.E., 1967: Electron Micrographs of Limestones and their Nannofossils. Princeton University Press, Princeton.

Flores, J.A., Sierro, F.J., 2007: Paleoceanography, biological proxies/coccolithophores. In: Elias, S. A. (Ed). Encyclopedia of Quaternary Science. Amsterdam: Elsevier, 1634 – 1646.

Forel, M.-B., Grădinaru, E., 2020: Rhaetian (Late Triassic) ostracods (Crustacea, Ostracoda) from the offshore prolongation of the North Dobrogean Orogen into the Romanian Black Sea shelf. European Journal of Taxonomy, 727, 1 – 83. 10.5852/ejt.2020.727.1183.

Fütterer, D., 1977: Distribution of calcareous dinoflagellates in Cenozoic sediments of site 366, eastern North Atlantic. Initial Reports Deep Sea Drilling Project, 41, 709 – 737.

Gallet, Y., Besse, J., Krystyn, L., Marcoux, J., 1996: Norian magnetostratigraphy from the Scheiblkogel section, Austria: constraint on the origin of the Antalya Nappes, Turkey. Earth and Planetary Science Letters 140 (1 – 4), 113 – 122. 10.1016/0012-821X(96)00044-1.

Gallet, Y., Krystyn, L., Marcoux, J., Besse, J., 2007: New constraints on the End-Triassic (Upper Niran-Rhaetian) magnetostratigraphy. Earth and Planetary Science Letters, 255 (3 – 4), 458 – 470. 10.1016/j.epsl.2007.01.004.

Garcés, E., Masó, M., Camp, J., 2002: Role of temporary cysts in the population dynamics of *Alexandrium taylori* (Dinophyceae). Journal of Plankton Research, 24 (7), 681–686. 10.1093/plankt/24.7.681.

Gardin, S., Krystyn, L., Richoz, S., Bartolini, A., Galbrun, B., 2012. Where and when the earliest coccolithophores? Lethaia. 45, 507 – 523. 10.1111/j.1502-3931.2012.00311.x.

Gattuso, J.-P., Allemand, D., Frankignoulle, M., 1999: Photosynthesis and calcification at cellular, organismal and community levels in coral reefs: a review on interactions and control by carbonate chemistry. Integrative and Comparative Biology, 39, 160 – 183. 10.1093/icb/39.1.160.

Germs, G.J.B., 1972: New shelly fossils from Nama Group, south west Africa. American Journal of Science, 272, 752 – 761. 10.2475/ajs.272.8.752.

Ginot, S., Goudemand, N., 2020: Global climate changes account for the main trends of conodont diversity but not for their final demise. Global and Planetary Change, 195, 103325. 10.1016/j.gloplacha.2020.103325.

Golonka, J., Embry, A., Krobicki, M., 2018: Chapter 2 – Late Triassic Global Plate Tectonics. In: Tanner, L.H., (Ed.) The Late Triassic World – Earth in a Time of Transition. Topics in Geobiology, Springer, 46, 27 – 57. 10.1007/978-3-319-68009-5.

Gottschling, M., Renner, S.S., Meier, K.J.S., Willems, H., Keupp, H., 2008: Timing deep divergence events in calcareous dinoflagellates, Journal of phycology, 44, 429 – 438. 10.1111/j.1529-8817.2008.00479.x.

Grădinaru, E., 1984: Jurassic rocks of North Dobrogea: a depositional-tectonic approach. Revue roumaine de Géologie, 28, 61 – 72.

Grădinaru, E., 2000: Introduction to the Triassic geology of North Dobrogea Orogen. In: Grădinaru E. (ed.) Workshop on the Lower-Middle Triassic (Olenekian-Anisian) Boundary: 5–37. 7–10 June 2000, Tulcea, Romania, Conference and Field Trip. Field Trip Guide, Bucharest.

Grotzinger, J., Watters, W., Knoll, A., 2000: Calcified metazoans in thrombolite-stromatolite reefs of the terminal Proterozoic Nama Group, Namibia. Paleobiology, 26, 334 – 359. 10.1666/0094-8373(2000)026<0334:CMITSR>2.0.CO;2.

Grotzinger, J.P., James, N.P., 2000: Precambrian Carbonates: Evolution of Understanding. In: Carbonate Sedimentation and Diagenesis in the Evolving Precambrian World, SEPM, Special Publication, 67. 1 – 20.

Hannah, L., 2022: Chapter 5 – Climate Change and the Earth System. In: Hannah, L., (Ed.) Climate Change Biology (Third Edition), Academic Press, 95 – 114. 10.1016/B978-0-08-102975-6.00005-4.

Hay, W.W., 2004: Carbonate fluxes and calcareous nannoplankton. In: Thierstein, H.R., Young, J.R. (Eds.), Coccolithophores. From Molecular Processes to Global Impact. Springer-Verlag, Berlin, 509 – 528.

Head, M., 1996: Chapter 30. Modern dinoflagellate cysts and their biological affinities. In: Palynology: Principles and applications. Ed. Jansonjus, J., McGregor, D.C. American Association of Stratigraphic Palynologists, Dallas, Texas, 3, 1197 – 1248.

Hibberd, D.J., 1976. The ultrastructure and taxonomy of the Chrysophyceae and Prymnesiophyceae (Haptophyceae): a survey with some new observations on the ultrastructure of the Chrysophyceae. Botanical Journal of the Linnaean Society, 72, 55 – 80.

Hippler, D., Schmitt, A.D., Gussone, N., Heuser, A., Stille, P., Eisenhauer, A., Nägler, T.F., 2003: Calcium isotopic composition of various reference materials and seawater: Geostandards Newsletter, 27 (1), 13 – 19. 10.1111/j.1751-908X.2003.tb00709.x.

Höll, C., Zonneveld, K.A.F., Willems, H., 1998: On the ecology of calcareous dinoflagellates: The Quaternary Eastern Equatorial Atlantic, Marine Micropaleontology, 33, 1 – 25. 10.1016/S0377-8398(97)00033-9.

Höll, C., Karwath, B., Rühlemann, C., Zonneveld, K.A.F., Willems, H., 1999: Palaeoenvironmental information gained from calcareous dinoflagellates: the late Quaternary eatern and western tropical Atlantic Ocean in comparison. Palaeogeography, Palaeoclimatology, Palaeoecology, 146 (1 – 4), 147 – 164. 10.1016/S0031-0182(98)00141-2.

Jafar, A.S., 1979: Taxonomy, stratigraphy and affinities of calcareous nannoplankton genus *Thoracosphaera* Kamptner. Proceeding IV, International Palynology Congress.

Jafar, A.S., 1983: Significance of Late Triassic calcareous nannoplankton from Austria and Southern Germany. Neues Jahrbuch für Geologie und Paläontologie, Abhandlungen, 166, 218 – 259.

Jain, S., 2020a: Calcareous Nannofossils. In: Fundamentals of Invertebrate Palaeontology. Springer Geology. Springer, New Delhi. 10.1007/978-81-322-3962-8_10.

Jain, S., 2020b: Dinoflagellates. In: Fundamentals of Invertebrate Palaeontology. Springer Geology. Springer, New Delhi. 10.1007/978-81-322-3962-8_4.

Jakob, I., Weggenmann, F., Posten, C., 2018: Cultivation of Emiliania huxleyi for cocclith production. Algal Research, 31, 47 – 59. 10.1016/j.algal.2018.01.013.

Janofske, D., 1987: Kalkige Nannofossillien aus der Ober-Trias (Rhät) der Nördlichen Kalkalpen. Berliner Geowissenschaftlichen Abhandlungen. 86, 45 – 67.

Janofske, D., 1990: Eine neue "Calcisphaere", *Carnicalyxia tabellata* n.g. n.sp. aus den Cassianer Schichten (Cordevol, unteres Karn) der Dolomiten. Berliner Geowissenschaftlichen Abhandlungen. 124, 259 – 269.

Janofske, D., 1992: Calcareous nannofossils of the Alpine Upper Triassic. In: Hamrsmid, B., Young, J.R., (Eds), Nannoplankton Research (Proceedings INA Conference). Knihovnicka ZPN, Hodonin, Cz. 87 – 109.

Janofske, D., Karwath, B., 2000: Oceanic calcareous dinoflagellates of the equatorial Atlantic Ocean: cyst-theca relationship, taxonomy and aspects on ecology. In: Karwath, B.,

Ecological studies on living and fossil calcareous dinoflagellates on the equatorial and tropical Atlantic Ocean. Berichte aus dem Fachbereich Geowissenschaften der Universität Bremen, 152, 94 – 136.

Kamptner, E., 1967: Kalkflagellaten-Skelettreste aus Tiefseeschlamm des Sfidatlantischen Ozeans. Annalen des Naturhistorischen Museums in Wien, 71, 117 – 198.

Kent, D.V., Olsen, P.E., Muttoni, G., 2017: Astrochronostratigraphic polarity time scale (APTS) for the Late Triassic and Early Jurassic from continental sediments and cor-relation with standard marine stages. Earth Science Reviews, 166, 153 – 180.

Kenter, J.A.M., Schlager, W., 2009: Slope angle and basin depth of the Triassic Platform-Basin transition at the Gosaukamm, Austria. Austrian Journal of Earth Science, 102, 15 – 22.

Keupp, H., 1981: Die kalkigen Dinoflagellaten-Zysten der borealen UnterKreide (Unter-Hauterivium bis Unter Albium). Facies, 5, 190.

Keupp, H., 1982: Die kalkigen Dinoflagellaten-Zysten des späten Apt und frühen Alb in Nordwestdeutschland. Geologisches Jahrbuch, 65, 307 – 363.

Keupp, H., 1992a: Calcareous dinoflagellate cysts from the Lower Cretaceous of Hole 761C, Wombat Plateau, eastern Indian Ocean. Proceedings of the Ocean Drilling Program, Scientific Results, 122, 497 – 509.

Keupp, H., 1992b: Die Flora kalkiger Dinoflagellaten-Zysten im mittleren Apt (Gargas) der Kernbohrung Himstedt 3 bei Hoheneggelsen/Niedersachsen. Berliner Geowissenschaftliche Abhandlungen, 3, 121 – 169.

Keupp, H., 1995a: Vertical distribution of calcareous dinoflagellate cysts of the Middle Aptian core section Hoheneggelsen KB 3 borehole, Lower Saxony, Germany. Neues Jahrbuch für Geologie und Paläontologie, Abhandlungen, 196 (2), 221 – 233.

Keupp, H., 1995b: Die kalkigen Dinoflagellaten-Zysten aus dem Ober-Albder Bohrung Kirchrode 1/91 (zentrales Niedersächsisches Becken, NW Deutschland). Berliner Geowissenschaftliche Abhandlungen, 16, 155 – 199.

Keupp, H., Mutterlose, J., 1984: Organismenverteilung in den D-Beds von Speeton (Unterkreide, England) unter besonderer Berück-sichtigung der kalkigen Dinoflagellaten-Zysten. Facies, 10, 153 – 178.

Keupp, H., Versteegh, G., 1989: Ein neues systematische Konzept für kalkige Dinoflagellaten-Zysten der Subfamilie Orthopithonelloideae Keupp 1987. Berliner Geowissenschaftliche Abhandlungen, 106, 207 – 219.

Knoll, A.H., 2003: Biomineralization and evolutionary history. In: Dove, P.M., De Yoreo, J.J., Weiner, S., (Eds.) Reviews in Mineralogy and Geochemistry. 329 – 356.

Kouchinsky, A., Bengtson, S., Runnegar, B., Skovsted, C., Steiner, M., Vendrasco, M., 2011: Chronology of early Cambrian biomineralization. Geological Magazin, 149 (2), 221 – 251. 10.1017/S0016756811000720.

Krystyn, L., 1980: Triassic conodont localities of the Salzkammergut region (Northern Calcareous Alps) – Abhandlungen der Geologischen Bundesanstalt. 35, 61 – 98.

Kucera, M., Morard R., 2019: Origin of planktonic foraminifera as a result of biotic recovery from thePermian-Triassic boundary crisis. Geophys Research Abstracts Vol. 21, EGU2019, 7619.

Lorenz, T., 1902: Geologische Studien im Grenzgebiet zwischen helvetischer und ostalpiner Fazies. II Dersüdliche Rhätikon, Berichte der Naturforschenden Gesellschaft zu Freiburg, 12, 35 – 95.

Love, G., Grosjean, E., Stalvies, C., Fike, D.A., Grotzinger, J.P., Bradley, A.S., Kelly, A.E., Bhatia, M., Meredith, W., Snape, C.E., Bowring, S.A., Condon, D.J., Summons, R.E., 2009: Fossil steroids record the appearance of Demospongiae during the Cryogenian period. Nature, 457, 718 – 721. 10.1038/nature07673.

Maloof, A.C., Rose, C.V., Beach, R., Samuels, B.M., Calmet, C.C., Erwin, D.H., Poirier, G:R., Yao, N., Simons, F.J., 2010a: Possible animals-body fossils in pre-Marinoan limestones from South Australia. Nature Geoscience, 3, 653 – 659. 10.1038/ngeo934.

Maloof, A.C., Porter, S.M., Moore, J.L., Dudás, F.Ö., Bowring, S.A., Higgins, J.A., Fike, D.A., Eddy, M.P., 2010b: The earliest Cambrian record of animals and ocean geochemical change. GSA Bulletin, 122 (11-12), 1731 – 1774. 10.1130/B30346.1.

Mandl, G. W., 2000: The alpine sector of the Tethyan shelf – Examples of Triassic to Jurassic sedimentation and deformation from the Northern Calcareous Alps. Mitteilungen der Österrike Geologie Gesellschaft, 92, 61 – 77.

Marshall, N., Lang, S., 2013: A New Sequence Stratigraphic Framework for the North West Shelf, Australia. In: Keep, M. and Moss, S.J. (Eds), The Sedimentary Basins of Western Australia 4: Proceedings of Petroleum Exploration Society of Australia Symposium. Petroleum Exploration Society of Australia, Perth. 1 – 32.

Martens, K., Schön, I., Meisch, C., Horne, D. J., 2008: Global diversity of ostracods (Ostracoda, Crustacea) in freshwater. Hydrobiologia, 595, 185 – 193. 10.1007%2Fs10750-007-9245-4.

Mattioli, E., Pittet, B., 2002: Contribution of calcareous nannoplankton to carbonate deposition: a new approach applied to the Lower Jurassic of central Italy. Marine Micropaleontology, 45, 175 – 190.

Monteiro, F.M., Bach, L.T., Brownlee, C., Bown, P., Rickaby, R.E.M., Poulton, A.J., Tyrrell, T., Beaufort, L., Dutkiewicz, S., Gibbs, S., Gutowska, M.A., Lee, R., Riebesell, U., Young, J., Ridgwell, A., 2016: Why marine phytoplankton calcify. Science Advances, 2 (7), 1501822. 10.1126/sciadv.1501822.

Morse, J.W., Mackensie, E.T., 1990: Geochemistry of Sedimentary Carbonates. Elsevier, Amsterdam, 707.

Moshkovitz, S., 1982: On the findings of a new calcareous nannofossil (*Conusphaera zlambachensis*) and other calcareous organisms in the Upper Triassic sediments of Austria. Eclogae Geologicae Helvetiae. 75, 611–619. 10.5169/seals-165245.

Nakov, T., Beaulieu, J.M., Alverson, A.J., 2018: Accelerated diversification is related to life history and locomotion in a hyperdiverse lineage of microbial eukaryotes (Diatoms, Bacillariophyta). New Phytologist, 219 (1), 462 – 473.

Ogg, J.G.,. 2012: Triassic. In: Gradstein, F. M., Ogg, J.G., Schmitz, M.D., Ogg, G.M. (Eds.), The Geologic Time Scale 2012, Amsterdam, Elsevier. 681 – 730. 10.1016/C2011-1-08249-8.

Ogg, J.G., Chen, Z.-Q., 2020: The Triassic Period. In: Gradstein, F. M., Ogg, J.G., Schmitz, M.D., Ogg, G.M. (Eds.), Geologic Time Scale 2020, Amsterdam, Elsevier. 903 – 953. 10.1016/B978-0-12-824360-2.00025-5.

Onoue, T., Yoshida, A., 2010: Depositional response to the Late Triassic ascent of calcareous plankton in pelagic mid-oceanic plate deposits of Japan. Journal of Asian Earth Sciences, 37, 312 – 321. 10.1016/j.jseaes.2009.08.013.

Oxford, M. J., Gregory, F. J., Hart, M. B., Henderson, A. S., Simmons, M. D., Watkinson, M. P., 2002: Jurassic planktonic foraminifera from the United Kingdom. Terra Nova, 14 (3), 205 – 209. 10.1046/j.1365-3121.2002.00410.x

Penny, A.M., Wood, R., Curtis, A., Bowyer, F., Tostevin, R., Hoffman, K.H., 2014: Ediacaran metazoan reefs from the Nama Group, Namibia. Science, 334 (6191), 1504 – 1506. 10.1126/science.1253393.

Pfiester, L. A., Anderson, D. M., 1987: Dinoflagellate reproduction. In: The biology of dinoflagellates (ed.) F. J. R., Taylor, Blackwell, Oxford, 611 – 648.

Pillevuit, A., 1993: Les blocs exotiques du Sultanats d'Oman. Mémoire de Géologie (Lausanne), 17, 249.

Porter, S. M., 2007: Seawater chemistry and early carbonate biomineralization. Science 316, 1302.

Porter, S., 2011: The rise of predators. Geology, 39 (6), 607 – 608. 10.1130/focus062011.1.

Preto, N., Kustatscher, E., Wignall, P.B., 2010: Triassic climates – State of the art and perspectives – Palaeogeography, Palaeoclimatology, Palaeoecology. 290, 1 – 10. 10.1016/j.palaeo.2010.03.015.

Preto, N., Rigo, M., Agnini, C., Bertinelli, A., Guaiumi, C., Borello, S., Westphal, H., 2012: Triassic and Jurassic calcareous nannofossils oft he Pizzo Mondello section: A SEM

study. Rivista Italiana di Paleontologia e Stratigrafia (Research in Paleontology and Stratigraphy). 118, 131 – 141. 10.13130/2039-4942/5994.

Preto, N., Agnini, C., Rigo, M., Sprovieri, M., Westphal, H., 2013a: The calcareous nannofossil Prinsiosphaera achieved rock-forming abundances in the latest Triassic of western Tethys: consequences for the $\delta^{13}C$ of bulk carbonate – Biogeosciences. 10, 6053 – 6068. 10.5194/bg-10-6053-2013.

Preto, N., Willems, H., Guaiumi, C., Westphal, H., 2013b: Onset of significant pelagic carbonate accumulation after the Carnian Pluvial Event (CPE) in the western Tethys – Facies. 59, 891 – 914. 10.1007/s10347-012-0338-9.

Prins, B., 1969: Evolution and stratigraphy of coccolothinids from the lower and middle lias. International Conference Planktonic Microfossils, Geneva. 2, 547 – 558.

Richoz, S., 2006: Stratigraphie et variations isotopiques du carbone dans le Permien supérieur et le Trias inférieur de quelques localités de la Néotéthys (Turquie, Oman et Iran). Mémoire de Géologie (Lausanne), 44, 1 – 251.

Richoz, R., Krystyn, L., Von Hillebrandt, A., Martindale, R., 2012: End-Triassic crisis events recorded in platform and basin of the Austrian Alps. The Triassic/Jurassic and Norian/Rhaetian GSSPs – *Journal of Alpine Geology*, 55, 321 – 374.

Richoz, S., Baud, A., Beauchamp, B., Grasby, S., Henderson, C., Krystyn, L., 2014: Khuff margin: slope to oceanic deposits (Permian-Triassic Allochthons and Exotics, Oman). In: The Khuff Formation. New perspective. (Poeppelreiter Ed.). EAGE Publications. Houten, The Nederlands, 55 – 76. ISBN 978-90-73834-42-2.

Richoz, S., Krystyn, L., 2015: The Upper Triassic events recorded in platform and basin of the Austrian Alps. The Triassic/Jurassic GSSP and Norian/Rhaetian GSSP candidate. Berichte der geologischen bundesanstalt, 111.

Ridgwell, A. J., Kennedy, M.J., Caldeira, K., 2003: Carbonate deposition, climate stability, Neoproterozoic ice ages, Science, 302, 859 – 862.

Ridgwell, A. J., 2005: A mid Mesozoic revolution in the regulation of ocean chemistry. Marine Geology, 217, 339 – 357.

Robinson, P.L., 1973: Paleoclimatology and continental drift. In: Tarling, D.H., Runcorn, S.K. (Eds.), Implications of continental drift to the Earth Sciences. Academic Press, London, 449 – 476.

Rost, B., Riebesell, U., 2004: Coccolithophores and the biological pump: responses to environmental changes. In: Thierstein, H. R., Young, J. R. (Eds.), Coccolithophores: from molecular processes to global impact, Berlin, Springer. 99 – 125. 10013/epic.21851.d001.

Roth, P.H., 1989: Ocean circulation and calcareous nannoplankton evolution during the Jurassic and Cretaceous. Palaeogeography, Palaeoclimatology, Palaeoecolohy, 74, 111 – 126.

Sarjeant, W.A.S., Lacalli, T., Gaines, G., 1987: The cysts and skeletal elements of dinoflagellates speculations on the ecological causes for their morphology and development. Micropaleontology, 33 (1), 1 – 36. 10.2307/1485525.

Schmitt, A.D., Chabaux, F., Stille, P., 2003: The calcium riverine and hydrothermal isotopic fluxes and the oceanic calcium mass balance. Earth and Planetary Science Letters, 281 (3-4), 169 – 187. 10.1016/S0012-821X(03)00341-8.

Scott, D.B., Medioli, F., Braund, R., 2003: Foraminifera from the Cambrian of Nova Scotia: The oldest multichambered foraminifera. Micropaleontology, 49 (2), 109 – 126. 10.2113/49.2.109.

Seghedi, A., 2001: The North Dobrogea orogenic belt (Romania): a review. In: Ziegler, P.A., Cavazza, W., Robertson, A.H.F., Crasquin-Soleau, S., (Eds.), Peri-Tethys Memoir 6: Peri-Tethyan Rift/Wrench Basins and Passive Margins. Paris: Mèmoire du Muséum National d'Histoire Naturelle, 237 – 257.

Sims, P. A., Mann, D. G., Medlin, L. K., 2006: Evolution of the diatoms: Insights from fossil, biological and molecular data. Phycologia, 45 (4), 361 – 402. 10.2216/05-22.1.

Sperling, E.A., Robinson, J.M., Pisani, D., Peterson, K.J., 2010: Where's the glass? biomarkers, molecular clocks, and microRNAs suggest a 200-Myr missing Precambrian fossil record of siliceous sponge spicules. Geobiology, 8, 24 – 36. 10.1111/j.1472-4669.2009.00225.x.

Stampfli, G.M., Borel, G.D., 2002: A plate tectonic model for the Paleozoic and Mesozoic constrained by dynamic plate boundaries and restored synthetic oceanic isochrones. Earth and Planetary Science Letters, 196 (1 – 2), 17 – 33. 10.1016/S0012-821X(01)00588-X.

Stanley, S.M., Hardie, L.A., 1998: Secular oscillations in the carbonate mineralogy of reef-building and sediment-prducing organisms driven by tectonically forced shifts in seawater chemistry. Palaeogeography, Palaeoclimatology, Palaeoecology, 144 (1 – 2), 3 – 19. 10.1016/S0031-0182(98)00109-6.

Stanley, S.M., 2006: Influence of seawater chemistry on biomineralization throughout Phanerozoic time: Paleontological and experimental evidence. Palaeogeography, Palaeoclimatology, Palaeoecology, 232, 214 – 236. 10.1016/j.palaeo.2005.12.010.

Stoecker, D. K., 2007: Mixotrophy among Dinoflagellates. The Journal of Eukaryotic Microbiology, 46 (4), 397 – 401. 10.1111/j.1550-7408.1999.tb04619.x.

Streng, M., Hildebrand-Habel, T., Willems, H., 2004: A proposed classification of archeopyle types in calcareous dinoflagellate cysts. Journal of Paleontology, 78 (3), 456 – 483.

Suan, G., Mattioli, E., Pittet, B., Maillot, S., Lecuyer, C., 2008: Evidence for major environmental perturbation prior to and during the Toarcian (Early Jurassic) oceanic anoxic event from the Lusitanian Basin Portugal. Paleoceanography, 23, PA1202. 10.1029/2007PA001459.

Suchéras-Marx, B., Mattioli, E., Allemand, P., Giraud, F., Pittet, B., Plancq, J., Escarguel, G., 2019: The colonization of the oceans by calcifying pelagic algae. Biogeosciences, 16, 2501 – 2510. 10.5194/bg-16-2501-2019.

Tangen, K., Brand, L.E., Blackwelder, P.L., Guillard, R.R.L., 1982: *Thoracosphaera heimii* (Lohman) Kamptner is a dinophyte: observations on its morphology and life cycle. Marine Micropaleontology, 7, 193 – 212.

Thierstein, H., R., 1976: Mesozoic calcareous nannoplankton biostratigraphy of marine sediments. Marine Micropaleontology, 1, 325 – 362. 10.1016/0377-8398(76)90015-3.

Tyrrell, T., Young, J.R., 2009: Coccolithophores. In: Steele, J.H., Turekian, K.K, Thorpe, S.A. (Eds). Encyclopedia of Ocean Sciences. Second Edition. Elsevier, 606 – 614.

Vink, A., Zonneveld, K.A.F., Willems, H., 2000: Distribution of calcareous dinoflagellate cysts in surface sediments of the western equatorial Atlantic Ocean, and their potential use in palaeoceanography. Marine Micropaleontology, 38 (2), 149 – 180. 10.1016/S0377-8398(99)00038-9.

Vink, A., Brune, A., Höll, C., Zonneveld, K.A.F., Willems, H., 2002: On the response of calcareous dinoflagellates to oligotrophy and stratification of the upper water coluön in the equatorial Atlantic Ocean. Palaeogeography, Palaeoclimatology, Palaeoecology, 178 (1 – 2), 53 – 66. 10.1016/S0031-0182(01)00368-6.

Vink, A., 2004: Calcareous dinoflagellate cysts in South and equatorial Atlantic surface sediments: diversity, distribution, ecology and potential for palaeoenvironmental reconstruction. Marine Micropaleontology, 50 (1 – 2), 43 – 88. 10.1016/S0377-8398(03)00067-7.

Wendler, I., Zonneveld, K.A.F., Willems, H., 2002: Production of calcareous dinoflagellate cysts in response to monsoon forcing off Somalia: a sediment trap study. Marine Micropaleontology, 46 (1 – 2), 1 – 11. 10.1016/S0377-8398(02)00049-X.

Willems, H., 1988: Kalkigen Dinoflagellaten-Zysten aus der oberkretazischen Schribkreide-Fazies N-Deutschlands (Coniac bis Maastricht). Senckenbergiana Lethaea, 68 (5 – 6), 433 – 477.

Willems, H., 1992: Kalk-Dinoflagellaten aus dem Unter-Maastricht der Insel Rügen. Zeitschrift für Geologische Wissenschaften, 20, 155 – 178.

Willems, H., 1996: Calcareous dinocysts from the Geulhemmerberg K/T boundary section (Limburg, SE Netherlands). Geologie en Mijnbouw, 75, 215 – 231.

Winter, A., Siesser, W.G., 1994: Coccolithophores. Cambridge, New York, NY: Cambridge University Press, First Edition. ISBN: 0-521-38050-2.

Wood, R., 2018: Exploring the drivers of early biomineralization. Emerging Topics in Life Sciences, 2 (2), 201 – 212. 10.1042/ETLS20170164.

Woodside Energy Ltd., 2007a: Well completion report Pluto-3 & ST1 Basic Data (WA-350-P, Carnarvon Basin). Unpublished report by Woodside Energy Ltd., publicly available from the NOPIMS website, www.nopims.ga.gov.au.

Woodside Energy Ltd., 2007b: Well completion report Pluto-4 Basic Data (WA-350-P, Carnarvon Basin). Unpublished report by Woodside Energy Ltd., publicly available from the NOPIMS website, www.nopims.ga.gov.au.

Young, J. R., Didymus, J. M., Bown, P. R., Prins, B., Mann, S., 1992: Crystal assembly and phylogenetic evolution in heterococcoliths. Nature, 356, 516 – 518.

Young, J. R., Bergen, J. A., Bown, P. R., Burnett, J. A., Fiorentino, A., Jordan, R. W., Kleijne, A., Van Niel, B.E., Romein, A. J. T., Von Salis, K., 1997: Guidelines for coccolith and calcareous nannofossils terminology. Palaeontology, 40, 875 – 912.

Young, J.R., Davis, S.A., Bown, P.R., Mann, S., 1999: Coccolith Ultrastructure and Biomineralisation. Journal of Structural Biology, 126, 195 – 215.

Young, J.R., Henriksen, K., 2003: Biomineralization within vesicles: the calcite of coccoliths. Reviews in Mineralogy and Geochemistry, 54, 189 – 215.

Zeebe, R.E., Westbroek, P., 2003: A simple model for the CaCO3 saturation stte of the ocean: The “Strangelove,” the “Neritan,” and the “Cretan” Ocean. Geochemistry, Geophysics, Geosystems, 4 (12), 1104. 10.1029/2003GC000538.

Ziegler, A.M., Eshet, G., McAllister Rees, P., Rothfus, T.A., Rowley, D.B., Sunderlin, D., 2003: Tracing the tropics across land and sea: Permian to present. Lethaia, 36, 227 – 254.

Zonneveld, K.A.F., Höll, C., Janofske, D., Karwath, B., Kerntopf, B., Rühlemann, C., Willems, H., 1999: Calcareous dinoflagellate cysts as palaeo-environmental tools. In: Fischer, G., Wefer, G. (Eds.), Use of Proxies in Paleoceanography: Examples from the South Atlantic. Springer, Berlin, 145 – 164.

Zonneveld, K.A.F., Brune, A., Willems, H., 2000: Spatial distribution of calcareous dinoflagellate cysts in surface sediments of the Atlantic Ocean between 13°N and 36°S. Review of Palaeobotany and Palynology, 111, 197 – 223.

Zügel, P., 1994: Verbreitung kalkiger Dinoflagellaten-Zysten im Cenoman/Turon von Westfrankreich und Norddeutschland. Courier Forschungsinstitut Senckenberg, 176, 1 – 159.

CHAPTER 2 - DEVELOPMENT OF EARLY CALCAREOUS NANNOPLANKTON IN THE LATE TRIASSIC (NORTHERN CALCAREOUS ALPS, AUSTRIA)

Isaline Demangel[1, 2], Zsófia Kovács[1, 2], Sylvain Richoz[1, 2], Silvia Gardin[3], Leopold Krystyn[4], Andre Baldermann[5], Werner E. Piller[1]

1 Institute of Earth Sciences, University of Graz, NAWI Graz Geocenter, Heinrichstrasse 26, 8010 Graz, Austria

2 Department of Geology, University of Lund, Sölvegatan 12, 22362 Lund, Sweden

3 Center for Research on Palaeobiodiversity and Palaeoenvironments, Sorbonne University, 4 place Jussieu (Case 104), 75252 Paris Cedex 05, France

4 Department of Palaeontology, University of Vienna, Althanstrasse 14, 1090 Vienna, Austria

5 Institute of Applied Geosciences, Graz University of Technology, NAWI Graz Geocenter, Rechbauerstrasse 12, 8010 Graz, Austria

Abstract

Calcareous nannofossils are considered to be the most productive calcifying organisms, but the impact of their emergence on the chemistry of the ocean in the Late Triassic is not understood yet. Evolutionary details of this bio-event are missing due to the scarcity of well-preserved outcrops worldwide. The current study focuses on the calcareous nannofossil assemblage of the middle Norian to lower Rhaetian at Sommeraukogel and Steinbergkogel in the Northern Calcareous Alps (Austria). The sediments were deposited on a topographic high on a deeper shelf at a palaeolatitude around 20–30°N. The steps in the emergence of pelagic calcifiers are documented by a scanning electron microscope (SEM) study. The First Occurrence (FO) of coccolith, not identified at a species level, was recorded in the middle Norian (Alaunian 3). The oldest *Crucirhabdus minutus* and *Archaeozygodiscus koessenensis* were observed in the late Norian (Sevatian) and were followed by the FO of *Crucirhabdus primulus* in the early Rhaetian. These observations suggest a rather slow temporal evolution of the first coccolithophorids, with millions of years from the ancestor *C. minutus* to *C. primulus*, and in between the evolution of the new genus *A. koessenensis*. Diagenetic overprinting of the sedimentary succession has affected the preservation degree of the calcareous nannofossils but

not the trend of their quantity in the studied samples, as proven by petrographic studies and trace element signatures of the calcareous sediments. This supports our quantitative estimates of the CaCO3 volume- and palaeo-fluxes due to the export productivity of the calcareous nannofossils, *Prinsiosphaera triassica*. Our results show the dominance and the increase in abundance of *Prinsiosphaera triassica* slightly above the Norian/Rhaetian boundary. However, calcareous nannofossils did not reach rock-forming abundances at this time and thus did not significantly influence the geochemical composition of the Western Tethys Ocean.

1. Introduction

The advent of biomineralization, and thus the ability to precipitate calcium carbonate (CaCO3) skeleton started in the Ediacaran (620 – 542 Ma) and progressed during the so-called "Cambrian Revolution", about 540 – 520 Ma ago (Wood et al., 2002). However, unfavourable environmental conditions, such as low nutrient levels in the photic zone, lower pH conditions and extensive carbonate mineral dissolution in the water column, has prevented the demonstration of significant planktonic calcification in the Paleozoic (Falkowski et al., 2004). It is only since the Late Triassic (237 – 201 Ma) that calcareous cysts, nannoliths and then coccoliths have started to contribute to the total calcium carbonate productivity in the surface oceans. After the Triassic/Jurassic mass extinction (~ 201 Ma), calcareous nannofossils have significantly contributed to the biogenic carbonate production in the oceans only since the Middle Jurassic (Suchéras-Marx et al., 2019). Since then, they are responsible for a huge accumulation of biogenic CaCO3 on the ocean floor. Now termed the mid-Mesozoic seawater revolution (Ridgwell, 2005), the initiation of the pelagic carbonate production has caused a major change in ocean chemistry. The latter is reflected by the shift from the "Neritan Ocean" of carbonate over-saturation and dominant biogenic shallow water CaCO3 production to the "Cretan Ocean", where large-scale biogenic-pelagic carbonate productivity led to lower saturation of the surface ocean with respect to CaCO3 and a stabilization of the deep-ocean alkalinity reservoir (Zeebe and Westbroek, 2003). The strong reinforcement of the biological pump and the step-wise establishment of a counter-pump (Rost and Riebesell, 2004), due to the calcifying plankton, enabled a higher regulation of the marine carbon cycle. The understanding of the driving factors causing this shift is of major importance to understand the biogeochemical evolution of the global ocean in the Mesozoic. However, until now comprehensive studies about the temporal evolution of calcareous nannofossils in the Late

Triassic are scarce and it remains questionable if and how their first occurrence has affected the biogeochemistry of the Cretan Ocean millions of years before the mid-Mesozoic seawater revolution.

Since the first discovery of calcareous nannoplankton, several studies have been carried out in older sedimentary records, e.g. in the Western Tethys Ocean (South Germany, Calcareous Alps in Italy and Austria), to pin point the First Occurrence (FO) of calcareous nannofossils in the Late Triassic (Gardin et al., 2012). Concerning coccolithophorids, Prins (1969) has described the first specimen of *Crucirhabdus primulus* from lower and middle Liassic sediments in England, France and Western Germany. Jafar (1983) has described the first *Crucirhabdus minutus* and recorded specimens of *C. primulus* from the base of the Rhaetian in the southern Bavarian (Germany). Later, Bown (1985) has reported the first *Archaeozygodiscus koessenensis* from the ammonite *Choristoceras marshi* Zone (upper Rhaetian) in the Weissloferbach section (Austria). Recently, Gardin et al. (2012) have reviewed all previously published reports on occurrences of coccolithophorids in the Late Triassic and re-assigned all of them to the Rhaetian. Their investigations in the Steinbergkogel section in the Northern Calcareous Alps (NCA) (Austria), a GSSP candidate for the Norian/Rhaetian boundary (Krystyn et al., 2007a, 2007b), reported by far the oldest occurrences of *C. minutus* and undetermined coccoliths. Gardin et al. (2012) have found specimens of *C. minutus* just above the Norian/Rhaetian boundary and undetermined coccoliths in uppermost Norian sediments. The semi-quantitative estimation of the calcareous nannoplankton content across the Late Triassic further revealed that only a few nannoliths and calcareous cysts appeared in the late Norian and a significant increase of *Prinsiosphaera triassica* occurred around the Norian/Rhaetian boundary (Gardin et al., 2012). Enhancing the global understanding of the nannofossils evolution in the Late Triassic, Preto et al. (2013a) presented a quantification of the main species, *Prinsiosphaera triassica*, in two Tethyan basins in Central and South Italy building 0 to 10% of the rock volume during the Norian, 20 to 40% in the middle Rhaetian and up to 60% in the late Rhaetian. Interestingly, coccolithophores have remained subordinate in the same timeframe.

To complement the existing view on the calcareous nannoplankton's early evolution and to understand better their importance on ocean chemistry, the occurrence of coccolithophorids was investigated by looking at middle Norian to lower Rhaetian sediments deposited on

topographic highs on a deeper shelf at Sommeraukogel and Steinbergkogel (NCA, Austria). In addition, this study presents quantitative estimates of the abundance and temporal evolution of calcareous nannofossils in the Steinbergkogel section. Furthermore, the potential impact of burial diagenesis is discussed regarding the presence and preservation degree of calcareous nannofossils. Finally, palaeo-fluxes of biogenic carbonate due to calcareous nannofossils productivity during the Late Triassic are presented and discussed in relation to long-term shifts in Cretan Ocean chemistry.

2. Geological settings

During the Late Triassic (237.0–201.3 Ma; Cohen et al., 2013), the NCA was located at the margin of the Western Tethys Ocean at palaeolatitudes around 20–30°N (Fig.2.1 a). The area was situated in the tropical climate zone with the maximum activity of the mega-monsoon system (Robinson, 1973; Preto et al., 2010) modulated by Milankovitch cycles (Ogg, 2012). During the Middle and Late Triassic, the NCA was a region characterized by the development of a large-scale carbonate platform system (Kenter and Schlager, 2009; Richoz and Krystyn, 2015), where predominantly carbonates were deposited with minor intercalated siliciclastic materials. Starting from the late Carnian (237–227 Ma), the widespread "Dachstein" carbonates have accumulated above siliciclastic deposits linked to the Carnian Humid Episode (e.g. Ruffell et al., 2015). The shelf area was composed of large lagoons and intra-platform basins extending toward the southeast with fringing reefs open to the open ocean (Fig.2.1 a, b). In the deeper-water offshore basin, pelagic limestones of the so-called Hallstatt facies developed (Richoz and Krystyn, 2015). The most recent study has proposed a palaeo-water depth for the Hallstatt depositional environment of at least 300 m, up to 500 m (Kenter and Schlager, 2009). Increased terrigenous input during the early Rhaetian has led to the demise of pelagic carbonate formation and hence resulted in the deposition of marly sediments of the Zlambach Formation, which accumulated on top of the Hallstatt Formation (Fig.2.1 b).

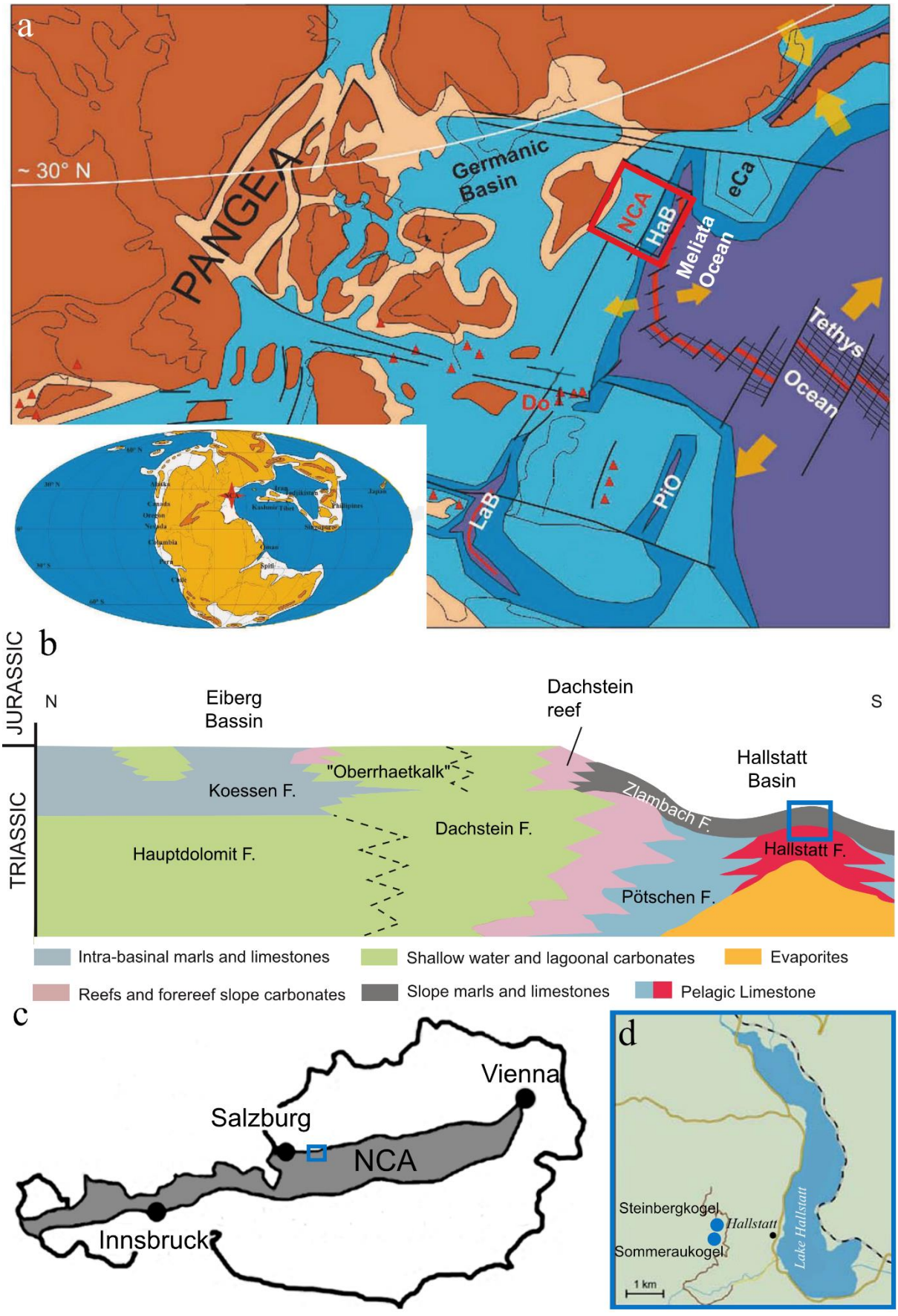
a
~ 30° N
PANGEA
Germanic Basin
NCA
HaB
eCa
Meliata Ocean
Tethys Ocean
Do
LaB
PiO
b
JURASSIC
TRIASSIC
N
S
Eiberg Bassin
Dachstein reef
Hallstatt Basin
"Oberrhaetkalk"
Koessen F.
Dachstein F.
Hauptdolomit F.
Zlambach F.
Hallstatt F.
Pötschen F.
Intra-basinal marls and limestones
Shallow water and lagoonal carbonates
Evaporites
Reefs and forereef slope carbonates
Slope marls and limestones
Pelagic Limestone
c
Vienna
Salzburg
NCA
Innsbruck
d
Steinbergkogel
Hallstatt
Sommeraukogel
Lake Hallstatt
1 km

Fig.2.1 – Geographic location and stratigraphy of the studied sections a) Global palaeogeographic reconstruction (insert) and regional palaeogeography of the Western Tethyan margin during the Late Triassic (reproduced from Hornung, 2007). The brown colour indicates the emerged land, the blue colour the shallow seas and the purple colour the deeper seas; the arrow indicates the rift opening and closing. NCA = Northern Calcareous Alps, eCA = east Carpathians, HaB = Hallstatt Basin, Do = Dolomites, PiO = Pinde Ocean, LaB = Lagonegro Basin. b) Schematic Triassic stratigraphy in the NCA, with locations of the topographic high within the mesopelagic Hallstatt and the terrigenous Zlambach formations at Sommeraukogel and Steinbergkogel sections (blue square)(modified after Kürschner et al., 2007). c) Distribution of the NCA within Austria and the location of the studied sections (blue square) (modified after Mandl, 2000). d) Map of the studied sections, Sommeraukogel and Steinbergkogel, near Hallstatt (Austria, modified after Gardin et al., 2012).

Due to the development of the Alpine fault belt in the Cretaceous, the Triassic successions are nowadays exposed within the central part of the Austrian NCA, a ~ 500 km long and ~ 20–50 km wide mountain range that is subdivided into three nappe complexes: Bajuvaric, Tirolic, and Juvavic (Mandl, 2000). The studied area belongs to the Juvavic nappe complex. The Hallstatt limestones and the marly sediments of the Zlambach Formation are well exposed at the Sommeraukogel section (47°33'44''N/13°37'36''E) and, ca. 300m northward, in an old quarry at Steinbergkogel (47°33'50''N/13°37'34''E) (Fig.2.1 c, d), at ca. 1245 m above sea level. Described in detail by Krystyn (1980), the Sommeraukogel section includes a 3.5 m thick late middle Norian (Halorites macer ammonoid Zone; Alaunian 3, age sub-division of the Austrian stratigraphic Chart; Piller et al., 2004), which consists of reddish limestone of Hallstatt Formation. The age is well established by the presence of the ammonoid Halorites macer as well as by the conodonts Epigondolella abneptis and E. vrielyncki (Fig.2.2). After an observation gap between the two sections, the proposed Norian/Rhaetian boundary is exposed at Steinbergkogel with sediments ranging from the upper Norian (Sevatian; ~ 209–204.5 Ma; Ogg, 2012) to the lower Rhaetian (Figs.2.1; 2.2). This well-studied profile (Krystyn, 1980; Krystyn et al., 2007a; Krystyn et al., 2007b; Krystyn, 2008; Hüsing et al., 2011; Gardin et al., 2012; Richoz et al., 2012; Richoz and Krystyn, 2015) is composed of four successive, well dated and overlapping sub-sections (Fig.2.2), which can be recognized in the beds' coding. The first sub-section, ST4, is composed of 21 m, mostly thick-bedded red limestones of the Hallstatt Formation extending from the Sevatian *E. bidentata* to the *E. bidentata – Misikella hernsteini* conodont Zone (Richoz and Krystyn, 2015). This facies is also exposed at the base of the overlapping sub-section STK A. From Bed 107 upward, the colour of the limestone changes to greyish, and contains a high bioclastic content until Bed 112 (Krystyn et al., 2007a,

2007b; Richoz and Krystyn, 2015). The base of Bed 111A records the FO of *Misikella posthernsteini* the proposed marker for the base of the Rhaetian. Most of sub-section STK A is overlapped by the sub-sections STK B and C. The sub-section STK B ends with occurrences of nodular limestones and marls, which mark the transition toward the greyish marls of the Zlambach Formation (Krystyn et al., 2007a).

The Hallstatt Formation is characterized by an abundant and very diverse invertebrate fauna, such as cephalopods (Mojsisovics, 1873–1902), bivalves (Kittl, 1912), gastropods (Koken, 1897) and braciopods (Bittner, 1890). A few exceptional occurrences of reef fossils have been recognized (Krystyn, 1980; Krystyn et al., 2007b; Richoz and Krystyn, 2015). The Hallstatt Formation also contains a diverse microfauna, including benthic foraminifers, sponge spicules, radiolarians, echinoderms, holothurian sclerites and conodonts (Mosher, 1968; Krystyn, 1980; Krystyn et al., 2007a, 2007b; Richoz and Krystyn, 2015). Conodonts and ammonoids biostratigraphy are cross-correlated with chemostratigraphy (δ13C isotopes) and magnetostratigraphy in order to establish time control and a high-resolution correlation between the different sub-sections (Fig.2.2) (Krystyn et al., 2007b, Hüsing et al., 2011). Normal marine salinity has prevailed during sediment deposition, as indicated by the continuous presence of stenohaline benthic organisms (echinoderms). The diverse benthic faunas and the high density of trace fossils indicate dominantly oxic conditions at the sea bottom throughout the accumulation of the successions (Richoz and Krystyn, 2015).

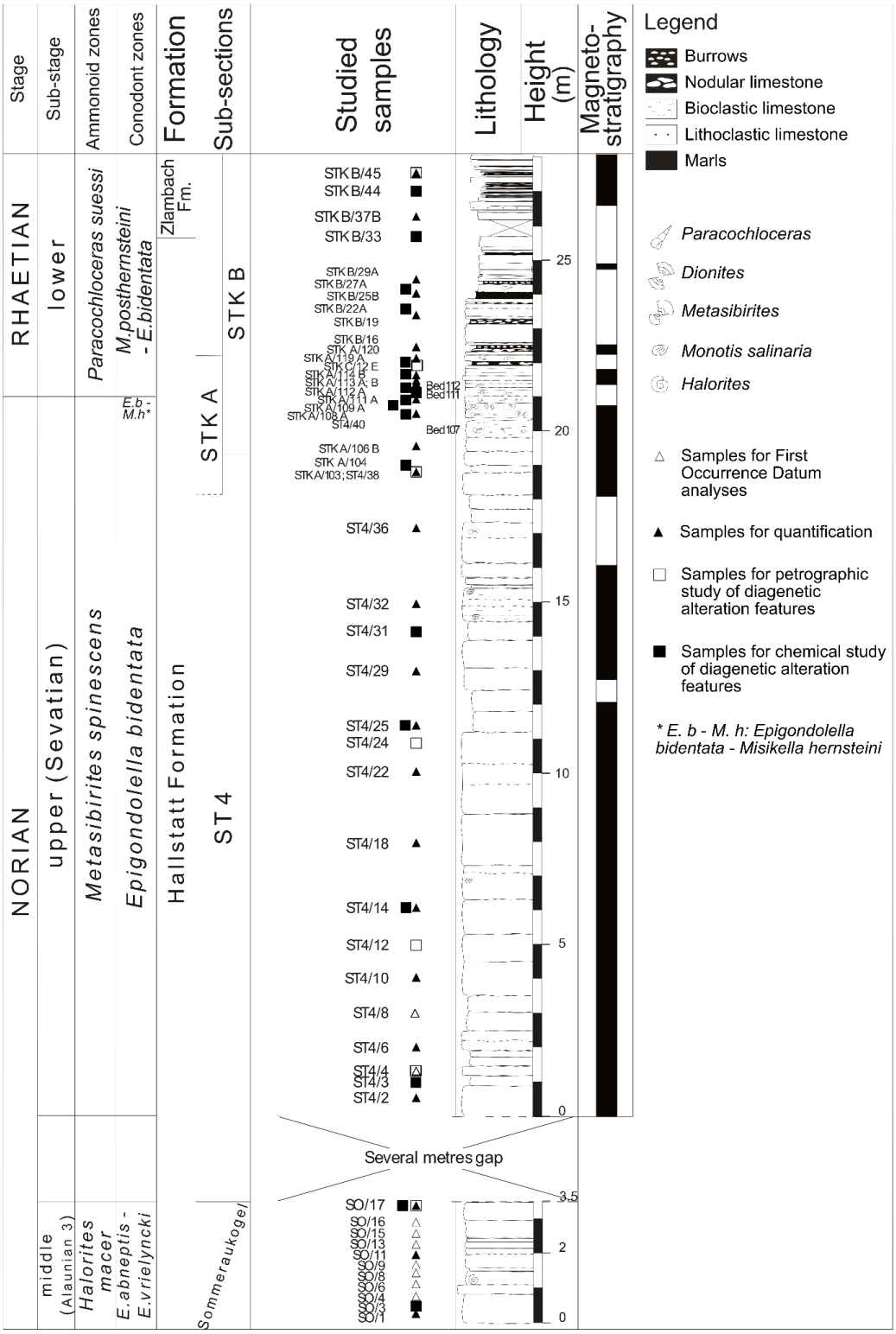

Fig.2.2 – Schematic lithological profile across the Hallstatt and Zlambach formations (middle Norian to lower Rhaetian), with conodont and ammonoid zones, and magnetostratigraphy. Lithological profile, age control and magnetostratigraphy are from Krystyn et al.

3. Material and method

3.1 *The study material*

A total of 62 samples were studied for calcareous nannofossils and their preservation. Calcareous nannofossil quantification was performed under the SEM on 27 samples (Fig.2.2, black triangles), with approximatively one sample every 1.5 m for Sommeraukogel, 2 m for ST 4, and 1 m for STK A and B. One sample from younger sediments (late Rhaetian, *Choristoceras marshi* Zone) exposed at the Eiberg section (NCA, Richoz et al., 2012) was also quantified to verify the robustness of our method regarding the point counting method used by Preto et al. (2013a). In addition to these samples taken for quantification, we increased the resolution in the middle and upper Norian (Sommeraukogel and ST4 sections) to constrain the FO of the coccolithophorids. 9 supplementary samples from Sommeraukogel and 2 from ST4 were observed under the SEM, but not quantified (Fig.2.2, open and black triangles). In addition, the effect of early diagenesis, such as dissolution and recrystallization of biogenic and abiogenic carbonates, on the preservation degree and abundance of calcareous nannofossils was investigated by a petrographic study conducted on a third set of 7 samples (Fig.2.2, open squares) and by a chemical study carried out on a set of 18 samples (Fig.2.2, black squares).

3.2 *Sample preparation, SEM study and quantification of nannofossil content*

To study the calcareous nannofossil content, SEM analyses were performed on solid rocks instead of the widely used smear and settling slide technique (e.g. Bown, 1998). Indeed, no calcareous nannofossils were found during smear slide observations carried out in an early phase of this study on both optical microscope and SEM. This is most likely attributable to the high degree of cementation of the limestone matrix embedding the nannofossils and preventing their extraction without breaking them down. The sample preparation, as described by Preto et al. (2013a, b), has been followed with slight modifications regarding the facies type and sample properties. Specifically, after an initial SEM inspection and qualitative evaluation of the nannofossil content of some fragments of rock samples with a Hitachi Tabletop Microscope TM3000 (Sorbonne University, UMP CNRS 7207 CR2P, Paris, France), the samples were cut in blocks with a surface of ~1 cm^2. The surfaces were polished with HV 600 and 1200 diamonds discs using deionized water. Afterwards, the blocks were etched for 15 seconds in 0.1 % HCl

solution and cleaned with distilled water in an ultrasonic bath for 7 seconds. The samples were dried overnight at 50 °C and finally coated with a 1 nm thin layer of platinum/palladium using a Cressington Sputter Coater 208HR.

The quantitative estimation of the calcareous nannofossil content was done with a TESCAN MIRA 3 electron microscope at Lund University. This SEM is equipped with an energy dispersive X-ray spectroscopy (EDS) detection system and a back-scattered electron (BSE) detector for chemical and compositional analysis of the samples. To reduce the effect of sample heterogeneity, surfaces perpendicular to the bedding plane were investigated (Chayes, 1954). Additionally, to verify the nannofossils content homogeneity on the sample surface, we analysed five transects of 1 cm length on one sample and two transects on five samples, all randomly selected. These investigations do not show any differences, proving the homogeneity of the materials. The repeatability and the potential error during counting were tested with two persons counting the same transect. Samples recounted by two persons shown only insignificant variation of one specimen. In each transect, only complete individuals of *P. triassica* were counted. The area of the SEM frame (21.9 x 21.9 µm) was chosen to cover an area larger than the biggest known calcareous nannofossils, i.e. *P. triassica* of ~11 µm. The absolute number of calcareous nannofossils per cm² was calculated using a slightly modified equation of Bordiga et al. (2015):

$$x = (N \times A) \div (f \times n) \qquad \text{(equation 1)}$$

where x is the absolute number of calcareous nannofossils per cm² of sediment, N denotes the total number of individuals counted, A is the area of the block (1 cm²), f is the area of one SEM frame in cm² (4.7961E^{-06}) and n refers to the number of frames analysed.

The carbonate flux linked to Late Triassic biogenic $CaCO_3$ production was calculated based on the absolute abundance of the dominant species, i.e. *P. triassica*. Due to the specific sample preparation applied in this study, i.e. using solid pieces of bulk rock, the total carbonate flux based on *P. triassica* cannot be calculated based on grams of powder, as described in several coccolith carbonate flux studies (e.g., Young and Ziveri, 2000; Bornemann et al., 2003; Erba and Tremolada, 2004; Suchéras-Marx et al., 2014). Therefore, the carbonate palaeo-flux (given in g *P. triassica* $CaCO_3$ cm^{-3} My^{-1}) linked to the main calcareous nannofossil was calculated using the following equation 2:

$$\text{Carbonate palaeo-flux} = M_{P.\ triassica} \times \text{sedimentation rate} \qquad \text{(equation 2)}$$

The sedimentation rate of the studied sections has been estimated ~5 m/Myr. Schlager (1969) has estimated a sedimentation rate of 3 m/Myr for the condensed limestones of the Hallstatt Formation, which seems to be appropriate for the condensed limestones of the Sommeraukogel section, but too less for Steinbergkogel. The estimation by Hüsing et al. (2011) of a 2 Myr duration for the uncondensed section ST4 would imply a sedimentation rate of 10 m/Myr. Ogg (2012), however, has proposed a longer duration for the Sevatian of 4.5 Myr, resulting in a sedimentation rate of ~5 m/Myr for section ST 4. Considering the median value (5 m/Myr) of those three estimates, we assume a similar sedimentation rate for the overlaying and microfacially corresponding quarry sections STK A, B and C than for ST4. However, in order to take into consideration the possible variations in sedimentation rate throughout the sections, the carbonate fluxes have been calculated applying the median values as well as the minimum (Schlager, 1969) and maximum sedimentation rate values (Hüsing et al., 2011). $M_{P.\ triassica}$ corresponds to the total mass of *P. triassica* (g $CaCO_3$) per cm^3 of a sample, as calculated following equation 3:

$$M_{P.\ triassica} = V_{P.\ triassica} \times \rho_{\text{calcite}} \qquad \text{(equation 3)}$$

$V_{P.\ triassica}$ represents the total volume of *P. triassica* in one cm^3 of a sample. The density of the calcite skeleton was assumed to be 2.7 g/cm^3 considering that *P. triassica* specimens consist of pure calcite, as confirmed by surface composition analyses of such species (Young and Ziveri, 2000). The total volume of *P. triassica* was obtained using equation 4:

$$V_{P.\ triassica} = \frac{4}{3\pi r^3} \times X \qquad \text{(equation 4)}$$

where r is the mean radius of *P. triassica* and X represents the total number of *P. triassica* in 1 cm^3 of a sample. X is obtained by converting the absolute abundance of *P. triassica* in cm^2 (x) into a volume fraction in cm^3. x, as calculated with equation 1, presents the abundance of *P. triassica* in an area of 1 cm^2 having, however, a volumetric dimension equal to the mean diameter of *P. triassica* in each sample. Therefore, X was calculated with the following equation:

$$X = \frac{x \times 1}{mean\emptyset} \qquad \text{(equation 5)}$$

The diameter (Ø) of *P. triassica* was obtained by length measurements (in replicates) on specimens showing distinct edges and clear half spheres. Note that the use of the mean diameter in equation 5 introduces a minor inaccuracy. Consequently, the standard error of the mean was computed and integrated into the error bars (1 σ) of the carbonate flux, ranging from 0.09 to 0.69.

Finally, the percentage of *P. triassica* at Steinbergkogel was computed following the equation 6 in order to ensure direct comparison with the study of Late Triassic Italian sections by Preto et al. (2013a):

$$\%\ P.triassica\ in\ the\ rock = \frac{VP.triassica \times 100}{mean\emptyset} \quad \text{(equation 6)}$$

3.3 *Geochemical analyses*

In order to investigate the impact of diagenesis on the preservation state of nannofossils, inductively coupled plasma atomic emission spectrometry (ICP-OES) analyses were conducted at the Institute of Applied Geosciences, Graz University of Technology (Austria). Indeed, changes in the concentration of critical trace elements (Na, Sr, Fe, Mn, etc.) can help to constrain the post-depositional alteration degree (Brand and Veizer, 1980). Acid digestion of the carbonate fraction (including dolomite) was carried out by reacting 0.050 g of the powdered sample with 5 drops of 6 % HNO_3 of suprapure grade and 50 mL of 2 % HNO_3 for 12 h at 80 °C. Afterwards, the acid-soluble fraction was separated by filtration through a 0.45 µm cellulose acetate membrane. Analyses were carried out on a Perkin Elmer OPTIMA 8300 to obtain the total aqueous concentration of major, minor and trace elements (Al, Ba, Ca, Cd, Co, Cr, Cu, Fe, K, Li, Mg, Mn, Na, Ni, Si, Sr, Zn) in each sample. The analytical precision (2 σ, 3 replicates) is better than ± 3 % for all elements, as determined by replicate analyses of NIST 1640a and SPS-SW2 Batch 130 standards (Baldermann et al., 2018 a, b).

4. Results

4.1 *The Late Triassic calcareous nannofossils record*

The calcareous nannofossils were identified following the criteria described in the taxonomic index in the supplementary material. The assemblage observed at Steinbergkogel is

comparable with other Triassic assemblages worldwide. It is composed of three coccolith species: *Archaeozygodiscus koessenensis, Crucirhabdus minutus* and *C. primulus* (Fig.2.3) three nannolith species: the incertae sedis *P. triassica* (Fig.2.4), *Eoconusphaera hallstattensis* (Fig.2.5) and, more rarely, *Carnicalyxia tabellata. Cassianospica curvata*, which is reported from other alpine locations (Janofske, 1990; Janofske, 1992; Gardin et al., 2012), was not observed in the studied samples. Calcareous (dino-)cysts are present in the studied samples, including *Thoracosphaera* specimens (*sensu* Jafar, 1983), *Obliquipithonella rhombica* and *Orthopithonella geometrica* (Fig.2.5). In addition, some undetermined calcispheres have been observed (Fig.2.6).

In general, during the Late Triassic, coccolithophorids increase slightly in abundance, starting in the middle Norian (Alaunian 3; sample SO/15). From the middle to upper Norian, they are present with only one specimen per investigated transect, but are not observed in every sample (Fig.2.7). The abundance of coccolithophorids increases slightly from the lower Rhaetian (around STK B/16), where they are present in most samples, reaching 2 – 3 specimens per transect (1 cm). Although the form observed in the middle Norian (SO/15) could not be identified at the species level it represents the oldest coccolith found so far (Fig.2.3 A). In the upper Norian (Sevatian; ST4/2), a well-preserved rim of *C. minutus* has been observed, representing the oldest *C. minutus* ever identified (Fig.2.3 B; Fig.2.7). *A. koessenensis* has been identified also in the upper Norian (ST4/6; Fig.2.3 C; Fig.2.7). Finally, only one specimen of *C. primulus* was observed in the lower Rhaetian (STK C/12E; Fig.2.3 D; Fig.2.7).

From the middle Norian to the lower Rhaetian, the observed coccoliths species do not vary in size. The nine measured specimens of *A. koessenensis* have a length between 2.00 and 2.80 μm, a width between 1.20 and 2.00 μm and a mean size of 2.35 x 1.53 μm (long times short axis). The five measured specimens of *C. minutus* have a mean size of 2.08 × 1.44 μm, with a length between 1.71 and 2.27 μm and a width between 1.18 and 1.61 μm. The single *C. primulus* specimen observed displays a length of 3.11 μm and a width of 2.13 μm. The preservation state of those coccolithophorids varies from good preservation of all elements composing the rim and the central area (Fig.2.3 E) to a comparably poor preservation degree with the only conservation of the rim without recognition of the elements (Fig.2.3 A).

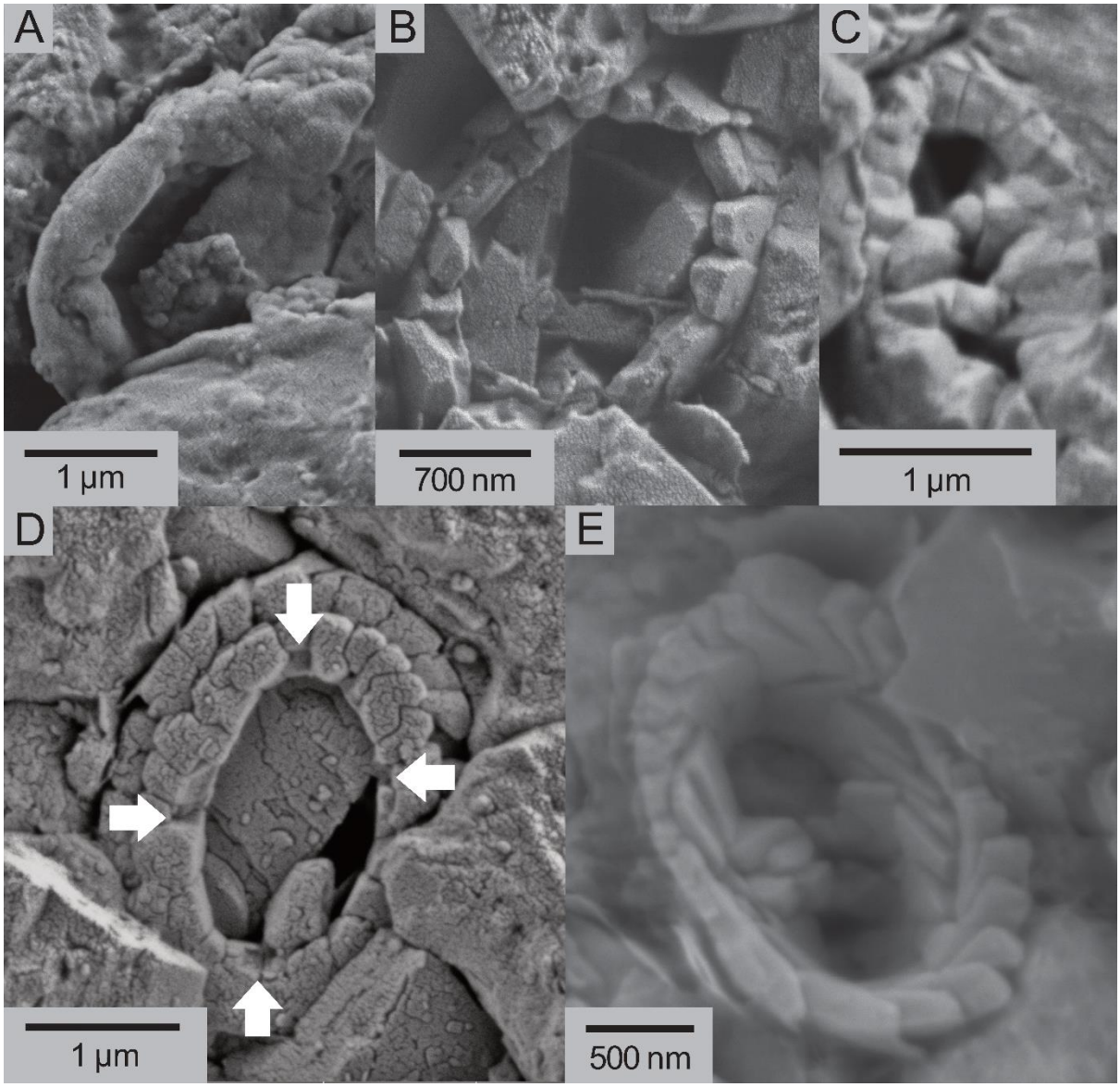

Fig.2.3 – SEM images showing the different coccolith species, the oldest specimens and the two preservation states observed at Steinbergkogel sections. A- Oldest, undetermined,coccolith (poorly preserved) from the middle Norian (sample SO/15); B- Distal view of the oldest *C. minutus* with a loxolith rim from the upper Norian (ST4/2); C- Proximal view of a well preserved *A. koessenensis* from the upper Norian (ST4/6); D - Proximal view of *C. primulus* from the lower Rhaetian (STK C/12E) with the anchor points shown with arrows; E- Well preserved *A. koessenensis* in distal view with the middle bar visible from the lower Rhaetian (STK B/37B).

Prinsiosphaera triassica is present in every sample from the middle Norian (Alaunian 3) to the lower Rhaetian (*P. suessi* Zone). These specimens exhibit a broad size range, from 4.93 to 12.92 µm (Fig.2.7). Forms of this taxon have been observed either broken with the inner part visible (Fig.2.4 A, B) or intact with the outer layer visible (Fig.2.4 C). The inner part, if well preserved, is composed of randomly oriented, well-defined groups of parallel, thin tabular,

rhombohedral calcite crystals (Fig.2.4 A). However, if the preservation is not good, the pristine structure is replaced by blocky calcite crystals (Fig.2.4 B). In case of poor preservation of the outer layer, this is also composed of blocky tabular calcite crystals parallel arranged (Fig.2.4 C).

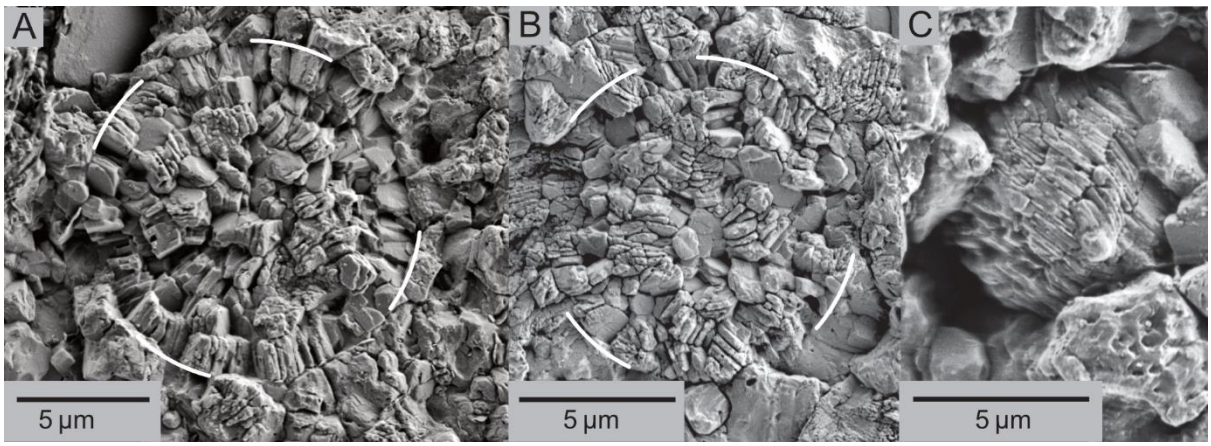

Fig.2.4 – SEM pictures representing A- Large *P. triassica*, well preserved (stage 3 in Bralower et al., 1991) with the inner part of the sphere visible and being composed of groups of parallel, thin tabular, rhombohedral calcite crystals randomly oriented (middle Norian; SO/11). B- *P. triassica*, poorly preserved (stage 4) compared to the specimen in A, only the inner part of the sphere is visible and is composed of blocky calcite crystals (lower Rhaetian; STK B/29 A). C- Outer layer of a complete *P. triassica*, poorly preserved (stage 4) and being composed of groups of parallel, thin tabular calcite crystals (upper Norian; ST4/25).

Eoconusphaera hallstattensis displays low abundances, with 2-3 specimens per transect (1 cm). The first occurrence is slightly before the onset of the Zlambach Formation in the lower Rhaetian (STK A/119 A) (Fig.2.5 A; 2.7). Most of the specimens were observed from the extremity of the truncated cone shape, only one specimen was observed in the side view with the inner part visible. The several extremities of specimens observed did not vary in appearance and size. They are characterized by an oval shape with a thick outer wall of vertical calcite lamellae enclosing the inner structure composed of radially arranged, vertical and elongated calcite lamellae. The long-axis oval-shape extremity ranges between 2.25 and 2.94 µm and between 1.57 and 1.96 µm for the short axes. The specimen observed in longitudinal view measured 2.30 µm in width and 4.00 µm in length.

The calcareous cysts specimens were observed in 10 samples (on 26). *Orthopithonella geometrica* (Fig.2.5 B) and *Thoracosphaera* (*sensu* Jafar, 1983; Fig.2.5 C) are rare with 1-2 specimens per transect (1 cm) from the middle to upper Norian but increase in abundance in

the lower Rhaetian, with 2-5 specimens per transect (1 cm). *Obliquipithonella rhombica* (Fig.2.5 D) is present in low abundance (1 specimen per transect) only in the lower Rhaetian. Concerning the size variation, *Orthopithonella geometrica* ranges between 8.10 and 10.00 µm and *Thoracosphaera* between 5.39 and 11.15 µm. In the case of *Obliquipithonella rhombica* only parts of the spheres were visible making the measurements of the complete diameter impossible.

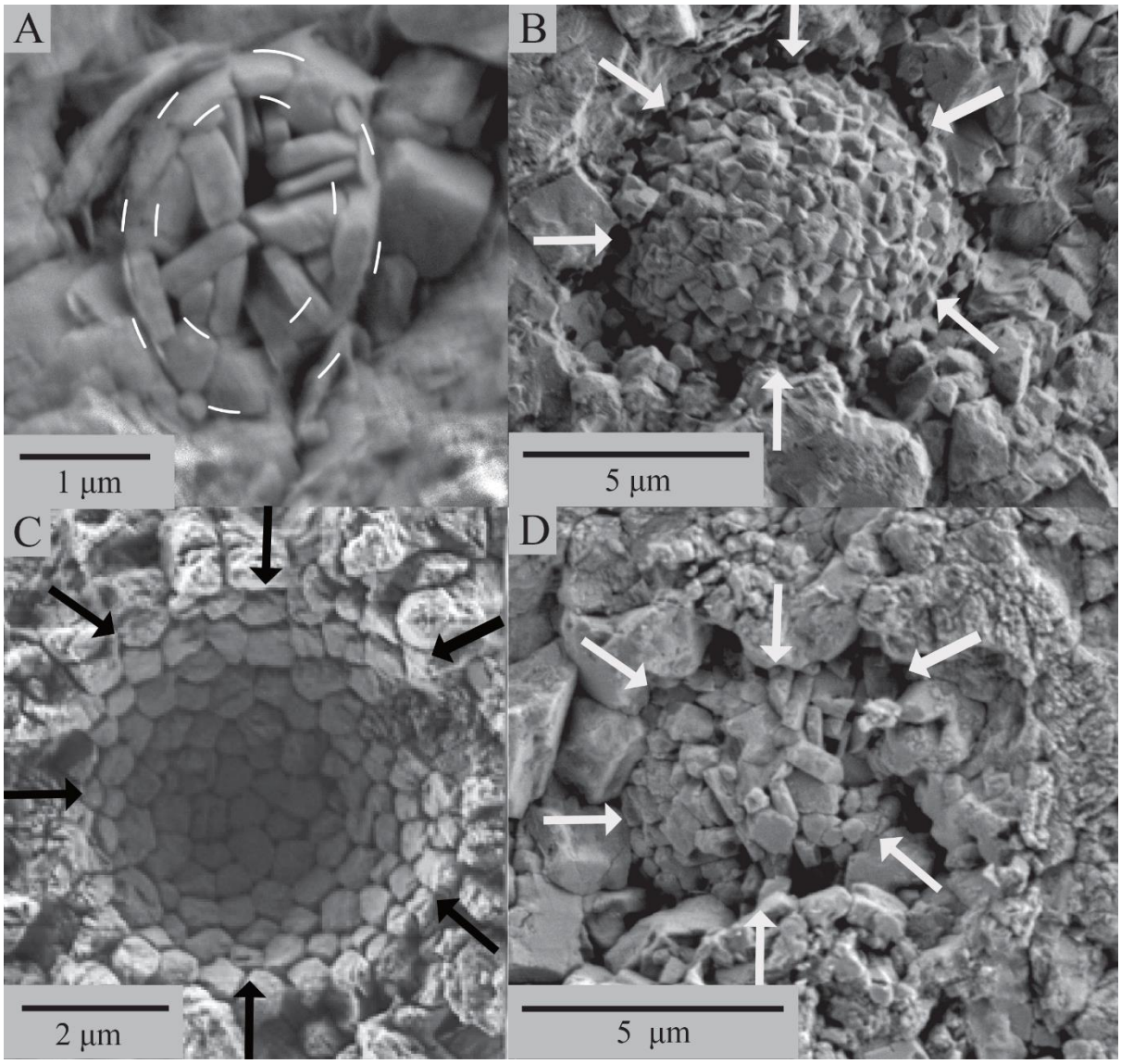

Fig.2.5 – SEM images displaying calcareous cysts and nannoliths of Steinbergkogel. A- Extremity view of *E. hallstattensis*, lower Rhaetian (STK B/37B); B- Calcite crystals arranged perpendicular to the outer wall of *Orthopithonella geometrica*, upper Norian (ST4/6); C- Bowl shaped *Thoracosphaera* (sensu Jafar, 1983), lower Rhaetian (STK A/119A); D- Calcite crystals randomly arranged, obliquely to the outer wall of *Obliquipithonella rhombica*, lower Rhaetian (STK B/25B).

The nannofossil assemblage also comprises some undetermined rounded calcareous structures (Fig.2.6 A – E) and calcispheres (Fig.2.6 F) . They were observed in low abundances throughout all studied sections, with 1-3 specimens per transect (1 cm). Calcispheres are more or less well preserved, with diameters ranging between 4.32 and 9.20 μm (Fig.2.6 F). The rounded calcareous structures (Fig.2.6 A – E) are composed of radially arranged, elongated calcite crystals. The centre of these spheres is either completely filled with blocky calcite crystals (Fig.2.6 B, C, D) or displays a small void (Fig.2.6 A, E). They range from 8.00 to 17.43 μm in size. EDS analyses revealed that these specimens consist mainly of Ca, O and C, indicating a calcitic composition. These structures are often observed in the middle to late Norian but rarely in the early Rhaetian.

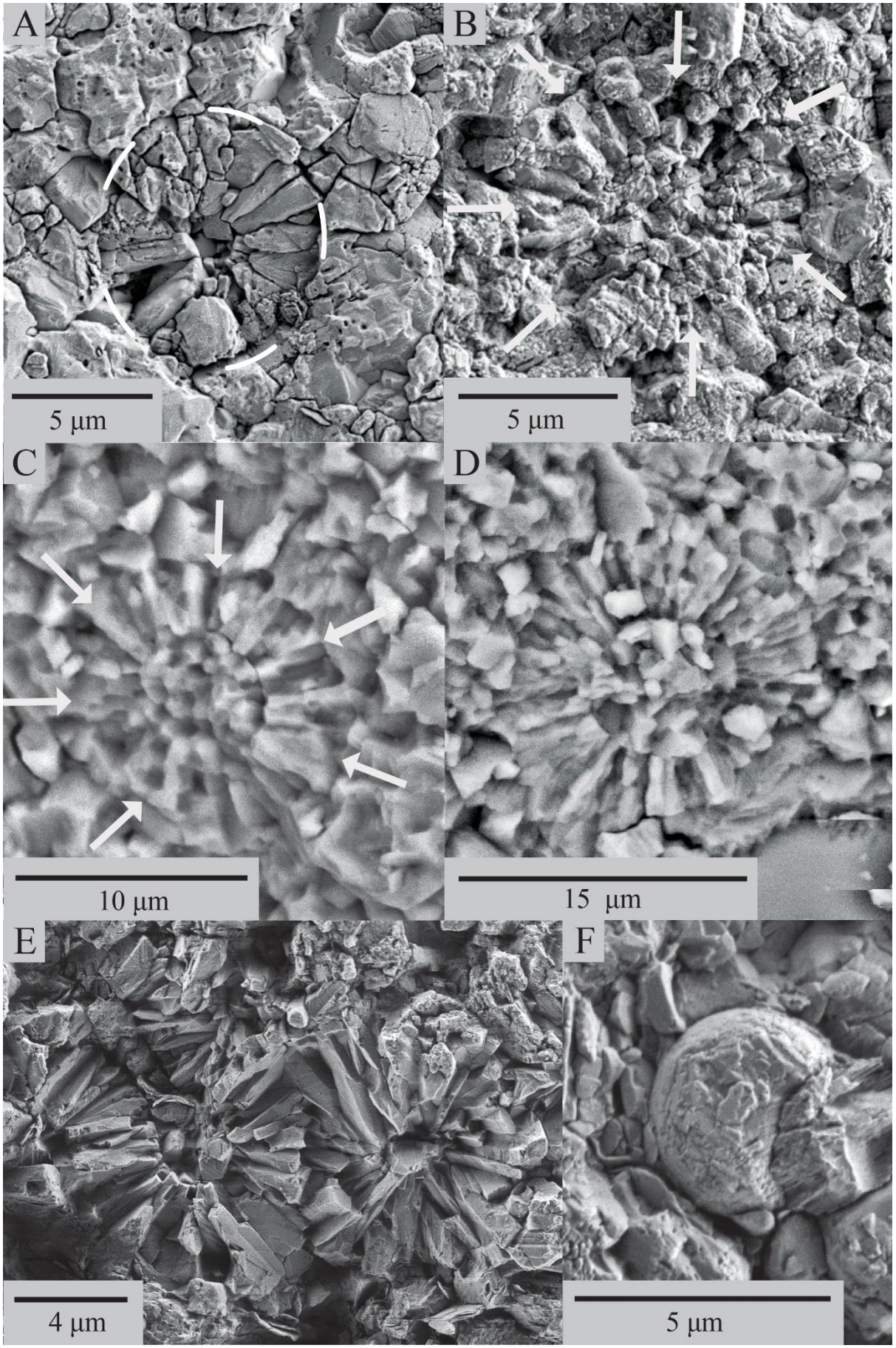
A
5 μm
B
5 μm
C
10 μm
D
15 μm
E
4 μm
F
5 μm

Fig.2.6 – SEM images of calcisphere-like structures with radially elongated calcite crystals; middle and upper Norian; samples: A) ST4/25, B) ST4/29, C) and D) SO/17, E) ST4/6; F) Calcisphere; lower Rhaetian (P. suessi Zone); at STK B/45.

4.2 *Prinsiosphaera triassica – abundance and carbonate flux*

The incertae sedis *P. triassica* is by far the most abundant calcareous nannofossil in the studied sections and in Upper Triassic sediments in general (Gardin et al., 2012; Preto et al., 2013a). This species clearly dominates the assemblage with a relative abundance > 87 % in all our samples, except for ST4/2 (50 %). The carbonate flux attributed to the absolute abundance of *P. triassica* shows a general increase around the Norian/Rhaetian boundary, from 0.2 to 56 g N_{CaCO_3} cm^{-3} Myr^{-1}, followed by a slightly decreasing trend toward the Zlambach Formation (Fig. 2.7). During the middle and late Norian (Sommeraukogel and ST4), the carbonate flux is low, i.e. below 10 g N_{CaCO_3} cm^{-3} Myr^{-1}, except for the samples SO/11, ST4/6 and ST4/36, which have values between 20 – 31 g N_{CaCO_3} cm^{-3} Myr^{-1}. In the uppermost Norian (STK A), the carbonate flux is fluctuating from 0.2 to 26 g N_{CaCO_3} cm^{-3} Myr^{-1}. This interval is followed by an increasing trend, reaching a maximum of 56 g N_{CaCO_3} cm^{-3} Myr^{-1} just above the Norian/Rhaetian boundary (STK B/16). Upward, a slight decrease in the carbonate flux is recorded toward the top of the section, with values ranging between 23 and 39 g N_{CaCO_3} cm^{-3} Myr^{-1}.

The absolute abundance of *P. triassica* (supplementary material Table S1) varies between 397 and 148,094 specimens per cm^2. From the middle Norian (Sommeraukogel) to the lowest Rhaetian (top of STK A) the absolute abundances are relatively stable below 20,000 specimens per cm^2, except for samples SO/11, ST4/6, and ST4/36, which show increasing values between 30,000 and 53,000 specimens per cm^2. Around the Norian/Rhaetian boundary, the absolute abundance values of *P. triassica* also scatter before increasing in the earliest Rhaetian, reaching a maximum of 148,094 specimens per cm^2, which is about 14 times higher than at the top of STK A. In the Zlambach Formation, the *P. triassica* absolute abundances show a gradual decrease with values between 50,000 and 110,000 specimens per cm^2. The average diameter of *P. triassica* does not vary significantly throughout the investigated sections, i.e. 8 ± 2 µm (Fig.2.7).

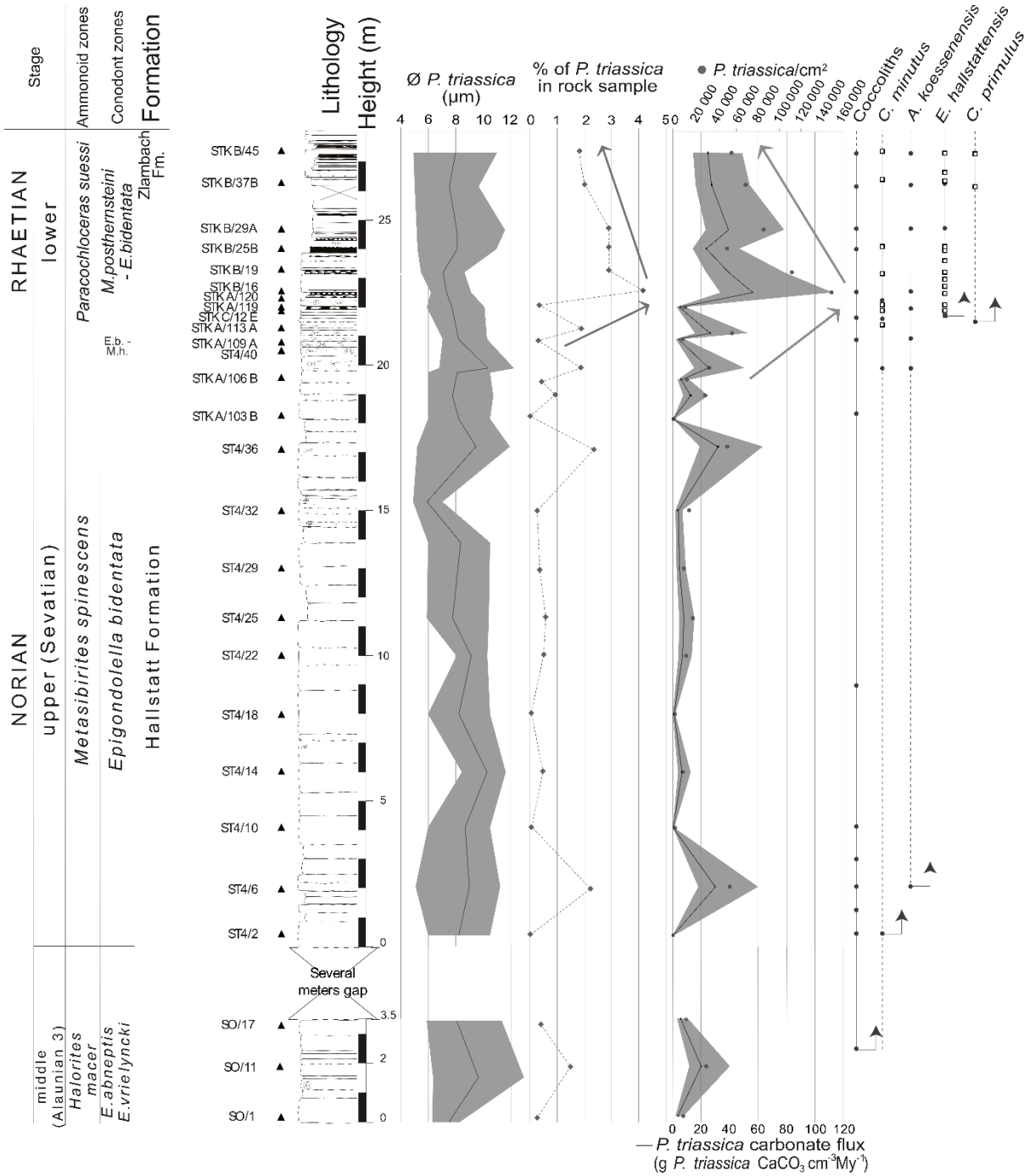

Fig.2.7 – Abundance of *P. triassica* across the Upper Triassic from Sommeraukogel and Steinbergkogel sections. Mean (black line) $CaCO_3$ palaeo-fluxes (g N_{CaCO3} cm^{-3} Myr^{-1}) were calculated assuming a sedimentation rate of 5 m/Myr, the grey area represent minimum (3m/Myr; Schlager, 1969) and maximum (10m/Myr; Hüsing et al., 2011) estimations of the sedimentation rate. The error bars link to the $CaCO_3$ fluxes and absolute abundance of *P. triassica* per cm^2 (black dots) are shown together with the percentages and the diameter (µm) of *P. triassica* in the sediment (black line corresponds to the mean diameter; the grey area indicates minimum and maximum sizes). On the right side, the arrows indicate the sample where the different species first occur, the black dots denote the

observed specimen(s) from this study, while the black squares those from Gardin et al. (2012). The dashed lines highlight the potential presence of specimens (from FO until the top of the section) and the solid lines show the continuous proof of specimens across the profile. Lithological profile and age control are from Krystyn et al. (2007b) for Steinbergkogel and from this study for Sommeraukogel. For abbreviations and credits see Fig. 2.2.

4.3 *Diagenetic alteration*

4.3.1 Petrographic observations

The carbonate matrix (i.e. micrite) of ten samples from different sections was studied with SEM to determine diagenetic alteration patterns (e.g., dissolution or overgrowth patterns of calcite) (Fig.2.8). On the micro-scale, the studied limestone samples are compact with low interstitial porosity. Some clay lenses are present and traces of star-shaped goethite or hematite crystals are visible. The only biogenic elements recognized are calcareous nannofossils. Besides these original signatures, the samples show signs of dissolution, including dissolution pits, micro-cracks, rough calcite surfaces with rounded edges, as well as recrystallization patterns, such as the transition of micrite to (poikilotopic) calcite spar and calcite step growth (Fig.2.8 C, D). The lower part of the section (SO/17, ST4/2, 4, 6 and 10) and the sample ST4/24 are dominated by dissolution features. From sample ST4/12 upward, the samples are dominated by overgrowth patterns of calcite, although dissolution features are still present. This implies very minor modifications of the pristine marine deposits during early diagenesis.

Three samples (ST4/2, 6 and 10), with high (52,718 *P. triassica*/cm^2) to very low (415 and 1 245 *P. triassica*/cm^2) nannofossil abundance, have been scrutinized in more detail. They all show the same degree of dissolution and the absence of overgrowth structures. Therefore, diagenesis-induced dissolution and partial recrystallization of the micrite matrix likely have had an influence on the preservation degree of calcareous nannofossils, as indicated before, but this effect seems to be insignificant on the trend of their quantified abundance (Fig.2.8 A, B).

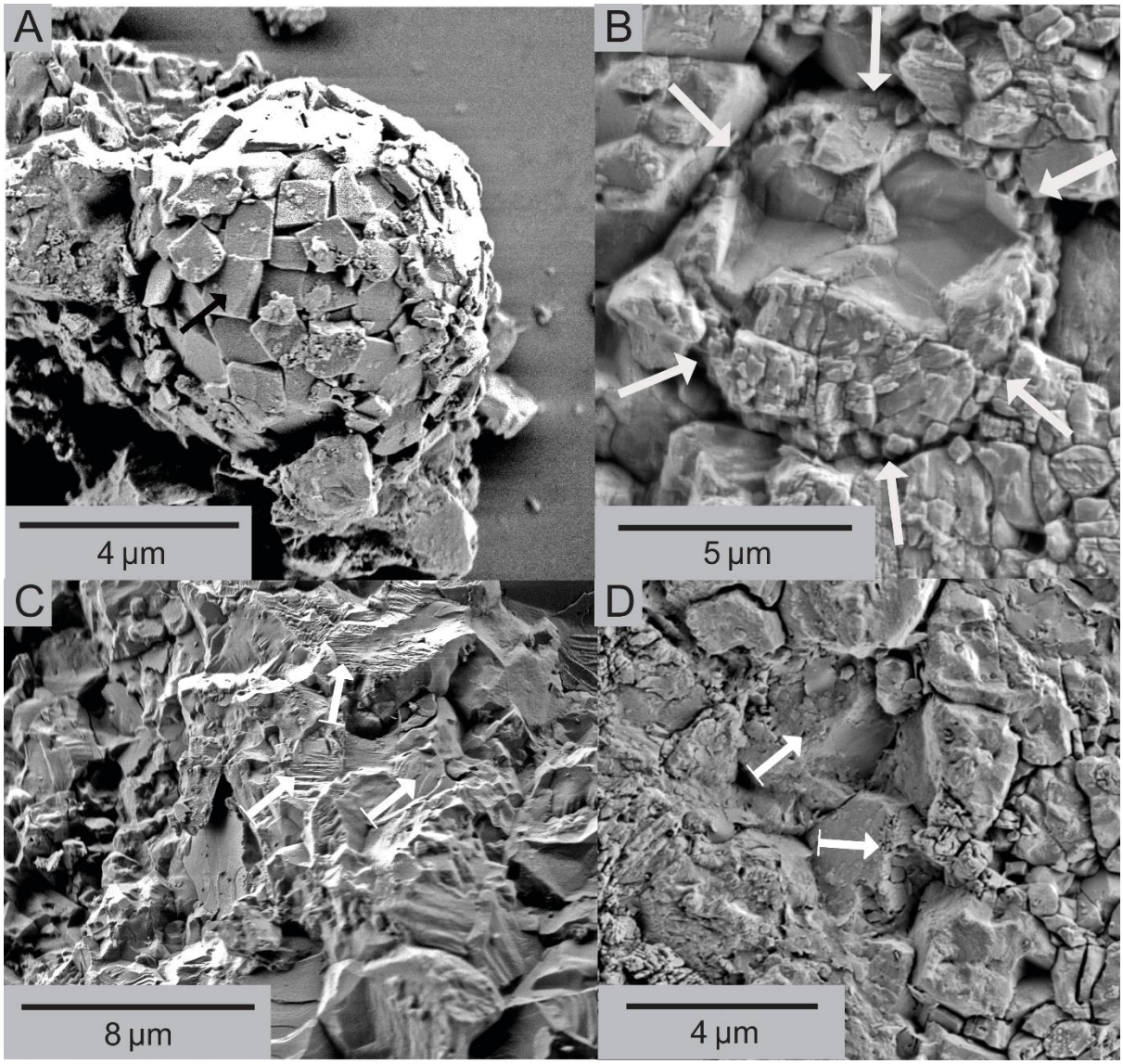

Fig.2.8 – SEM images showing dissolution and overgrowth patterns within the carbonate matrix and calcareous nannofossils from Sommerkogel and Steinbergkogel sections. A- Recrystallized *P. triassica* covered by calcite crystals, lower Rhaetian, STK A/119A; B- *Orthopithonella geometrica* filled by secondary calcite, lower Rhaetian, STK B/29A; C- Overgrowth features of calcite (step growth), upper Norian, ST4/38; D- Dissolution pits (marked with arrows) and recrystallization patterns, upper Norian, ST4/2.

4.3.2 Chemical composition of the samples

The impact of marine diagenesis on the calcareous samples was investigated by analyzing the elemental composition of selected samples (Table S2). Independent from their stratigraphic position, all samples display high Ca contents (34.9 ± 2.2 wt.%, on average) reflecting the dominance of carbonate minerals (i.e. > 80-95 wt.% of calcite). Low contents of Mg (0.7 ± 0.3

wt.%), Fe (0.3 ± 0.2 wt.%), Si (0.7 ± 0.4 wt.%), Al (0.3 ± 0.2 wt.%) and K (0.1 ± 0.1 wt.%) likely correspond to minor abundances of detrital dolomite, Fe-oxyhydrates and siliciclastic components, like quartz, feldspar and clay minerals. The Al/Ca vs. Fe/Ca cross-plot shows a positive linear correlation (R^2 = 0.84; Fig.2.9 A), indicating that almost all Fe belongs to the detritic fraction and is thus neither of diagenetic origin nor part of the micritic matrix. The relatively high Na (260 ± 120 ppm) and Sr (410 ± 330 ppm) contents and the low Mn (200 ± 130 ppm) contents (Fig.2.9 B) document the majority of the carbonate fraction to be pristine-marine, as recrystallization due to diagenesis produces carbonates that are depleted in Na and Sr, but relatively enriched in Fe and Mn (e.g. Baldermann et al., 2015). These data collectively suggest that diagenetic overprinting was minimal.

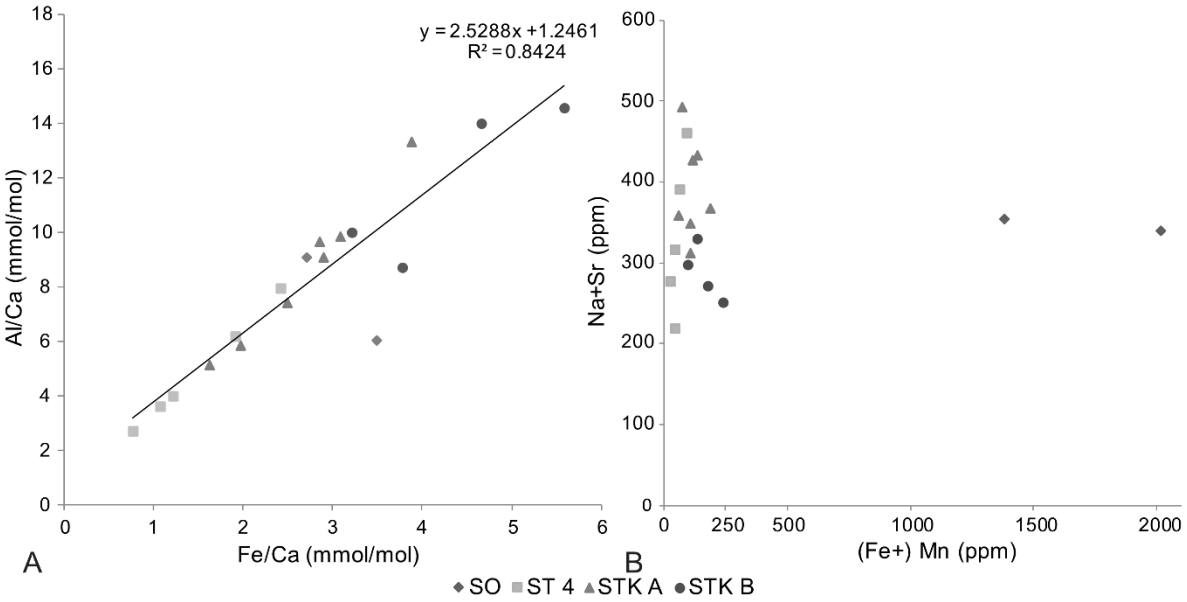

Fig.2.9 – Cross plot of A: Al/Ca and Fe/Ca; B: Na+Sr versus Mn from sub-sections ST4 and STK A, B and Na+Sr versus Fe+Mn from Sommeraukogel.

5. Discussion

5.1 *Upper Triassic coccolithophorids*

5.1.1 Oldest occurrence of coccolithophorids

Until this study, the oldest occurrence of the coccolithophorids has been reported just below the Norian/Rhaetian boundary at Steinbergkogel (Gardin et al., 2012). Bown et al. (1991) and Gardin et al. (2012) have proposed that the main location of evolutionary activity

during both the Late Triassic and Early Jurassic seems to have taken place in the subtropical/tropical Western Tethys. In addition, molecular clocks suggest the earliest origin of potentially calcifying haptophytes, so-called Calcihaptophycidae (De Vargas et al., 2007), between 270 – 240 Myr for SSU rDNA (Small SubUnit ribosomal DeoxyriboNucleic Acid) and at 200 Ma for LSU rDNA (Large SubUnit ribosomal DeoxyriboNucleic Acid) (De Vargas et al., 2007). Our results fall in between these two estimations, 227 – 209 Myr.

Indeed, we observed the oldest occurrence of coccoliths in the Alaunian 3 (mid-Norian) in sample SO/15 (around 215 Ma, unfortunately, the Norian is poorly constrained in term of radiometric dating). Although this specimen is not ideally preserved (Fig.2.3 A), we propose the FO of the coccoliths is in the middle Norian. In addition, rim shapes were observed in samples below the oldest observed coccoliths, but their overall poor preservation state does not allow a confident identification as coccoliths. These observations support the hypothesis of an older appearance of coccoliths, as previously hypothesised by Erba (2006) and Gardin et al. (2012), especially in an environment with higher preservation potential. Nonetheless, the minute size, the scarcity and the simple shape of these early specimens observed in the middle and upper Norian might indicate that these could be the earliest primitive forms.

The specimens observed in ST4/2 (upper Norian) have a clearly visible protolith rim with a small size (length 2.13 µm, width 1.57 µm), allowing a confident identification as *C. minutus.* Belonging to upper Norian (lower Sevatian) sediments, this FO of *C. minutus* is the oldest reported so far. This species is considered to be the ancestor of the Late Triassic coccolithophorids, as argued by Bown (1987) and Gardin et al. (2012), and therefore it should be present already from at least the middle Norian, according to our observations. Due to stronger dissolution features in the middle Norian Sommeraukogel section, the identification of the coccoliths at species level was difficult, however, in the middle Norian SO/17 sample a form similar to *C. minutus* was observed, suggesting that the first occurrence of this species might go back to the middle Norian and might represent the ancestor of the coccolithophorids. Indeed, compared to other well-preserved *C. minutus* from the lower Rhaetian (e.g. in sample STK A/119 A), this specimen presents an oval shape and is composed of partly visible outer elements and of a central knob, which is typical for this species (see supplementary material, figure S1).

In the upper Norian, just above the first truly identified *C. minutus* (ST4/2), a well-preserved specimen of *A. koessenensis* was observed in sample ST4/6, with a clear loxolith rim and a double bar crossing the central area. This represents the oldest *A. koessenensis* observed so far. *Crucirhabdus primulus* has been previously reported in lower Rhaetian sediments (STK B/28 by Gardin et al., 2012). In the present study, a specimen of *C. primulus* with a double rim structure was found in the lower Rhaetian (sample STK C/12 E). The cross present in the centre area, typical for this species, is missing but the four symmetric anchor points are still visible. Concerning the nannoliths, the FO of *E. hallstattensis* is in the lower Rhaetian (sample STK A/119A;equivalent to STK B/12G in Gardin et al. (2012). All other nannoliths are present already from the base of the Sommeraukogel section because their FO is older than the timespan of our studied sections.

5.1.2 Evolution of early coccolithophorids

The investigation of middle Norian to lower Rhaetian sediments allowed us to follow the early evolution of coccolithophorids and nannoliths throughout the Late Triassic. Previously, Bralower et al. (1991) have proposed that *C. primulus* is the ancestor of a lineage, which gave rise to *C. minutus* and *A. koessenensis*. Bralower et al. (1991) have based this lineage on the stratigraphic succession of the taxa at the Wombat Plateau (N-W Australia) and by the development of their characteristic rim structure, i.e. protolithic in *C. primulus*, protolithic or loxolithic in *C. minutus* and loxolithic in *A. koessenensis*. In contrast, Thierstein (1976), Jafar (1983), Bown (1987) and, more recently, Gardin et al. (2012) have proposed another lineage with *C. minutus* giving rise to *C. primulus*.

The stratigraphic apparition observed in this study is in good agreement with the proposed second lineage. We propose an evolution consistent with the trend recognized in our data in the coccolithophorids structural evolution and size, i.e. from a protolith-subvertical rim toward a more loxolith rim and from small sized *C. minutus* (1.6 to 2.4 µm), over medium sized *A. koessenensis* (1.9 to 3.2 µm) to bigger specimens of *C. primulus* (3 to 5 µm). We suggest *C. minutus* as the ancestor of *C. primulus* and the FO of the genus *Archaeozygodiscus* in between, representing either an independent lineage (see Fig. 4, Bown, 1987) or a new branch evolving from the *Crucirhabdus* lineage. During the late Norian/earliest Rhaetian the diversity of the coccolithophorids is very low with only three species described during the ~6.3 Myr recorded

in our study section. The speciation rate greatly accelerated in the early Jurassic, with 1.7 new species per million years (Bown et al., 1991). Coccolithophorids reached their maximum diversity during the late Cretaceous, which is ~120 Myr after their first occurrence in the sedimentary record (Bown et al., 1991).

5.2 *Preservation of calcareous nannofossils*

During the Late Triassic, sediments from Sommeraukogel and Steinbergkogel were deposited on a deeper shelfat palaeo-water depths of approximately 300 to 500 m (Kenter and Schlager, 2009), thus largely above the lysocline. However, partial dissolution and recrystallization of the micritic matrix (Berner, 1982) and nannofossils have occurred, as indicated by our petrographic and geochemical results. Changes in the trace element composition can occur during early marine and burial diagenesis (Land and Epstein, 1970; Budd and Land, 1990; Saller and Moore, 1991). Burial diagenesis can lead to sediments depleted in Sr and Na and enriched in Mn and eventually Fe and Zn (Turekian, 1972, Brand and Veizer, 1980). As shown before, especially the redox-sensitive elements Mn (and Fe) occur in low concentrations and show no correlation with the carbonate content. The comparably high Sr values (average: 162 ppm) suggest no pervasive diagenetic overprinting, corroborating the hypothesis of an open-marine depositional environment characterized by a low sedimentation rate (Coimbra et al., 2015). Middle and upper Jurassic successions of Ammonitico Rosso type sediments show similar Sr values (50 to 250 ppm; Price and Sellwood, 1994; Préat et al., 2006; Coimbra et al., 2015). The trace element signal clearly argues against a significant diagenetic impact, although an influence on the preservation degree of the nannofossil is possible (Price and Sellwood, 1994; Derry, 2010; Coimbra and Olóriz, 2012; Coimbra et al., 2015).

Dissolution features are clearly visible, especially in the middle Norian at Sommeraukogel, hindering the observation of small coccoliths. However, the diagenetic alteration was not sufficient to change significantly the quantification results, as only the preservation degree but not the abundance trend of calcareous nannofossils was affected in the analysed samples. *Prinsiosphaera triassica* specimens show dissolution features, comparison of the specimens observed in the studied sections with the preservation stages established by Bralower et al. (1991) indicates stage one (well-preserved specimens with intact outer layer)

and stage two (partly etched outer layer) to be absent. Indeed, all specimens of *P. triassica* display either stage three (entire inner layer) or stage four (etched inner layer) of preservation with less preserved specimens having secondary blocky calcite crystals. *Prinsiosphaera triassica* also shows some overgrowth features associated with early diagenesis, i.e. crystallization of neomorphic calcite on the whole surface (Fig 2.8 A). This process has also affected the calcareous cysts *Orthopithonella geometrica* and *Obliquipithonella rhombica*, which display secondary calcite crystals within the hollow sphere (Fig.2.8 B). Coccoliths are also affected by calcite overgrowth, frequently covering the rims and the central elements and preventing sometimes the precise identification of the specimens. At Steinbergkogel, Gardin et al. (2012) have hypothesized that variations in the preservation degree could impact the quantification results. Our careful control on diagenesis demonstrates the influence of dissolution of calcite matrix and overgrowth of calcite spar on the preservation of the specimens. However, the abundance trend of calcareous nannofossils does not seem to be affected, as confirmed by the fact that three samples with different abundance show similar dissolution features and justifying our quantitative estimates of carbonate palaeo-fluxes.

5.3 *Undertermined calcispheres*

The assignment to a calcareous nannofossil species of the second type of calcispheres possessing axial rays around a central structure is not straightforward (Fig.2.6 A – E). These structures are composed of Ca, C, O and minor amounts of Mg, which is indicative of a Ca-carbonate mineralogy. The low Sr content supports a primary calcite structure rather than an aragonitic one, which is typical for calcareous nannofossils. Such specimens have been reported first by Di Nocera and Scandone (1977) in Middle to Upper Triassic deep-water sediments from several localities of the Western Tethys (Italy, Austria, Montenegro, and Greece). They were described as *Nannoconus* sp. with circular shape and an axial canal. The specimen identified in this study is irregularly filled with calcite and surrounded by radial crystals that probably formed during diagenesis (Di Nocera and Scandone, 1977; see Fig. 3 a – c). Later, Bellanca et al. (1993) have reported similar structures from Sicilian sections of Carnian age and argued for a strong link to *Nannoconus* sp. These morphotypes have a conical or spherical shape and are composed of plates that are spirally arranged around a canal, similar to the *incertae sedis* shape presented here. However, it is important to highlight that *Nannoconus* sp. is only known from the Upper Jurassic, that is 50 Myr younger (Bown and

Cooper, 1998) compared to what is reported in this study. Recently, in upper Carnian sediments from Italy, Preto et al. (2012; 2013a; 2013b) have described similar specimens first as *Thoracosphaera* related specimens, then as calcareous dinocysts from the "*Pithonella*" group, with epitaxial overgrowth as a consequence of diagenesis. These authors proposed these forms to be a recrystallization artefact with calcite crystal rays growing in open space and having rhombohedral terminations. However, we did not observe any of these rhombohedral terminations, preventing the identification as recrystallized calcareous cysts (Preto et al., 2012; 2013a; 2013b) or as early form of *Nannoconus* sp. (Di Nocera and Scandone, 1977; Bellanca et al. 1993).

5.4 *Evolution and palaeo-flux of Prinsiosphaera triassica*

5.4.1 P. triassica size evolution

Data from the Wombat Plateau (NW Australia) indicate that *P. triassica* size increases from 6 μm during the middle Norian to 9 μm in the upper Rhaetian (Bralower et al., 1991). Clémence et al. (2010) reported a size reduction during the latest Rhaetian, just before the mass-extinction, with assemblages dominated by large *P. triassica* (~10 μm) to assemblages poor in *P. triassica* presenting a small size (< 5 μm). Bottini et al. (2016) have also shown a trend from large (10.5 to 13 μm) to medium and small sized specimens in an Italian section during the latest Rhaetian. Our data show a wide range in size, which varies from 4.93 μm to 12.92 μm (Fig.2.7). The maximum value is about 3 – 4 μm bigger than the maximum values reported by Clémence et al. (2010) and Bralower et al. (1991), respectively, but in the range of Bottini et al., (2016). In our dataset, specimens larger than 11 μm are often present. However, a size increase or decrease over time, as observed by Bralower et al. (1991), Clémence et al. (2010) and Bottini et al., (2016) has not been observed in this study from the middle Norian to the early Rhaetian. These observations could suggest that a significant size variation did not occur before the middle Rhaetian but later, close to the end-Triassic mass extinction.

5.4.2 Prinsiosphaera triassica abundance and related carbonate flux

The nannofossil assemblage observed at Steinbergkogel is representative for other Upper Triassic marine successions. *Prinsiosphaera triassica* dominates the assemblage with a relative abundance > 85 % in most samples, which has been observed in other Upper Triassic sections

of the Western Tethys Ocean (Fisher et al., 1976; Wiedmann et al., 1979; Jafar, 1983; Gardin et al., 2012; Preto et al., 2013a). The estimation of the carbonate palaeo-flux is an important proxy to estimate the contribution of these main calcifiers to the total marine carbonate export production during the Late Triassic. The progressive increase of *P. triassica* abundance, reaching 56 g N_{CaCO_3} cm^{-3} Myr^{-1} just above the Norian/Rhaetian boundary, highlights the transition from a *P. triassica*-poor to a *P. triassica*-rich period and predicts the successful evolution of this species in the late Rhaetian. The percentage of *P. triassica* (related to rock volume) in the uppermost Norian varies between 0.3 and 1.0 % and reaches a maximum of 4.2 % in the lower Rhaetian. This corresponds to the first step of increase before reaching the rock-forming abundance in the late Rhaetian, as described by Preto et al. (2013a). This first increase is followed by a slight decrease in abundance at the end of the studied section. This diminution co-occurs with the FO of the Upper Triassic nannoliths, *E. hallstattensis*, and a change in lithology, marked by the transition to the marly sediments of the Zlambach Formation. Those two observations raise the question of possible competition between these two species and/or possible negative feedback induced by a shift in the depositional environment, i.e. increase of the clay input of the Zlambach Formation. Indeed, nannoplankton is sensitive to changes in the trophic conditions (e.g., Winter and Siesser, 1994; Thierstein and Young, 2004; Erba, 2006). The change to a marlier lithology, possibly parallel to an increase in the nutrient concentration, could have been unfavourable for *P. triassica*.

Our quantitative results are in accordance with the semi-quantitative values obtained for the same time interval and at the same location (Gardin et al., 2012). However, our percentages of *P. triassica* per rock volume during the Norian are slightly lower than the results published by Preto et al. (2013a). Considering the analysed intervals in both studies, the direct comparison of results is only possible during *M. bidentata*, *M. hernsteini* and *P. andrusovi* zones (upper Norian, corresponding to our sub-section ST4). For ST4, our percentages are low, ranging between 0.01 and 2.3 % (Fig.2.7). Preto et al. (2013a) have reported at Pizzo Mondello (Sicanian Basin, Sicily – shallow sea) stable values below 3 % during the *M. bidentata* Zone (base of ST4), followed by an increase to 20 % during the *M. hernsteini* and the *P. andrusovi* zones (top of ST4). At Pignola-Abriola (Lagonegro Basin – open marine), Preto et al. (2013a) have presented values with an opposite trend compared to Pizzo Mondello. Indeed, at the end of the *M. bidentata* Zone the volume of *P. triassica* is around 10 % and decreases below 5 %

during the *M. hernsteini* and *P. andrusovi* zones (top of ST4). The differences can reflect the different palaeo-depositional environments, i.e., closer to the coastline and shallower at Pizzo Mondello, pelagic marine deposits at Pignola-Abriola and a hemipelagic setting in this study. Preto et al. (2013a) have suggested that *Prinsiosphaera* was more common in a shallower environment (Pizzo Mondello, Sicanian Basin) than in open marine settings (Pignola-Abriola, Lagonegro Basin). This is confirmed by the deeper shelf setting of Sommeraukogel and Steinbergkogel. Additionally, Preto et al. (2013a) have used a point-counting method on a rock surface, resulting in an overestimation of the calculated amount per cm^3. We calculated a percentage utilizing the total volume of *P. triassica*, computed on the basis of the absolute abundance in respect to the rock volume, which likely leads to an underestimation of the real abundance per cm^3. Moreover, in our study only complete specimens were counted, while Preto et al. (2013a) have counted even small single elements, which they have interpreted as broken parts of *P. triassica*. The most successful time of *P. triassica* has likely occurred later in the Rhaetian. During the late Rhaetian, at Pizzo Mondello, Preto et al. (2013a) have reported *P. triassica* as a rock-forming nannofossil with an abundance up to 60 % of the rock volume. At Pignola-Abriola, the maximum abundance in the *M. ultima* Zone is only around 20 %. The analysis of a sample from the Eiberg section (NCA), corresponding to a late Rhaetian intraplatform basin in Austria, confirms the observations of Preto et al. (2013). The quantification of this sample follows the preparation and calculation method developed in this study and shows that *P. triassica* represents 30 % of the rock volume, which is equal to 45 % of the rock surface in the upper Rhaetian sediments. The increase to a rock-forming abundance, as described by Preto et al. (2013a), has therefore occurred only during the late Rhaetian, but is preceded by an at least 15-fold increase during the early Rhaetian (from 0.3 to 4.2% of the rock volume).

Conclusion

The quantitative investigation on the calcareous nannofossil content at Sommeraukogel and Steinbergkogel sections (Northern Calcareous Alps, Austria) provides new insights into the evolution of the early calcareous nannofossils during the Late Triassic. The following observations have been made:

1. The oldest coccolithophorids can be traced at least back to the middle Norian (SO/15 – *Halorites macer* Zone).

2. The oldest *C. minutus* and *A. koessenensis* were observed in the late Norian (ST4/2 and ST4/6 – *Metasibirites spinescens* Zone).

3. *C. primulus* was first observed in the early Rhaetian (STK C/12E – *Paracochloceras suessi* Zone).

The evolution of the earliest coccolithophorids started with the appearance of *C. minutus* giving rise to *C. primulus. Archaeozygodiscus* appears between these two taxa, representing the emergence of an independent lineage or of a new evolutionary branch from the *Crucirhabdus* spp. lineage. This diversification was relatively slow, taking several million years and the morphological changes observed include the modification of the rim structure from a protolith-subvertical rim to a loxolith rim and an increase in size. Besides the evolution of the coccolithophorids, *Prinsiosphaera triassica* dominates the calcareous nannofossil assemblages during the Late Triassic. The increasing abundance of *P. triassica* from the late Norian to the earliest Rhaetian does not reach rock-forming proportions but is interpreted as the onset of its later successful evolution in the late Rhaetian. The low abundance of *P. triassica* in the early Rhaetian suggests that the Cretan Ocean was still not established in the Western Tethys at this time.

Acknowledgements: This research was supported by the Austrian Science Foundation (Project P 29497-P29 to Sylvain Richoz) and « RESPECT » (A major evolutive Revolution : the Emergence and Spreading of PElagic Calcifiers in the late Triassic) PICS-CNRS project to Silvia Gardin. Gerald Auer and Dorothee Hippler are acknowledged for their help in the early scientific discussions and Franz Tscherne for his assistance during sample preparation for SEM. The detailed and constructive comments of two anonymous reviewers and of guest editor Yadong Sun were very helpful during the revision of this manuscript.

References

Baldermann, A., Deditius, A.P., Dietzel, M., Fichtner, V., Fischer, C., Hippler, D., Leis, A., Baldermann, C., Mavromatis, V., Stickler, C.P., Strauss, H., 2015. The role of bacterial sulfate reduction during dolomite precipitation: Implications from Upper Jurassic platform carbonates. Chemical Geology. 412, 1 – 14. 10.1016/j.chemgeo.2015.07.020.

Baldermann, A., Grießbacher, A.C., Baldermann, C., Purgstaller, B., Letofsky-Papst, I., Kaufhold, S., Dietzel, M., 2018a. Removal of Barium, Cobalt, Strontium, and Zinc from Solution by Natural and Synthetic Allophane Adsorbents. Geosciences. 8(9), 309, 1 – 22. 10.3390/geosciences8090309.

Baldermann, A., Mavromatis, V., Frick, P.M., Dietzel, M., 2018b. Effect of aqueous Si/Mg ratio and pH on the nucleation and growth of sepiolite at 25 °C. Geochimica et Cosmochimica Acta. 227, 211 – 226. 10.1016/j.gca.2018.02.027.

Baumann, K.H., 2004. Importance of size measurements for coccoliths carbonate flux estimates. Micropaleontology. 50, 35 – 43. 10.2113/50.Suppl_1.35.

Bellanca, A., Di Stefano, E., Di Stefano, P., Erba, E., Neri, R., Pirini Radrizzani, C., 1993. Ritrovamento di ‘‘Calcisfere’’ e nannofossili calcarei in terreni carnici della Sicilia. Paleopelagos. 3, 91 – 96.

Berner, R.A., 1982. Early diagenesis as a theoretical approach. – Princeton, Princeton University Press, NJ, Princeton Series in Geochemistry. Earth Surface Processes and landforms. 7, 197 – 198. 10.1002/esp.3290070212.

Bittner, A. 1890. Brachiopoden der alpinen Trias. – Abhandlungen der kaiserlich – königlichen Geologischen Reichsanstalt. 14, VI+325.

Bordiga, M., Bartol, M., Henderiks, J., 2015. Absolute nannofossil abundance estimates: Quantifying the pros and cons of different techniques – Revue de micropaléontologie. 58, 155 – 165. 10.1016/j.revmic.2015.05.002.

Bornemann, A., Aschwer, U., Mutterlose, J., 2003. The impact of calcareous nannofossils on the pelagic carbonate accumulation across the Jurassic–Cretaceous boundary. Palaeogeography, Palaeoclimatology, Palaeoecology. 199, 187 – 228. 10.1016/S0031-0182(03)00507-8.

Bottini, C., Jadoul, F., Rigo, M., Zaffani, M., Artoni, C., Erba, E., 2016. Calcareous nannofossils at the Triassic/Jurassic boundary: Stratigraphic and paleoceanographic characterization. Rivista Italiana di Paleontologia e Stratigrafia (Research in Paleontology and Stratigraphy). 122(3), 141 – 164. 10.13130/2039-4942/7726.

Bown, P.R., 1985. Archaeozygodiscus gen. nov. and other Triassic coccoliths. INA Newsletter. 7, 32 – 35.

Bown, P.R., 1987. The structural Development of Early Mesozoic Coccoliths and its Evolutionary and Taxonomic Significance. Abhandlungen der Geologischen Bundesanstalt. 39, 33 – 49.

Bown, P.R., Burnett, J.A., Gallagher, L.T., 1991. Critical events in the evolutionary history of calcareous Nannoplankton. Historical Biology. 5(2-4), 279 – 290. 10.1080/10292389109380407.

Bown, P.R., 1998. Calcareous Nannofossil Biostratigraphy. London: Chapman & Hall, First Edition. ISBN: 0-412-78970-1.

Bown, P.R., Cooper, M.K.E., (1998). Jurassic. In: Bown, P.R. (Ed), Calcareous nannofossil biostratigraphy. London, Chapman & Hall, British Micropalaeontological Society Publication Series. 315, 34 – 85.

Bralower, T.J., Bown, P.R., Siesser, W.G., 1991. Significance of Upper Triassic nannofossils from the Southern Hemisphere (ODP Leg 122, Wombat Plateau, N.W. Australia) – Marine Micropaleontology. 17, 119 – 154. 10.1016/0377-8398(91)90025-2.

Brand, U., Veizer, J., 1980. Chemical diagenesis of a multicomponent carbonate-system – 1: trace elements. Journal of Sedimentary Petrology. 50, 1219–1236. 10.1306/212F7BB7-2B24-11D7-8648000102C1865D.

Budd, D.A., Land, L.S., 1990. Geochemical imprint of meteoric diagenesis in Holocene ooid sands, Schooner Cays, Bahamas: correlation of calcite cement geochemistry with extant groundwaters. Journal of Sedimentary Petrology. 60, 361 – 378. 10.1306/212F919C-2B24-11D7-8648000102C1865D.

Chayes, F., 1954. The theory of thin-section analysis. Journal of Geology. 62, 92 – 101. 10.1086/626135.

Clémence, M.E., Gardin, S., Bartolini, A., Paris, G., Beaumont, V., Guex, J., 2010. Bentho-planktonic evidence from the Austrian Alps for a decline in sea-surface carbonate

production at the end of the Triassic. Swiss Journal of Geosciences. 103, 293 – 315. 10.1016/j.palaeo.2010.05.021.

Cohen, K. M., Finney, S. C., Gibbard, P.L., Fan, J.-X., 2013; updated v 2018/08. The ICS International Chronostratigraphic Chart. Episodes 36, 199 – 204.

Coimbra, R., Olóriz, F., 2012. Geochemical evidence for sediment provenance in mudstones and fossil-poor wackestones (Upper Jurassic, Majorca Island). Terra Nova. 24, 437 – 445. 10.1111/j.1365-3121.2012.01082.x.

Coimbra, R., Immenhauser, A., Olóriz, F., Rodríguez-Galiano, V., Chica-Olmo, M., 2015. New insights into geochemical behaviour in ancient marine carbonates (Upper Jurassic Ammonitico Rosso): Novel proxies for interpreting sea-level dynamics and palaeoceanography. Sedimentology. 62, 266 – 302. 10.1111/sed.12148.

Demangel, I., Howe, R., Gardin, S., Richoz, S. 2021: *Eoconusphaera hallstattensis* sp. nov. and review of the Rhaetian genus *Eoconusphaera*. *Journal of Nannoplankton Research*. 39 (1), 77 – 87.

Derry, L.A., 2010. A burial diagenesis origin for the Ediacaran Shuram-Wonoka carbon isotope anomaly. Earth and Planetary Science Letters. 194, 152 – 162. 10.1016/j.epsl.2010.03.022.

De Vargas, C., Aubry, M.P., Probert, I., Young, J., 2007. Origin and evolution of coccolithophores: from coastal hunters to oceanic farmers. In: Falkowski, P.G., Knoll, A.H. (Eds), Evolution of Aquatic Photoautotrophs, Boston, Elsevier. 251 – 285.

Di Nocera S., Scandone P., 1977. Triassic nannoplankton limestones of deep basin origin in the central Mediterranean region. Palaeogeography, Palaeoclimatology, Palaeoecology. 21, 101 – 111. 10.1016/0031-0182(77)90008-6.

Ehrenberg, C. G., 1836. Bemerkungen über feste mikroskopische anorganische Formen in den erdigen und derben Mineralien. – Abhandlungen der Königlich Preussischen Akademie der Wissenschaften Berlin. 1836, 84 – 85.

Erba, E., Tremolada, F., 2004. Nannofossil carbonate fluxes during the Early Cretaceous: Phytoplamkton response to nitrification episodes, atmospheric CO_2, and anoxia. Paleoceanography. 19, PA1008. 10.1029/2003PA000884.

Erba, E., 2006. The first 150 million years history of calcareous nannoplankton: Biosphere-geosphere interactions. Palaeogeography, Palaeoclimatology, Palaeoecology. 232, 237 – 250. 10.1016/j.palaeo.2005.09.013.

Falkowski, P. G., Katz, M. E., Knoll, A. H., Quigg, A., Raven, J. A., Schofield, O., Taylor, F. J. R., 2004. The Evolution of Modern Eukaryotic Phytoplankton. Science. 305 (5682), 354 – 360. 10.1126/science.1095964.

Fischer, A.G., Honjo, S., Garrison, R.A.E., 1967. Electron Micrographs of Limestones and their Nannofossils. Princeton, Princeton University Press, NJ. 157.

Gardin, S., Krystyn, L., Richoz, S., Bartolini, A., Galbrun, B., 2012. Where and when the earliest coccolithophores? Lethaia. 45, 507 – 523. 10.1111/j.1502-3931.2012.00311.x.

Gottschling, M., Renner, S.S., Meier, K.J.S., Willems, H., Keupp, H., 2008. Timing deep divergence events in calcareous dinoflagellates. Journal of Phycology. 44, 429 – 438. 10.1111/j.1529-8817.2008.00479.x.

Hornung, T., 2007. The "Carnian Crisis" in the Tethys realm: multistratigraphic studies and paleoclimates constraints. PhD-Thesis. pp 233, 1 CD, Universität Innsbruck.

Hüsing, S.K., Deenen, M.H.L., Koopmans, J.G., Krijgsman, W., 2011. Magnetostratigraphic dating of the proposed Rhaetian GSSP at Steinbergkogel (Upper Triassic, Austria): Implications for the Late Triassic time scale. – Earth and Planetary Science Letters. 302, 203 – 216. 10.1016/j.epsl.2010.12.012.

Jafar, S.A., 1983. Significance of Late Triassic calcareous Nannoplankton from Austria and Southern Germany. Neues Jahrbuch für Geologie und Paläeontologie. 166, 218 – 259.

Janofske, D., 1987. Kalkige Nannofossillien aus der Ober-Trias (Rhät) der Nördlichen Kalkalpen. Berliner Geowissenschaftlichen Abhandlungen. 86, 45 – 67.

Janofske, D., 1990. Eine neue "Calcisphaere", *Carnicalyxia tabellata* n.g. n.sp. aus den Cassianer Schichten (Cordevol, unteres Karn) der Dolomiten. Berliner Geowissenschaftlichen Abhandlungen. 124, 259 – 269.

Janofske, D., (1992). Calcareous nannofossils of the Alpine Upper Triassic. In: Hamrsmid, B., Young, J.R., (Eds), Nannoplankton Research (Proceedings INA Conference). Knihovnicka ZPN, Hodonin, Cz. 87 – 109.

Kenter, J.A.M., Schlager, W., 2009. Slope angle and basin depth of the Triassic Platform-Basin Transition at the Gosaukamm, Austria. Austrian Journal of Earth Sciences. 102, 15 – 22.

Kittl, E. 1912. Materialien zu einer Monographie der Halobiidae und Monotidae der Trias. Palaeontologie der Umgebung des Balatonsees. 2(4), 1 – 129.

Koken, E. 1897. Die Gastropoden der Trias um Hallstatt. – Abhandlungen der kaiserlich – königlichen geologischen Reichsanstalt. 17, 1 – 112.

Krystyn, L., 1980. Triassic conodont localities of the Salzkammergut region (Northern Calcareous Alps) – Abhandlungen der Geologischen Bundesanstalt. 35, 61 – 98.

Krystyn, L., Richoz, S., Gallet, Y., Bouquerel, H., Kürschner, W.M., Spötl, C., 2007a. Updated bio-and magnetostratigraphy from Steinbergkogel (Austria), candidate GSSP for the base of the Rhaetian stage. – Albertiana. 36, 164 – 173.

Krystyn, L., Bouquerel, H., Kuerschner, W.M., Richoz, S., Gallet, Y., 2007b. Proposal for a candidate GSSP for the base of the Rhaetian stage. In: Lucas, S.G., Spielmann, J.A. (Eds), The Global Triassic – New Mexico Museum of Natural History and Science Bulletin 41. 189 – 199.

Krystyn, L. 2008. The Hallstatt pelagics – Norian and Rhaetian Fossillagerstaetten of Hallstatt. – Berichte der Geologischen Bundesanstalt. 76, 76-98.

Kürschner, W. M., Bonis, N.R., Krystyn, L., (2007): Carbon-isotope stratigraphy and palynostratigraphy of the Triassic-Jurassic transition in the Tiefengraben section – Northern Calcareous Alps (Austria). Palaeogeography, Palaeoclimatology, Palaeoecology. 244, 257 – 280. 10.1016/j.palaeo.2006.06.031.

Land, L.S., Epstein, S., 1970. Late Pleistocene diagenesis and dolomitization, North Jamaica. Sedimentology. 14, 187 – 200. 10.1111/j.1365-3091.1970.tb00192.x.

Mandl, G.W., 2000. The Alpine sector of the Tethyan shelf - Examples of Triassic to Jurassic sedimentation and deformation from the Northern Calcareous Alps. – Mitteilungen der Österreichischen Geologischen Gesellschaft. 92, 61 – 78.

Martin, R.E., 1995. Cyclic and secular variation in microfossil biomineralization – clues to the biogeochemical evolution of Phanerozoic oceans. Global and Planetary Change. 11, 1 – 13. 10.1016/0921-8181(94)00011-2.

Mosher, L.C., 1968. Triassic conodonts from western North America and Europe and their correlation. – Journal of Paleontology. 42(4), 895 – 946. http://www.jstor.org/stable/1302396

Moshkovitz, S., 1982. On the findings of a new calcareous nannofossil (*Conusphaera zlambachensis*) and other calcareous organisms in the Upper Triassic sediments of Austria. Eclogae Geologicae Helvetiae. 75, 611–619. 10.5169/seals-165245.

Mojsisovics, E.V., 1873, 1875, 1902. Das Gebirge um Hallstatt. Die Mollusken-Faunen der Zlambach- und Hallstätter Schichten; Suppl.: Die Cephalopoden der Hallstätter Kalke. – Abhandlungen der Geologischen Reichsanstalt. 6: H1(1873), H2(1875), Suppl.(1902).

Ogg, J.G., 2012. Triassic. In: Gradstein, F. M., Ogg, J.G., Schmitz, M.D., Ogg, G.M. (Eds), The Geologic Time Scale 2012, Amsterdam, Elsevier. 681 – 730. 10.1016/C2011-1-08249-8.

Piller, W. E., Egger, H., Erhart, C. W., Gross, M., Harzhauser, M., Hubmann, B., van Husen, D., Krenmayr, H.-G., Krystyn, L., Lein, R., Lukeneder, A., Mandl, G.W., Rögl, F., Roetzel, R., Rupp, C., Schnabel, W., Schönlaub, H. P., Summersberger, H., Wagreich, M., Wessely, G., 2004. Die stratigraphische Tabelle von Österreich 2004 (sedimentäre Schichtfolgen). Kommission für die paläontologische und stratigraphisce Erforschung Österreichischen Akademie der Wissenschaften und Österreichische Stratigraphische Kommission.

Préat, A., Morano, S., Loreau, J. P., Durlet, C., Mamet, B., 2006. Petrography and biosedimentology of the Rosso Ammonitico Veronese (middle-upper Jurassic, north-eastern Italy). Facies. 52(2), 265 – 278. 10.1007/s10347-005-0032-2.

Preto, N., Kustatscher, E., Wignall, P.B., 2010. Triassic climates – State of the art and perspectives – Palaeogeography, Palaeoclimatology, Palaeoecology. 290, 1 – 10. 10.1016/j.palaeo.2010.03.015.

Preto, N., Rigo, M., Agnini, C., Bertinelli, A., Guaiumi, C., Borello, S., Westphal, H., 2012. Triassic and Jurassic calcareous nannofossils oft he Pizzo Mondello section: A SEM study. Rivista Italiana di Paleontologia e Stratigrafia (Research in Paleontology and Stratigraphy). 118, 131 – 141. 10.13130/2039-4942/5994.

Preto, N., Agnini, C., Rigo, M., Sprovieri, M., Westphal, H., 2013a. The calcareous nannofossil Prinsiosphaera achieved rock-forming abundances in the latest Triassic of western Tethys: consequences for the $\delta^{13}C$ of bulk carbonate – Biogeosciences. 10, 6053 – 6068. 10.5194/bg-10-6053-2013.

Preto, N., Willems, H., Guaiumi, C., Westphal, H., 2013b. Onset of significant pelagic carbonate accumulation after the Carnian Pluvial Event (CPE) in the western Tethys – Facies. 59, 891 – 914. 10.1007/s10347-012-0338-9.

Price, G.D., Sellwood, B.W., 1994. Palaeotemperatures indicated by Upper Jurassic (Kimmeridgian – Tithonian) fossils from Mallorca determined by oxygen isotope composition. Palaeogeography, Palaeoclimatology, Palaeoecology. 110, 1 – 10. 10.1016/0031-0182(94)90106-6.

Prins, B., 1969. Evolution and stratigraphy of coccolothinids from the lower and middle lias. International Conference Planktonic Microfossils, Geneva. 2, 547 – 558.

Richoz, R., Krystyn, L., Von Hillebrandt, A., Martindale, R., 2012. End-Triassic crisis events recorded in platform and basin of the Austrian Alps. The Triassic/Jurassic and Norian/Rhaetian GSSPs – Journal of Alpine Geology. 55, 321 – 374.

Richoz, S., Krystyn, L., 2015. The Upper Triassic events recorded in platform and basin of the Austrian Alps. The Triassic/Jurassic GSSP and Norian/Rhaetian GSSP candidate – Berichte der Geologischen Bundesanstalt. 111.

Ridgwell, A., 2005. A Mid Mesozoic Revolution in the regulation of ocean chemistry. Marine Geology. 217, 339 – 357. 10.1016/j.epsl.2005.03.006.

Robinson, P.L., 1973. Paleoclimatology and continental drift. In: Tarling, D.H., Runcorn, S.K. (Eds.), Implications of continental drift to the Earth Sciences (v2). New York, Academic Press. 1184, 449 – 476.

Rood, A.P., Hay, W.W., Barnard, T., 1973. Electron microscope studies of lower and middle Jurassic coccoliths. Eclogae Geologicae Helvetiae. 66(2), 365 – 382. 10.5169/seals-164197.

Rost, B., Riebesell, U., 2004. Coccolithophores and the biological pump: responses to environmental changes. In: Thierstein, H. R., Young, J. R. (Eds.), Coccolithophores: from molecular processes to global impact, Berlin, Springer. 99 – 125. 10013/epic.21851.d001.

Ruffell, A., Simms, M.J., Wignall, P.B., 2015. The Carnian Humid Episode of the late Triassic: a review. Geological Magazine. 153, 271 – 284. 10.1017/S0016756815000424.

Saller, A.H., Moore, C.H., 1991. Geochemistry of meteoric calcite cements in some Pleistocene limestones. Sedimentology. 38, 601 – 621. 10.1111/j.1365-3091.1991.tb01011.x.

Schlager, W., 1969. Das Zusammenwirken von Sedimentation und Bruchtektonik in den triadischen Hallstätterkalken der Ostalpen. – Geologische Rundschau. 59, 289 – 308.

Suchéras-Marx, B., Giraud, F., Mattioli, E., Gally, Y., Barbarin, N., Beaufort, L., 2014. Middle Jurassic coccolith fluxes: A novel approach by automated quantification. Marine Micropaleontology. 111, 15 – 25. 10.1016/j.marmicro.2014.06.002.

Suchéras-Marx, B., Mattioli, E., Allemand, P., Giraud, F., Pittet, B., Plancq, J., Escarguel, G., 2019. The colonization of the oceans by calcifying pelagic algae. Biogeosciences. 16, 2501–2510. 10.5194/bg-16-2501-2019.

Thierstein, H., R., 1976. Mesozoic calcareous nannoplankton biostratigraphy of marine sediments. Marine Micropaleontology, 1, 325 – 362. 10.1016/0377-8398(76)90015-3.

Thierstein, H.R., Young, J.R. (2004): Coccolithophores: From molecular processes to Global Impact. Berlin, Springer-Verlag. 1–29. 10.1007/978-3-662-06278-4.

Tollmann, K., 1995. Weitere beobachtungen an Rhätischen nannofossilien der Tethys. Geolologisch-Paläontologische Mitteilungen Innsbruck. 20, 1 – 10.

Turekian, K.K., 1972. Chemistry of the Earth. Holt, Rinehart, Winston, New-York, 131.

Wiedmann, J., Fabricius, F., Krystyn, L., Reitner, J., Ulrichs, M., 1979. Über Umfang und Stellung des Rhaet. Newsletter on Stratigraphy. 8, 133 – 152. 10.23689/fidgeo-817.

Winter, A., Siesser, W.G., 1994. Coccolithophores. Cambridge, New York, NY: Cambridge University Press, First Edition. ISBN: 0-521-38050-2.

Wood, R.A., Grotzinger, J.P., Dickson, J.A.D., 2002. Proterozoic modular biomineralized metazoan from the Nama Group, Namibia. Science. 296, 2383 – 2386. 10.1126/science.1071599.

Young, J.R., Ziveri, P., 2000. Calculation of coccolith volume and its use in calibration of carbonate flux estimates. Deep-Sea Research, II. 47, 1679 – 1700. 10.1016/S0967-0645(00)00003-5.

Zeebe, R. E., Westbroek, P. 2003. A simple model for the CaCO3 saturation state of the ocean: the “Strangelove”, the “Neritan”, and the “Cretan” Ocean. Geochemistry, Geophysics, Geosystems. 4, 1 – 26. 10.1029/2003GC000538.

Supplementary material

Taxonomic index of calcareous nannofossil taxa reported in this study with some remarks .

Archaeozygodiscus koessenensis Bown, 1985

Remarks: *A. koessenensis* was identified following the original description of Bown (1985) as an elliptical coccolith with a loxolith rim structure imbricating in an anticlockwise direction and having a size ranging from 1.9 to 3.2 µm. The inner part holds a thick bar with a circular hole in the middle.

Carnicalyxia tabellata Janofske, 1990

Remarks: *C. tabellata* has an oval-shape with a size of 19.4 µm in length and 14.3 µm in width. The single-layer wall of this specimen is composed of more or less parallel rhombohedral calcite crystals forming a 45º angle to the wall surface.

Cassianospica curvata Janofske, 1992

Remarks: *C. curvata* was described as a curved-shape calcareous nannofossil, which is composed of two rows of calcite elements.

Conusphaera zlambachensis Moshkovitz, 1982; emended Bown and Cooper, 1989; Demangel et al., 2021.

Crucirhabdus minutus Jafar, 1983

Remarks: *C. minutus* is a tiny, elliptical coccolith with a size ranging between 1.6 to 2.4 µm. The inner area of the rim is composed of a cross supporting a central spine, which appears as two knobs under the OM. Concerning the rim elements orientation, Bown (1985) has defined a protolith rim, while Bralower et al. (1991) have outlined the possibility of both protolith and loxolith structures. In this study, we consider the protolith rim as belonging to *C. minutus*, but the loxolith rim without preserved inner structure (i.e. a bar or a cross) was not determined at a species level.

Crucirhabdus primulus Prins, 1969

Remarks: *C. primulus* has a size between 3 to 5 µm and exhibits an elliptical shape. Rood et al. (1973) and Janofske (1987) have described this species with a loxolith rim with imbricated

elements. Bown (1987) and Bralower et al. (1991) have defined the species to be composed of vertical to sub-vertical elements, forming a protolith rim. In this study, *C. primulus* was considered as a species presenting a loxolith rim with imbricated elements in a clockwise direction (Rood et al., 1973; Janofske, 1987). The central area of the rim is marked by a cross-shaped element, which is not always preserved.

Eoconusphaera hallstattensis Demangel et al., 2021 Remarks: *E. hallstattensis* was first described in Demangel et al. (2021) has a conic shape and is truncated at both ends, with a dome on the larger extremity. The mantle is composed of elongated lamellae. The inner core is composed of vertical, radially arranged lamellae joining in the centre part without forming a canal. The FO of this species has been assigned to the base of the Rhaetian (*P. suessi* Zone) (Demangel et al., 2021).

Obliquipithonella rhombica Jafar, 1983 ; emended Janofske, 1987

Remarks: *O. rhombica* possesses calcitic external elements oblique to the wall, and the mean size is smaller with a diameter around 6 µm.

Orthopithonella geometrica Jafar, 1983 ; emended Janofske, 1987

Remarks: *O. geometrica* has an empty spherical shape with external elements perpendicular to the wall and a mean diameter around 9 µm.

Prinsiosphaera triassica Jafar, 1983

Remarks: P. triassica is the main carbonate producer among calcareous nannofossils during the Late Triassic in the Western Tethys Ocean (Preto et al., 2013b). *Prinsiosphaera triassica* was originally described by Jafar (1983) as a spherical to hemispherical form with a depression at one end and being composed of thin, tabular calcite rhombohedra arranged in parallel groups, randomly positioned to form the calcareous nannofossil. Bralower et al. (1991) have explained the diversity of *P. triassica* as an etching effect, defining four distinct stages of preservation, ranging from the smooth outer layer to the etched inner layer, composed of unorganised groups of parallel, tabular, calcite.

Thoracosphaera sp. Jafar, 1983; emended Bralower, 1991

Remarks: *Thoracosphaera* was recognized here as a bowl- or hat-shape calcareous dinocyst with a size between 5 to 13 µm. However, Gottschling et al. (2008) were sceptical regarding the affinities of the Late Triassic specimens to the current Thoracosphaeraceae family due to missing characteristics (i.e. archeopyle and paratabulation) and a stratigraphic gap between the Late Triassic and the late Middle Jurassic forms.

Sample's number	**Calcispheres**	**Coccolithophorids**	***A. koessenensis***	***C. minutus***	***C. primulus***	***P. triassica***	***E. hallstattensis***	***Obliquipithonella rhombica***	***Orthopithonella geometrica***	***Thoracosphaera* (*sensu* Jafar, 1983)**	**Total**	Absolute number of nannofossils/cm² (N/cm²)	Absolute number of *P. triassica*/cm² (N/cm²)	Relative abundance of *P.triassica* (%)
SO/1	0	0	0	0	0	23	0	0	1	0	**24**	9962.64	9547.53	95.83
SO/11	2	0	0	0	0	78	0	0	1	1	**82**	32559.06	30970.81	95.12
SO/17	0	0	0	0	0	27	0	0	0	0	**27**	12328.76	12328.76	100
ST4/2	0	0	0	1	0	1	0	0	0	0	**2**	830.22	415.11	50
ST4/6	0	1	1	0	0	127	0	0	2	0	**131**	54379.41	52718.97	96.94
ST4/10	0	0	0	0	0	3	0	0	0	0	**3**	1245.33	1245.33	100
ST4/14	0	0	0	0	0	19	0	0	0	0	**19**	8675.79	8675.79	100
ST4/18	0	0	0	0	0	3	0	0	0	0	**3**	1268.39	1268.39	100
ST4/22	0	0	0	0	0	27	0	0	0	0	**27**	11741.68	11741.68	100
ST4/25	2	0	0	0	0	42	0	0	0	0	**44**	19134.59	18264.84	95.45
ST4/29	0	0	0	0	0	25	0	0	0	0	**25**	9926.54	9926.54	100
ST4/32	1	0	0	0	0	29	0	0	0	0	**30**	15096.29	14593.08	96.66

ST4/36	0	0	0	0	0	100	0	0	0	0	**100**	50320.96	50320.96	100
ST4/40	2	0	0	0	0	29	0	0	1	1	**33**	14233.64	12508.35	87.87
STK A/ 103	0	0	0	0	0	1	0	0	0	0	**1**	397.06	397.06	100
STK A/106B	0	0	0	0	0	69	0	0	0	0	**69**	29761.25	29761.25	100
STK A/109A	0	0	0	0	0	74	0	0	0	0	**74**	33513.76	33513.76	100
STK A/113A	1	0	0	0	0	22	0	0	0	0	**23**	9132.42	8735.35	95.65
STK C/12E	1	1	0	1	0	114	0	1	1	1	**120**	56180.97	55076.25	95
STK A/120	0	0	0	0	0	29	0	0	0	0	**29**	10944.81	10944.81	100
STK B/16	0	1	1	0	0	327	0	1	1	0	**331**	149906.16	148094.60	98.79
STK B/19	0	0	0	0	0	245	0	0	0	0	**245**	110957.73	110957.73	100
STK B/25B	3	2	0	0	0	111	0	1	3	2	**123**	56164.38	50684.93	90.24
STK B/29A	1	2	1	0	0	205	3	0	5	0	**217**	90078.87	85097.55	94.47
STK B/37B	1	1	2	0	0	164	2	0	2	2	**174**	72229.14	68078.04	94.25
STK B/45	1	0	1	0	0	108	0	0	0	1	**111**	56316.59	54794.52	97.29
Total	**18**	**10**	**6**	**2**	**0**	**2036**	**5**	**3**	**17**	**8**	**2106**			

Table S 1- Quantification values of the different calcareous nannofossils, the absolute abundances in specimens/ cm2, the relative abundance of *P. triassica* for the 25 samples analysed at Steinbergkogel sections.

Analyte Name	Ca	Mg	Fe	Si	Al	K	Na	Sr	Mn
Calib Units	wt.%	wt.%	wt.%	wt.%	wt.%	wt.%	Ppm	ppm	ppm
SO/3	33.140	0.460	0.124	0.429	0.203	0.081	206.209	149.977	130.247
SO/17	37.207	0.898	0.179	0.335	0.152	0.062	200.953	141.426	211.890
ST4/3	35.040	0.552	0.118	0.455	0.187	0.079	288.436	173.133	90.822
ST4/14	36.046	0.543	0.038	0.127	0.065	0.073	115.121	162.415	22.328
ST4/25	39.239	0.646	0.104	0.393	0.163	0.051	177.209	214.589	61.562
ST4/31	35.756	0.519	0.060	0.190	0.096	0.033	149.800	166.597	44.893
STK A/104	33.812	0.823	0.116	0.376	0.170	0.064	165.820	148.755	101.032
STK A/108A	33.596	0.683	0.132	0.483	0.219	0.133	304.651	190.122	68.802
ST4/40	36.023	0.567	0.054	0.187	0.087	0.070	42.345	177.842	44.391
STK A/109	34.610	0.441	0.094	0.288	0.137	0.051	196.027	154.211	98.242
STK A/111A	33.137	0.738	0.178	0.698	0.298	0.149	275.422	153.075	110.909
STK A/112A	33.506	0.844	0.134	0.462	0.205	0.100	283.927	150.242	130.086
STK A/114B	33.278	0.529	0.142	0.520	0.222	0.078	210.944	159.102	181.122
STK A/119B	34.189	0.496	0.076	0.270	0.119	0.113	179.763	181.236	53.741
STK B/22A	33.498	0.832	0.150	0.509	0.225	0.123	115.574	156.222	175.816
STK B/27A	33.583	0.513	0.218	0.699	0.315	0.115	156.477	141.210	96.499
STK B/33	33.231	0.422	0.258	0.721	0.325	0.115	193.829	136.578	132.152
STK B/44	33.609	0.472	0.177	0.436	0.197	0.052	98.126	153.880	237.242

Table S 2 – Inductively coupled plasma atomic emission spectroscopy values for the Calcium, Magnesium, Iron, Silicon, Aluminium and Potassium measured in weight percent (wt. %) and for the Sodium, Strontium, Manganese measured in part per million (ppm) for the 18 samples analyzed from Steinbergkogel sections.

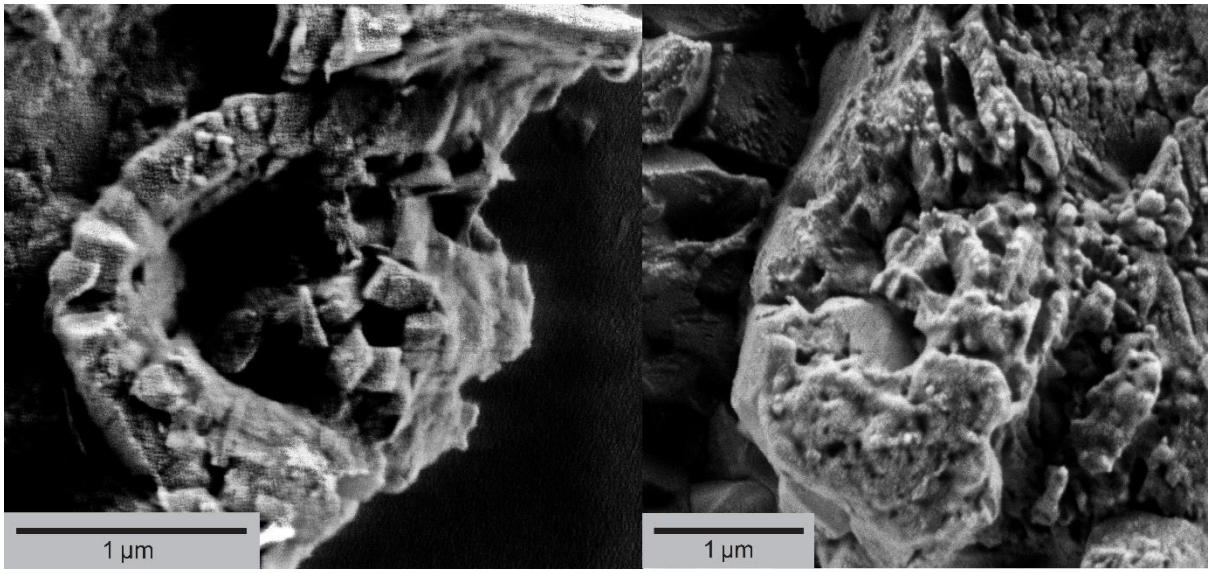

Figure S 1- Comparison between a *C. minutus* observed in the lower Rhaetian in the sample STK A/119 A and a overgrowth *C. minutus*-like with the poible central spine preserved, observed in the middle Norian in sample SO/17.

CHAPTER 3 - *EOCONUSPHAERA HALLSTATTENSIS*, SP. NOV. AND REVIEW OF THE RHAETIAN GENUS *EOCONUSPHAERA*

J. Nannoplankton Res., 39(1), 2021, pp. 77–87 ISSN 1210-8049 Printed by The Sheridan Press, USA

Isaline Demangel*

Institute of Earth Sciences, University of Graz, NAWI Graz Geocenter, Heinrichstraße 26, 8010 Graz, Austria & Department of Geology, University of Lund, Sölvegatan 12, 22362 Lund, Sweden; isaline.demangel@geol.lu.se

Richard Howe

Ellington Geological Services, 1414 Lumpkin Road, Houston, TX 77043, USA; richard.howe@ellingtongeo.com

Silvia Gardin

Centre de Recherche en Paléontologie, Sorbonne Université, Paris, France; silvia.gardin@upmc.fr

Sylvain Richoz

Institute of Earth Sciences, University of Graz, NAWI Graz Geocenter, Heinrichstraße 26, 8010 Graz, Austria & Department of Geology, University of Lund, Sölvegatan 12, 22362 Lund, Sweden; sylvain.richoz@geol.lu.se

Manuscript received 24th February, 2020; revised manuscript accepted 26th March, 2021

Abstract

The genus *Eoconusphaera* is among the few calcareous nannofossil genera that occur in the Upper Triassic. The calcareous nannofossil assemblages of three Rhaetian sections—two from the Austrian Northern Calcareous Alps and one from offshore north-western Australia—were studied using scanning electron and/or transmitted-light microscopy. Significant structural differences were observed in the inner structures of conical Rhaetian forms belonging to *Eoconusphaera*, which prompted a revision of *Eoconusphaera zlambachensis* and the description of a new species, *E. hallstattensis* sp. nov.

Keywords Calcareous nannofossils, Upper Triassic, Rhaetian, nannoliths, coccoliths, *Eoconusphaera zlambachensis*, *hallstattensis*, new species, Tethys Ocean, Tethyan, Austria, Australia

1. Upper Triassic genus *Eoconusphaera*: State of art and historical background

The first records of the family Eoconusphaeraceae go back to the 1980s with the original description of *Conusphaera zlambachensis* by Moshkovitz (1982) from the lower Rhaetian

Zlambach Formation of Austria. *Conusphaera zlambachensis* was originally described as an elongated cone, truncated at both ends, with an inner part of inclined laths and an outer mantle of vertical non-imbricating plates. One year later, Jafar (1983) described a new genus and species, *Eoconusphaera tollmanniae,* from the same area and formation. The description and figures (p. 228, figs 1-3) of *E. tollmanniae* correspond very closely with the illustrations of *C. zlambachensis* in Moshkovitz (1982, p1. 1, figs 1 – 10).

The genus *Eoconusphaera* was described by Jafar (1983) as differing from the upper Jurassic – mid-Cretaceous (Tithonian-Aptian) genus *Conusphaera* in having a dome at the broader end and lacking an axial "canal". Numerous published illustrations of *Conusphaera mexicana* (e.g. Bown and Cooper, 1989, pl. 5.2, fig. 4) show that it can have a domed shape at its wide end, so this criterion cannot be used to separate the two genera. *Conusphaera* also lacks an axial "canal", in the sense of an axial cavity running vertically up the conical nannofossil. A dark optical suture, rather than a central canal, can be seen down the axis when viewed under crossed nicols of the light microscope (e.g. Bown and Cooper, 1989, pl. 4.16, fig. 3). This optical suture is simply the axis from which the calcite laths that fill the central core radiate from, and is similar in both *Conusphaera* and *Eoconusphaera zlambachensis*. For these reasons, the two genera cannot be separated in the way intended by Jafar (1983), but instead by the inclination of the inner laths (Moshkovitz, 1982) and their disjunct stratigraphic occurrence.

Posch and Stradner (1987) discussed the detailed structure of *E. zlambachensis* and showed that the outer mantle consists of elongated, smooth, vertically-oriented plates enclosing an inner core made of 7 or 8 bundles of thin calcite laths that are obliquely stacked within each bundle – an ultrastructure which is unique to *E. zlambachensis*.

Janofske (1987) regarded the genus *Eoconusphaera* as superfluous, and recombined *E. tollmanniae* into *Conusphaera*. She regarded the species *zlambachensis* and *tollmanniae* as differing in the orientation of the inner laths – vertical in *tollmanniae* and inclined in *zlambachensis*. This distinction between the two species is not clearly shown by any of her illustrations, and has not been followed subsequently. Kristan-Tollmann (1988) regarded *E. tollmanniae* as a junior synonym of *C. zlambachensis*, making *C. zlambachensis* the type species of *Eoconusphaera* when she recombined it into *Eoconusphaera*.

A new investigation of Upper Triassic sediments from the Steinbergkogel and Zlambach sections in the Northern Calcareous Alps (NCA, Austria) has led to the observation of two different conical forms. To clarify the taxonomy and descriptions of the species belonging to the genus *Eoconusphaera*, we investigated them using both scanning electron and transmitted-light microscopy in order to observe and describe in detail the ultrastructural characteristics of these species. We added and compared LM observations made on another section, from the Northern Carnarvon Basin (NCB) in Australia, to give a more global perspective to our descriptions.

2. Materials and methods

During the Rhaetian (208.5 – 201.4 Ma; Ogg and Chen, 2020), the Austrian sections were located around 25° N (Gallet et al., 1996), on the western margin of the Neo-Tethys Ocean and the Australian sections from the Northern Carnarvon Basin, were at around 30 °S along the southern margin of the Neo-Tethys Ocean. Of the two Austrian sections analysed, the Steinbergkogel section (47.5639°, 13.6261°), is located west of the Hallstatt lake at around 1245 m above sea level (Fig.3.1). It represents a topographic high with red condensed limestone on a deep ramp setting (Richoz and Krystyn, 2015; Demangel et al., 2020; Kovács et al., 2020). The chronologically younger Kleiner Zlambach section (47.6389°, 13.6593°), is located 3 km north of the Hallstatt lake along the Kleiner Zlambach River at around 870 m height (Fig.3.1) and represents a toe-of-slope palaeo-setting with limestone and marl deposition (Richoz and Krystyn, 2015, Kovács et al., 2020; Galbrun et al., 2020).

The Australian material is from the Pluto-3 and 4 petroleum exploration wells (Woodside, 2007a, b), drilled in the Northern Carnarvon Basin, offshore Western Australia. Pluto-3 was drilled in 584.6 m water depth at -19.9119°, 115.1613° and Pluto-4 was drilled in 970.6 m water depth at -19.8487°, 115.165°. The samples studied here come from conventional cores taken in the Brigadier Formation, an offshore marine marl, deposited in a wide and shallow epicontinental sea between Australia and Greater India (Marshall and Lang, 2013). The Brigadier Formation is Rhaetian in age, based on the *Ashmoripollis reducta* spore/pollen zone and the *Dapcodinium priscum* and *Rhaetogonyaulax rhaetica* dinoflagellate zones, correlated to the Rhaetian by Helby et al. (1987, 2004).

A total of 55 samples were analysed from Austria, 24 from the 28 m thick Steinbergkogel section, and 31 from the 55 m thick Zlambach section. Two samples were examined from northwestern Australia, from cores taken in the petroleum exploration wells, Pluto 3 and 4. Smear slides for the Austrian samples were prepared following the description of Bordiga et al. (2015). The fresh rock surfaces were powdered and 0.05 g of the rock powder was mixed with 50 mL of buffered ammonia. With a micropipette, 1.5 mL of the solution were put on the coverslip and homogenised by aspiration and release. The coverslip was dried slowly, below 50°C, to avoid aggregates of sediments and mounted on the slide using Norland Optical Adhesive before drying with a UV lamp. For the Australian samples, smear slides were prepared following the methods of Bown (1998). Light microscope observations were performed on the Austrian samples with an Olympus BX50 microscope with a magnification of 2500x, and on the Australian samples with a Leitz Ortholux microscope with a magnification of 1000x. The SEM samples were prepared mainly following the method of Preto et al. (2013a, b): the samples were cut in blocks of 1 cm^2 and polished with 600 and 1200 diamonds discs using deionized water. These blocks were etched for 15 seconds in 0.1% HCl and cleaned for 7 seconds in an ultrasonic bath with distilled water. The samples were dried overnight in the oven at 50°C and finally coated with 1nm of platinum/palladium using a Cressington Sputter Coater 208HR. The observations were done with a TESCAN MIRA 3 electron microscope at Lund University.

Fig.3.1 – A) Global map of the Late Triassic with the Northern Calcareous Alps (red star) and the Northern Carnarvon Basin (red point) (modified from Scotese, 2004; Golonka, 2007, Nakada et al., 2014). B) Simplified map of Austria with the studied sections (red stars) and two localities cited in the literature (blue stars; modified from Gardin et al., 2012). C) Map of northwestern Australia, showing Pluto 3 and 4 in the Northern Carnarvon Basin (red circle; modified from Marshall and Lang, 2013).

3. Systematic palaeontology

The studied sections contain several calcareous nannofossil species characteristic of the Rhaetian. The spherical nannolith *Prinsiosphaera triassica* is abundant, as are the two species of *Eoconusphaera* described here, *E. zlambachensis* and *E. hallstattensis* sp. nov. Three species of coccolithophorids were observed, *Crucirhabdus minutus*, *C. primulus* and

Archaeozygodiscus koessenensis. Three calcisphere species are also present, *Thoracosphaera* sp., *Obliquipithonella* sp. and *Orthopithonella* sp.

The species belonging to the genus *Eoconusphaera* are considered by most workers as nannoliths, of unknown affinity. However, the following evidence shows a likely affinity to the coccolithophorids. Their morphology (conical shape, outer mantle with narrow vertical elements, core filled with complexly arranged elements, and also size; Figure 3.2) is similar to the coccolith species *Calcivascularis jansae* Wiegand (1984), which occurs in the Lower Jurassic (Sinemurian – lower Toarcian). Although *C. jansae* has a similar overall morphology to *Eoconusphaera*, it is not closely related, as its evolution from the protolith coccolith genus *Mitrolithus* is well understand (Young et al., 1986, Bown, 1987). *Eoconusphaera* and the coccolithophorids seem to have a similar palaeoenvironmental preference with first occurrences in the same palaeolatitude (i.e. subtropical) (Jafar, 1983; Gardin et al., 2012; Demangel et al., 2020). They both seem to occur and evolve first in subtropical zones, getting dispatched to the tropical zone only during the latest Rhaetian, while other nannoliths such as *Prinsiosphaera triassica* are present in both palaeolatitudes since the Norian (Jafar, 1983; Bralower et al., 1991). However, these species could not be assigned to either *Crucirhabdus* or *Archaeozygodicus*. The absence of a proximal cycle in the specimens observed under light microscopy prevent us from inferring a clear affinity with *Crucirhabdus,* and the presence of an outer cycle of vertical, non-imbricating elements does not correspond to *Archaeozygodiscus*.

The optical birefringence was investigated under polarized light with a gypsum plate to observe the crystallographic orientation. In both species, the outer mantle in N-S position appears yellow on the left-hand side and blue on the right-hand side (*E. hallstattensis*: Pl. 1 15d, 17b; *E. zlambachensis*: Pl. 2 10b, 11b, 13d, 14b) then goes into extinction at 45° (*E. hallstattensis*: Pl. 1 15b, 17d; *E. zlambachensis*: Pl. 2 10d, 13b, 14d). This suggested sub-radial orientations with the c-axes tapering for the outer mantle. The inner core elements show minimum birefringence in the N-S and E-W positions then yellow colour at 45° suggesting sub-vertical c-axes. This set of orientations is common among the Upper Triassic coccoliths (Young et al., 1992) giving new evidence for an affinity between them and *Eoconusphaera*.

The formal definition of our new species is presented below in accordance with the *International Code of Nomenclature for algae, fungi, and plants* (*Shenzhen Code*) (Turland et al., 2018).

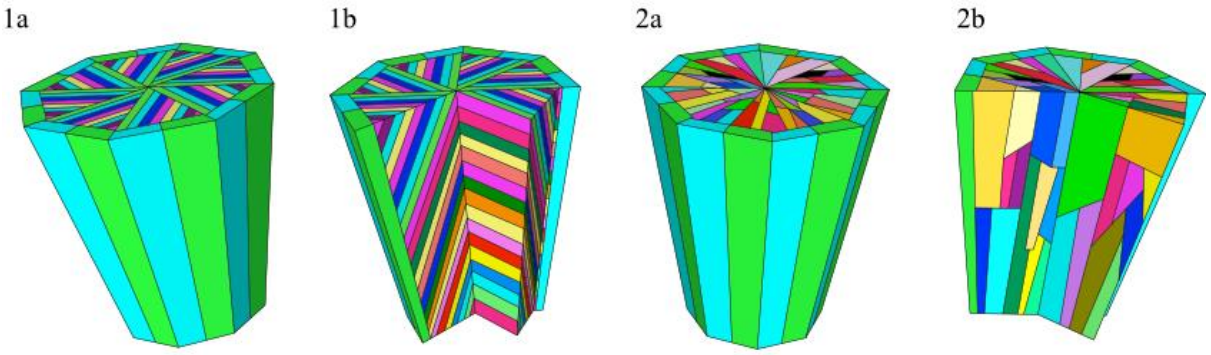

Fig.3.2 – Schematic representation of 1: *Eoconusphaera zlambachensis*; 2: *E. hallstattensis* with a: the outer mantle and top view and b: the inner core view showing the orientation of the inner laths. Note that the colours aid visualization of the structure but have no particular significance.

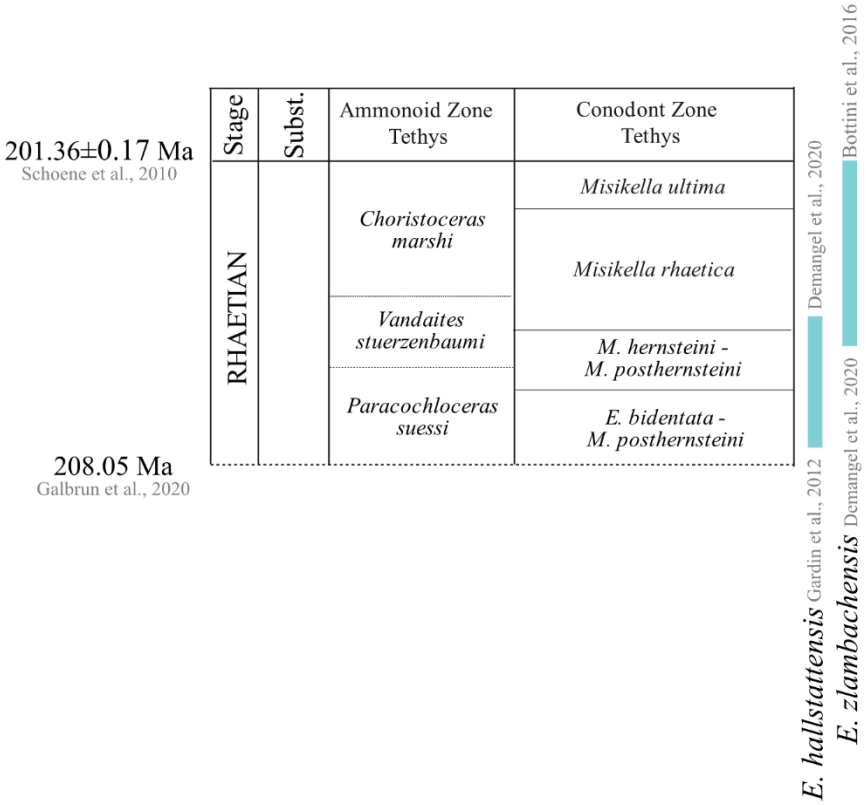

Fig.3.3 – Rhaetian biozonation based on ammonoids and conodonts for the Tethys realm (Galbrun et al., 2020, Ogg et al., 2020) along with the ranges of the *Eoconusphaera* species discussed here.

Family **EOCONUSPHAERACEAE** Kristan-Tollmann, 1988

Genus *Eoconusphaera* Jafar, 1983

Eoconusphaera hallstattensis sp. nov.

Plate 1, figs 1 – 18

1991 *Eoconusphaera zlambachensis* (Moshkovitz, 1982) Bown & Cooper (1989) Bralower et al.: pl. IX, figs 7-11, ?*non* fig. 6

2012 *Eoconusphaera zlambachensis* (Moshkovitz, 1982) Kristan-Tollmann (1988) Gardin et al.: figs. 6 J-I

2020 *Eoconusphaera hallstattensis* (Moshkovitz, 1982) Kristan-Tollmann (1988) Demangel et al.: fig 5 A.

Derivation of name: This species is named after the Hallstatt Formation, Northern Calcareous Alps (Austria), where the first specimens of this new species were found.

Diagnosis: Elliptical (Pl. 1, fig. 3) to sub-circular (Pl. 1, fig. 8) conical nannofossil, truncated at both ends with a flat to domed distal end (Pl. 1, figs 1; 7; 10; 11 – 12; 14 – 15; 16; 18). The outer mantle of elements is composed of tall, flat, laths vertically oriented without imbrication or overlap (Pl. 1, figs 1; 3; 4; 7; 9; 10). The number of outer elements observed is at least 12-14, though overgrowth can obscure this number. The inner core is composed of tall, thin elements that are oriented vertically to sub-vertically, and radially in plan view. No canal is visible, only a central suture corresponding to the radiating axis of the inner core laths (Pl. 1, figs 3; 8; 16; 18). The inner elements are of different lengths, and irregularly overlap each other. They end in a flat to domed shape on the wide end of the truncated cone. Under the light microscope, this species presents a trapezoid shape with the flat outer mantle clearly visible and showing first order grey high birefringence (Pl. 1, figs 2; 11 - 18). The inner part appears as if composed of several undulating bars of different length or small blocks, parallel to the outer mantle elements. The undulation effect is a result of the bundles of overlapping inner elements. At the wide end of the nannofossil, the core can protrude beyond the outer mantle

(Pl. 1, figs 1; 10; 14 – 15; 16c; 18a). The height of *E. hallstattensis* ranges from 2.0 (Pl. 1, fig. 17) to 5.8 µm, the width at the wide end varies from 1.1 to 3.1 µm and the width at the narrow end, between 1.0 and 2.4 µm.

Differentiation: *E. hallstattensis* and *E. zlambachensis* exhibit many similarities under the SEM, but show distinctly different organisation of the elements in the core, with irregularly overlapping vertical laths in *E. hallstattensis* n. sp. and clearly oblique bundles of regularly arranged laths in *E. zlambachensis*. Also, *E. hallstattensis* n. sp. nov. does not show an axial suture under crossed nicols, while *E. zlambachensis* does. The two species can be easily distinguished under the light microscope due to their different inner structure. Finally, the two species are dominant in distinct stratigraphic intervals: *E. hallstattensis* is abundant during the early Rhaetian (*Paracochloceras suessi* to the base of *Vandaites stuerzenbaumi* ammonoids zones; *Epigondolella bidentata* - *Misikella posthernsteini* and *M. posthernsteini*- *Misikella hernsteini* conodonts zones) while *E. zlambachensis* dominates in the middle and late Rhaetian (*V. stuerzenbaumi* and *Choristoceras marshi* ammonoids zones; *Misikella rhaetica* and *Misikella ultima* conodonts zones) (Fig. 3.3).

E. hallstattensis sp. nov. differs from *Calcivascularis jansae* (Wiegand, 1984) (Sinemurian - Toarcian) by its disjunct stratigraphic level, and distinctly different ultrastructure of the central core. *C. jansae* has vertical laths in the lower part of the core, with a complex spine above this which fills the central area, while *E. hallstattensis* has irregularly overlapping vertical laths filling the core.

Remarks: *E. hallstattensis* presents a broad range of size from low and stubby (Pl. 1, figs 4; 17 - 18) to high and narrow (Pl.1, figs 5; 16) with several medium-sized specimens in between (Pl 1, figs 1; 6; 7; 9; 11; 11 - 15). The height varies between 2.4 and 5.8 µm, the width at the distal end between 1.1 and 3.1 µm and the width at the proximal end between 1.0 and 2.4 µm. The thickness of the mantle and the inner laths can vary mostly due to the preservation, thus the appearance of the inner laths under the light microscope can vary from long bars to small blocks. *E. hallstattensis* presents a protolith outer wall with small, low rim specimens being only slightly higher than the similar protolith rim of *C. minutus*, suggesting they could be closely related.

Holotype: Plate 1, fig. 1. Catalogue number 219913 (Pl.1, fig.1). Collection of Universalmuseum Joanneum, Department for Geology and Palaeontology, Graz, Austria.

Dimensions: Holotype length = 2.6 µm; Holotype large diameter = 1.6 µm; Holotype narrow diameter = 1.4 µm.

Paratypes: Plate 1, figs 2 – 5. Catalogue numbers 219913 (sample Zl 6.4202 for the paratype figs 2; 3; 5) and 219915 (samples Zl 35.9311 for the paratype Fig. 4). Collection of Universalmuseum Joanneum, Department for Geology and Palaeontology, Graz, Austria.

Type locality: Holotype from Kleiner Zlambach, Northern Calcareous Alps, Austria (section base: 46.6464°, 13.673°; top: 46.6457°, 13.6675°).

Type level: Lower Rhaetian (*Paracochloceras suessi ammonoids Zone; Epigondolella bidentata - Misikella posthernsteini* conodonts Zone), Upper Triassic, sample Zl 6.4202, 6.4 m above the base of the Kleiner Zlambach section.

Geographical occurrence: The oldest specimens reported so far are at the base of the Rhaetian in the Steinbergkogel section (Gardin et al., 2012). This species is rare in the Hallstatt Formation of the Steinberkogel section (Demangel et al., 2020), and is widespread in the Zlambach Formation of the examined samples of the Kleiner Zlambach section (both oceanic-open Hallstatt basin, Northern Calcareous Alps, Austria). This species was also observed in the Kössen Formation (intraplatform Eiberg basin, Northern Calcareous Alps, Southern Germany; Janofske, 1987) and in ODP Leg 122 (Wombat Plateau; North-West Australia) where the species has a low abundance (rare to few; Bralower et al., 1991; SG unpublished data, 2017). It is common in the lower Rhaetian in the Northern Carnarvon Basin of Western Australia (RH, unpublished data, 2018).

Stratigraphical occurrence: This species ranges through the Rhaetian (Upper Triassic) from the *Paracochloceras suessi* to the *V. stuerzenbaumi* ammonoids zones (*E. bidentata – M. posthernsteini* to *M. rhaetica* conodonts zones) in Austria and in the lower Rhaetian, i.e in the *R. rhaetica* dinoflagellate zone in Australia. The highest occurrence of the species observed so far is in the upper *V. stuerzenbaumi* ammonoid Zone/ *M. rhaetica* conodont Zone in the Zlambach Formation of the Northern Calcareous Alps, Austria.

Eoconusphaera zlambachensis (Moshkovitz, 1982), Bown and Cooper, 1989, emend. Demangel, Howe, Gardin, Richoz

Plate 2, figs 1 – 17

1982 *Conusphaera zlambachensis* Moshkovitz: pp. 612 – 613, pl. 1, figs 1 – 10 (Holotype = figs 1 – 3)

1983 *Eoconusphaera tollmanniae* Jafar: pp. 228-229, figs. 6, 1-3

1987 *Conusphaera zlambachensis* Moshkovitz (1982) Janofske: p. 49, pl. 2, figs 6-8

1987 *Conusphaera tollmanniae* (Jafar, 1982) Janofske: p. 49, pl. 2, figs 1-5

1987 *Conusphaera zlambachensis* Moshkovitz (1982) Bown: p.72, pl. 11, fig 1-3; pl. 15, figs. 13-14.

1987 *Conusphaera zlambachensis* Moshkovitz (1982) Posch & Stradner: p. 232, text-fig. 6, pl. 1, figs 1-7

1988 *Eoconusphaera zlambachensis* (Moshkovitz, 1982) Kristan-Tollmann: p. 77

1989 *Eoconusphaera zlambachensis* (Moshkovitz, 1982) Kristan-Tollmann, 1988 – Bown and Cooper: p. 104, Pl. 5.1, figs 1 – 8

1995 *Eoconusphaera zlambachensis* (Moshkovitz, 1982) Kristan-Tollmann, 1988 – Kristan-Tollmann: pp. 2 - 4, pl.1, figs. 1-6.

2010 *Eoconusphaera zlambachensis* (Moshkovitz, 1982) Kristan-Tollmann (1988) Clemence et al.: fig. 11 c, k

2016 *Eoconusphaera zlambachensis* (Moshkovitz, 1982) Kristan-Tollmann (1988) Bottini et al.: figs. 5 – 8.

Derivation of name: Species name was given after the Zlambach Marl (now called Zlambach Formation) where the first specimens were found.

Original Diagnosis: "*Elongated cone, truncated at both ends, composed of some 35 to 40 inner calcitic lamellae, closely packed and radiating from the centre of the cone. When viewed from the narrower base, the lamellae are seen to be inclined and arranged in a sinistrally turning spindle (Pl. 1, figs 3, 4, 6 [in Moshkovitz, 1982; herein, Pl. 2, figs 2, 3, 5, 8]). The outer surface of the cone is covered by elongated, smooth plates, each one separated from the other [herein Pl.2, figs 2, 5, 7]. In LM, the form is too small to reveal the fine details of the lamellae and only the general conical shape and the cover plates, which in many specimens have fallen out (Pl. 1, figs 4, 5 [in Moshkovitz, 1982]) could be discerned (Pl. 1, figs 7, 8 [in Moshkovitz, 1982])"*.

Emended description: In addition to the presence of a core with approximately eight bundles of radially arranged (Posch and Stradner, 1987), our observations highlighted additional characteristics, i.e. the inclination of the calcite laths (between 150 and 159º, Pl. 2, figs 2; 5; 8). Similar to *E. hallstattensis*, specimens were observed with a dome-shape on the wider extremity formed by an extension of the inner laths (Pl. 2, figs 3; 5; 11; 14; 16), which can be enclosed by the outer mantle of elements if preserved (Pl. 2, figs 3; 11; 12; 14). Less frequently and only observed under the SEM, *Eoconusphaera zlambachensis* can also present a dome structure on the narrow extremity, formed by the outer mantle laths joining at the top and more or less closing the extremity regarding preservation (Pl. 2, fig. 2). Under the light microscope, *E. zlambachensis* shows also a more trapezoid shape than that of *E. hallstattensis* n. sp. Because the laths of the inner core in *E. zlambachensis* are very thin (< 0.5 µm thick), they cannot be distinguished from each other optically. Hence, the inner core appears as a homogenous birefringent block at all angles to the polariser. A thin dark line, reflecting the central axis, from which the laths of the inner core radiate, is visible in some orientations.

Differentiation: *E. zlambachensis* differs from *E. hallstattensis* by the inclination of the laths in the inner core, its appearance under the light microscope (see description above), more circular extremities and its dominance in the *V. stuerzenbaumi* and *C. marshi* ammonoids zones, *M. rhaetica* and *M. ultima* conodonts zones.

Dimensions of observed specimens: In our study, the length of the specimens varies between 2.2 µm and 4.8 µm, with the width of the wide end varying between 1.4 µm and 3 µm, the width of the narrow end varying from 1 µm to 2.5 µm. Holotype dimensions: Length = 8 µm; width of wide end = 5 µm and width of narrow end = 3.5 µm (Moshkovitz, 1982).

Geographical occurrence: According to Moshkovitz (1982): widespread in the Zlambach Formation (oceanic-open Hallstatt basin) at Fischerwiese and Roßmoosgraben sections, less frequent in the Kössen Formation (intraplatform Eiberg basin) at Kendlbachgraben section. According to Jafar (1983): not common in Fischerwiese section (Zlambach Formation) and rare in Ampelsbach section (Kössen Formation). Bown and Cooper reported a high abundance (i.e. 10 – 20 specimens per field of view at 1000x, 50% of the assemblage) at Weißloferbach section (Kössen Formation). According to Kristan-Tollmann (1995), the species is as common as *P. triassica* in the Grünbachgraben section (Zlambach Formation). Clemence et al. (2010) report a high relative abundance in Eiberg (i.e. 20 – 40 % of the assemblages) and a lower one in Tiefengraben (i.e. 10 – 15 %) (both Kössen Formation). All localities are from the Northern Calcareous Alps, Austria. Bralower et al., (1991) report this species being common in the Upper Triassic of the Wombat Plateau, offshore Western Australia. It is very common (up to 100 – 150 specimens per field of view at 1000x) in the Brigadier Formation in the Northern Carnarvon Basin, offshore Western Australia (RH, unpublished data, 2018).

Stratigraphic range: Upper Triassic, Rhaetian (lower *V. stuerzenbaumi* Zone - *C. marshi* ammonoids zones, *M. posthernsteini-M. hernsteini* Zone to the *M. ultima* conodonts Zone).

Remarks: This specimens called *E. zlambachensis* by Bralower et al. (1991) do not closely resemble the holotype of this species. The inner core in these specimens, figured on light microscope photographs (Bralower et al., 1991, pl. IX, figs 7 – 11), do not show the typical continuous birefringence pattern of *E. zlambachensis*, so they are considered here to belong to *E. hallstattensis* n. sp.

The specimens illustrated by Bottini et al. (2016) in Pl. 1, figs 5 – 8 are poorly preserved, but under the light microscope show continuous laths in the core, which suggests they are closer to *Eoconusphaera zlambachensis* than *E. hallstattensis* sp. nov. which has discontinuous laths in the core.

Conclusion

This study clarifies the taxonomy of the two species in the genus *Eoconusphaera* in the Late Triassic. A new species, *E. hallstattensis*, is described with two differentiating

characteristics: the absence of an axial suture under crossed nicols and the presence of numerous overlapping vertical inner laths, which appear as undulating bars under the light microscope. *E. zlambachensis* has been emended to include the inner inclined (~154°) laths arranged in bundles, sometimes with a dome shape on the wider extremity like *E. hallstattensis* but also, less frequently, on the narrow extremity. In addition to the different structural characteristics (inner laths shape and orientation), these two species dominate in different stratigraphic intervals. *E. hallstattensis* first occurs in the *P. suessi* Zone and dominates from the *P. suessi* until the base of the *V. stuerzenbaumi* zone. *E. zlambachensis* appears at the base of the *V. stuerzenbaumi* and dominates during the *V. stuerzenbaumi* and *C. marshi* zones. We suggest that these two species might be useful biostratigraphic markers for the latest Triassic in the Western Tethys.

Acknowledgements This research was supported by the Austrian Science Foundation (Project P 29497-P29 to Sylvain Richoz). The SEM observations were supported by the Royal Physiographic Society of Lund (grand to Isaline Demangel). We thank Werner E. Piller for his advice for the taxonomic description and his help during the early stage of the manuscript improving the English. We strongly thank Jeremy Young for his careful review, his suggestion and help to integrate crystallographic orientation analyses to improve the manuscript. We also thank Matt Hampton for his critical comments and interesting interpretations.

References

Bordiga, M., Bartol, M., Henderiks, J., 2015. Absolute nannofossil abundance estimates: Quantifying the pros and cons of different techniques. Revue de micropaléontologie, 58: 155 – 165. 10.1016/j.revmic.2015.05.002.

Bottini, C., Jadoul, F., Rigo, M., Zaffani, M., Artoni, C., Erba, E., 2016. Calcareous nannofossils at the Triassic/Jurassic boundary: Stratigraphic and paleoceanographic

characterization. Rivista Italiana di Paleontologia e Stratigrafia (Research in Paleontology and Stratigraphy), 122(3): 141 – 164. 10.13130/2039-4942/7726.

Bown, P.R., 1987. Taxonomy, evolution, and biostratigraphy of Late Triassic-Early Jurassic Calcareous Nannofossils. Special paper in Paleontology, 38: 1 – 118.

Bown, P.R., Cooper, M.K.E., 1989. Conical calcareous nannofossils in the Mesozoic. In: Crux, J.A., Heck, S.E. (Eds.), Nannofossils and their applications. Br. Micropaleontology Society, Ellis Horwood, Chichester: 98 – 106.

Bown, P.R., 1998. Calcareous Nannofossil Biostratigraphy. Chapman & Hall, First, London.

Bralower, T.J., Bown, P.R., Siesser, W.G., 1991. Significance of Upper Triassic nannofossils from the Southern Hemisphere (ODP Leg 122, Wombat Plateau, N.W. Australia) – Marine Micropaleontology, 17: 119 – 154. 10.1016/0377-8398(91)90025-2.

Clémence, M.E., Gardin, S., Bartolini, A., Paris, G., Beaumont, V., Guex, J., 2010. Bentho-planktonic evidence from the Austrian Alps for a decline in sea-surface carbonate production at the end of the Triassic. Swiss Journal of Geosciences, 103: 293 – 315. 10.1016/j.palaeo.2010.05.021.

Demangel, I., Kovacs, Z., Richoz, S., Gardin, S., Krystyn, L., Baldermann, A., Piller, W. E., 2020. Development of early calcareous nannoplankton in the Northern Calcareous Alps (Austria) in the Late Triassic. Global and Planetary Change, 193, 103254, 10.1016/j.gloplacha.2020.103254.

Galbrun, B., Boulila, S., Krystyn, L., Richoz, S., Gardin, S., Bartolini, A., (2020): « Short » or « long » Rhaetian? Astronomical calibration of Austrian key sections. Global and Planetary Change. 192, 103253. 10.1016/j.gloplacha.2020.103253.

Gallet, Y., Besse, J., Krystyn, L., Marcoux, J., 1996. Norian magnetostratigraphy from the
Scheiblkogel section, Austria: constraint on the origin of the Antalya Nappes, Turkey. Earth and Planetary Science Letters 140 (1 – 4), 113 – 122. 10.1016/0012-821X(96)00044-1.

Gardin, S., Krystyn, L., Richoz, S., Bartolini, A., Galbrun, B., 2012. Where and when the earliest coccolithophores? – Lethaia, 45: 507 – 523. 10.1111/j.1502-3931.2012.00311.x.

Golonka, J., (2007): Late Triassic Early Jurassic palaeogeography of the world. Palaeogeography, Palaeoclimatology, Palaeoecology, 244, 297 – 307. 10.1016/j.palaeo.2006.06.041.

Helby, R., Morgan, R., Partridge, A.D., 1987. A palynological zonation of the Australian Mesozoic. In Jell, P.A. (Ed.), Studies in Australian Mesozoic Palynology. Association of Australasian Palaeontologists Memoir, 4, 1 – 85.

Helby, R., Morgan, R., Partridge, A.D., 2004. Updated Jurassic–Early Cretaceous dinocyst zonation NWS Australia. Geoscience Australia, ISBN 1 920871 01 2.

Jafar, S.A., 1983. Significance of Late Triassic calcareous Nannoplankton from Austria and Southern Germany. Neues Jahrbuch für Geologie und Paläeontologie, 166: 218 – 259.

Janofske, D., 1987. Kalkige Nannofossillien aus der ober-Trias (Rhät)der Nördlichen kalkalpen. Berliner geowissenschaftliche abhandlungen, 86: 45 – 67.

Kovacs, Z., Demangel, I., Richoz, S., Hippler, D., Baldermann, A., Krystyn, L., 2020. New constraints on the evolution of $^{87}Sr/^{86}Sr$ of seawater during the Upper Triassic. Global and Planerary Change, 192, 103255, 10.1016/j.gloplacha.2020.103255.

Kristan-Tollmann, E., 1988. Coccolithen aus den alterenallgiiuschichten (alpiner lias, sinemur) von timor, indonesian. Geologisch-Paläontologische Mitteilungen Innsbruck, 15: 71 – 83.

Kristan-Tollmann, E., 1995. Weitere Beobachtungen an Rhätischen nannofossilien der Tethys. Geologisch-Paläontologische Mitteilungen Inssbruck, 20: 1 – 11.

Marshall, N., Lang, S., 2013. A New Sequence Stratigraphic Framework for the North West Shelf, Australia. In: Keep, M. and Moss, S.J. (Eds), The Sedimentary Basins of Western Australia 4: Proceedings of Petroleum Exploration Society of Australia Symposium. Petroleum Exploration Society of Australia, Perth. 1 – 32.

Moshkovitz, S., 1982. On the findings of a new calcareous nannofossil (*Conusphaera zlambachensis*) and other calcareous organisms in the Upper Triassic sediments of Austria. Eclogae Geologicae Helvetiae, 75: 611 – 619. 10.5169/seals-165245.

Nakada, R., Ogawa, K., Suzuki, N., Takahashi, S., Takahashi, Y., (2014): Late Triassic compositional changes of eolian dusts in the pelagic Panthalassa: response to the continental climatic change. Palaeogeography, Palaeoclimatology, Palaeoecology, 393, 61 – 75. 10.1016/j.palaeo.2013.10.014.

Ogg, J.G., Chen, Z.-Q., Orchard, M. J., Jiang, H.S., (2020): The Triassic Period. In: Gradstein, F. M., Ogg, J.G., Schmitz, M.D., Ogg, G.M. (Eds), The Geologic Time Scale 2020, Amsterdam, Elsevier. 903 – 953. 10.1016/B978-0-12-824360-2.00025-5.

Posch, F., Stradner, H., 1987. Report on Triassic Nannoliths from Austria. Abhandlungen der Geologischen Bundesanstalt, 39: 231 – 237.

Preto, N., Agnini, C., Rigo, M., Sprovieri, M., Westphal, H., 2013a. The calcareous nannofossil *Prinsiosphaera* achieved rock-forming abundances in the latest Triassic of western Tethys: consequences for the $\delta^{13}C$ of bulk carbonate – Biogeosciences, 10: 6053 – 6068. 10.5194/bg-10-6053-2013.

Preto, N., Willems, H., Guaiumi, C., Westphal, H., 2013b. Onset of significant pelagic carbonate accumulation after the Carnian Pluvial Event (CPE) in the western Tethys – Facies, 59: 891 – 914. 10.1007/s10347-012-0338-9.

Richoz, S., Krystyn, L., 2015. The Upper Triassic events recorded in platform and basin of the Austrian Alps. The Triassic/Jurassic GSSP and Norian/Rhaetian GSSP candidate – Berichte der Geologischen Bundesanstalt, 111.

Schoene, B., Guex, J., Bartolini, A., Schaltegger, U., Blackburn, T.J., (2010). Correlating the end-Triassic mass extinction and flood basalt volcanism at the 100 ka level. Geology, 35 (5), 387 – 390. 10.1130/G30683.1.

Scotese, C.R., (2004): A continental drift flipbook. The Journal of Geology, 112, 729 – 741. 10.1086/424867.

Turland, N. J., Wierema, J. H., Barrie, F. R., Greuter, W., Hawksworth, D.L., Herendeen, P. S., knapp, S., Kusber, W.-H., Li, D.-Z., Marhold, K., May, T.W., McNeill, J., Monro, A. M., Prado, J., Price, M. J. & Smith, G. F. (eds.) 2018: *International Code of Nomenclature for algae, fungi, and plants (Shenzhen Code) adopted by the Nineteenth International Botanical Congress Shenzhen, China, July 2017.* Regnum Vegetabile 159. Glashütten: Koeltz Botanical Books. 10.12705/Code.2018.

Wiegand, G. E., 1984. Two New Genera of Calcareous Nannofossils from the Lower Jurassic. Journal of Paleontology, 58 (4), 1151 – 1155.

Woodside Energy Ltd., 2007a. Well completion report Pluto-3 & ST1 Basic Data (WA-350-P, Carnarvon Basin). Unpublished report by Woodside Energy Ltd., publicly available from the NOPIMS website, www.nopims.ga.gov.au.

Woodside Energy Ltd., 2007b. Well completion report Pluto-4 Basic Data (WA-350-P, Carnarvon Basin). Unpublished report by Woodside Energy Ltd., publicly available from the NOPIMS website, www.nopims.ga.gov.au.

Young, J. R., Teale, C. T. & Bown, P. R., 1986. Revision of the stratigraphy of the Longobucco Group (Liassic, southern Italy); based on new data from nannofossils and ammonites. Eclogae Geologicae Helvetiae, 79(1), 117 – 135.

Young, J. R., Didymus, J. M., Bown, P. R., Prins, B., Mann, S., 1992. Crystal assembly and phylogenetic evolution in heterococcoliths. Nature, 356, 516 – 518.

Plate 1

Eoconusphaera hallstattensis SEM & LM images. 1–15: Zlambach, Austria; 16–18: Australia

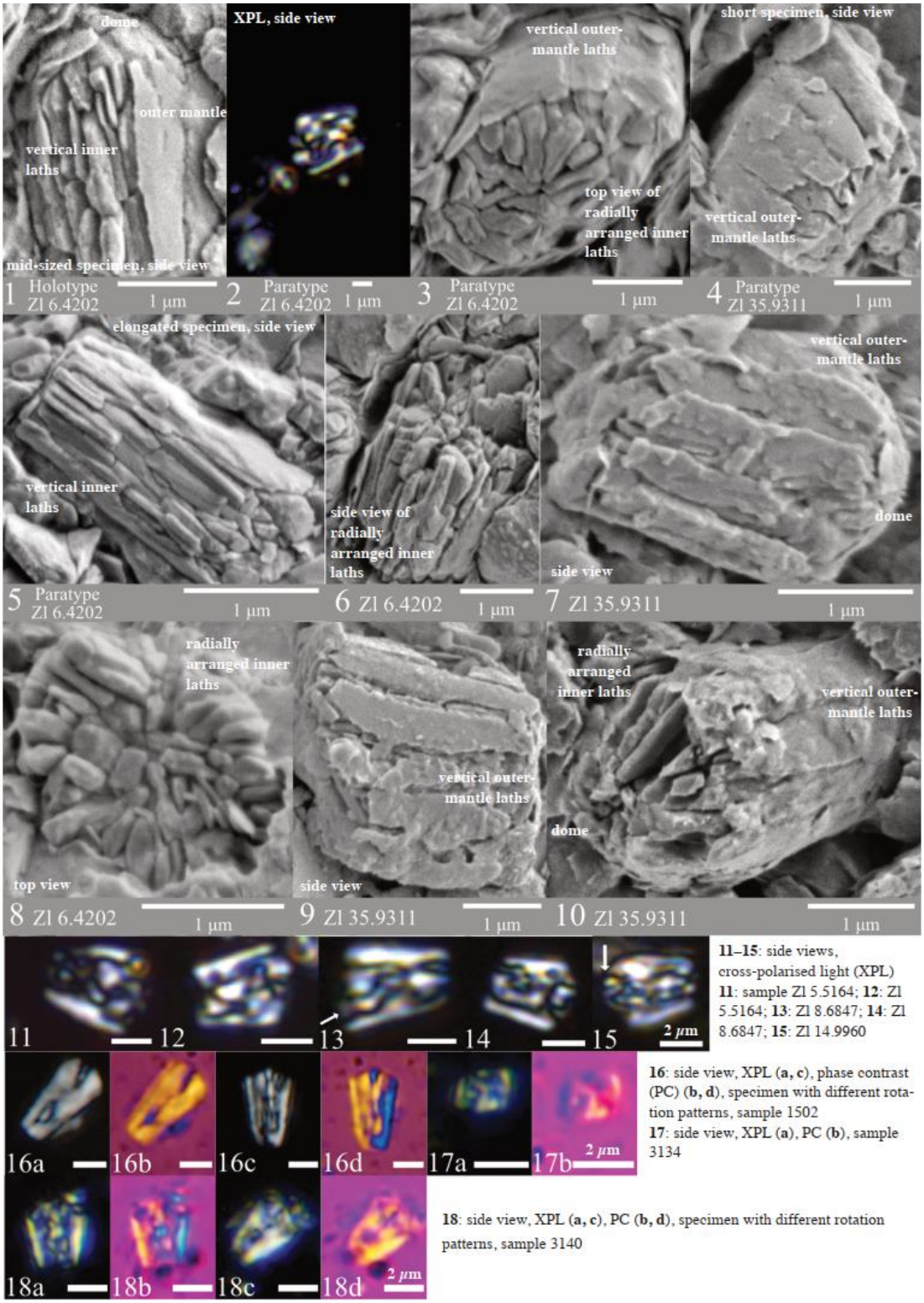

11–15: side views, cross-polarised light (XPL) **11**: sample Zl 5.5164; **12**: Zl 5.5164; **13**: Zl 8.6847; **14**: Zl 8.6847; **15**: Zl 14.9960

16: side view, XPL (**a, c**), phase contrast (PC) (**b, d**), specimen with different rotation patterns, sample 1502
17: side view, XPL (**a**), PC (**b**), sample 3134

18: side view, XPL (**a, c**), PC (**b, d**), specimen with different rotation patterns, sample 3140

Plate 2

Eoconusphaera zlambachensis SEM & LM images. 1–12: Zlambach, Austria; 13–17: Australia

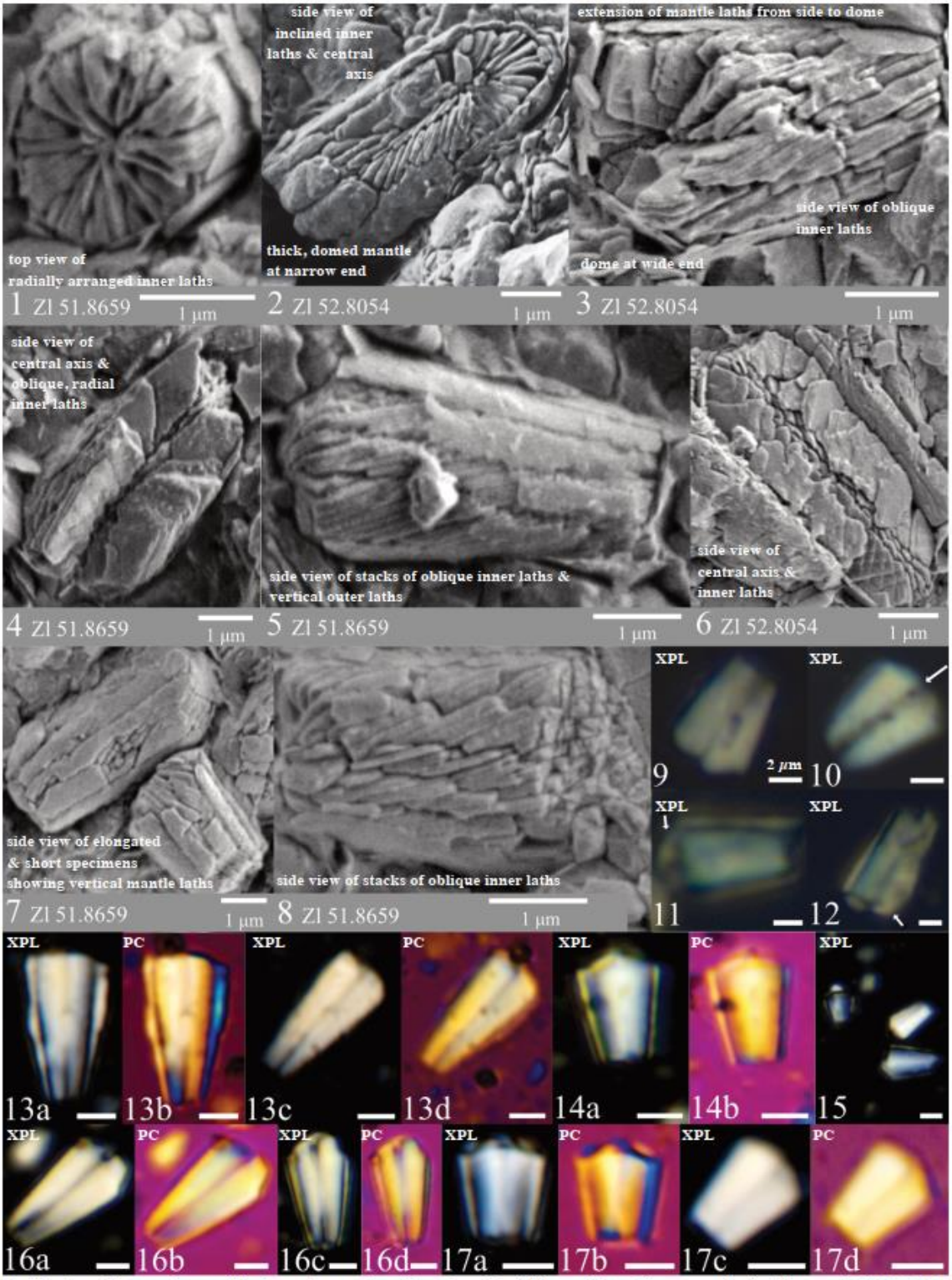

9–12: side views of four specimens with a dome shape at the wide end, mantle visible as pale lateral bars, central axis dark, sample Zl 51. 8659. **13**: side view of specimen with different rotation patterns, sample 1499. **14**: side view, sample 3143. **15**: side view of three specimens, sample 3150. **16**: side view of specimen with different rotation patterns, sample 3146. **17**: side view of specimen with different rotation patterns, sample 1501

CHAPTER 4 – LATE TRIASSIC CALCAREOUS NANNOFOSSILS IN NORTH DOBROGEAN OROGEN (ROMANIA): FIRST EVIDENCE FOR THE PALAEO-TETHYS

Isaline Demangel [1,2], Eugen Grădinaru [3]

[1] *Institute of Earth Sciences, University of Graz, NAWI Graz Geocenter, Graz, Austria*

[2] *Department of Geology, University of Lund, Lund, Sweden*

[3] *Department of Geology, Faculty of Geology and Geophysics, University of Bucarest, Bd. Bălcescu Nicolae 1, 010041 Bucharest, Romania.*

Keywords: *Prinsiosphaera triassica*; *Eoconusphaera zlambachensis*; Rhaetian; Frecătei; Borehole 816 LV; palaeo-Tethys

Abstract

Analyses of Upper Triassic sediments from five sections in North Dobrogea (Romania) has revealed the presence of two calcareous nannofossil species, *Prinsiosphaera triassica* and *Eoconusphaera zlambachensis.* Both were common, when present in the sample, and allowed us to assign the sediments to the Rhaetian. Coccolith-like forms were also observed rising the possibility of their presence in Romania in well-preserved sections. This constitutes the first record of Late Triassic calcareous nannofossils in the Paleo-Tethys Ocean.

1. Introduction

Calcareous nannofossil assemblages from the Late Triassic are dominated by the incertae sedis *Prinsiosphaera triassica*. This species is known at least since the middle Norian (Alaunian) (Fischer et al., 1967) below the first appearance of the coccolithophorids, observed also from the middle Norian (Alaunian – *Halorites macer* ammonoid Zone) (Demangel et al., 2020) and the Eoconusphaeraceae reported since the lower Rhaetian (*Paracochloceras suessi* Zone) (Demangel et al., 2021). From the middle Rhaetian (*V. stuerzenbaumi* Zone), the sub-species *P. triassica crenulata* appears (Demangel et al., submitted). Calcareous nannofossils are well described and reported from the Neo-Tethys and western Europe such as in Austria, England, France, Germany, Italy (e.g. Prins, 1969; Moshkovitz, 1982; Jafar, 1983; Janofske, 1987; Posch and Stradner, 1987; Bown, 1987; Bown and Cooper, 1989; Bralower et al., 1991; Bown, 1998, Gardin et al., 2012, Preto et al., 2013, Demangel et al., 2020, 2021). Record of

Late Triassic calcareous nannofossils in Palaeo-Tethys and Eastern Europe are almost inexistent. Koiava et al. (2015) reported calcareous nannofossils including *Prinsiosphaera triassica*, *Crucirhabdus minutus* and *C. primulus* from Georgia (Caucasus). The specimens illustrated seems badly preserved with overgrowth of the calcite crystals. The identifications are doubtful, i.e. lack of circular structure and inner calcite lamellae for the specimens reported as *P. triassica* (Plate 1, 1 – 6) and the coccoliths rims and inner structure are not visible for the specimens 16 and 18 (Plate 1) define as *C. minutus* and *C. primulus*. However, the specimen 17 (Plate 1), reported as a *C. primulus*, present a clear rim with a size corresponding to the Upper Triassic coccoliths but the inner structure in not visible so the identification at the species level is not possible. In this study, we investigated five sections of the North Dobrogea (Romania) to observe a possible trace of calcareous nannoplankton existence during the Norian and Rhaetian.

2. Geological settings and stratigraphic data

North Dobrogea, in Romania, is an Alpine fold and thrust belt, commonly named the north Dobrogean Orogen (Săndulescu, 1984, 1995). It is located in the south of the Danube Delta and northwest of Black Sea. The North Dobrogea Orogen (NDO) is tectonically bounded by the Galaţi-Sf. Gheorghe Fault, at north, and the Peceneaga-Camena Fault, at south (Fig. 4.1). The NDO corresponds to a Late Permian-Middle Triassic rifted basin that was inverted during Late Triassic, Jurassic and Early Cretaceous tectonic phases. It is placed at the western tip of the Paleo-Tethys issued Cimmerian Orogenic System, which extends eastwards with the Mountainous Crimea, North Caucasus and continues furthermore to the Asian Cimmerides (Şengör, 1984, 1986). The NDO is composed of four tectonic units, Măcin, Consul, Niculiţel and Tulcea, forming a system of nappes that are overthrusted north-easterly (Săndulescu, 1984; Visarion et al., 1990).

The Triassic sedimentary series has the widest and most representative development in the Tulcea Unit, unconformably overlying a Variscan basement. The carbonate sedimentation, which started in the early Spathian and lasted during the Middle and Late Triassic, developed with basinal facies westwards and a complex carbonate platform that extends eastwards in the Tulcea Unit. The Triassic of North Dobrogea is well known for its Tethyan-type facies and richness in various groups of fossils (Peters, 1867: Arthaber, 1906; Kittl, 1908; Simionescu,

1910, 1913, 1927; Tozer, 1984; Mirăuţă & Gheorghian, 1975; Mirăuţă & Iordan, 1982; Mirăuţă et al., 1984, 1993; Grădinaru, 1984, 1995, 2000; Crasquin-Soleau & Grădinaru, 1996; Grădinaru et al., 2007; Grădinaru & Sobolev, 2006; Sebe et al., 2013; Popa et al., 2014; Cavin & Grădinaru, 2014; Nützel et al., 2018; Grădinaru & Gaetani, 2019; Forel & Grădinaru, 2018, 2020, 2021; Gale et al., 2021; Friesenbichler et al., 2021).

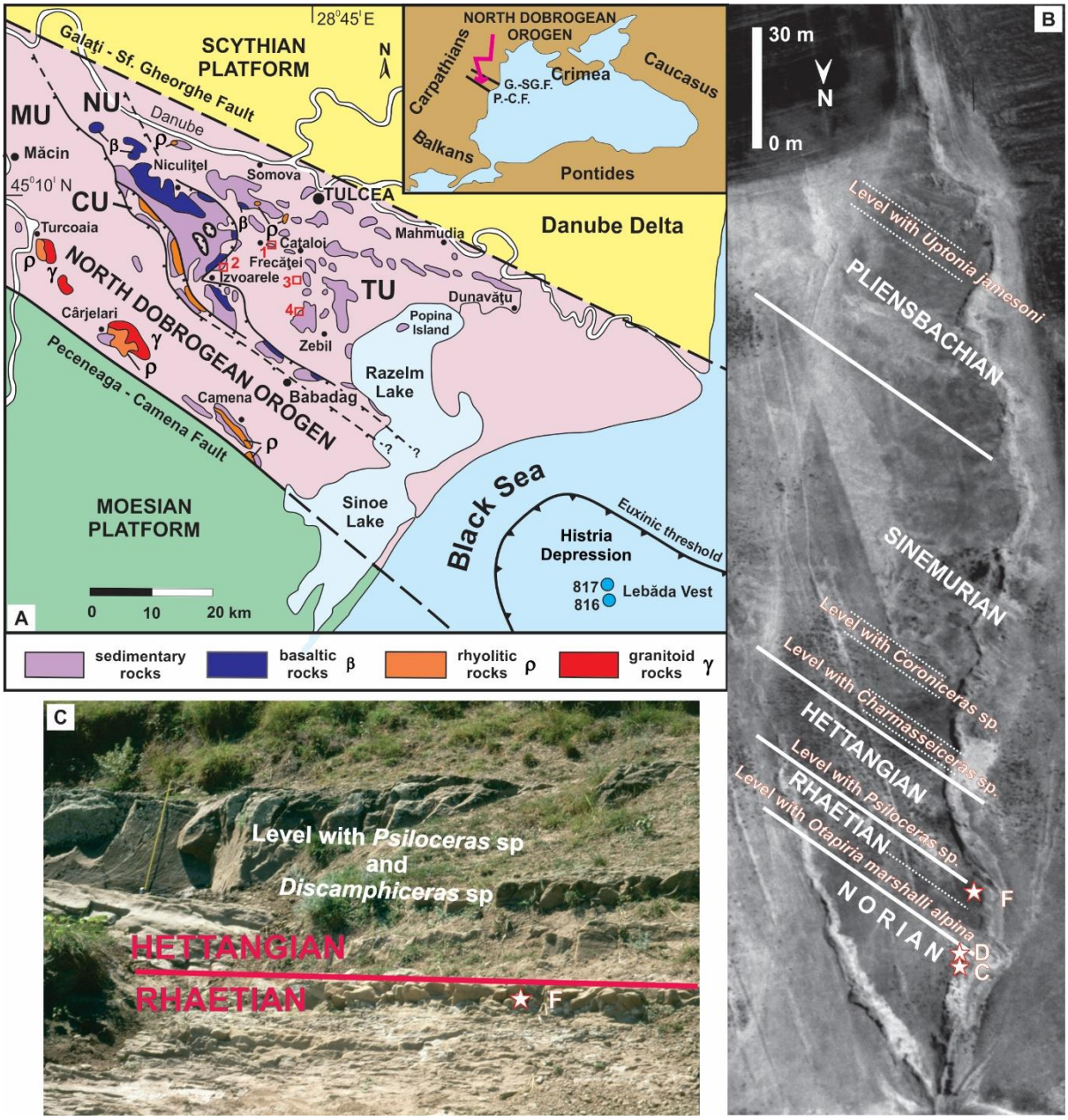

Fig.4.1 – A: Tectonostratigraphic map of the North Dobrogean Orogen showing the distribution of Triassic rocks and localities that provided nannofossils. MU: Măcin Unit, CU: Consul Unit, NU: Niculiţel Unit, TU: Tulcea Unit (modified and completed after Grădinaru 2000). 1, Frecăţei; 2, Izvoarele; 3, Mihail Kogălniceanu borehole;

4, Rândunica; 816 LV borehole. Inset map shows the regional location of the North Dobrogean Orogen. B – The right-bank ravine, 1.5 east of Frecăţei village, which exposes the succession from the upper Norian (Sevatian 1) to the lower Pliensbachian, showing the location of samples Frecăţei C, D and F. C – Photo of the Rhaetian-Hettangian boundary showing the location of sample Frecăţei F.

Norian and Rhaetian carbonates rocks are rare in the Tulcea Unit. There are only few localities where the Norian and Rhaetian deposits are exposed or identified in boreholes. Almost of them are developed in basinal facies, and these are occurring in isolated oucrops located along the right-bank of the Teliţa river, from west of Cataloi till east of Frecaţei villages (Fig. 4.1 A) (Grădinaru, 1984; Mirăuţă et al., 1993), and also in a narrow strip underlying the frontal part of the Niculiţel Unit, mainly north of the Izvoarele village (Fig. 4.1 A) (Grădinaru, 2011). Rhaetian deposits were drilled near the Mihail Kogălniceanu village (Antonescu & Baltreş, 1998). Only a single locality, south of the Rândunica village exposes Norian and Rhaetian sections located on the outer rim of the carbonate platform (Mirăuţă & Gheorghian, 1975).

As after investigation, nannofossil assemblage have been found only in Frecatei section (see result part), we describe in detail here only this section.

The Frecăţei section, located approximately 1.5 km east of the homonymous village, is exposed in a ravine located on the right-bank of the Teliţa river (Fig. 4.1B). This section, which exposes a continuous succession from the Norian till the lower Pliensbachian offers the unique opportunity in North Dobrogea to study the transition from the basinal facies of the Upper Triassic carbonate succession to the deep-water siliciclastic turbidite succesion of the Lower Jurassic (Grădinaru, 1984; Grădinaru, 2005). The Frecăţei section exposes around the Triassic-Jurassic boundary the following succession, in ascending order:

A - an alternance of nodular gray marly limestones and marls, no more than 5 m in thickness, with black shells of crashed ammonoids, commonly represented by arcestids, rare specimens of *Paracladiscites multilobatus* (Bronn), and of nautiloids, such as *Proclydonautilus spirolobus* (Dittmar). Mirăuţă et al. (1993) reported rich foraminiferal and ostracod assemblages indicating the upper Norian (Sevatian). The presence in other exposures, located in the Muchea Verde area, near the Poşta village, of the ammonoid *Sagenites quinquepunctatus*, together with bivalves of the *Monotis* (*Monotis) salinaria-haueri* group, is diagnostic for the *Sagenites quinquepunctatus* Zone of the upper Norian, which in terms of the

actual standard Triassic time scale corresponds to the lower Sevatian (= Sevatian 1) (see Krystyn, 2008; Grădinaru & Sobolev, 2011). Samples Frecăţei A1-2 and B come from this part of section.

B - a package, no more than 1.0 m thick, of gray-mauvish, sandy limestones with pyrite. Mirăuţă et al. (1993) reported the occurrence of the conodont *Norigondolella steinbergensis* (Mosher), and a rich upper Norian (Sevatian) foraminiferal assemblage including "*Vidalina*" sp., *Ophthalmidium fusiforme* (Trifonova), *Ophthalmidium* sp., and frequently Tolypamminidae (Mirăuţă et al. 1993). Samples Frecăţei C and D are from this part of the section.

C - a package, around 10 m thick, of gray calcareous siltstones with *Zoophycos*-type fucoids, which exposes a coquina, around 5.5 m thick, with the Rhaetian bivalve *Otapiria marshalli alpina* Zapfe. Sample Frecăţei E is from this interval.

D – a bed, 0.25 m thick, of grey mudstone, whitish on weathering surfaces, with black bioturbations, and bearing nodules of reddish limestone at upper part represents sample Frecăţei F.

E – a succession of thick-bedded calcareous siltstones to fine-grained sandstones, from 1.0 to 1.40 m thick, with *Zoophycos*-type fucoids, separated by thin layers of dark grey clays. Poorly preserved specimens of Hettangian ammonoids, identified as *Psiloceras* sp. and *Discamphiceras* sp, document the start of the Lower Jurassic deposition, which continues upwards with siliciclastic turbidites, made up of grey-greenish thick-bedded, fine-grained sandstones to argillaceous siltstones and rare intercalations of black clays. A few levels with ammonoids document the Sinemurian to lower Pliensbachian stratigraphic interval (Fig. 4.1).

Outside the onshore territory of North Dobrogean, Triassic carbonate rocks were intercepted in several boreholes drilled during the 1980s in the eastwards offshore extension of the NDO into the western continental shelf of the Black Sea (Grădinaru et al., 1989). A particular case is the Rhaetian carbonate rocks drilled by the boreholes 816 and 817 Lebăda Vest.

The lithological and stratigraphical relationships show that the Rhaetian carbonate rocks drilled in the boreholes 816 and 817 Lebăda Vest (LV) are allochthonous, being incorporated

in Middle Jurassic black argillites (Grădinaru et al., 1989). The rich and diverse ostracod assemblage extracted by Forel and Grădinaru (2020) and also the foraminiferal assemblage described by Gale et al. (2021) constrain the Rhaetian age of the drill core CM31 limestone in the borehole 817 LV. This is also supported by the brachiopod fauna, which includes *Euxinella anatolica* (Bittner), *Fissirhynchia fissicostata* (Suess), and *Rhaetina pyriformis* (Suess), and it, besides the foraminiferal assemblages, is similar to that of the allochthonous Rhaetian limestone in the Mountainous Crimea as recorded by Dagys (1974), Kotlyar et al. (1999) and Korchagin et al. (2003).

3. Material and methods

A total of seventeen samples from five different localities of the North Dobrogea, Romania (Fig. 4.1) were analysed for their calcareous nannofossil content under both light microscope (LM) and Scanning Electron Microscope (SEM). Seven Upper Triassic samples are from Frecătei section (A1, A2, B, C, D, E, F) and three samples from Izvoarele section (144 with 2 pieces and 237). Date in the Rhaetian based on ostracods, foraminifers and conodonts (Forel and Grădinaru, 2020), three samples come from Borehole 817 Lebăda Vest (LV), drill core CM 31 (depth interval 2623.85 – 2623.90 m, 2623.90 – 2624.00 m, 2623.00 – 2625.00 m), three from borehole 816 LV, core CM 9 (2650.20 – 2650.25 m), core CM 10 (2699.30 – 2699.55 m) and core CM 11 (2807.70 – 2808.00 m) and one from Răndunica section. Finally, two samples belong to Vaşcău section with an approximative Rhaetian age.

The smear slides were prepared according to the method described in Bordiga et al. (2015). A fresh rock surface was powdered and dried overnight, 0.05 g of powder were add to 50mL of buffered ammonia. After shaking, 1500 µL of the solution were put on the coverslip previously humidified. The solution was slowly dried below 50°C to avoid aggregates of sediments. The coverslip was mounted on the slide using Norland Optical Adhesive and fixed with a UV lamp. Observations of the smear slide were performed using an Olympus BX50 light microscope with a magnification of x2500. The illustrations were taken using a camera Olympus SC50.

The samples for the SEM were prepared according to the method described in Demangel et al. (2020). Fresh surfaces of $1cm^2$ were cut perpendicular to the bedding and polish with powder at 800 mesh per inch using distillate water. The blocks were etched for 15 seconds in

0.1% HCl and briefly cleaned in the ultrasonic bath with distillate water. The samples were dried overnight at 50°C and coated with 1nm of platinum/palladium using Cressington Sputter Coater 208HR. The SEM observations were done with a TESCAN MIRA 3 electron microscope at Lund University (Sweden).

4. Results

The observations under SEM revealed a moderate diagenetic alteration for all the studied samples with dissolutions patterns (e.g. pits, cracks and rounded edges) (Fig.4.2 A). The resulting poor preservation of the samples and the clay content forming layers on the surface analysed (Fig.4.2 B) brought difficulty to observed and identified potential calcareous nannofossil. Several samples (816 LV – CM9; Frecatei C; Frecatei D) showed forms like calcareous nannofossils (i.e. *P. triassica*, coccoliths, *E. zlambachensis*) (Fig.4.3) but uncertainty remains concerning affiliation to calcareous nannofossil due to the poor preservation.

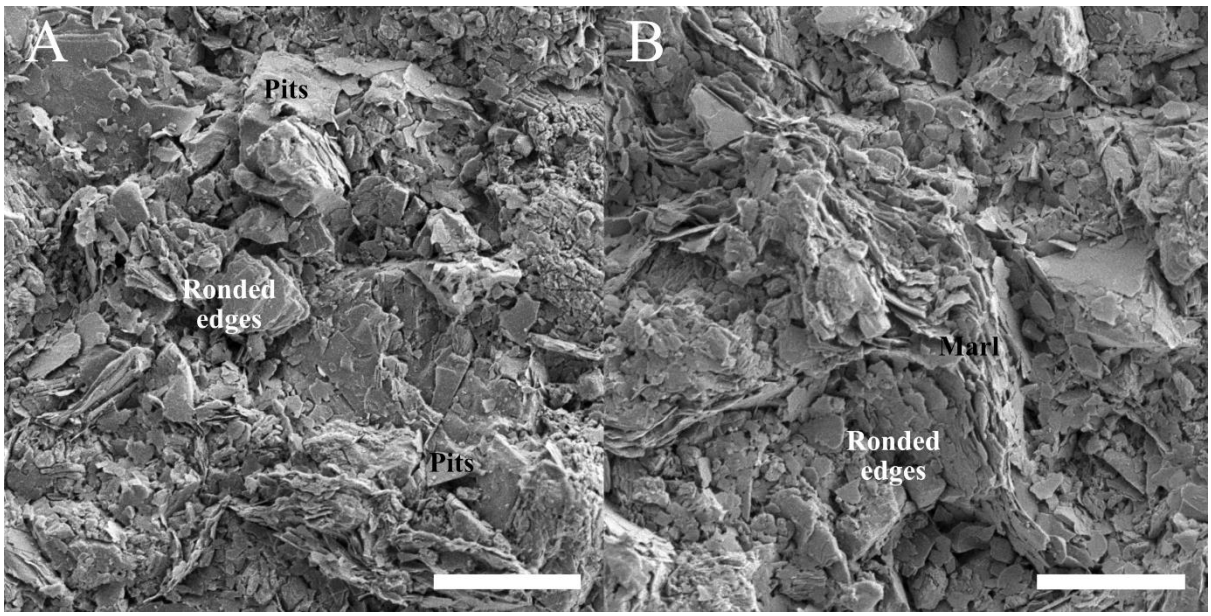

Fig.4.2 – Scanning electron microscope images illustrating A- Dissolution patterns on the matrice such as the rounded edges on the calcite cristals, pits on the surface and cracks; B- Clay layer covering the surface of the observed sample. Scale bar = 5µm.

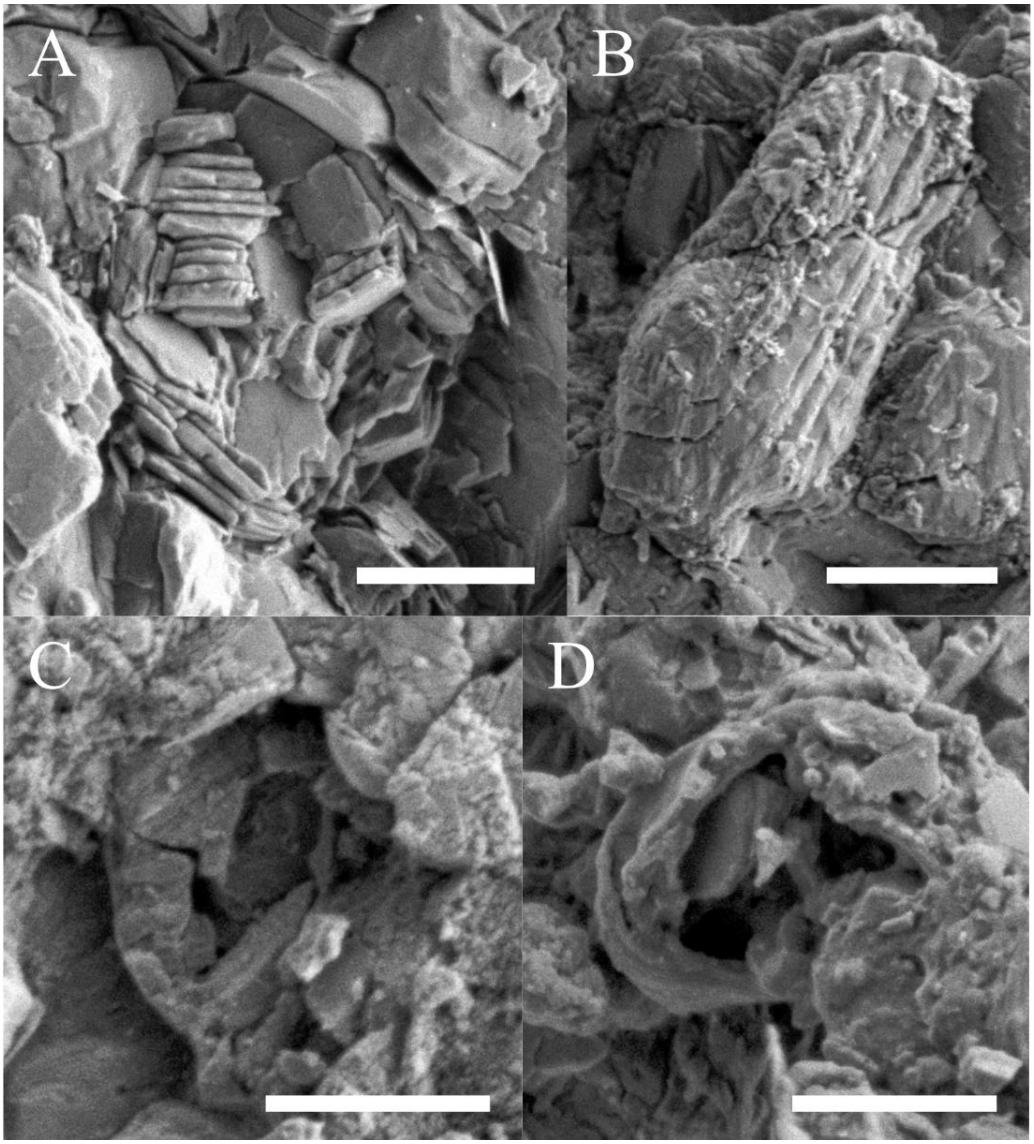

Fig.4.3. – Scanning electron microscope pictures representing A- *Prinsiosphaera triassica*-like from Frecatei C, B - Outer lamellae of an *Eoconuspheara* sp.-like from borehole 816 LV - Core CM 9; C – Coccoliths-like from borehole 816 LV – Core CM 9; D – Coccoliths-like form from Frecatei F (Rhaetian). Scale bar = 2µm.

However, the sample from Frecatei F presented calcareous nannofossils including the two Upper Triassic nannoliths species, *Prinsiosphaera triassica* (Fig.4.4) and *Eoconusphaera zlambachensis* (Fig.4.5) recognised with the characteristic oblique inner lamellae. The two species present a low abundance in the samples with less than 20 specimens per transect of smear slide (24mm) and small blocks (1cm). The two species were observed with relatively bad preservation showing dissolution features as described above.

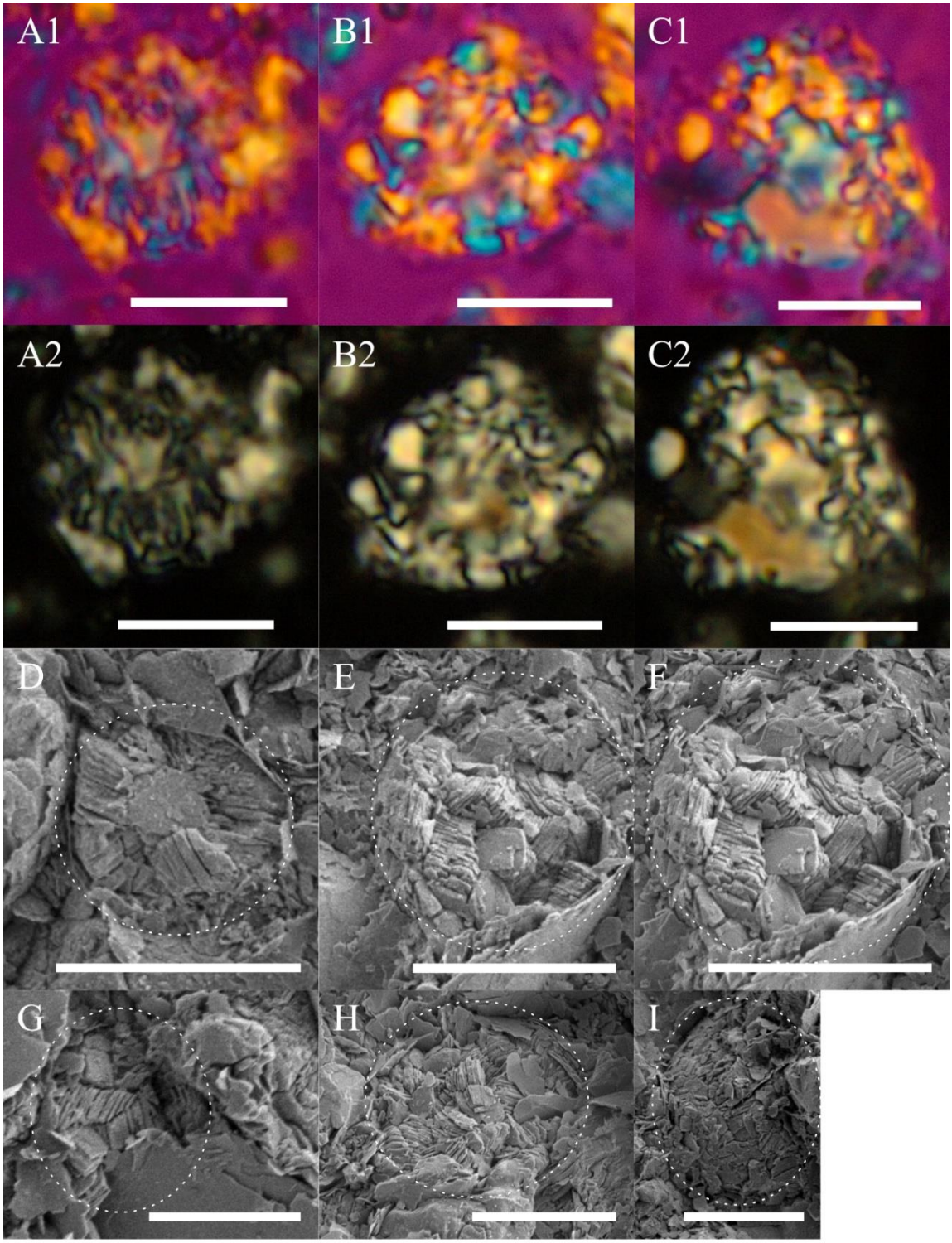

Fig.4.4 – Representation of *Prinsiosphaera triassica* from Frecatei F sample under a light microscope (A – C) (Scale bar = 10 µm) with phase contrast (1), polarised-light (2) and under a scanning electron microscope (D – I) (Scale bar = 5 µm).

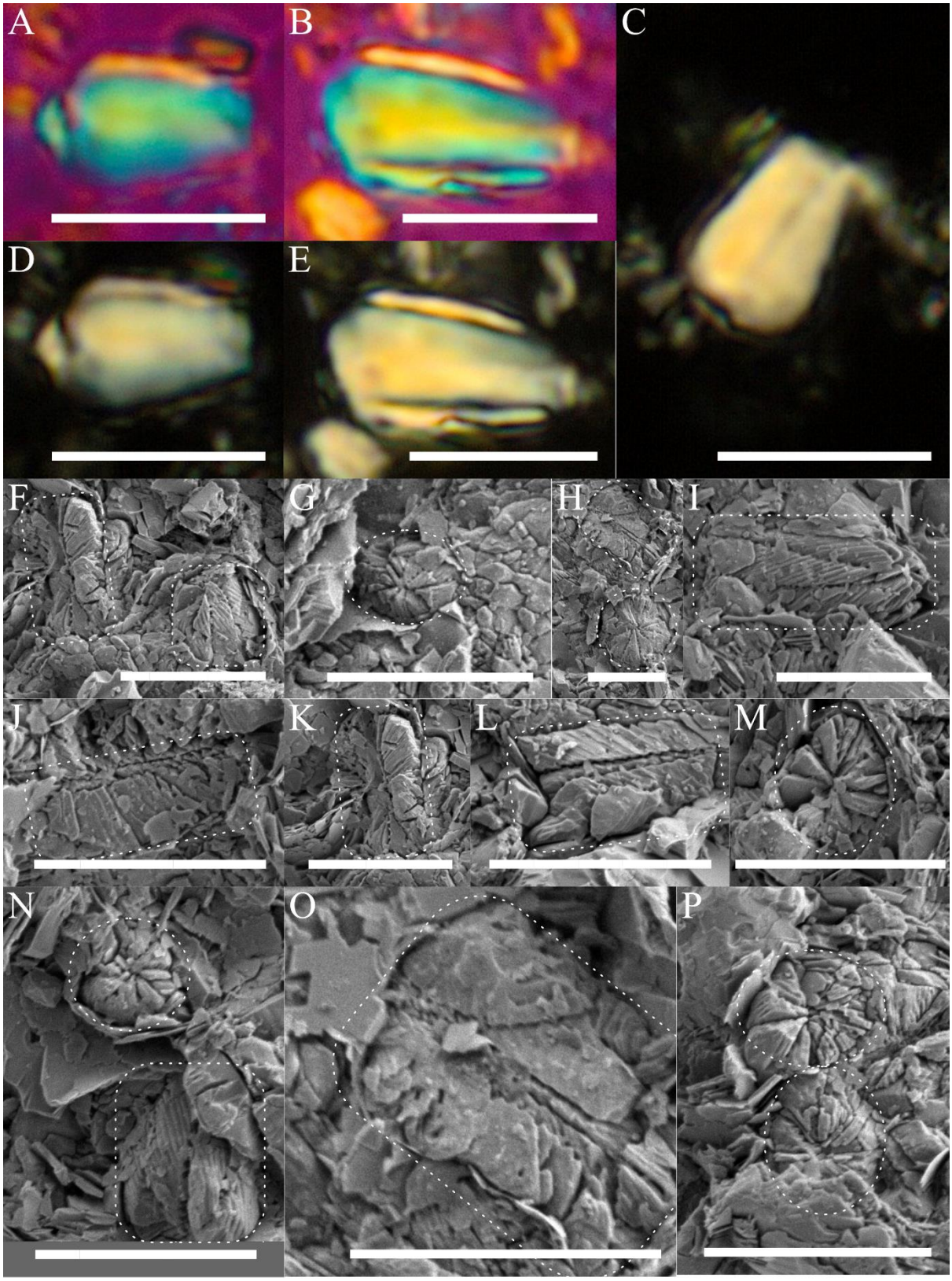
A
B
C
D
E
F
G
H
I
J
K
L
M
N
O
P

Fig.4.5 – Representation of *Eoconusphaera zlambachensis* from Frecatei F (Rhaetian) observed under an optical microscope (A – E)(Scale bar = 10 µm)with phase contrast (A – B) and with polarised light (C – E) and observed under the scanning electron microscope (F – P) (Scale bar = 5 µm).

5. Discussions

Calcareous nannofossils were observed, so far, only from the Neo-Tethys Ocean both in the Western Tethys and Southern Tethys. During the Late Triassic, North Dobrogea (Romania) was located in the Paleo-Tethys Ocean, which is north of the Neo-Tethys Ocean, enclosed between Laurasia and Cimmeria. This study illustrates the first evidence of calcareous nannofossils in the Paleo-Tethys (North Dobrogea, Romania) with the two nannoliths *Prinsiosphaera triassica* and *Eoconusphaera zlambachensis*. The sub-species *P. triassica crenulata* and other common upper Triassic calcispheres, i.e. *Orthopithonella geometrica*, *Obliquipithonella rhombica* and *Thoracosphaera wombatensis* were not observed. However, this fact does not necessarily indicates an inexistence of those species in the Palaeo-Tethys Ocean, but rather that more investigations are needed to constrain the assemblage. *Crucirhabdus minutus*, *C. primulus* and *Archaeozygodiscus koessenensis* could not be found but coccoliths-like specimens were observed questioning the presence of the coccolithophorids in the Palaeo-Tethys Ocean during the latest Triassic.

According to Stampfli & Kozur (2006), and Kovács et al. (2011), sedimentation took place during the Late Triassic on the Laurasian margin of the Pangea, including the actual territory of North Dobrogea, which was situated between 35° (earlyNorian) and 50° (latest Rhaetian) of the northern palaeolatitude.The present-day remote location of the North Dobrogean Triassic, which is located outside the Mediterranean Alpine-type Triassic, is interpreted as the result of post-Triassic large-scale horizontal displacements of the Tethyan terranes due to the opening of the West Black Sea Basin (e.g. Grădinaru 1988; Okay et al. 1994; Banks and Robinson 1997; Gaetani et al. 2000).

Despite poor preservation, *P. triassica* was identified with the characteristic inner part being composed of randomly oriented groups of parallel, thin tabular, rhombohedral calcite crystals. *E. zlambachensis* was observed with only the inner part preserved. The inner organisation of the lamellae enables the differentiation between *E. hallstattensis* presenting vertically arranged lamellae and *E. zlambachensis* possessing inclined lamellae (Demangel et

al., 2021). The specimens of Frecatei F are observed with inner lamellae inclined typically for *E. zlambachensis*. In the Neo-Tethyan domain, this last species is known from the middle Rhaetian (*Vandaites stuerzenbaumi* Zone) (Demangel et al., 2021) and is not observed after the end-Triassic mass extinction. Using this proxy for chronostratigraphy in the Palaeo-Tethys Ocean, the sample from Frecatei F can be dated to the middle to upper Rhaetian (Demangel et al., 2021). This imply that the Triassic Jurassic boundary is located at Frecatei between the grey whitish mudstone (called bed D) and the succession E of dark grey thick-bedded calcareous siltstones to fine-grained sandstones.

Conclusions

The section Frecatei F in North Dobrogea (Romania) record the two Upper Triassic nannoliths, *Prinsiosphaera triassica* and *Eoconusphaera zlambachensis*. This assemblage helps to date the sample to the Rhaetian (from *Vandaites stuerzenbaumi* Zone). Possible remains of coccolithophorids were observed in Frecatei F and borehole 816 LV - core CM 9. This last section also shows possible *E. zlambachensis* and possible *P. triassica* were observed in Frecatei C. Early investigation of Upper Triassic sediments from North Dobrogea revealed apart from the preservation degree, good potential for further analyses of calcareous nannofossils.

Acknowledgements

The SEM observations were supported by the Royal Physiographic Society of Lund (grand to Isaline Demangel). We thank Sylvain Richoz for his contribution during the early versions of this article.

References

Antonescu, E., Baltreş, A., (1998): Palynostratigraphie de la Formation de Nalbant (Trias-Jurassique) de la Dobrogea du Nord et des formations jurassiques du sous-sol du Delta du Danube (Plate-forme Scythienne). Geo-Eco-Marina, 3: 159 – 187.

Arthaber, G. von**.,** **(**1906): Die alpine Trias des Mediterran-Gebietes. In Lethaea geognostica II. Teil, Mesozoicum, Band I: 223 – 475. Verlag der E. Schweizerbart'schen Verlagshandlung (E. Nägele), Stuttgart.

Banks, C.J, Robinson, A.G., (1997): Mesozoic Strike-Slip Back-Arc Basins of the Western Black Sea Region. In: Robinson, A.G., (ed.). Regional and petroleum geology of the Black Sea and surrounding region. Vol. 68. AAPG Memoir; 53–61. 10.1306/m68612c5.

Bordiga, M., Bartol, M., Henderiks, J., (2015): Absolute nannofossil abundance estimates: Quantifying the pros and cons of different techniques – Revue de micropaléontologie, 58, 155 – 165. 10.1016/j.revmic.2015.05.002.

Bown, P.R. (1987): Taxonomy, evolution, and biostratigraphy of Late Triassic-Early Jurassic Calcareous Nannofossils. Special paper in Paleontology, 38: 1 – 118.

Bown, P.R., Cooper, M.K.E. (1989): Conical calcareous nannofossils in the Mesozoic. In: Crux, J.A., Heck, S.E. (Eds.), Nannofossils and their applications. Br. Micropaleontology Society, Ellis Horwood, Chichester: 98 – 106.

Bown, P.R., (1998). Triassic. In: Bown, P.R. (Editor), *Calcareous nannofossil biostratigraphy*. British Micropalaeontological Society Publication Series. Chapman & Hall, 29-33.

Bralower, T.J., Bown, P.R., Siesser, W.G., (1991): Significance of Upper Triassic nannofossils from the Southern Hemisphere (ODP Leg 122, Wombat Plateau, N.W. Australia) – Marine Micropaleontology, 17, 119 – 154. 10.1016/0377-8398(91)90025-2.

Cavin, L., Grădinaru, E., (2014): *Dobrogeria aegyssensis*, a new early Spathian (Early Triassic) coelacanth from North Dobrogea (Romania). Acta Geologica Polonica, 64 (2): 147 – 173.

Crasquin-Soleau, S., Grădinaru, E., (1996): Early Anisian ostracode fauna from the Tulcea Unit (Cimmerian North Dobrogean Orogen, Romania). Annales de Paléontologie, 82, 59 – 116.

Dagys, A.S., (1974): Triassic brachiopods. Trudy Instituta Geologii i Geofiziki Novosibirsk, 214, 1 – 323.

Demangel, I., Kovacs, Z., Richoz, S., Gardin, S., Krystyn, L., Baldermann, A., Piller, W. E., (2020): Development of early calcareous nannoplankton in the Northern Calcareous Alps (Austria) in the Late Triassic. Global and Planetary Change, 193, 103254.

Demangel, I., Howe, R., Gardin, S., Richoz, S., (2021): Eoconusphaera hallstattensis, new species, and review of the Rhaetian genus Eoconusphaera. Journal of nannoplankton research, 39 (1), 77 – 87.

Demangel, I., Kovács, Z., Gardin, S., Krystyn, L., Piller, W.E., Baldermann, A., Richoz, S., submitted: Fate of the calcareous nannofossils during the Rhaetian (Late Triassic): Evidence from the Northern Calcareous Alps (Austria).

Dinu, C., Wong, H.K., Tambrea, D., Matenco, L., 2005: Stratigraphic and structural characteristics of the Romanian Black Sea Shelf. Tectonophysics, 410, 417 – 435. 10.1016/j.tecto.2005.04.012.

Fischer, A.G., Honjo, S., Garrison, R.A.E., (1976): Electron Micro-graphs of Limestones and their nannofossils. Princeton University Press, Princeton.

Forel, M.-B., Grădinaru, E., (2018): First report of ostracods (Crustacea) associated with Bithynian (Anisian, Middle Triassic) *Tubiphytes*-microbial reef in the North Dobrogean Orogen (Romania). Papers in Palaeontology, 4(2), 211 – 244.

Forel, M.-B., Grădinaru, E., 2020: Rhaetian (Late Triassic) ostracods (Crustacea, Ostracoda) from the offshore prolongation of the North Dobrogea Orogen into the Romanian Black Sea shelf. European Journal of Taxonomy, 727, 1 – 83. 10.5852/ejt.2020.727.1183.

Forel, M.-B., Grădinaru, E., (2021): A unique diversity hotspot for Polycopidae (Ostracoda) in the Triassic of North Dobrogea. Historica Biology, online article. 10.1080/08912963.2021.1959577

Friesenbichler, E., Hautmann, M., Grădinaru, E., Bucher, H., (2021): A highly diverse bivalve fauna from a Bithynian (Anisian, Middle Triassic) *Tubiphytes*-microbial buildup in North Dobrogea (Romania). Papers in Palaeontology, 7(1), 447 – 495.

Gaetani, M., Lozowski, V., Szulc, J., Arche, A., Calvet, F., Lopez-Gomez, J., Hirsch, F., (2000). Olenekian (245-243 Ma), Early Ladinian (238-235 Ma), Late Norian (215-212 Ma). In: Dercourt, J., Gaetani, M., Vrielynck, B., Barrier, E., Biju-Duval, B., Brunet, M.F., Cadet, J.P., Crasquin, S., Săndulescu, M., (Eds.). Atlas Peri-Tethys, Palaeogeographical maps. Paris: Crasquin, S. Coord; 27 – 48. CCGMCGMW, and Explanatory Notes.

Gale, L., Grădinaru, E., Kolar-Jurkovšek, T., Forel, M.-B., Korat, L., (2021): Rhaetian foraminifers from the western Black Sea shelf: new evidence for heterozoan carbonate factories in the Palaeotethys. Rivista Italiana di Paleontologia e Stratigrafia, 127(3), 673 – 687.

Gardin, S., Krystyn, L., Richoz, S., Bartolini, A., Galbrun, B., (2012): Where and when the earliest coccolithophores? Lethaia. 10.1111/j.1502-3931.2012.00311.x.

Golonka, J., Embry, A., Krobicki, M., (2018): Chapter 2 – Late Triassic Global Plate Tectonics. In: Tanner, L.H., (Ed.) The Late Triassic World – Earth in a Time of Transition. Topics in Geobiology, Springer, 46, 27 – 57. 10.1007/978-3-319-68009-5.

Grădinaru, E., (1984): Jurassic rocks of North Dobrogea: a depositional tectonic approach. Review of Roumanian Geology, 28, 61 – 72.

Grădinaru, E., (1988): Jurassic sedimentary rocks and bimodal volcanics of the Peceneaga-Camena Fault. Studii și cercetări de geologie, geofizică, geografie, Seria Geologie, 33, 97 – 121.

Grădinaru, E., Dinu, C., Dragastan, O., (1989): Stratigraphy of the Dobrogean Continental Shelf of the Black Sea. In Almăşan B. (Ed.) - Conditions for the Generation, Migration and Accumulation of Hydrocarbons on the Romanian Continental Shelf of the Black Sea. Internal Report, vol. 1: III.39-85. Faculty of Geology and Geophysics, Bucharest University, Bucharest. [in Romanian].

Grădinaru, E., (1995): Mesozoic rocks in North Dobrogea: an overview. In: Săndulescu, M., Grădinaru, E., (Eds), Field Guidebook, Central and North Dobrogea, Romania, October 1-4, 1995. IGCP Project No. 369, Comparative Evolution of Peri-Tethyan Rift Basins: 17 – 26. Geological Institute of Romania, Bucharest.

Grădinaru, E., (2000): Introduction to the Triassic Geology of North Dobrogea Orogen - an overview of the Triassic System in the Tulcea Unit and the ammonoid biostratigraphy. In Grădinaru, E., (Ed.) - Workshop on the Lower- Middle Triassic (Olenekian-Anisian) boundary, 7-10 June 2000, Tulcea, Romania, Conference and Field Trip. Field Trip Guide: 5 – 37. Romanian Academy & University of Bucharest, Faculty of Geology and Geophysics, Bucharest.

Grădinaru, E., (2000): Triassic-Jurassic boundary events in North Dobrogea (Romania) as recorded in basinal marine environments. 5th Field Workshop of IGCP 458, Transdanubian Range (Hungary) and Northern Calcareous Alps (Austria), 5-10 September 2005, Poster.

Grădinaru, E., Sobolev, E.S., (2006): Ammonoid and Nautiloid Biostratigraphy around the Olenekian–Anisian Boundary in the Tethyan Triassic of North Dobrogea (Romania): Correlation with the Boreal Triassic. In: Boreal Triassic 2006, Abstracts and Pro-ceeding of the Geological Society of Norway, 3: 56 – 58.

Grădinaru, E., Orchard, M.J., Nicora, A., Gallet, Y., Besse, J., Krystyn, L., Sobolev, E.S., Atudorei, N-V., Ivanova, D., (2007): The Global Boundary Stratotype Section and Point (GSSP) for the base of the Anisian Stage: Deşli Caira Hill, North Dobrogea, Romania. Albertiana. 36:54–71.

Grădinaru, E., Sobolev, E.S., (2010): First record of *Rhabdoceras suessi* (Ammonoidea, Late Triassic) from the Transylvanian Triassic Series of the Eastern Carpathians (Romania) and a review of its biochronology, paleobiogeography and paleoecology. Central European Geology, 53(2-3), 261 – 309. 10.1556/ceugeol.53.2010.2-3.8

Grădinaru, E., (2011): Occurrence of the Bivalvia Monotis (Monotis) salinaria-haueri group in the Upper Norian (Upper Triassic) of Tulcea Unit, North Dobrogean Orogen. 8th Romanian Symposium on Paleontology, Bucharest, 29-30 September 2011.Abstract Book, 57.

Grădinaru, E., Gaetani, M., (2019): Upper Spathian to Bithynian (Lower to Middle Triassic) brachiopods from North Dobrogea (Romania). Rivista Italiana di Paleontologia e Stratigrafia, 125(1), 91 – 123.

Jafar, S.A., (1983): Significance of Late Triassic calcareous Nannoplankton from Austria and Southern Germany. Neues Jahrbuch für Geologie und Paläeontologie, 166, 218 – 259.

Janofske, D., (1987): Kalkige Nannofossillien aus der ober-Trias (Rhät)der Nördlichen kalkalpen. Berliner geowiss. Abh, 86, 45 – 67.

Kittl, E., (1908): Beiträge zur Kenntnis der Triasbildungen der nordöstlichen Dobrudscha. Denkschriften der Kaiserlichen Akademie der Wissenschaften, Mathematisch-Naturwissenschaftliche Klasse, 81, 447 – 532.

Koiava, K., Mosar, J., Gavtadze, T., Kvaliashvili, L., Mauvilly, J., 2015: Late Triassic Calcareous Nannoplankton from Georgia and New Age of Moshevani Suite (Caucasus). In 13th Swiss Geoscience Meeting, Basel, 185 – 186.

Kotlyar, G.V., Baud, A., Pronina, G.P., Zakharov, Y.D., Vuks, V.Ja., Nestell, M.K., Belyaeva, G.V., Marcoux, J. (1999): Permian and Triassic exotic limestone blocks of the Crimea. In: Crasquin-Soleau S., De Wever P. (Eds.) - Peri-Tethys: stratigraphic correlations 3. *Geodiversitas*, 21, 299 – 323.

Korchagin, O.A., Kuznetsova, K.I., Bragin, N.Yu., (2003): Find of early planktonic foraminifers in the Triassic of the Crimea. Doklady Earth Science, 390, 482 – 486.

Kovács, S., Sudar, M., Grădinaru, E., Gawlick, H.-J., Karamata, S., Haas, J., Péró, Cs., Gaetani, M., Mello, J., Polák, M., Aljinovic, D., Ogorelec, B., Kolar-Jurkovšek, T., Jurkovšek, B., Buser, S., (2011): Triassic evolution of the tectonostratigraphic units of the Circum-Pannonian Region. Jahrbuch der Geologischen Bundesanstalt, 151, 199 – 280.

Krystyn, L., (2008): An ammonoid-calibrated Tethyan conodont time scale of the late Upper Triassic. Berichte der Geologischen Bundesanstalt, 76, 9 – 11.

Mirăuţă, E., Gheorghian, D., (1975): Norian conodonts and foraminifers from North Dobrogea. Dări de Seamă ale Şedinţelor, 61, 47 – 76.

Mirăuţă, E., Iordan, M., (1982): New Triassic fossiliferous localities in the Tulcea Zone (North Dobrogea*).* Dări de Seamă ale Şedinţelor – Instutul de Geologie şi Geofizică, 66(3), 15 – 22.

Mirăuţă, E., Iordan, M., Gheorghian, D., (1984): New biostratigraphic data on the Triassic from the Somova– Sarica Hill area (Tulcea zone, North Dobrogea). Dări de Seamă ale Şedinţelor – Instutul de Geologie şi Geofizică, 68(4), 35 – 48.

Mirăuţă, E., Gheorghian, D., Bădiceanu, M., (1993): Données biostratigraphiques sur la Formation de Cataloi (Dobrogea de Nord, Roumanie). Romanian Journal of Stratigraphy, 75, 21 – 27.

Moshkovitz, S., (1982): On the findings of a new calcareous nannofossil (Conusphaera zlambachensis) and other calcareous organisms in the Upper Triassic sediments of Austria. Eclogae Geologicae Helvetiae, 75, 611 – 619. 10.5169/seals-165245.

Nützel, A., Kaim, A., Grădinaru, E., (2018): Middle Triassic (Anisian, Bithynian) gastropods from North Dobrogea (Romania) and their significance for gastropod recovery from the end-Permian mass extinction event. Papers in Palaeontology, 4(4), 477 – 512.

Okay, A, Şengör, A.M.C., Görür, N., (1994): Kinematic history of the opening of the Black Sea and its effect on the surrounding regions. Geology. 22(3), 267 – 270. 10.1130/0091-7613(1994)022<0267:khotoo>2.3.co;2.

Peters, K.F., (1867): Grundlinien zur Geographie and Geologie der Dobrudscha. Denkschriften der Kaiserlichen Akademie der Wissenschaften, 27, 83 – 207.

Popa, L., Panaiotu, C.E., Grădinaru, E., (2014): An early Middle Anisian (Middle Triassic) *Tubiphytes* and cement crusts-dominated reef from North Dobrogea (Romania): facies, depositional environment and diagenesis. Acta Geologica Polonica, 64(2), 189 – 206.

Posch, F., Stradner, H., (1987): Report on Triassic Nannoliths from Austria. Abh. Geol. B.-A., 39, 231 – 237.

Preto, N., Agnini, C., Rigo, M., Sprovieri, M., Westphal, H., *2013(> The calcareous nannofossils Prinsiosphaera achieved rock/forming abundances in the latest Triassic of western Tethys> consequences for the δ13C of bulk carbonate. Biogeosciences, 10, 6053 – 6068. 10.5194/bg-10-6053-2013.

Prins, B., (1969): Evolution and stratigraphy of coccolothinids from the lower and middle lias. International Conference Planktonic Microfossils, Geneva, 2, 547 – 558.

Săndulescu, M., (1984): Geotectonics of Romania. Editura Tehnică, Bucharest, 336. [in Romanian]

Săndulescu, M., (1994): Overview on Romanian Geology. In: "ALCAPA II". Romanian Journal of Tectonics and Regional Geology, 75 (suppl. 2): 3 – 15.

Săndulescu, M., (1995): Dobrogea within the Carpathian Foreland. In: Săndulescu, M., Grădinaru, E., (Eds.) – IGCP Project No. 369, Comparative Evolution of PeriTethyan Rift Basins. Central and North Dobrogea, Romania, October 1-4, 1995. Field Guidebook: 1-4. Geological Institute of Romania & University of Bucharest, Faculty of Geology and Geophysics, Bucharest.

Sebe, O-G., Crasquin, S., Grădinaru, E., (2013): Early and Middle Anisian deep-water ostracods (Crustacea) from North Dobrogea (Romania). Revue de Paléobiologie, 32, 509 – 529.

Şengör, A.M.C., (1984): The Cimmeride orogenic system and the tectonics of Eurasia. Geological Society of America Special Paper, 195, 1 – 82.

Şengör, A.M.C., (1986): Die Alpiden und die Kimmeriden: die verdoppelte Geschichte der Tethys. Geologische Rundschau, 75, 501 – 510.

Simionescu, I., (1910): Studii geologice și paleontologice din Dobrogea. III. Fauna triasicã dela Deşli Caira. La faune triasique de Deşli Caira. Academia Româna, Publicațiunile Fondului Vasile Adamachi, 26, 465 – 494.

Simionescu, I., (1913): Studii geologice și paleontologice din Dobrogea. VI. Fauna amoniților triasici dela Hagighiol. Les ammonites triasiques de Agighiol. Academia Româna, Publicațiunile Fondului Vasile Adamachi, 34, 271 – 370.

Simionescu, I., (1927): Aperçu géologique sur la Dobrogea. In Guide des excursions. Association pour l'avancement de la géologie des Carpates. Deuxième réunion en Roumanie: 353 – 378. Cultura Naţională, Bucarest.

Stampfli, G.M., Kozur, H.W., (2006): Europe from the Variscan to Alpine cycles. In Gee D.G. & Stephenson R.A. (Eds.) - European Lithosphere Dynamics. Memoir 32, 57 – 82. Geological Society of London.

Tozer, E.T., (1984): The Trias and its ammonoids: the evolution of a time scale. Miscellaneous Report, Geological Survey of Canada. 35, 171. 10.4095/ 119548.

Visarion, M., Săndulescu, M., Roşca, V., Stănică, D., Atanasiu, L., (1990): La Dobrogea dans le cadre de l'avant pays carpatique. Revue Roumaine de Géophysique, 34, 55 – 65.

CHAPTER 5 – FATE OF CALCAREOUS NANNOFOSSILS DURING THE RHAETIAN (LATE TRIASSIC): EVIDENCE FROM THE NORTHERN CALCAREOUS ALPS (AUSTRIA)

Isaline Demangel[1,2], Zsófia Kovács[1,2], Silvia Gardin[3], Leopold Krystyn[4], Werner E. Piller[1], Andre Baldermann[5], Sylvain Richoz[1,2]

1 Institute of Earth Sciences, University of Graz, NAWI Graz Geocenter, Heinrichstrasse 26, 8010 Graz, Austria

2 Department of Geology, University of Lund, Sölvegatan 12, 22362 Lund, Sweden

3 Center for Research on Palaeobiodiversity and Palaeoenvironments, Sorbonne University, 4 place Jussieu (Case 104), 75252 Paris Cedex 05, France

4 Department of Palaeontology, University of Vienna, Althanstrasse 14, 1090 Vienna, Austria

5 Institute of Applied Geosciences, Graz University of Technology, NAWI Graz Geocenter, Rechbauerstrasse 12, 8010 Graz, Austria

Abstract

Calcareous nannofossils evolved in the global ocean from the Carnian (early Late Triassic) and have contributed to the accumulation of biogenic calcium carbonate in marine sediments since then. Bio-diversification and bio-productivity became more significant in the Rhaetian (Late Triassic), representing an important period to understand the dynamics of calcareous nannofossils evolution. The calcareous nannofossil content of the Zlambach section, Northern Calcareous Alps, Austria, was qualitatively and quantitatively investigated using both scanning electron and light microscopy. The nannolith, *Prinsiosphaera triassica* dominate the assemblage and increases slightly in abundance in the lower Rhaetian, followed by a small-scale short-term increase during the middle Rhaetian and reaches rock-forming abundance in the upper Rhaetian. A systematic size decrease is recorded from the lower Rhaetian onwards, possibly due to changes in the palaeo-environment. The abundance of *P. triassica* is affected by the occurrence of a second nannolith, *Eoconusphaera hallstattensis*, in the lower Rhaetian. The latter species is constrained to a relatively short interval, from the upper *Paracochloceras suessi Zone* (lower Rhaetian) and disappeared during the lower *Vandaites stuerzenbaumi* Zone (middle Rhaetian), fewly after the occurrence of a second Eoconusphaeraceae species*: E. zlambachensis.* When, *E. hallstattensis* last occurs, the sub-species *Prinsiosphaera triassica crenulata* is observed with

characteristic parallel calcite lamellae. The coccolithophorids are present in low abundance, increasing slightly in the middle Rhaetian. The lower-middle Rhaetian record of coccoliths confirm a rather slow temporal diversification of the first coccolithophorids.

Isaline Demangel [isaline.demangel@geol.lu.se], Institute of Earth Sciences, University of Graz, NAWI Graz Geocenter, Graz, Austria, Department of Geology, University of Lund, Lund, Sweden; Zsófia Kovács [zsofia.kovacs@geol.lu.se], Institute of Earth Sciences, University of Graz, NAWI Graz Geocenter, Graz, Austria, Department of Geology, University of Lund, Lund, Sweden; Silvia Gardin [silvia.gardin@upmc.fr], Centre de Recherche sur la Paléobiodiversité et les Paléoenvironnements, Sorbonne Université, Paris, France; Leopold Krystyn [leopold.krystyn@univie.ac.at], Department of Palaeontology, University of Vienna, Althanstrasse 14, 1090 Vienna, Austria; Werner E. Piller [werner.piller@uni-graz.at], Institute of Earth Sciences, University of Graz, NAWI Graz Geocenter, Graz, Austria; Andre Baldermann [baldermann@tugraz.at], Institute of Applied Geosciences, Graz University of Technology, NAWI Graz Geocenter, Rechbauerstrasse 12, 8010 Graz, Austria; Sylvain Richoz [sylvain.richoz@geol.lu.se], Institute of Earth Sciences, University of Graz, NAWI Graz Geocenter, Graz, Austria, Department of Geology, University of Lund, Lund, Sweden.

The (co-)authors have no conflict of interest to declare.

1. Introduction

The Late Triassic is a key interval for calcareous nannofossil evolution, and so for understanding their subsequent expansion in the oceans and their importance in present-day marine ecosystems. This period records the First Occurrence (FO) of calcareous nannofossils in the Carnian, their early evolution in the Rhaetian and their near-extinction at the Triassic/Jurassic boundary. Investigations on the oldest calcareous nannofossils are numerous (e.g., Prins, 1969; Deflandre, 1970; Di Nocera & Scandone, 1977; Moshkovitz, 1982; Jafar, 1983; Bown, 1985, 1987; Janofske, 1987, 1992; Posch & Stradner, 1987; Bralower et al., 1991; Bellanca et al. 1993; Erba 2006; Gardin et al. 2012; Preto et al. 2013; Demangel et al. 2020) and have allowed tracing of the FO back to the Carnian with the occurrence of three calcispheres, *Obliquipithonella prasina* (Janofske, 1992) and *Orthopithonella misurinae* (Janofske, 1992), *Carnicalyxia tabellata* (Janofske, 1992). The most abundant Triassic calcareous nannofossil, *Prinsiosphaera triassica* (Fischer et al., 1967) (calcisphere incertae sedis), and the coccolithophorids appeared in the middle Norian, followed by the occurrence of the Eoconusphaeraceae (nannolith) in the lower Rhaetian (Demangel et al., 2020). Attention was given to the end-Triassic, recording one of the "Big-Five" extinctions just before the Triassic/Jurassic boundary (e.g., Clémence et al., 2010; Preto et al., 2012; Bottini et al., 2016).

During this event, the red-plastid containing lineages, primarily dinoflagellates, nannoliths Eoconusphaeraceae, *P. triassica* and coccolithophorids, experienced high extinction rates (Richoz et al., 2012). However, in between their appearance (Carnian to the lower Rhaetian) and the end-Triassic event (upper Rhaetian - *Choristoceras marshi* Zone), the evolution of the early calcareous nannofossils is poorly investigated. Preto et al., (2013) have presented a quantification of the most abundant species, *P. triassica*, in two Tethyan basins in Central and South Italy: they contribute 0 to 10 % of the total rock volume during the Norian, 20 to 40 % in the middle Rhaetian and up to 60 % in the late Rhaetian in more proximal settings and between 0 to 20 % in more distal settings. On the contrary, Demangel et al. (2020) have presented a quantification of *P. triassica* at Steinbergkogel in the Austrian Northern Calcareous Alps (NCA): They account for 0 to 2 % of the total rock volume during the Norian and for 2 to 4 % during the lowermost Rhaetian in distal settings.

To document the missing information on the early evolution of the calcareous nannofossils, this study focuses on the *Paracochloceras suessi* and *Vandaites stuerzenbaumi* ammonoid Zones, covering the lower and middle Rhaetian at the Zlambach section (Austria – Northern Calcareous Alps). The impact of diagenesis on the preservation of the nannofossils record was investigated based on traces elements contents using Inductively Coupled Plasma-Optical Emission Spectrometry (ICP-OES) measurements. Scanning Electron Microscopy (SEM) and Optical Microscopy (OM) were used to obtain qualitative and quantitative estimates of the abundance and temporal evolution of the lower to middle Rhaetian calcareous nannofossils.

2. Geological settings

During the Rhaetian (208.50 – 201.36 Myr; Galbrun et al., 2020), the Austrian NCA were located at a palaeo-latitude around 25° N (Gallet et al., 1996), on the western margin of the Neo-Tethys Ocean (Fig. 5.1). Along with the opening of the Neo-Tethys Ocean, this region was characterized by the development of widespread carbonate platform systems during the Middle and Late Triassic (Mandl, 2000; Richoz & Krystyn, 2015). The Dachstein carbonate platform has spread from the late Carnian until the middle Rhaetian (Krystyn et al., 2009). During the middle Rhaetian, parts of the platform deepened and subsequently changed into a basinal setting before an increase of the terrigenous influx occurred, marking the shift back to

more proximal sedimentation in the late-middle Rhaetian (Kovács et al., 2020). The Zlambach facies was deposited in a toe-of-slope to open-marine basin environment and represents the interspace between the Dachstein platform and the Hallstatt basin (Fig. 5.1). This facies comprises alternations of autochthonous, bioturbated marlstones and subordinate marly micritic limestone of greyish colour with episodically embedded fine-grained calciturbidites of allochthonous origin and other mud/debris flows (Matzner, 1986; Krystyn, 1987, 1991; Richoz et al., 2012; Richoz & Krystyn, 2015; Galbrun et al., 2020) (Fig. 5.2). The allodapic limestone beds appear as grainstones to packstones with stylolites at the layer boundaries (Matzner, 1986) and contain abundant reworked corals with encrusting organisms as well as some calcisponges and bryozoans (Richoz & Krystyn, 2015). The autochthonous sedimentary rocks contain some ostracodes, radiolarians, ammonoids including *Paracochloceras suessi*, *Vandaites stuerzenbaumi* and *Choristoceras marshi.* The ammonoids are used in parallel with rare conodonts and foraminifera for biostratigraphic correlation (Piller, 1978; Matzner, 1986; Richoz & Krystyn, 2015; Galbrun et al., 2020). Some marlstone horizons are rich in corals (Frech, 1890), have a diverse foraminifera fauna (Kristan-Tollmann, 1964; Piller, 1978) and contain non-segmented calcareous sponges, spongiomorphs, hydrozoans, solenoporaceans, bryozoans, brachiopods, echinoderms, serpulids and ostracodes. Additionally, abundant pollen and spores are recognizable throughout the entire Zlambach Formation (Krystyn & Kuerschner, 2005), which is at least 150 m thick.

3. Material and methods

The herein studied section, called Kleiner Zlambach, represents a 55 m thick profile, which covers the lower part of the Zlambach Formation, i.e. the *P. suessi* and *V. stuerzenbaumi* Zones (Fig.5.2), until the base of the *C. marshi* Zone. The remaining part of the last zone is covered at this outcrop. The Kleiner Zlambach section is located in the Austrian NCA at around 870 m altitude, about 3 km north of the Hallstatt lake and 2 km east of the village Bad Goisern along the Kleiner Zlambach river (47.642278, 13.659267) (Fig.5.2).

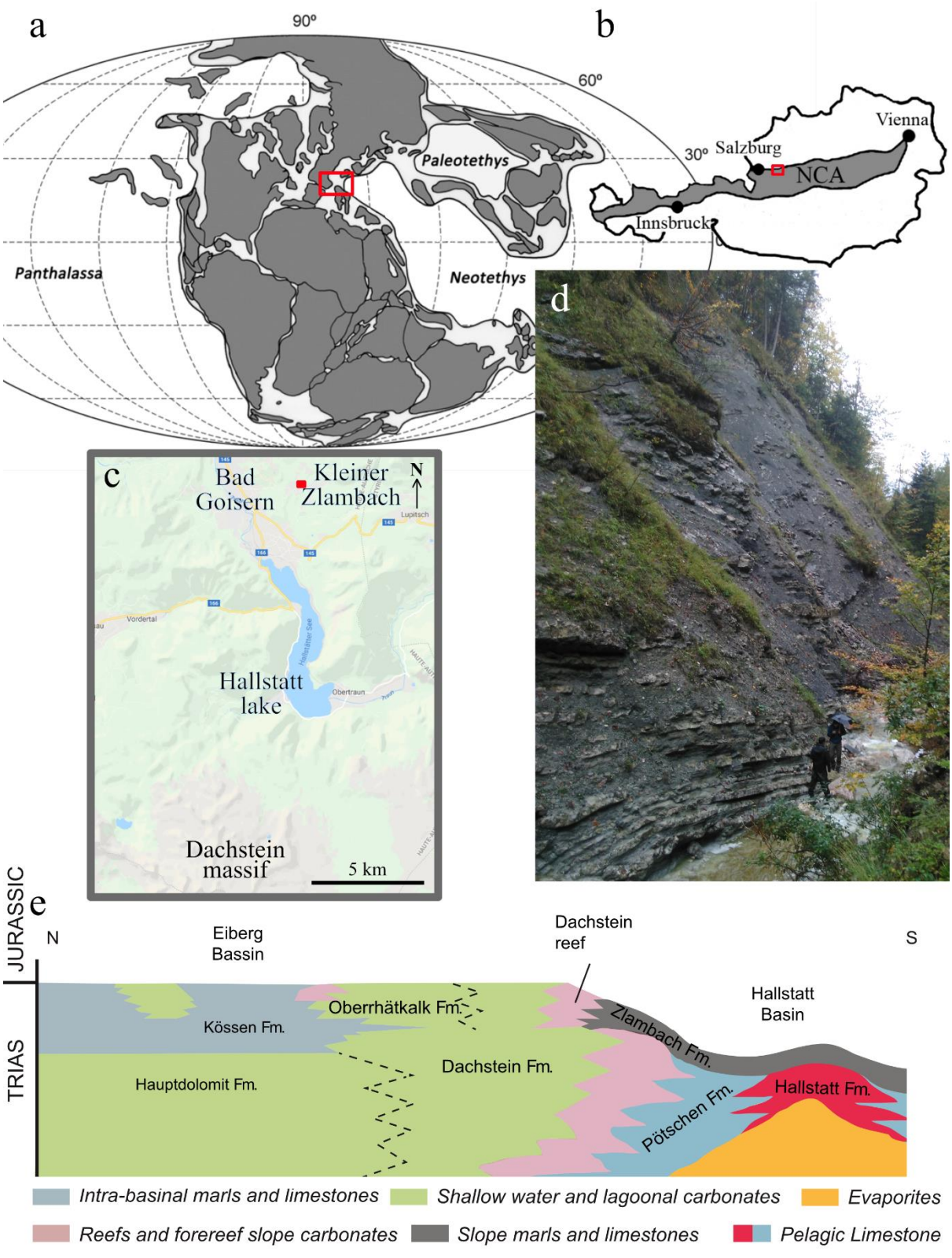

Fig.5.1 – Location and stratigraphy of the studied section at Kleiner Zlambach, Austria, Northern Calcareous Alps (NCA). a) Global palaeo-geographic reconstruction during the Late Triassic with the NCA (red square) located at

the Western Neo-Tethys margin (modified from Scotese, 2004; Golonka, 2007; Nakada et al., 2014). b) Location of the Zlambach section (red square) in the central NCA (modified after Schorn & Neubauer, 2014). c) Location of the Kleiner Zlambach (red square) in the Salzkammergut region of Austria north of the Dachstein summit, Hallstatt lake and village Bad Goisern. d) Outcrop at the Kleiner Zlambach section (people for scale are ca. 1.80 m tall). The base of the section shown here is at 40 m on the section log (Fig.5.2). e) Schematic Triassic stratigraphy of the NCA, with locations of the Zlambach Formation (grey zone) (Modified after Kürschner et al., 2007).

3.1 *Sampling and nannofossils quantification*

A total of 31 samples (Fig.5.2) were prepared following the smear slide preparation technique of Bordiga et al., (2015). The bulk rock samples were gently disintegrated by scratching the freshly prepared rock surfaces, then 0.05 g of dried, pulverized materials were mingled with 50 mL of a buffered ammonia solution. Using a micropipette, 1500 µL of the suspensions were transferred to coverslips and left to dry at a temperature below 50° C to avoid aggregation of sediment particles and nannofossils. The preparations were mounted on standard glass slides using Norland Optical Adhesive and dried with an UV lamp. The samples are named according to their positions in metres along the studied profile (Fig.5.2).

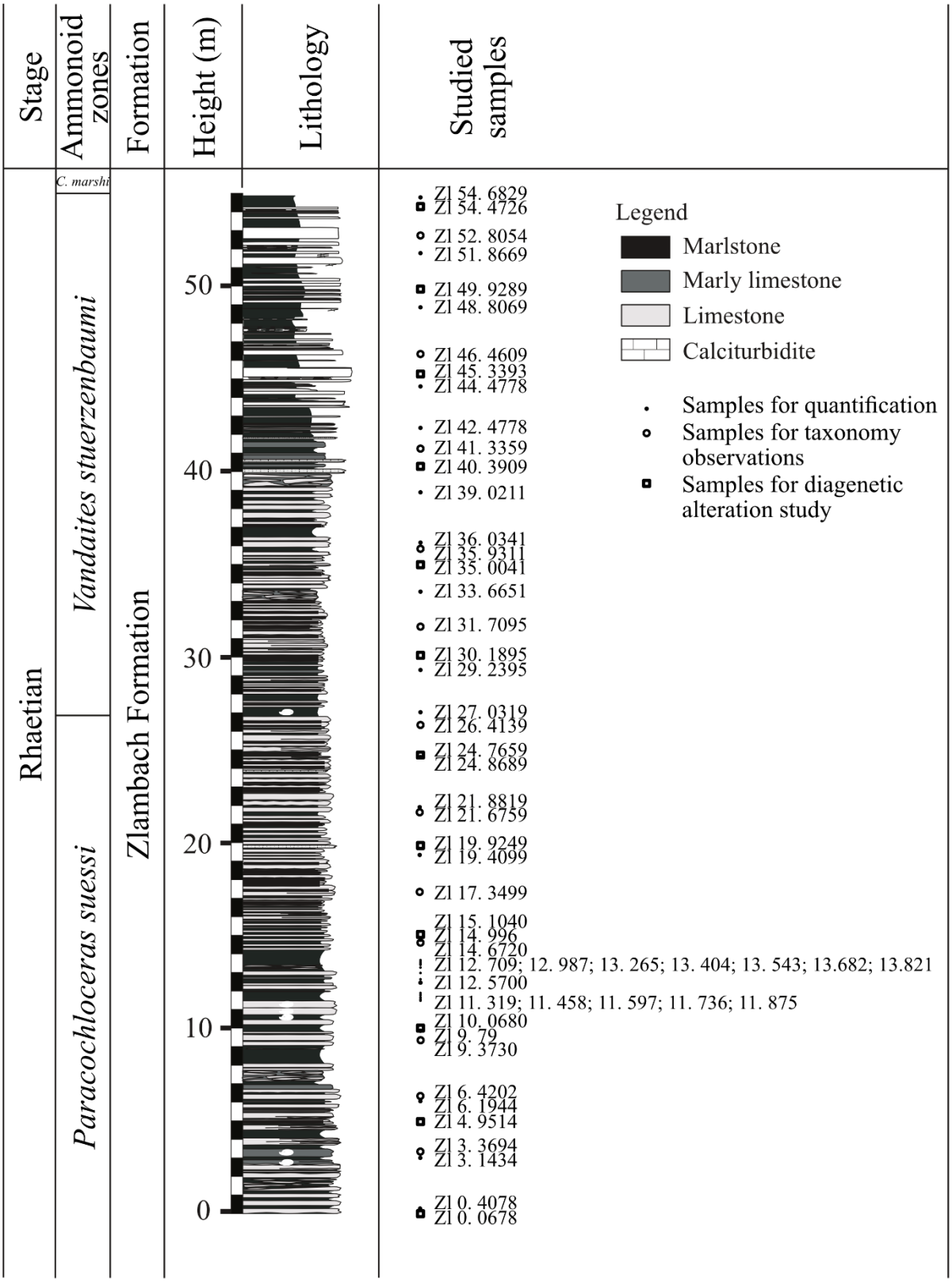
Stage
Ammonoid zones
Formation
Height (m)
Lithology
Studied samples
Rhaetian
C. marshi
Vandaites stuerzenbaumi
Paracochloceras suessi
Zlambach Formation
50
40
30
20
10
0
Zl 54. 6829
Zl 54. 4726
Zl 52. 8054
Zl 51. 8669
Zl 49. 9289
Zl 48. 8069
Zl 46. 4609
Zl 45. 3393
Zl 44. 4778
Zl 42. 4778
Zl 41. 3359
Zl 40. 3909
Zl 39. 0211
Zl 36. 0341
Zl 35. 9311
Zl 35. 0041
Zl 33. 6651
Zl 31. 7095
Zl 30. 1895
Zl 29. 2395
Zl 27. 0319
Zl 26. 4139
Zl 24. 7659
Zl 24. 8689
Zl 21. 8819
Zl 21. 6759
Zl 19. 9249
Zl 19. 4099
Zl 17. 3499
Zl 15. 1040
Zl 14. 996
Zl 14. 6720
Zl 12. 709; 12. 987; 13. 265; 13. 404; 13. 543; 13.682; 13.821
Zl 12. 5700
Zl 11. 319; 11. 458; 11. 597; 11. 736; 11. 875
Zl 10. 0680
Zl 9. 79
Zl 9. 3730
Zl 6. 4202
Zl 6. 1944
Zl 4. 9514
Zl 3. 3694
Zl 3. 1434
Zl 0. 4078
Zl 0. 0678
Legend
Marlstone
Marly limestone
Limestone
Calciturbidite
Samples for quantification
Samples for taxonomy observations
Samples for diagenetic alteration study

Fig.5.2 – Lithology and biostratigraphy of the Rhaetian Zlambach Formation with ammonoid zones and location of the studied samples

The samples were observed using an Olympus BX50 light microscope at a magnification of x2500. Two transects taken along the short axis (24 mm) of each slide were quantified, one at the middle and one at ¼ of the extremity. The average of both transects was consider for the calculation of the relative and absolute abundances. All the species presents in the studied samples were quantified. The relative abundances of each species were calculated with respect to the whole nannofossils assemblages. The absolute abundance of nannofossils per gram of bulk sediment (Nanno/g) was calculated for each species and obtained following the equation developed in Bordiga et al., (2015):

$$X = (Nanno \times A) \div (f \times n \times W) \quad \text{(equation 1)}$$

Where X is the absolute nannofossil abundance per gramme of sediment (Nanno/g), $Nanno$ is the average number of nannofossil counted on the two transect per sample, A is the area of the coverslip (768 mm^2), f is the area of one field of view (FOV: 0.0078 mm^2), n is the number of FOVs counted (240) and W is the weight of dry sediment placed on the coverslip (g) after dilution.

The nannofossils accumulation rate was calculated following the equation 2 (modified from Suchéras-Marx et al., 2014):

Nannofossil accumulation rate (nannofossils / cm^2 / Myr) = X × sedimentation rate × $\rho_{sediment}$

(equation 2)

Where X is the absolute nannofossils abundance (Nanno/g) calculated via equation 1. The bulk sedimentation rate chosen here is 15.97 m / Myr, as estimated by Galbrun et al. (2020) by cyclostratigraphy for the Zlambach Formation. The rate is considered to be linear as similar values have been obtained over the duration of the *P. suessi* Zone (1.83 Myr) and *V. stuerzenbaumi* Zone (1.63 Myr) and is verified further by the identical number of 405 000 years cycles in each ammonoid zone (Galbrun et al., 2020). $\rho_{sediment}$ corresponds to the measured sediment/rock density obtained from 25 samples including nineteen on small pieces of rocks for each quantified samples and six on larger rocks (around one kilogram) to control the density

obtain on small pieces. The density range from 1.8 to 3.2 g/cm^3 with an average for both set of rock at 2.4 g/cm^3. For the limestones, the density was calculated following the basic method of mass per rock volume measurements. For marlstones and marly limestones, the density was calculated using the respective sample mass divided by the difference of the sample mass to water mass in a known water volume, before and after immersion of the sample.

To ensure direct comparison with the study results of the Upper Triassic Italian sections reported by Preto et al., (2013) and understand the contribution to carbonate deposition of the main calcifier, the percentage of *P. triassica* in the sediment (wt% $CaCO_{3P.\ triassica}$) was calculated with equations 3 and 4. Therefore, the volume of all *P. triassica* (cm^3) was determined following equation 3, considering the mean radius (r) calculated for each samples in order to take into account the size variation thought the studied succession. The use of the mean radius introduces a minor inaccuracy; therefore, the standard error of the mean was computed ranging from 0.08 to 0.27 and integrated into the error bars (1 σ) of the wt% $CaCO_{3P.\ triassica}$. The mass of the total volume of *P. triassica* ($M_{P.\ triassica}$ g $CaCO_3$) was computed following equation 4. The density of the test was assumed to be 2.7 g/cm^3 referring to the calcite mineralogy of *P. triassica* specimens (Young & Ziveri, 2000).

$$V_{P.\ triassica} = \frac{4}{3\pi r^3} \times X \qquad \text{(equation 3)}$$

$$M_{P.\ triassica} = V_{P.\ triassica} \times \rho_{calcite} \qquad \text{(equation 4)}$$

3.2 *SEM samples preparation*

Twelve samples were prepared for a Scanning Electron Microscopy (SEM) study to observe details of the structure as well as structural and size changes of the calcareous nannofossils over time. We followed the method described in Demangel et al., (2020): The samples were cut in blocks with a surface of 1 cm^2 and then polished with 600 and 1200 diamonds discs using deionized water. The blocks were etched for 15 seconds in 0.1% HCl solution and cleaned for 7 seconds in an ultrasonic bath with distilled water. The samples were dried overnight at 50 °C and finally coated with 1 nm of platinum/palladium using a Cressington Sputter Coater 208HR. The SEM analyses were done with a TESCAN MIRA 3 electron microscope at Lund University.

3.3 *Diagenetic study*

The degree of diagenetic alteration of the samples was estimated based on common enrichment or depletion trends of major and minor elements (Na, Sr, Fe, Mn, etc.) recorded in the carbonate fraction obtained with inductively coupled plasma optical emission spectroscopy (Brand & Veizer, 1980; Baldermann et al., 2020). A total of 12 samples was analysed across the entire sections with a vertical resolution between 5 to 6 m. Acid digestion of the carbonate fraction (including dolomite) was carried out by reacting 0.050 g of the powdered sample with 5 drops of 6 % HNO_3 of suprapure grade and 50 mL of 2 % HNO_3 for 12 h at 80 °C. Afterwards, the acid-soluble fraction was separated by filtration through a 0.45 µm cellulose acetate membrane. Chemical analyses were carried out on a Perkin Elmer OPTIMA 8300 at the Institute of Applied Geosciences, Graz University of Technology, to obtain the total aqueous concentrations of Al, Ba, Ca, Cd, Co, Cr, Cu, Fe, K, Li, Mg, Mn, Na, Ni, Si, Sr and Zn in each sample. The analytical precision (2σ, 3 replicates) is better than ± 3 % for all elements, as determined by replicate analyses of NIST 1640a, in-house and SPS-SW2 Batch 130 standards (Baldermann et al., 2018 a, b).

4. Results

4.1 *The Rhaetian calcareous nannofossils assemblage at Zlambach section*

The Rhaetian interval at the Zlambach section presents almost all of the Upper Triassic calcareous nannofossils known so far. The Prinsiosphaeraceae are present with two sub-species, *Prinsiosphaera triassica* (Fig.5.3) and *P. triassica crenulata* (Jafar, 1983; Fig. 5.4). Two conical forms are present with *Eoconusphaera hallstattensis* (Demangel et al., 2021; Fig. 5.5) then *Eoconusphaera zlambachensis* (Moshkovitz, 1982; Fig. 5.6). Three calcispheres probably related to the Dinophyceae were observed, including *Orthopithonella geometrica* (Jafar, 1983; Fig. 5.7 A), *Obliquipithonella rhombica* (Janofske, 1987; Fig. 5.7 B) and *Thoracosphaera wombatensis* (Bralower et al., 1991; Fig. 5.7 C). The coccolithophorids are present with *Crucirhabdus minutus* (Jafar, 1983; Fig. 5.8 A), *Archaeozygodicus koessenensis* (Bown, 1985; Fig. 5.8 B) and *C. primulus* (Prins, 1969; Fig. 5.8 C). Additionally, one coccolith-like specimen was observed but not identified at the species level (Fig. 5.9). Finally, the nannolith *Carnicalyxia tabella* is barely observable, whereas *Cassianospica curvata* (Janofske,

1992) and *Hayococcus floralis* (Jafar, 1983) were not observed in this study, even though they were observed in time-equivalent Rhaetian sediments at other localities (e.g. Bralower et al., 1991; Janofske, 1992; Bown & Cooper, 1998; Bottini et al., 2016).

Along the section, *P. triassica* was observed in good preservation state with two different subspecies (Fig. 5.3). Mainly, *P. triassica* appears intact or broken in half with the outer and inner part being composed of randomly oriented groups of parallel, thin tabular, rhombohedral calcite crystals (Fig. 5.3). In sample Zl 42, 4778 some specimens of *P. triassica crenulata* also occur, consisting groups of parallel, thin tabular, rhombohedral calcite crystals which are similarly oriented and appear as striation (Fig. 5.4).

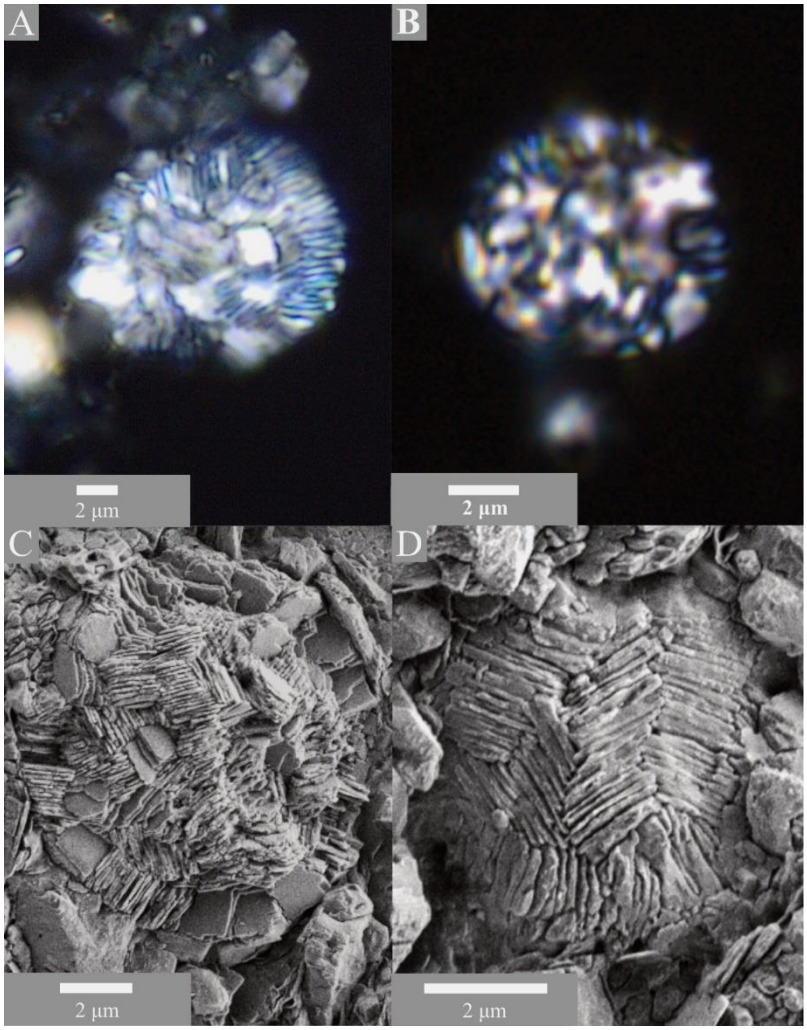

Fig.5.3 – *Prinsiosphaera triassica* in LM with XPL (A, B) and similar specimens under the SEM (C, D). The inner part of the calcisphere is well-preserved and composed of groups of calcite lamellae. Within each group the

lamellae are stacked parallel to each other. Between groups the orientation appears random. Specimens from the lower Rhaetian, samples: Zl 5.5164 (A, B), ZL 6.4202 (C, D)

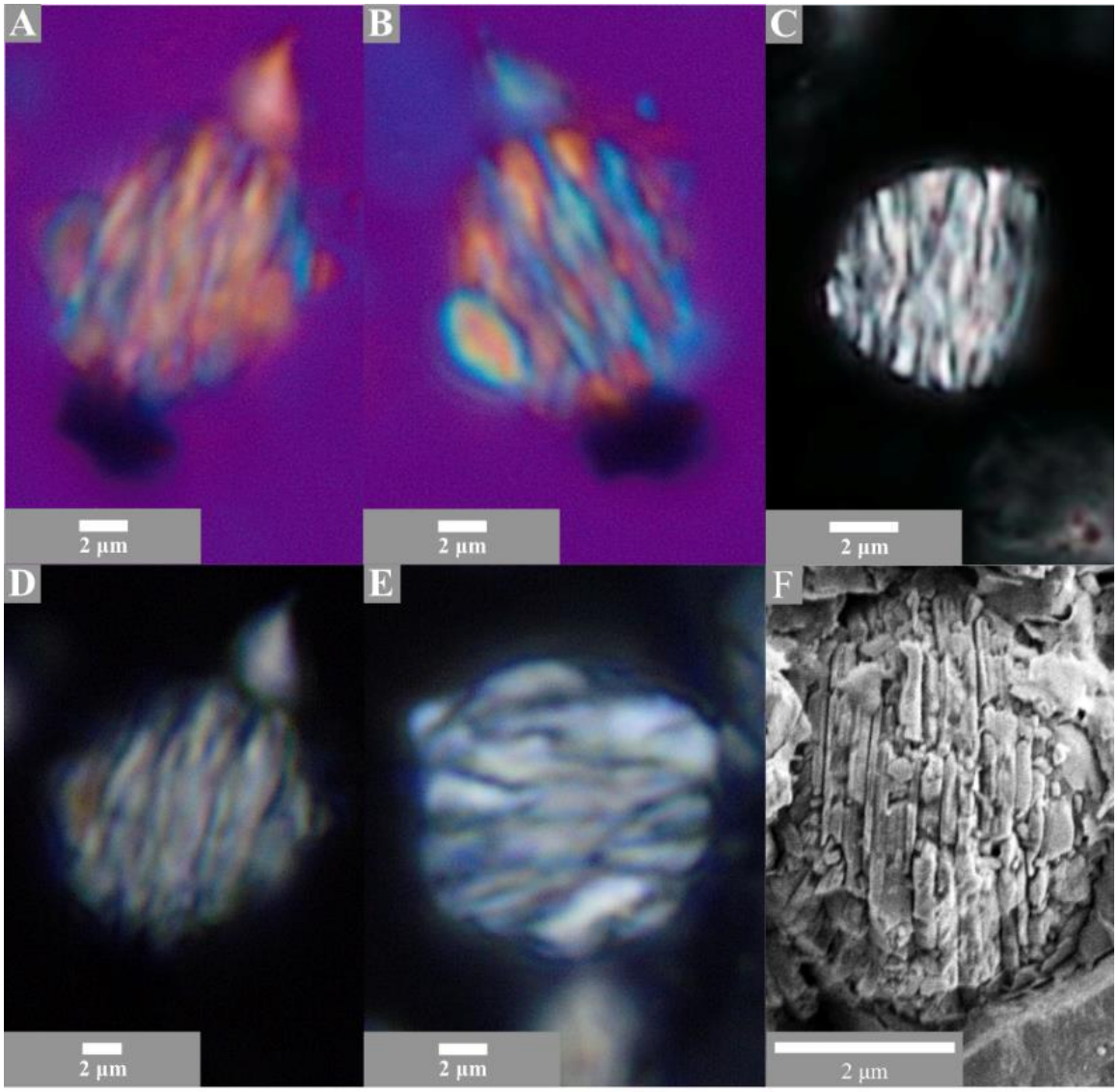

Fig.5.4 – *Prinsiosphaera triassica crenulata* (Jafar 1983) in LM (A – E) with XPL and gypsum plate (A, B) and under SEM (F). Specimens present calcite lamellae organised in stripes, from the middle Rhaetian, samples ZL 52.8554.

The Eoconusphaeraceae family is present throughout the Zlambach section. Two different species were observed with a dominance at two specific intervals: *E. hallstattensis* (Fig.5.5) is present from the base of the section (*Paracochloceras suessi* Zone – lower Rhaetian) to sample Zl 29. 2395 (*Vandaites stuerzenbaumi* Zone – middle Rhaetian). Above, *E. zlambachensis* (Fig.5.6) appears and dominates from sample Zl 33. 6651 (*Vandaites*

stuerzenbaumi Zone – middle Rhaetian) until the top of the section, with the persisting presence of few *E. hallstattensis* specimens after the transition.

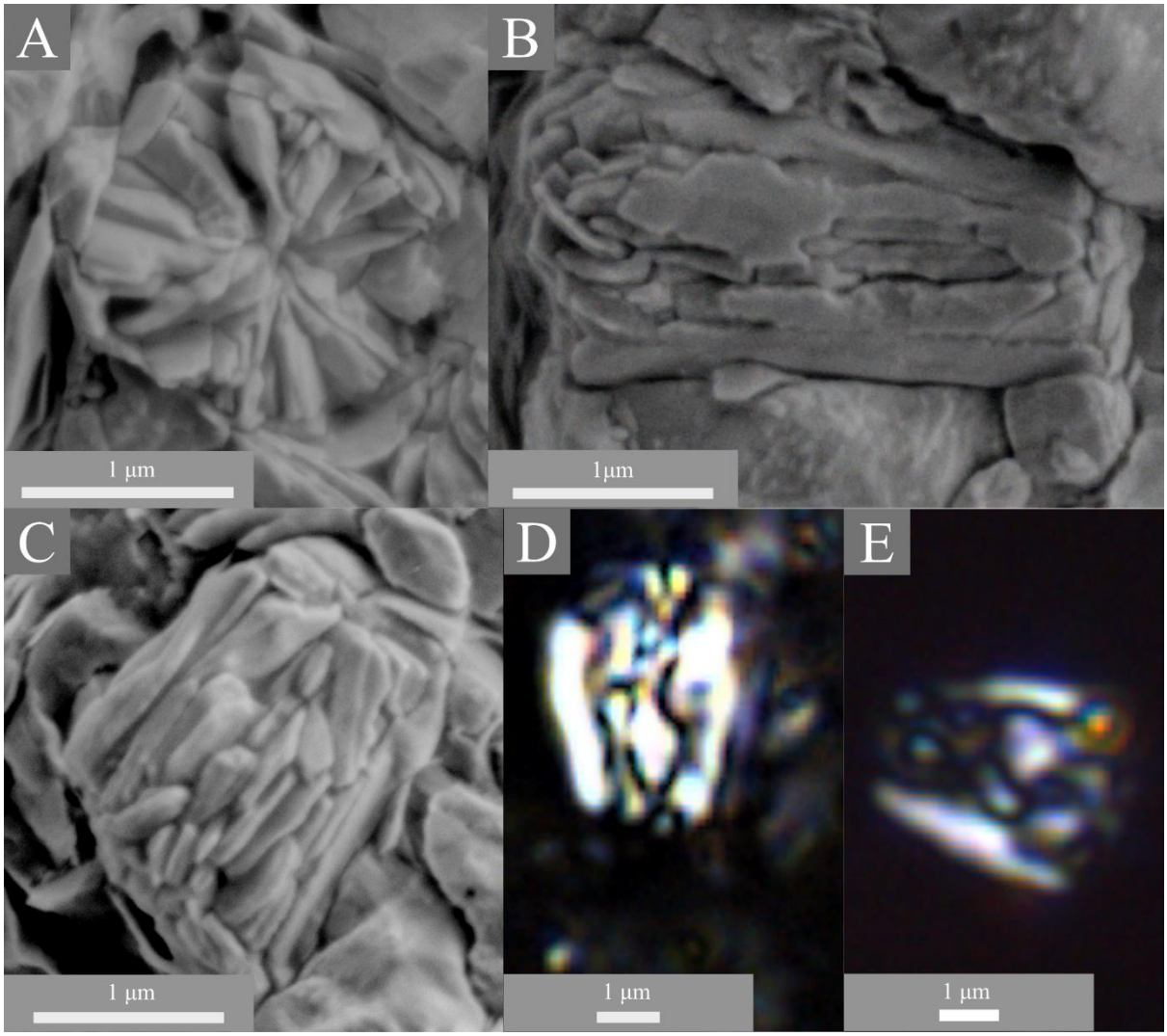

Fig.5.5 – *Eoconusphaera hallstattensis* observed under SEM (A – C; sample Zl 6.4202) and in LM with XPL (D, E) with A) top view; B) Side view showing the external and internal lamellae; C) Side/top view showing the inner part with vertical lamellae; D) Side view showing the dome shape at the distal (broader) extremity of the specimen (Zl 14.9960) ; E) Side view (Zl 5.5164).

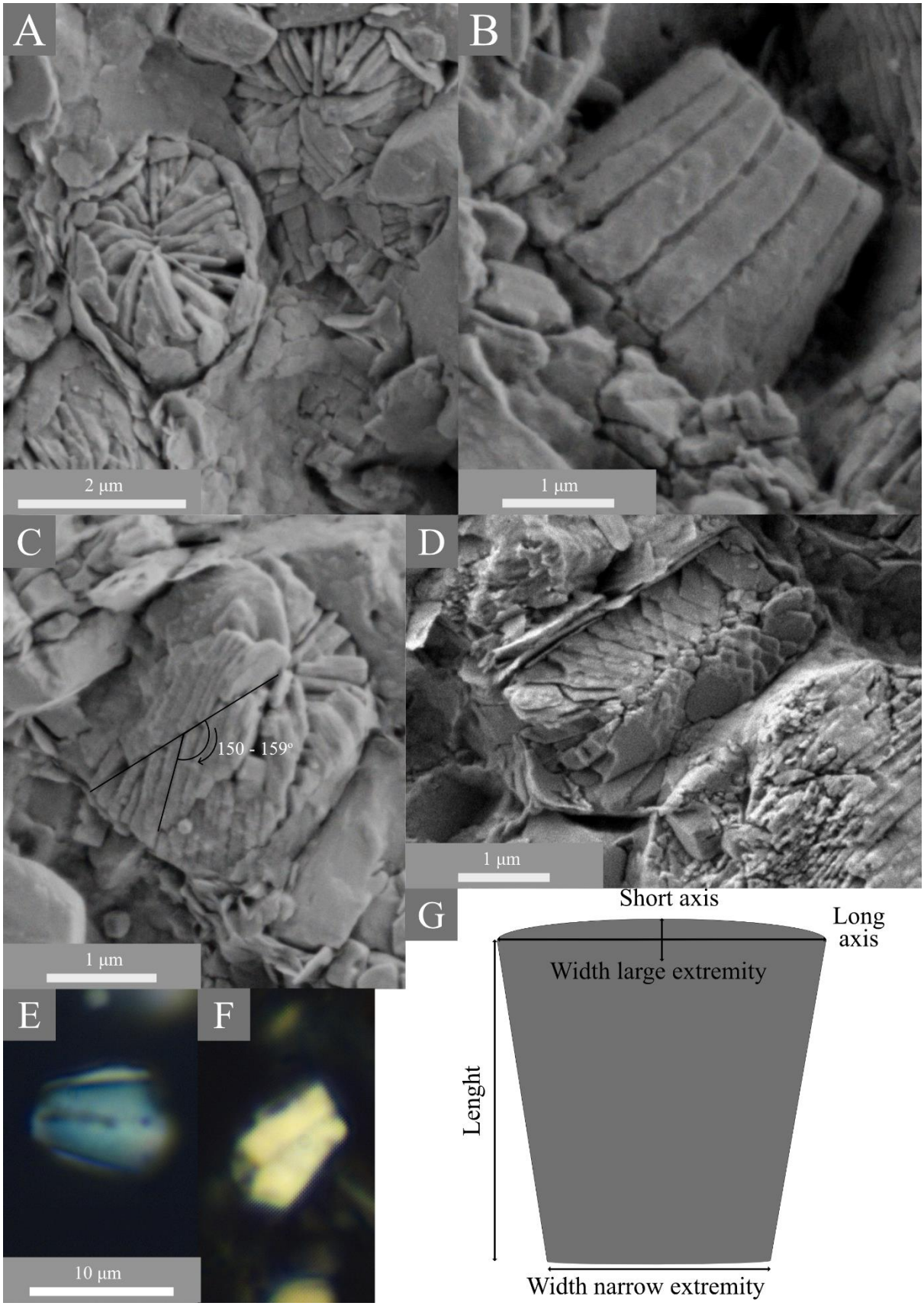
A
2 µm
B
1 µm
C
150 - 159°
1 µm
D
1 µm
E
F
10 µm
G
Short axis
Long axis
Width large extremity
Lenght
Width narrow extremity

Fig.5.6 – *Eoconusphaera zlambachensis* under the SEM (A – D) and in LM (E, F) with A) Top view of two specimens (Zl 51.8669); B) Side view showing the external lamellae (Zl 51.8669); C) Side/top view showing the rows of oblique lamellae (Zl 51.8669); D) Side view showing the central suture, the oblique lamellae and the external lamellae (Zl 52.8554); E, F) Side view of two specimens observed in two different extinction pattern (Zl 54.6829); G) Schematic view showing the measurements done on the Eoconusphaeraceae.

Calcispheres (other than *P. triassica*) are present in almost all of the samples, except for the interval between 11.3 and 11.7 m and at 12.9 m, but sometimes they are represented by only one or two species. Among the three species identified, *Obliquipithonella rhombica* (Fig. 5.7 B) is the most abundant (present in 21 out of 31 samples), followed by *Orthopithonella geometrica* (Fig. 5.7 A) and *Thoracosphaera wombatensis* (Fig. 5.7 C). The three species do not vary in shape across the investigated section. The mean sizes of *Thoracosphaera wombatensis*, *Orthopithonella geometrica* and *Obliquipithonella rhombica* are 7 (± 2) µm, 8 (± 2) µm and 9 µm, respectively.

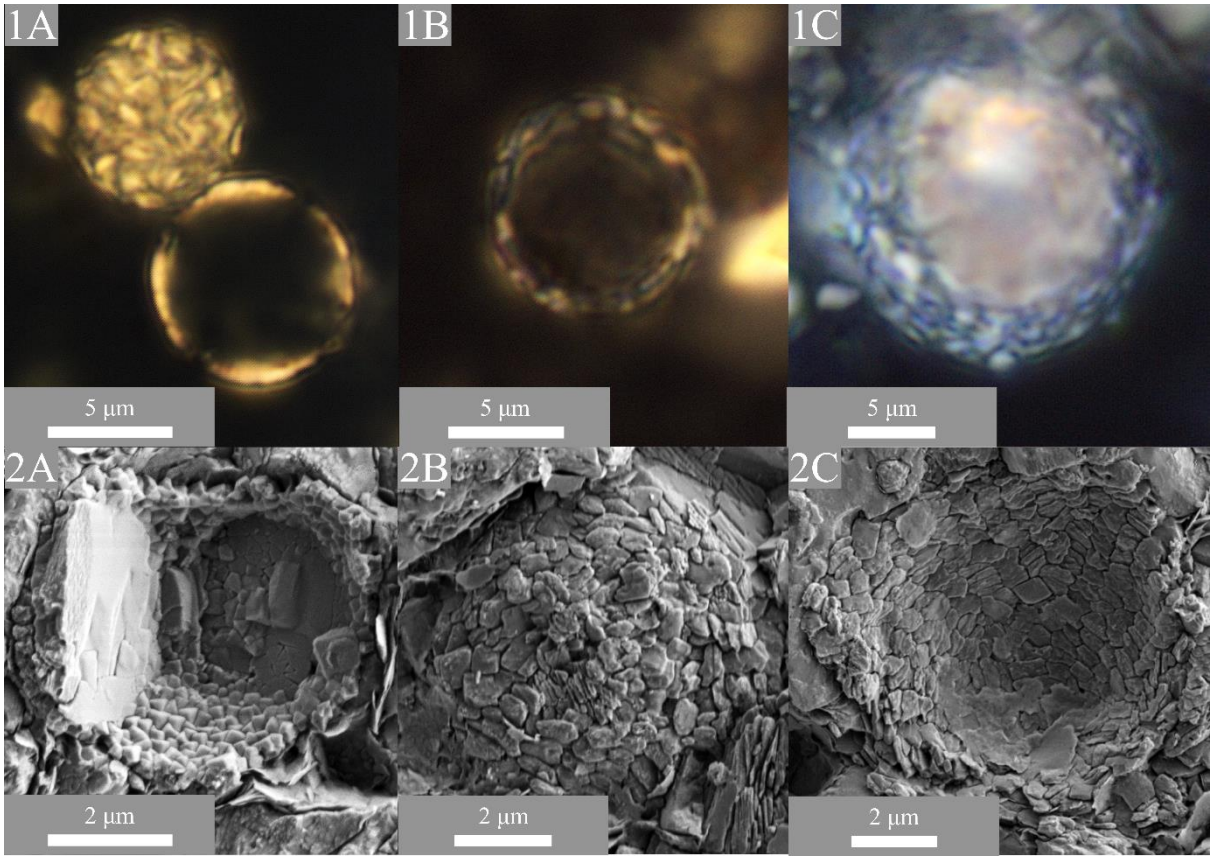

Fig.5.7 – Calcispheres under LM with XPL (1; Zl 39.0211) and under SEM (2). A) *Orthopithonella geometrica* (lower Rhaetian; Zl 6.4202, 2A). B) *Obliquipithonella rhombica* (lower Rhaetian; Zl 52.8554, 2B). C) *Thoracosphaera wombatensis* (middle Rhaetian; Zl 52.8554, 2C).

Coccolithophorids are presents in every sample, except for sample Zl 13.682, however, some specimens remain undetermined at the species level due to lack of characteristic structures. The three coccolithophorids species do not vary in shape and size during the Rhaetian: *C. minutus* and *C. primulus* have a mean size of 2.4 µm × 1.7 µm and *A. koessenensis* has a mean size of 3 µm × 2 µm.

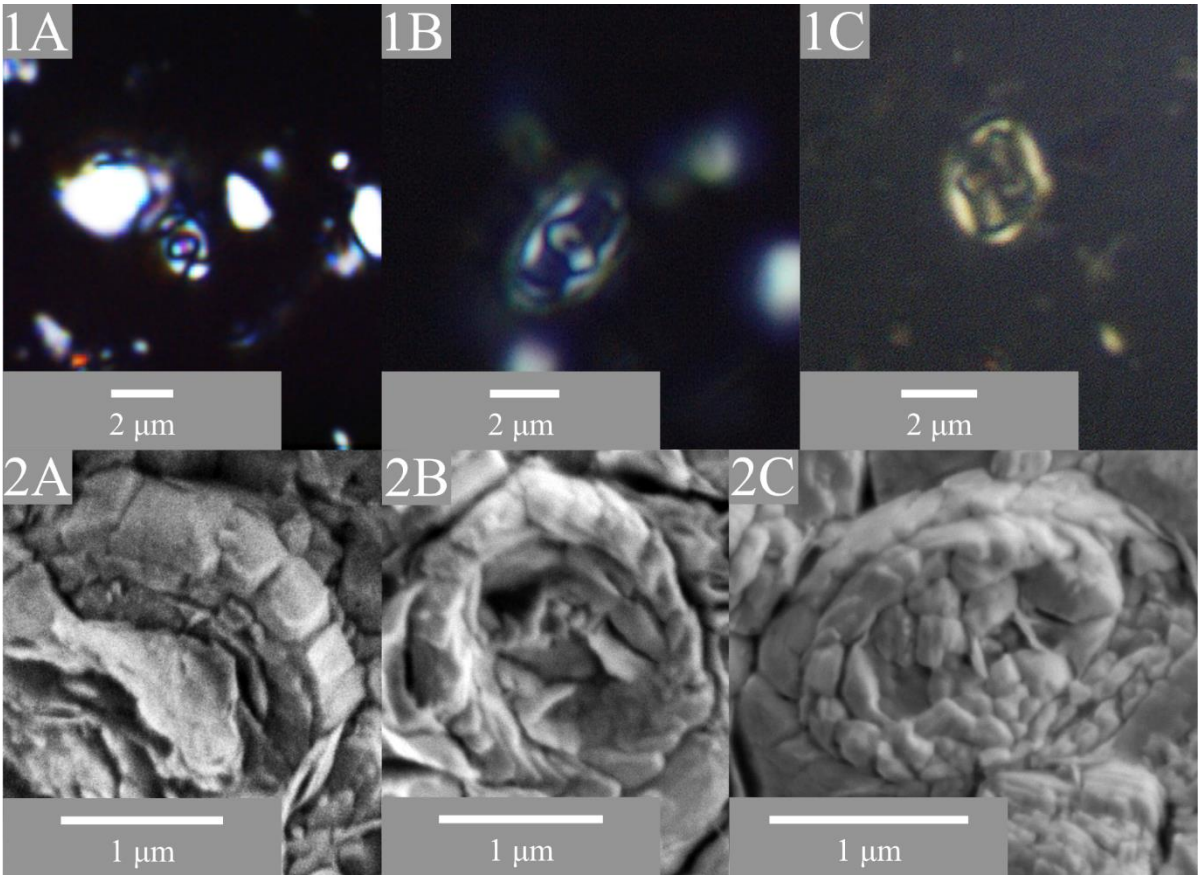

Fig.5.8 – Coccoliths in LM with XPL (1) and under SEM from sample Zl 6.4202 (2) with A) *Crucirhabdus minutus* (lower Rhaetian; Zl 5.5164, 1A); B) *Archaeozygodiscus koessenensis* (lower Rhaetian; Zl 8.6847, 1B). C – *Crucirhabdus primulus* (lower Rhaetian; Zl 14.9960, 1C).

A possible coccolith was observed in sample Zl 6.1944. It has an oval-shape, a length of 5 µm and a width of 4 µm and presents an oval, opened, central area likely filled by a central spine visible as knobs under light microscope. With polarized light, it shows a weakly birefringent rim with kinked isogyres (Fig. 5.9). Its structure differs from Upper Triassic heterococcoliths which are murolith presenting narrow, bicyclic rims with an outer cycle made of V-units. However this specimens (Fig. 5.9) seems to have a narrow central area and a wide

rim similar to placolith presenting well developed R-unit rim (e.g. Watznaueriaceae). Alternatively, the structure can be related to the holococcolith such as the *calculites* presenting a proximal plate of four blocks, a central spine and appears entirely bright in cross polarised light. Only one specimen has been observed under the light microscope so far, and more investigation is needed to prove that it is a real component of the coccoliths assemblage or an artefact, although contamination is a lower risk since the smear slides were prepared in a sterile clean room with the samples from the Zlambach section only.

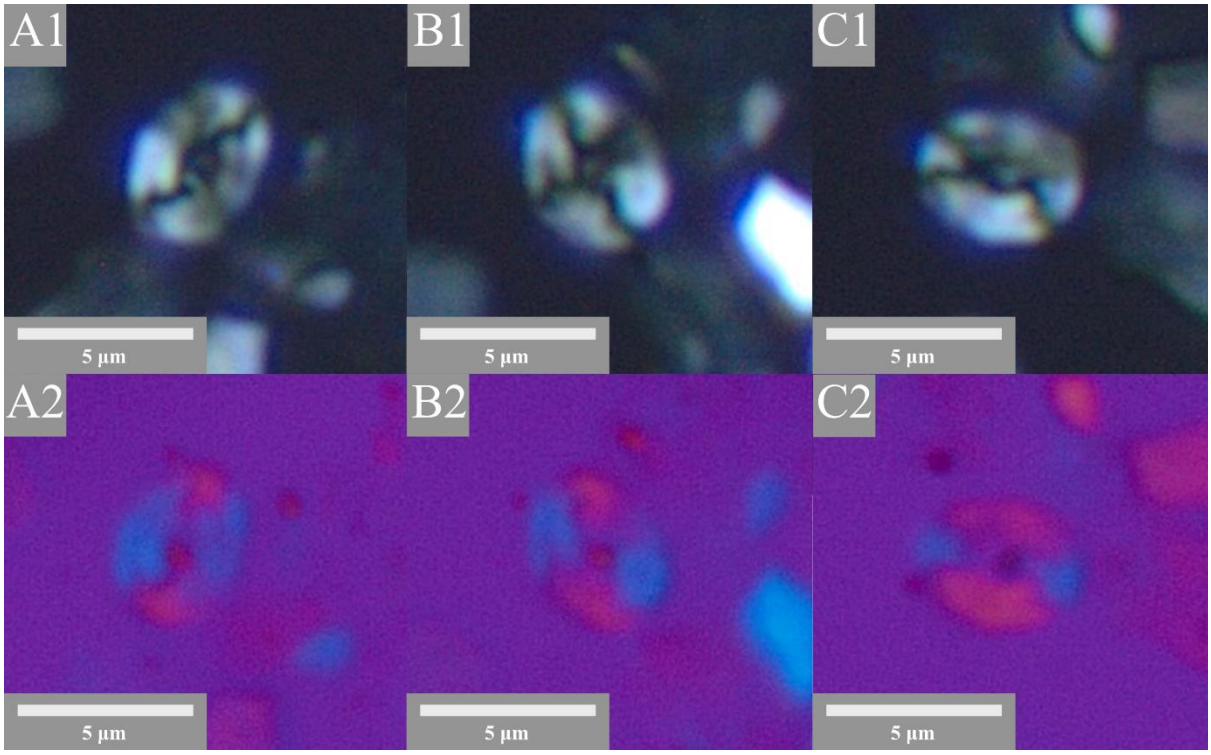

Fig.5.9 – Specimen of an unknown coccolith, sample Zl 6.1944 from the Lower Rhaetian in LM with XPL (1) and gypsum plate (2).

4.2 *Calcareous nannofossils abundance*

The nannofossils assemblage is mostly dominated by the calcisphere, *P. triassica* (Fig. 5.3) with relative abundances between 32 and 88 % (Fig. 5. 10), while the sub-species *P. triassica crenulata* is presents with low abundance (Fig. 5.4). The conical nannoliths, *Eoconusphaera hallstattensis* (Fig. 5.5) and *Eoconusphaera zlambachensis* (Fig. 5.6) show relative abundances of between 5 and 67 %. In five samples (out of 19 samples), they are even more abundant than *P. triassica*. The calcispheres (*P. triassica* not included), *Orthopithonella*

geometrica (Fig. 5.7 A), *Obliquipithonella rhombica* (Fig. 5.7 B) and *Thoracosphaera wombatensis* (Fig. 5.7 C), display relatively abundances between 0.1 and 33 %, if present in the sample. Throughout the section, the dominant species, i.e. *Obliquipithonella rhombica* shows an abundance between 1 and 32 specimens per transect, reaching the maximum in sample Zl 42.4778. *Orthopithonella geometrica* is present in many samples (20 of 31). The abundance of this species varies between 1 and 15 specimens per transect with its maximum in sample Zl 13.682. *Thoracosphaera wombatensis* is present in 15 out of 31 samples with a low abundance between 1 and 9 specimens per transect, reaching its maximum in sample Zl 42.4778. The three coccolithophorids, *Crucirhabdus minutus* (Fig. 5.8 A), *Archaeozygodiscus koessenensis* (Fig. 5.8 B) and *Crucirhabdus primulus* (Fig. 5.8 C), represent a minor part of the total nannofossils assemblage with relative abundances between 0.2 and 8 %, if present. *Crucirhabdus minutus* dominates the coccolithophorids, followed by the undetermined specimens, *C. primulus* and *A. koessenensis*. *C. minutus* is present in most of the samples (23 of 31) reaching a maximum abundance during the *V. stuerzenbaumi* Zone, with 51 specimens per transect at 36 m. *Crucirhabdus primulus* was observed in 19 samples (of 31), with two slight increases in abundance, reaching 5 and 10 specimens per transect at 9.8 and 36 m, respectively. *A. koessenensis* is scarce in the lower to middle Rhaetian and present only in 10 samples (of 31). This species reaches a maximum of 3 to 4 specimens per transect in the middle Rhaetian between 36 and 42.5 m in the section. The same trends in abundance were recognized for the undetermined specimens with 1 and 9 specimens per transect along the section and two increases reaching 20 and 28 specimens per transect at 9.8 and 36 m in the profile, respectively (Fig. 5.11).

The absolute abundance of each species present in the assemblage are represented in the figure 5.11. The nannofossils accumulation rate varies between 1.5×10^9 and 3.5×10^{10} (nannos / cm^2 / Myr) (Fig. 5.10). The nannofossils accumulation rate show an increases toward 10 m reaching 9×10^9 (nannos / cm^2 / Myr). After a slight decrease the value higher again around 20 m to 1×10^{10} (nannos / cm^2 / Myr). Minimum values are reaches around 30 m with 8×10^8 (nannos / cm^2 / Myr). The maximum nannofossil accumulation rate is reach at 36 m with 3.5×10^{10}, then decrease to 3.5×10^9 (nannos / cm^2 / Myr) at the top of the section.

The wt% $CaCO_{3}$ *P. triassica* varies between 0.3 and 19 %, with fluctuation throughout the Zlambach section, however, four distinctive increases are recognizable (Fig. 5.10). In the *P.*

suessi Zone, the percentage of *P. triassica* increases gradually to reach 14 % from the base of the section until 10 m. After a sudden decrease, an abrupt increase is seen at 13 m in the profile reaching a maximum concentration of 19 % in the bulk rock. Up-section the concentration of *P. triassica* drops, followed by another gradual increase to 13 % at 22 m. Afterwards, the concentration of *P. triassica* decreases again until the *V. stuerzenbaumi* Zone and subsequently stabilises until the FO of *E. zlambachensis*. The maximum abundance of the nannoliths and coccolithophorids comes along with a percentage increase up to 18 % in the rock record. Toward the top of the Zlambach section, the percentage decreases gradually.

All the data are available online: 10.17632/r62z95vzn8.1.

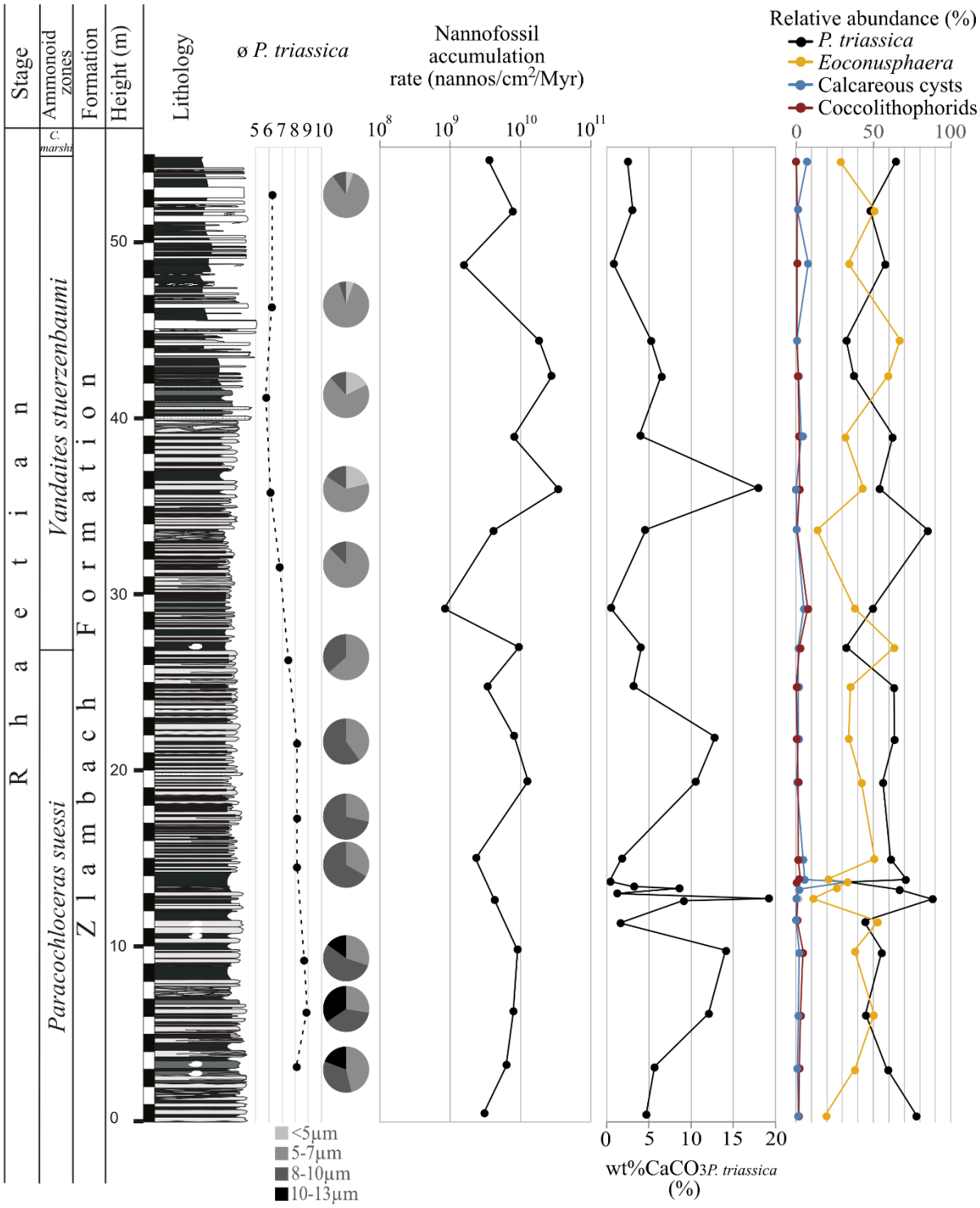

Fig.5.10 – Compilation of the calcareous nannofossils record at the Kleiner Zlambach section. 1st column - Lithology of the Rhaetian Zlambach Formation with the *P. triassica* size variation and pie charts showing the percentage of the different size clusters. 2nd column – Nannofossil accumulation rate including all species present

(nannos/cm^2/Myr). 3rd column - Concentration of *P. triassica* (%) in the sediment. 4th column - Relative abundance (%) of all calcareous nannofossils observed in the samples.

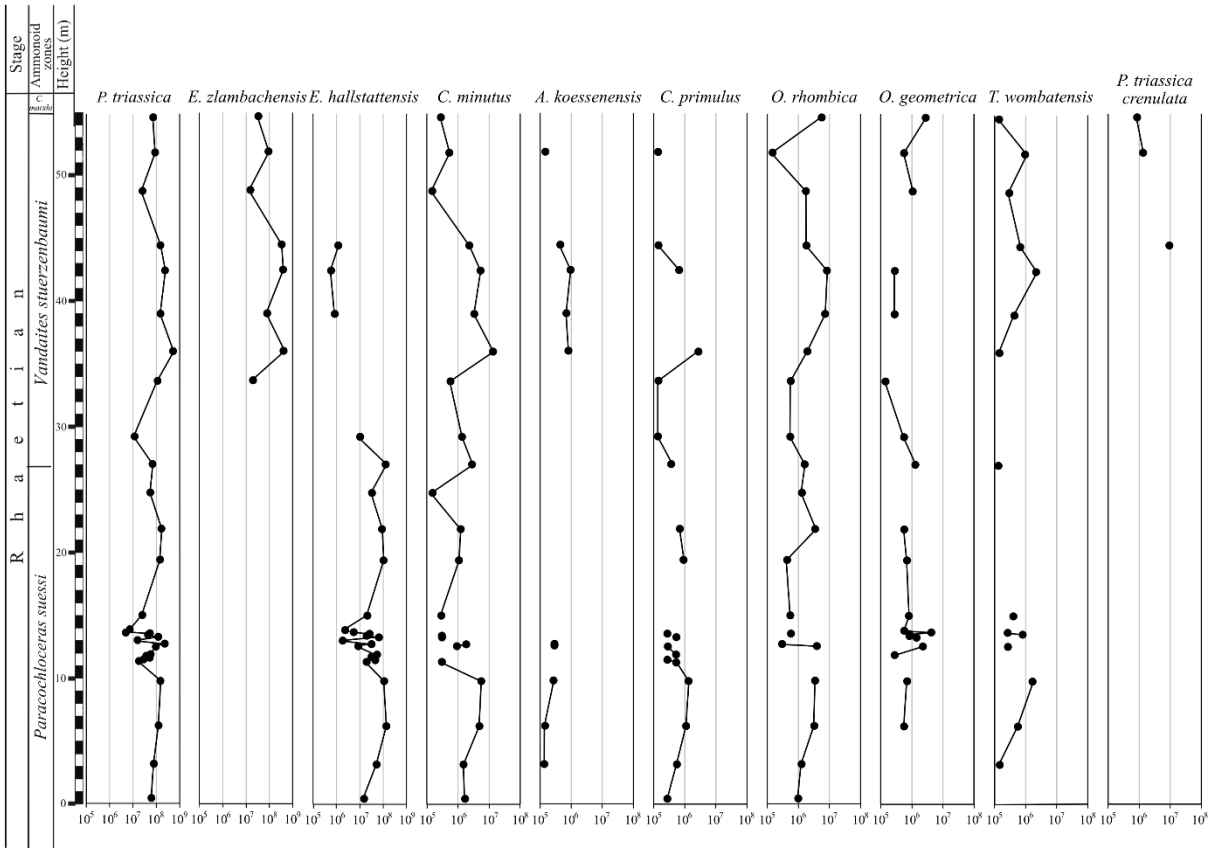

Fig.5.11 –.Absolute abundance of the different species present in the assemblage at the Zlambach section.

4.3 *Nannolith size variation*

4.3.1 Prinsiosphaera triassica

The size of *P. triassica* in the section varies between 4 and 12 µm with the mean diameter ranging from 9 µm in the lower Rhaetian to 6 µm in the middle Rhaetian, ± 0.2 and ± 0.5 µm (1 σ) respectively (Fig. 5.10). The *P. suessi* Zone records a broad range of *P. triassica* sizes, which vary from medium (5 – 7 µm), large (8 – 10 µm) and up to very large (11 – 13 µm). From the top of the lower Rhaetian until the base of the middle Rhaetian, the very large sized type of *P. triassica* disappears, replaced by the small sized type of *P. triassica* (< 5 µm) (Fig. 5.10). There is a marked decrease in the mean size of *P. triassica* around the *P. suessi* – *V. stuerzenbaumi* zones boundary.

4.3.2 Eoconusphaeraceae

The size variation of the two species, *E. hallstattensis*, *E. zlambachensis*, was measured on 67 and 48 specimens, respectively, in SEM. The specimens were observed in side view, which allows measuring of the total length and width of the distal (broad) and proximal (narrow) extremity of the truncated cone-shaped nannolith (Fig. 5.6 G). The specimens were also observed in top view making measurements of the long and short axis of the oval-shaped extremity possible. *E. hallstattensis* has a length between 2 and 6 µm (mean = 3.5 µm), a width between 1 and 3 µm for the distal extremity (mean = 2 µm) and between 1 and 2.6 µm for the proximal extremity (mean = 1.7 µm). In top view, *E. hallstattensis* has a long axis between 1.7 and 4.5 µm (mean = 3 µm) and a short axis between 1.3 and 3 µm (mean = 2 µm). *E. zlambachensis* has a length between 2 and 5 µm (mean = 3 µm) and a width between 1.5 and 3.5 µm for the distal extremity (mean = 2 µm) and between 1 and 2.5 µm for the proximal extremity (mean = 1.7 µm). In top view, *E. zlambachensis* has a long axis between 2 and 3.5 µm (mean = 2.5 µm) and a short axis between 1 and 3 µm (mean = 2 µm). The inclination angle of the inner lamellae of *E. zlambachensis* (Fig. 5.6 C) varies between 150º and 159º (determined based on the analysis of 17 specimens).

E. hallstattensis and *E. zlambachensis* have a broad range of sizes across the section, but these also vary within the same sample. Their sizes range from large and small to long and narrow with all size types in-between (Fig. 5.12). The size measurements do not show any clusters of sizes, but a rather continuous size range for both species. Figure 12 highlights the similar size range of the two species.

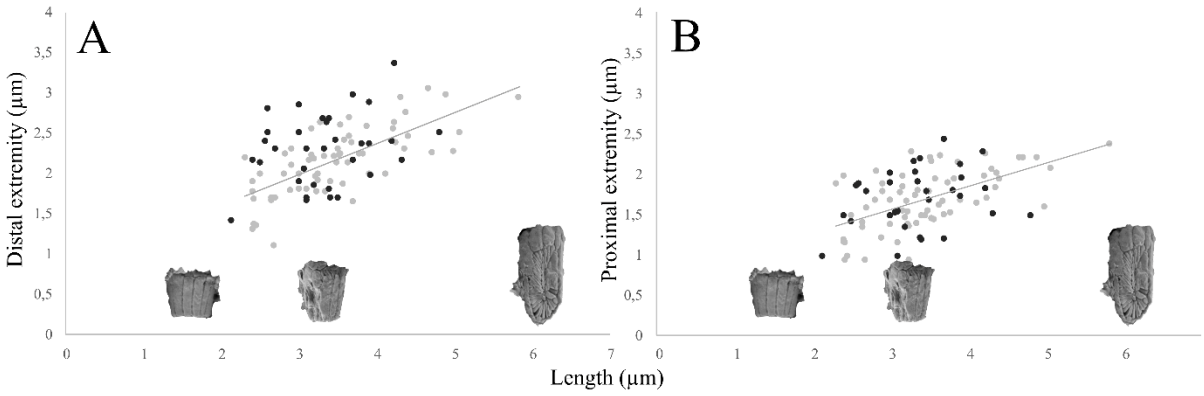

Fig.5.12 – Cross plot of the length of *E. hallstattensis* (grey dots) and *E. zlambachensis* (black dots) versus A: broad extremity (distal) width and B: narrow extremity (proximal) width.

4.4 *Calcareous nannofossils preservation and diagenetic impact*

The bulk samples are composed of micritic limestones with dominantly calcite mineralogy and contain some clay minerals but barely dolomite. The sole biogenic components recognized in the sample set are calcareous nannofossils. Their identification is sometimes difficult due to partly highly abundant clay minerals, which cover the nannofossils. Some dissolution patterns are visible in the samples, such as dissolution pits, rough calcite surfaces and rounded particle edges of the abiogenic material. However, no recrystallization patterns (calcite step-growth, transitions of micrite to calcite spar, dolomitization) are visible. Therefore, a large diagenetic impact on calcareous nannofossils preservation degree and abundance can be reasonably ruled out. Moreover, the *P. triassica* specimens appear with all inner or outer calcite lamellae visible, which can be assigned to stage 3 (relatively good preservation degree) applying the classification of Bralower et al., (1991). The two *Eoconusphaera* species do not seem to be impacted by diagenesis either. Indeed, their inner structure, i.e. the lamellae, the core and the inclination of *E. zlambachensis*, is still intact and visible. The calcareous cysts and the coccolithophorids also appear in good preservation with their structure and all characteristic elements clearly visible.

The impact of diagenesis was also studied through analysis of the elemental composition (Table 1) of the limestone beds. The chemical composition is similar for almost all of the samples analysed, except for sample Zl 19.9249. The latter represents a calciturbidite layer, which has a markedly higher Mg (3 wt%), Fe (1.3 wt%), Si (2.8 wt%), Al (1.2 wt%) and K (0.3 wt%) content and lower Ca content (15.9 wt%), compared to the other samples. These have a high Ca content ranging between 30.6 and 39 wt%, as well as minor Mg (0.7 – 1.8 wt%), Fe (0.2 – 0.6 wt%), Si (0.5 – 1.6 wt%), Al (0.2 – 0.7 wt%) and K (0.1 – 0.2 wt%) contents. This composition reflects the dominant $CaCO_3$ mineralogy with a minor presence of dolomite, Fe-(hydr)oxides and clay minerals (see also Kovács et al., 2020). The Al/Ca vs. Fe/Ca cross-plot shows a positive linear correlation ($R^2 = 0.82$; Fig. 5.13 A), indicating that all Fe has a continental-detrital origin and thus cannot be used as an indicator for diagenesis. However, the relatively high Na (268 – 605 ppm) and Sr (630 – 1156 ppm) contents and the low Mn (221 – 475 ppm) content (Fig. 5.13 B) argue against overprinting of the pristine chemical composition of the rocks during burial diagenesis, which would lead to a depletion in Na and Sr and

enrichment in Mn (e.g. Baldermann et al., 2015; Kovacs et al., 2020; Demangel et al., 2020) not observed here.

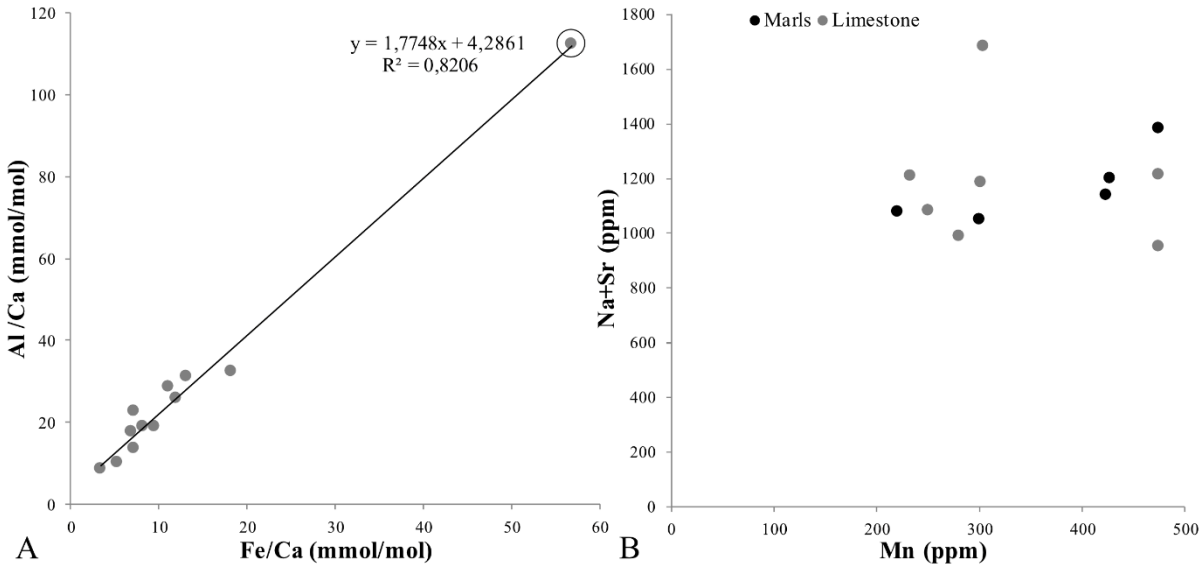

Fig.5.13 – Cross plot of A: Al/Ca (mmol/mol) and Fe/Ca (mmol/mol); B: Na+Sr (ppm) versus Mn (ppm).

5. Discussion

5.1 *Upper Triassic Calcareous nannofossils affinity*

The quantitative investigation of the calcareous nannofossils at the Zlambach section bring new information to understand the affinities of the Upper Triassic calcifiers. Orthopithonelloideae and Obliquipithonelloideae were suggested to belong to the calcifying dinoflagellates (Janofske, 1992) as *O. misurinae* presents a circular opening similar to an archeopyle (opening in the wall typical for the dinocyst) and *O. prasina* presents a wall ultrastructure close to the wall of Cretaceous dinocyst (Janofske, 1992). Thus, the Norian-Rhaetian species, *Orthopithonella geometrica* and *Obliquipithonella rhombica* were first described as cyst from calcareous dinoflagellates, and then this affinity was questioned as characteristics from the dinocysts such as the opening in the wall (archeopyle) or the tabulation (number and position of articulated plates) are not always recognized. Calcareous dinoflagellate cysts are resistant to adverse conditions (Fensome et al., 1993) and their formation is often triggers by changes in temperature, nutrients and/or light availability (Pfiester and Anderson, 1987). During *V. stuerzenbaumi* Zone (middle Rhaetian), major

turnover and occurrence of high latitude palynological assemblage suggest a cooling event. Additionally, the productivity of the platform dropped leading to reduced availability of nutrients (see below *Prinsiopshaera triassica size decrease*). Those palaeoenvironmental perturbations occurring along with the increase in *Orthopithonella geometrica* and *Obliquipithonella rhombica* and the decrease of the other calcareous nannofossils support an affinity of those two species to the Dinophyceae.

Thoracosphaera wombatensis is included in the Thoracosphaeroideae belonging to the dinophyceae (Gottschling et al. 2008). However, *T. wombatensis* was also suggested to belong to the nannolith Schizosphaerellaceae (Streng et al., 2004). In the studied section, *T. wombatensis* is rare but its abundance show similar fluctuation than the other calcareous dinoflagellates, especially *O. rhombica*. However, the abundance of *T.wombatensis* at the topmost section do not increase as the abundance of *Orthopithonella geometrica* and *Obliquipithonella rhombica*. Indeed, the calcareous sphere produce by the *Thoracosphaera* species corresponds to coccoid, vegetative phase with a calcareous wall produce after asexual division (Tangen et al., 1982) and not triggers by environmental changes. This different mode of formation explain the inverse abundance variation at the top of the section subject to cooling event and decrease in nutrient availability. The calcareous wall formation of the extant species *Thoracosphaera heimii* is described with rhombic and irregular, polygons, early grown crystals. Such structure can be observe in the species of *T. wombatensis* observe in the NCA (Fig. 5.7) (Demangel et al., 2020). Those observations are in favour to an affiliation of *T. wombatensis* to the Dinophyceae.

The subspecies *Prinsiosphaera triassica crenulata* was first described by Jafar (1983) from the Zlambach section. Named after its crenulated or wavy structure (Fig. 5.4), the subspecies has a spherical shape made of wavy striation, corresponding to calcite lamellae oriented parallel to each other. Bralower et al. (1991) rejected this subspecies and hypothesized that these structures are the result of etching and overgrowth processes associated with diagenesis. However, our observations show striation features similar to those reported by Jafar (1983), under both LM and SEM, which supports the validity of the subspecies *P. triassica crenulata*. From our observation, this species occurs in the middle Rhaetian (*V. stuerzenbaumi* Zone) with a low abundance. *P. triassica crenulata* was also reported from the Southern Tethys Ocean (the North West Shelf of Australia) with a distinct acme in the Rhaetian (Rutledge et

al., 2015). Ten specimens were measured and all have a diameter between 12 and 13 µm, which is higher than the mean diameter of 7 µm reported by Jafar (1983). More size measurements from different localities and time intervals are needed to confirm the potential specific size of *P. triassica crenulata*.

The *Eoconusphaera* species observe in this study are classified as nannolith due to their unknown origin. However, this Upper Triassic conical genus can be compared to the three other conical genera present in the Meosozoic, i.e. Mitrolithus, Calcivascularis (Lower Jurassic) and Conusphaera (uppermost Jurassic to Lower Cretaceous). They are all classified as coccoliths and as the *Eoconusphaera* sp., they present an outer cycle of vertical, non-imbricating elements described as a protolithic rim. The rim of all those conical forms present a broad range of size including low rim of ~ 2 µm, similar to the protolith rim of the Upper Triassic coccolith ancestor *Crucirhabdus minutus*. Additionnaly, the abundance of the *Eoconusphaera* sp. and *C. minutus* at Zlambach section, show a high co-variation (see at 27 m, 42 m and 44 m). Those observations support the hypothesis that *E. hallstattensis* and *E. zlambachensis* descend from *C. minutus* and are related to the coccolithophorids.

5.2 *Calcareous nannofossils evolution during the Rhaetian at Zlambach section*

Studies on Upper Triassic calcareous nannofossils are mainly concentrated on the Norian/Rhaetian boundary and the Rhaetian stage. As highlighted by the figure 5.14, few studies focuse on Carnian and none on lower Norian (Lacian). Additional, investigations on Carnian and Norian sediments are needed to better constrain the evolution of early calcifiers. During the Late Triassic, different groups of calcareous nannofossils including dinocysts, nannoliths and coccoliths, started to diversify slowly and increased in abundance in the rock record (Gardin et al., 2012; Preto et al., 2013; Demangel et al., 2020). The nannofossil accumulation rate mainly fluctuate around 9×10^9 (nannos / cm^2 / Myr) but reach around 36 m a maximum at 3.5×10^{10} (nannos / cm^2 / Myr). Those value corresponds with the lower Jurassic nannofossil accumulation rate fluctuating around 10^9 (nannofossil m^2 yr^{-1}) during the Sinemurian (Suchéras-Marx et al., 2019).

The cysts from calcareous dinoflagellates present a low diversification with two species in the lower Carnian (Cordevolian), i.e. *Obliquipithonella prasina* (Janofske, 1992), *Orthopithonella misurinae* (Janofske, 1992) occurring in the Western Tethys and seems to

disappear during the Cordevolian/Julian turnover event (Fig. 5.14). The sister taxa *Orthopithonella geometrica* (Jafar, 1983) is observed from the mid-Norian (Alaunian 3) in the Western Tethys (Demangel et al., 2020) and the Southern Tethys Ocean (Bralower et al., 1991). *Obliquipithonella rhombica* (Janofske, 1987) evolved from the lower Rhaetian and is observed only in the Western Tethys (Demangel et al., 2020). In the Zlambach section, both *O. geometrica* and *O. rhombica* present a low abundance but *O. rhombica* is more numerous. The Thoracosphaeroideae are present only with *T. wombatensis* presenting a very low abundance. This species was first described in the Southern Tethys (Bralower et al., 1991) but also occurs in the Western Tethys from the mid-Norian (Fig. 5.14) (Demangel et al., 2020).

The incertae sedis, *Prinsiosphaera triassica*, is first describe from the mid-Norian in the Western Tethys (Fischer et al., 1967) but observed at the same time in the Southern Tethys (Bralower et al., 1991). In all localities analysed, this species dominates the assemblages of calcareous nannofossils (Bralower et al., 1991; Gardin et al., 2012; Preto et al., 2013; Demangel et al., 2020), except in some interval in this study. In the Western Tethys, the percentages of *P. triassica* composing the rocks (wt% $CaCO_{3P.\ triassica}$) were estimated in Italian (Pizzo Mondello, Pignola-Abriola) and Austrian sections (Steinbergkogel, Zlambach). In the Austrian section, *P. triassica* composes less than 2 % of the rock record during the Norian, reaching 5 % in the early Rhaetian (*P. suessi* Zone) (Demangel et al., 2020). At the Zlambach section, the wt% $CaCO_{3P.\ triassica}$ varies globally around 5 % with two increases around 15 % in the lower Rhaetian (*P. suessi* Zone) and two up to 20 % in the lower and middle Rhaetian (*V. stuerzenbaumi* Zone). Those values corroborate the quantification of Preto et al. (2013) at Pignola-Abriola (Lagonegro Basin, Italy), fluctuating between 0 and 20 % in the Norian and Rhaetian. *Prinsiosphaera triassica* did thus not reach rock-forming abundance in the Hallstatt and Lagonegro basins at this time.

From the lower Rhaetian (*P. suessi* Zone), *Eoconusphaera hallstattensis* (Demangel et al., 2020) and from the middle Rhaetian (*V. stuerzenbaumi* Zone) *Eoconusphaera zlambachensis* are present in the Western and Southern Tethys Ocean. We recently revised their taxonomy (Demangel et al., 2021). In the Zlambach section, *E. zlambachensis* is more abundant than *E. hallstattensis*, reaching maximum abundance in the middle Rhaetian (*V. stuerzenbaumi* Zone). In the Zlambach section, the first occurrence of *P. triassica crenulata* in the middle *V. stuerzenbaumi* Zone (middle Rhaetian) corresponds to the last occurrence of *E.*

hallstattensis. Throughout the Rhaetian, three zones can be recognized first *E. hallstattensis* alone, then *E. hallstattensis*/*E. zlambachensis* and *E. zlambachensis*/*Prinsiosphaera triassica crenulata*. Those three species could be used as biostratigraphic markers in the Rhaetian in the Northern Calcareous Alps.

Known since the mid-Norian, the coccolithophorids evolved slowly in diversity throughout the Upper Triassic (Demangel et al., 2020) (Fig. 5.14). During the Norian, two species occur with low abundance: *Crucirhabdus minutus* (Jafar, 1983) and then *Archaeozygodicus koessenensis* (Bown, 1985). From the lower Rhaetian, a third species, *Crucirhabdus primulus* (Prins, 1969), appeared and it is the only coccolithophores species known to have survived after the end-Triassic mass extinction (Fig. 5.14). During middle Rhaetian, coccolithophorids show a slight increase in abundance reaching 7.5 % of relative abundance, but they remain the least abundant type of calcareous nannofossils during the Late Triassic. *Crucirhabdus minutus*, the suggested ancestor is the far most abundant coccoliths species.

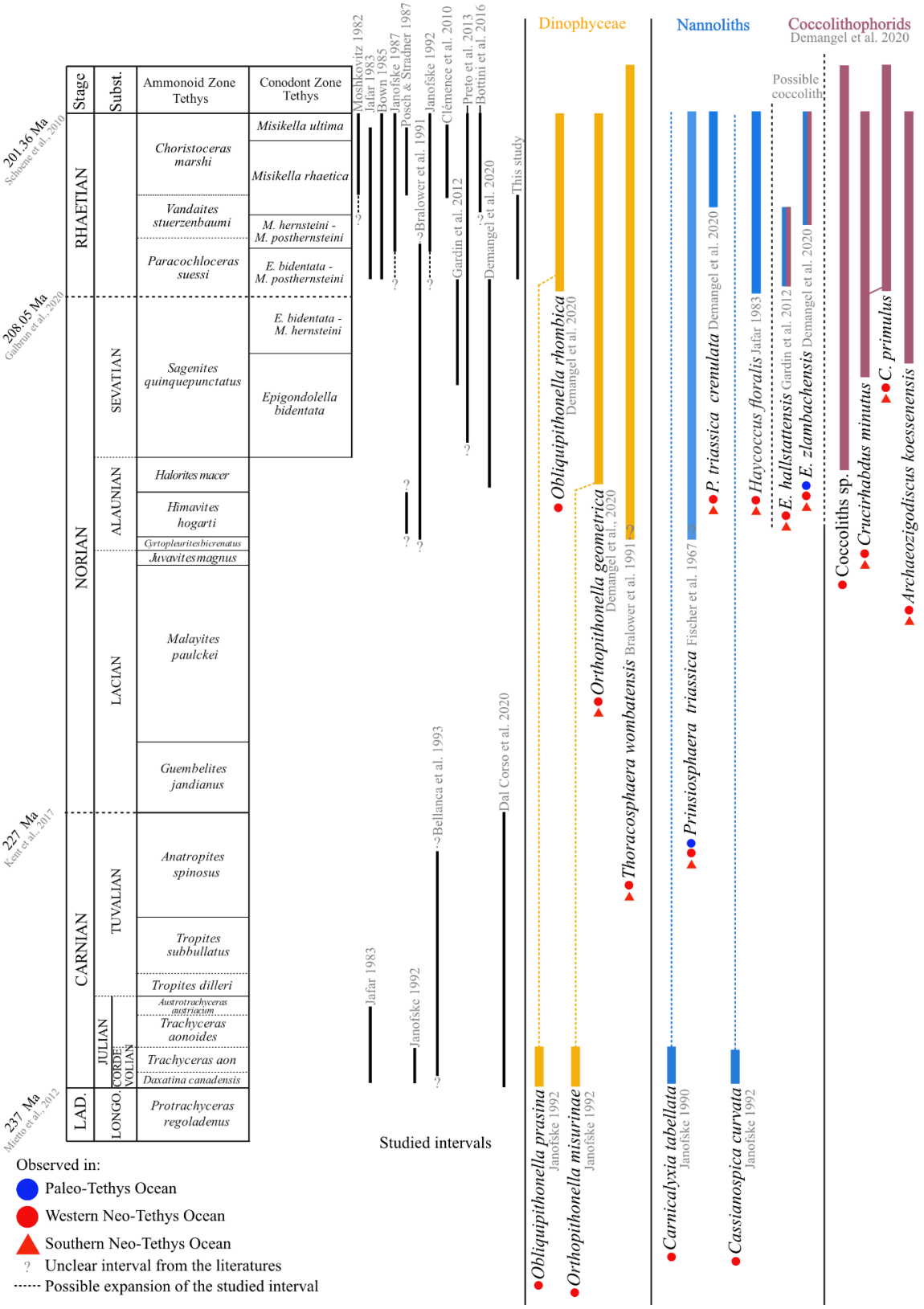

Fig.5.14 – Late Triassic biozonation based on ammonoids and conodonts for the Tethyan realm (Galbrun et al., 2020; Ogg et al., 2020) along with the calcareous nannofossils ranges of the Upper Triassic.

5.3 *Size variation of the nannoliths*

5.3.1 The Eoconusphaeraceae

Concerning the size evolution of the Eoconusphaeraceae, Bralower (1991) and Kristan-Tollmann (1995) have reported on the evolution of *C. zlambachensis* from a short, stubby shape (length: 2 to 4 µm, average: 3 µm) to a narrow, elongated form (length: 3 to 6 µm, average: 5 µm). Our results reveal a broad range of sizes for both *E. hallstattensis* and *E. zlambachensis*, ranging from short and stubby to long and narrow shapes with a broad range of medium sizes in-between. Our measurements corroborate the average size range of 3 to 5 µm previously reported by Bralower et al. (1991), however, in our study, no temporal evolution of the Eoconusphaeraceae shapes were observed, as many sizes were found in single samples (Fig. 5.12).

5.3.2 Prinsiosphaera triassica size decrease

After its appearance in the middle Norian, *P. triassica* has a constant size (Demangel et al., 2020) but from the top of *P. suessi* Zone a decrease in size is recorded, from 9 to 6 µm on average, which is accompanied with the disappearance of the very large size group of *P. triassica* (10 – 13µm). During the latest Rhaetian (*C. marshi* Zone), Clémence et al. (2010) also reported (i) a decrease in size of *P. triassica* until the extinction of the species and (ii) did not record very large size specimens in another Austrian section (Eiberg). During the latest Rhaetian, Bottini et al. (2016) also reported a size decrease of *P. triassica* in the Italian Southern Calcareous Alps (Italcementi active quarri), however, they recognized the presence of very large sized *P. triassica* (10 – 13 µm) too. They measured a decrease in size from very large (10 – 13 µm) to small (< 5 µm) with the smallest sizes recorded just before the Triassic/Jurassic boundary during the "initial negative Carbon Isotope Excursion (CIE)". The observation of very large specimens in Italy during the latest Rhaetian suggest a local perturbation in the NCA during the middle Rhaetian leading to the size decrease of the population of *P. triassica*.

In our study, the size variations do not correlate to the abundance variations of the other main calcareous nannofossils (Fig. 5.15 A). Thus, a possible competition between species seems unlikely to explain the size decrease. The size and the abundance of *P. triassica* do not

covary, as shown for the end-Triassic mass-extinction as well (Bottini et al., 2016), and hence most likely reflect a perturbation of nannoplankton biocalcification. Clémence et al. (2010) explained the size decrease of *P. triassica* observed during the late Rhaetian either by a local cooling event or a change in seawater chemistry, i.e. lower pH, and suggested warm seawater to be favourable for the bio-productivity of *P. triassica*. Calcareous nannoplankton are highly sensitive to environmental changes (Brand, 1994), such as seawater temperature and chemistry (Clémence et al., 2010; Peti & Thibault, 2017), to nutrient and light availability (Clark & Watkins, 2020; Wulff et al., 2020) and to climatic changes (Möller et al., 2020). The effects of any of these changes are species-dependent and could lead to variations in both abundance and size.

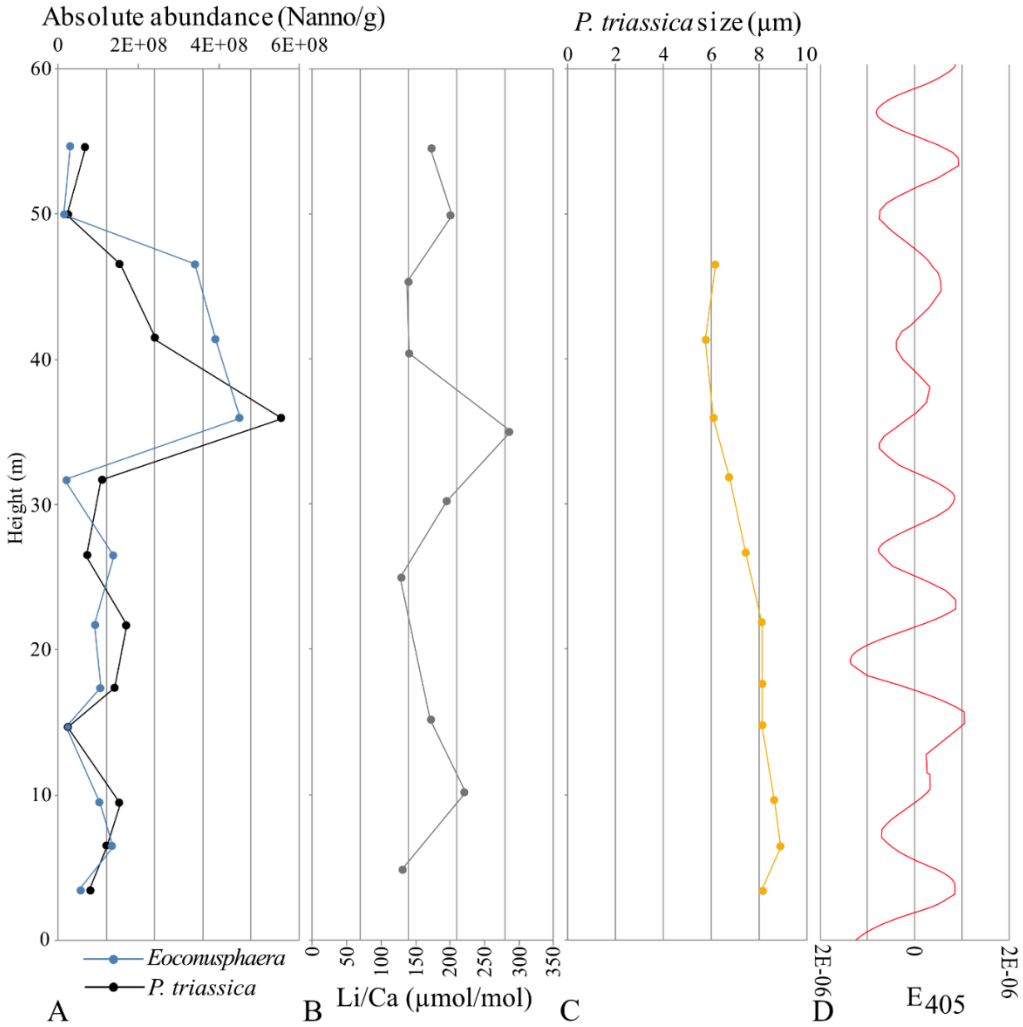

Fig.5.15 – Graphic with A: Absolute abundance of P. triassica and the two Eoconusphaera species (E. hallstattensis, E. zlambachensis) (Nanno/g); B: Li/Ca ratios; C: size variation of P. triassica; D: Eccentricity calculated at Zlambach from magnetosusceptibility measurements by Galbrun et al. (2020).

The Late Triassic in the NCA was characterized by the long term development of the large Dachstein carbonate platform which grew basinward (Fig. 5.1, 5.16). During the middle Rhaetian and contemporaneous with the afore mentioned northern platform retreat, the progradation also slows down at its southern margin. Explained by a platform productivity drop, this led to a pelagic cover developing over the platform margin (Krystyn et al., 2009) and to a reduction in the export of shallow biogenic carbonate to the adjacent Zlambach basin. In the studied section, this process is reflected in (i) pulses of increasing terrigenous input around 36 m and above 40 m and (ii) a change from calcareous marlstones to marlstone at 36 m (Fig. 5.16). The Li/Ca ratio (Fig. 5.15 B), a sensitive indicator of continental influx, also highlights an increased terrestrial contribution, reaching a maximum at 36 m followed by a decrease until 40 m in the section (Kovacs et al., 2020). The decrease in size of *P. triassica* observed from the base of the section onward to 40m could thus be explained by a reduced continentally-derived nutrient availability.

Moreover, the beds cropping out between 35 m and 45 m record a unusual abundance of ammonoids *Cochloceras, Cycloceltites* and *Vandaites* (Richoz & Krystyn 2015; Galbrun et al., 2020) and conodonts (*Norigondolella, Epigondolella*) which are otherwise only sporadically represented or even missing throughout the remaining section. A concurrent burst of the dinoflagellate cysts *Heibergella aculeata* and *Dapcodinium priscum* as well as a turnover in the miospore record were interpreted by Kürschner et al. (2008) as indications of a cooling event and a related transition to more humid conditions. We suggest an inflow of cooler water from the North importing those new assemblages and possibly leading to a change in salinity influencing the calcareous producers. Those palaeo-environment changes could have added stress on the calcifiers community, which after a steady size reduction starting at 22 m of the section would explain the noticeable size minimum of *P. triassica* between 36 and 42 m up-section.

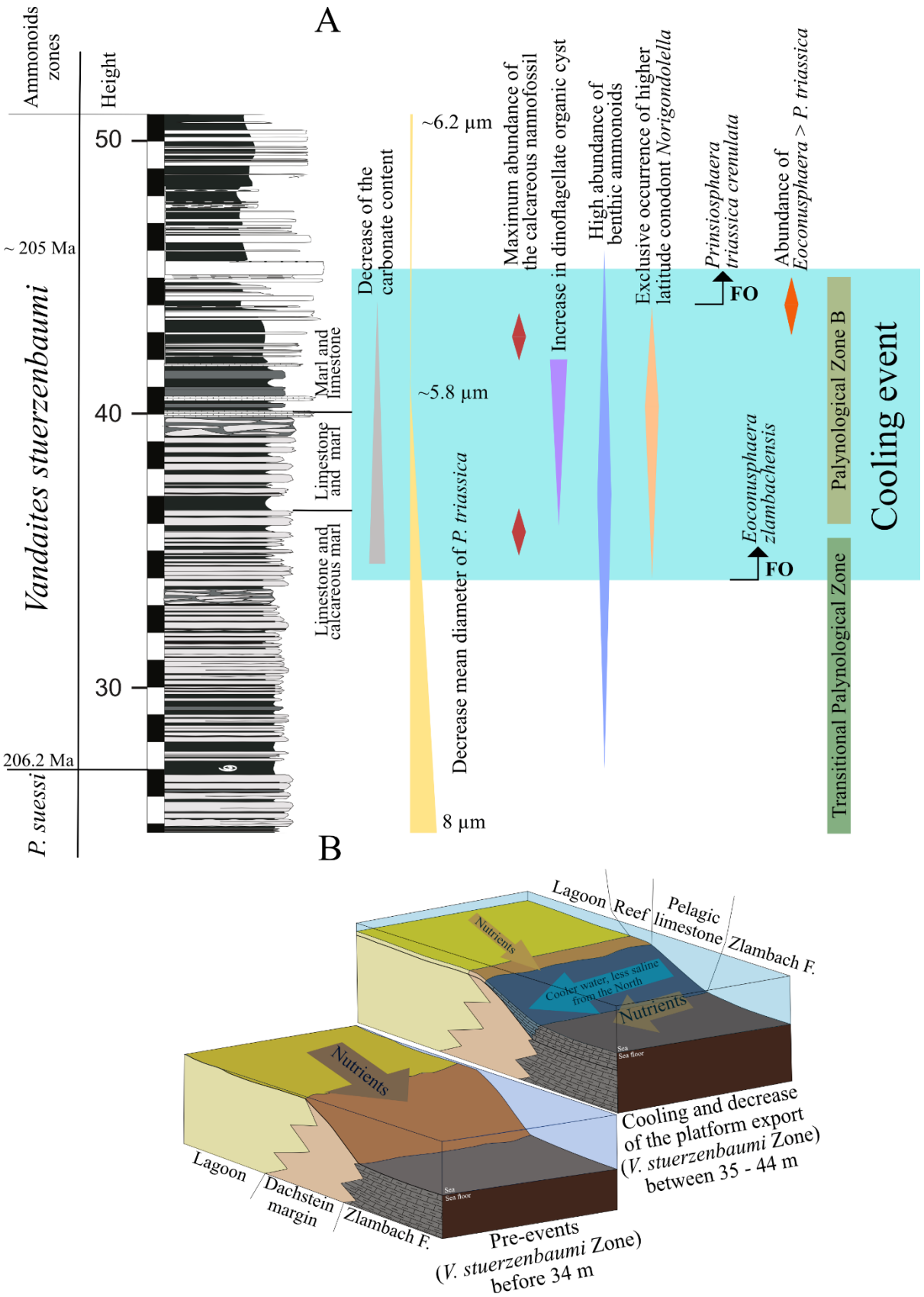
A
Ammonoids zones
Height
50
40
30
~ 205 Ma
206.2 Ma
Vandaites stuerzenbaumi
P. suessi
Marl and limestone
Limestone and marl
Limestone and calcareous marl
~6.2 µm
~5.8 µm
8 µm
Decrease of the carbonate content
Decrease mean diameter of P. triassica
Maximum abundance of the calcareous nannofossil
Increase in dinoflagellate organic cyst
High abundance of benthic ammonoids
Exclusive occurrence of higher latitude conodont Norigondolella
Prinsiosphaera triassica crenulata
FO
Abundance of Eoconusphaera > P. triassica
Eoconusphaera zlambachensis
FO
Palynological Zone B
Transitional Palynological Zone
Cooling event
B
Lagoon
Reef
Pelagic limestone
Zlambach F.
Nutrients
Cooler water, less saline from the North
Nutrients
Sea
Sea floor
Nutrients
Cooling and decrease of the platform export (V. stuerzenbaumi Zone) between 35 - 44 m
Lagoon
Dachstein margin
Zlambach F.
Sea
Sea floor
Pre-events (V. stuerzenbaumi Zone) before 34 m

Fig.5.16 – Main events occurring during the Rhaetian at Zlambach section with A: Schematic representation of the First Occurrences and qualitative abundance fluctuation of the microfossils, conodont and carbonate content suggesting a cooling event during the Rhaetian at Zlanbach section. Organic dinoflagellate and palynological zonation from Kürschner et al., 2008. B: Schematic 3D blocks diagrams representing the evolution of the Dachstein carbonate platform and the suggested events occurring during the Rhaetian at Zlambach, i.e. decrease of the carbonate export from the platfrom and cooling event.

Conclusions

The Northern Calcareous Alps bear a great potential to study the early evolution of calcareous nannofossils. The calcareous nannofossils assemblage records a maximum abundance during the middle Rhaetian, which comes along with the first occurrence of *E. zlambachensis* (oblique inner lamellae), henceforth dominating over *E. hallstattensis* (vertical inner lamellae). *Prinsiosphaera triassica crenulata* was observed with distinct striation patterns, confirming the validity of this subspecies initially described by Jafar (1983). The disappearance of the very large sized *P. triassica* (10 – 13 µm) and a continuous decrease in size of *P. triassica* are recorded in the lower Rhaetian (*P. suessi* Zone; the base of Zlambach section). The minimum size is reach in the middle Rhaetian, which may be the result of regional palaeo-environmental changes. At first, the decreasing carbonate export of the Dachstein platform could have reduced the influx of nutrients from continental sources available for the calcareous nannofossils. Second, cooling event as evidenced by a major turnover in the ammonoids, dinoflagellates cysts and miospores assemblages recorded in the middle Rhaetian (*V. stuerzenbaumi* Zone), could have impacted the nannolith size. During the early and middle Rhaetian, *P. triassica* did not reach rock-forming abundance and contributed with < 20 % to the rock record. We suggest a good adaptability of *P. triassica* and other nannoliths to warm and proximal water masses, probably with sufficient nutrient availability.

Acknowledgements

This research was supported by the Austrian Science Foundation (Project P 29497-P29; grant to Sylvain Richoz) « RESPECT » (A major evolutive **R**evolution : the **E**mergence and **S**preading of **PE**lagic **C**alcifiers in the late **T**riassic) PICS-CNRS project to Silvia Gardin. The SEM observations were supported by the Royal Physiographic Society of Lund (grant to Isaline Demangel). We thank Nicolas Thibault for the valuable scientific discussion.

References

Baldermann, A., Deditius, A.P., Dietzel, M., Fichtner, V., Fischer, C., Hippler, D., Leis, A., Baldermann, C., Mavromatis, V., Stickler, C.P. & Strauss, H. 2015: The role of bacterial sulfate reduction during dolomite precipitation: Implications from Upper Jurassic platform carbonates. *Chemical Geology*, 412, 1–14.

Baldermann, A., Grießbacher, A.C., Baldermann, C., Purgstaller, B., Letofsky-Papst, I., Kaufhold, S. & Dietzel, M. 2018a: Removal of Barium, Cobalt, Strontium, and Zinc from Solution by Natural and Synthetic Allophane Adsorbents. *Geosciences* 8, 309, 1–22..

Baldermann, A., Mavromatis, V., Frick, P.M. & Dietzel, M. 2018b: Effect of aqueous Si/Mg ratio and pH on the nucleation and growth of sepiolite at 25°C. *Geochimica et Cosmochimica Acta* 227, 211–226.

Baldermann, A., Mittermayr, F., Bernasconi, S.M., Dietzel, M., Grengg, C., Hippler, D., Kluge, T., Leis, A., Lin, K., Wang, X., Zünterl, A. & Boch, R. 2020: Fracture dolomite as an archive of continental palaeo-environmental conditions. *Communications Earth and Environment* 1, 35.

Bellanca, A., Di Stefano, E., Di Stefano, P., Erba, E., Neri, R. & Pirini Radrizzani, C. 1993: Ritrovamento di ‘‘Calcisfere’’ e nannofossili calcarei in terreni carnici della Sicilia. *Paleopelagos* 3, 91–96.

Bordiga, M., Bartol, M. & Henderiks, J. 2015: Absolute nannofossil abundance estimates: Quantifying the pros and cons of different techniques. *Revue de micropaléontologie* 58, 155–165.

Bottini, C., Jadoul, F., Rigo, M., Zaffani, M., Artoni, C. & Erba, E. 2016: Calcareous nannofossils at the Triassic/Jurassic boundary: Stratigraphic and paleoceanographic characterization. *Rivista Italiana di Paleontologia e Stratigrafia (Research in Paleontology and Stratigraphy)* 122, 141–164.

Bown, P.R. 1985: Archaeozygodiscus gen. Nov. and other Triassic coccoliths. *INA Newsletter* 32–35.

Bown, P.R. 1987: The structural Development of Early Mesozoic Coccoliths and its Evolutionary and Taxonomic Significance. *Abhandlungen der Geologischen Bundesanstalt* 39, 33–49.

Bown, P.R. & Cooper, M.K.E. 1998: Jurassic. In, Bown, P. R. (ed.) Calcareous Nannofossil Biostratigraphy. *British Micropalaeontological Society Publication Series* 34–85.

Bralower, T.J., Bown, P.R. & Siesser, W.G. 1991: Significance of Upper Triassic nannofossils from the Southern Hemisphere (ODP Leg 122, Wombat Plateau, N.W. Australia). *Marine Micropaleontology* 17, 119–154.

Brand, U. & Veizer, J. 1980: Chemical diagenesis of a multicomponent carbonate-system - 1: Trace elements. *Journal of Sedimentary Petrology* 50, 1219–1236.

Brand, L.E. 1994: Physiological ecology of marine coccolithophores, in Winter, A., and Siesser, W.G., eds., Coccolithophores: Cambridge, UK, *Cambridge University Press* 39–49.

Clark, W. B. & Watkins, D. K. 2020: A quantitative analysis of calcareous nannofossils across a late oligocene paleolatitudinal transect of the North Atlantic Ocean. *Marine Micropaleontology* 158, 101892.

Clémence, M.E., Gardin, S., Bartolini, A., Paris, G., Beaumont, V. & Guex, J. 2010: Bentho-planktonic evidence from the Austrian Alps for a decline in sea-surface carbonate production at the end of the Triassic. *Swiss Journal of Geosciences* 103, 293–315.

Dal Corso, J., Preto, N., Agnini, C., Hohn, S., Merico, A., Willems, H., Gianolla, P., 2020: Rise of calcispheres during the Carnian Pluvial Episode (Late Triassic). Global and Planetary Change, 200, 103453.

Deflandre, G.M. 1970: *Présence de nannofossiles calcaires (coccolithes et* Incertae sedis) *dans le Siluro-dévonien d'Afrique du Nord.* Comptes rendus hebdomadaires des séances de l'Académie des sciences. Série D, *Sciences naturelles* 2916–2921.

Demangel, I., Kovács, Z., Richoz, S., Gardin, S., Krystyn, L., Baldermann, A. & Piller, W. E. 2020: Development of early calcareous nannoplankton in the Northern Calcareous Alps (Austria) in the Late Triassic. *Global and Planetary Change* 193, 103254.

Demangel, I., Howe, R., Gardin, S. & Richoz, S. 2021: *Eoconusphaera hallstattensis*, new species, and review of the Rhaetian genus *Eoconusphaera*. *Journal of Nannoplankton Research*, 39 (1), 77 – 87.

Di Nocera S. & Scandone P. 1977: Triassic nannoplankton limestones of deep basin origin in the central Mediterranean region. *Palaeogeography, Palaeoclimatology, Palaeoecology* 21, 101–111.

Erba, E. 2006: The first 150 million years history of calcareous nannoplankton: Biosphere-geosphere interactions. *Palaeogeography, Palaeoclimatology, Palaeoecology* 232, 237–250.

Fischer, A.G., Honjo, S. & Garrison, R.A.E. 1967: Electron Micrographs of Limestones and their Nannofossils. Princeton University Press, Princeton.

Frech, F. 1890: Die Korallen der Trias. - I. Die Korallen der juvavischen Triasprovinz. *Paläontographica* 37, 1–116.

Galbrun, B., Boulila, S., Krystyn, L., Richoz, S., Gardin, S. & Bartolini, A. 2020: « Short » or « long » Rhaetian? Astronomical calibration of Austrian key sections. *Global and Planetary Change* 192, 103253.

Gardin, S., Krystyn, L., Richoz, S., Bartolini, A. & Galbrun, B. 2012: Where and when the earliest coccolithophores? *Lethaia* 45, 507–523.

Goddéris, Y., Donnadieu, Y., de Vargas, C., Pierrehumbert, R. T., Dromart, G. & van de Schootbrugge, B. 2008: Causal or casual link between the rise of nannoplankton calcification and a tectonically-driven massive decrease in Late Triassic atmospheric CO_2? *Earth and Planetary Science Letters* 267, 247–255.

Golonka, J. 2007: Late Triassic Early Jurassic palaeogeography of the world. *Palaeogeography, Palaeoclimatology, Palaeoecology* 244, 297–307.

Gottschling, M., Renner, S.S., Meier, K.J.S., Willems, H., Keupp, H., 2008: Timing deep divergence events in calcareous dinoflagellates, Journal of phycology, 44, 429 – 438. 10.1111/j.1526-8817.2008.00479.x.

Hannisdal, B., Henderiks, J. & Liow, L.H. 2012: Long-term evolutionary and ecological responses of calcifying phytoplankton to changes in atmospheric CO_2. *Global Change Biology* 18, 3504–3516.

Iglesias-Rodriguez, M.D., Halloran, P.R., Rickaby, R.E.M., Hall, I.R. & Colmenero-Hidalg, E. 2008: Phytoplankton Calcification in a High-CO_2 World. *Science* 320, 336–340.

Jafar, S.A. 1983: Significance of Late Triassic calcareous Nannoplankton from Austria and Southern Germany. *Neues Jahrbuch für Geologie und Paläeontologie* 166, 218–259.

Janofske, D. 1987: Kalkige Nannofossillien aus der ober-Trias (Rhät)der Nördlichen kalkalpen. *Berliner geowissenschatliche Abhandlungen* 86, 45–67.

Janofske, D. 1990: Eine neue 'Calcisphaere' Carnicalyxia tabellata n.g. n.sp. aus den Cassianer Schichten (Cordevol, unteres Karn) der Dolomiten. *Berliner Geowissenschaftliche Abhandlungen* 124, 259–269.

Janofske, D. 1992: Kalkiges Nannoplankton, insbesondere kalkige Dinoflagellaten-Zysten der alpinen Ober-Trias: Taxonomie, Biostratigraphie und Bedeutung für die Phylogenie der Peridiniales. *Berliner Geowissenschaftliche Abhandlungen* 4, 1–53.

Kovács, Z., Demangel, I., Richoz, S., Hippler, D., Baldermann, A. & Krystyn, L. 2020: New constraints on the evolution of $^{87}Sr/^{86}Sr$ of seawater during the Upper Triassic. *Global and Planetary Change* 192, 103255.

Kristan-Tollmann, E. 1964: Die Foraminiferen aus rhätischen Zlambachmergeln der Fischerwiese bei Aussee, Salzkammergut. *Jahrbuch der Geologischen Bundesanstalt* 10, 1–189.

Krystyn, L. 1987: Zur Rhät-Stratigraphie in den Zlambach-Schichten (vorläufiger Bericht). *Österreichische Akademie der Wissenschaften, Sitzungsberichte der Mathematisch-Naturwissenschaftlichen Klasse*, Abteilung 1, 196, 21–36.

Krystyn, L. 1991: Die Fossillagerstätten der alpinen Trias. In: Nagel, D., Rabeder, G., (Eds): Exkursionen im Jungpaläozoikum und Mesozoikum Österreichs, *Österreichische Paläontologische Gesellschaft*, Wien, 23–78.

Krystyn, L. & Kuerschner, W. M. 2005: Biotic events around the Norian – Rhaetian boundary from a Tethyan perspective. *Albertiana 32*, 17–20.

Krystyn, L., Mandl, G.W. & Schauer, M. 2009: Growth and termination of the Upper Triassic platform margin of the Dachstein area (Northern Calcareous Alps, Austria). *Austrian Journal of Earth Sciences* 103, 23–33.

Kürschner, W.M., Krystyn, L. & Richoz, S. 2008: An integrated palaeontological, geochemical and palynological study of the Rhaetian Zlambach marls in the Northern Calcareous Alps (Austria). *Berichte geologischen Bundesanstalt* 76, 13–14.

Mandl, G. W. 2000: The alpine sector of the Tethyan shelf – Examples of Triassic to Jurassic sedimentation and deformation from the Northern Calcareous Alps. *Mitteilungen der Österrike Geologie Gesellschaft* 92, 61–77.

Matzner, C. 1986: Die Zlambach-Schichten (Rhät) in den Nördlichen Kalkalpen: Eine Plattform-Hang-Beckenentwicklung mit allochthoner Karbonatsedimentation. *Facies* 14, 1–104.

Moshkovitz, S. 1982: On the findings of a new calcareous nannofossil (Conusphaera zlambachensis) and other calcareous organisms in the Upper Triassic sediments of Austria. *Eclogae Geologicae Helvetiae* 75, 611–619.

Möller, C., Bornemann, A., Mutterlose, J. 2020: Climate and paleoceanography controlled size variations of calcareou nannofossils during the Valanginian Weissert Event (Early Cretaceous). *Marine Micropaleontology* 157, 101875.

Nakada, R., Ogawa, K., Suzuki, N., Takahashi, S. & Takahashi, Y. 2014: Late Triassic compositional changes of eolian dusts in the pelagic Panthalassa: response to the continental climatic change. *Palaeogeography, Palaeoclimatology, Palaeoecology* 393, 61–75.

Ogg, J.G., 2012: Triassic. In: Gradstein, F. M., Ogg, J.G., Schmitz, M.D. & Ogg, G.M. (Eds), The Geologic Time Scale 2012, Amsterdam, *Elsevier*, 681–730.

Ogg, J.G., Chen, Z.-Q., Orchard, M. J. & Jiang, H.S. 2020: The Triassic Period. In: Gradstein, F. M., Ogg, J.G., Schmitz, M.D., Ogg, G.M. (Eds), The Geologic Time Scale 2020, Amsterdam, *Elsevier*. 903–953.

Peti, L. & Thibault, N. 2017: Abundance and size changes in the calcareous nannofossil Schizosphaerella - Relation to sea-level, the carbonate factory and palaeoenvironmental change

from the Sinemurian to earliet Toarcian of the Paris Basin. *Palaeogeography, Palaeoclmatology, Palaeoecology* 485, 271–282.

Piller, W. 1978: Involutinacea (Foraminifera) der Trias und des Lias. Beiträge Paläontologie Österreich, 5, 1–164.

Posch, F. & Stradner, H. 1987: Report on Triassic Nannoliths from Austria. *Abhandlungen Der Geologischen Bundesanstalt* 39, 231–237.

Preto, N., Rigo, M., Agnini, C., Bertinelli, A., Guaiumi, C., Borello, S. & Westphal, H. 2012: Triassic and Jurassic calcareous nannofossils oft he Pizzo Mondello section: A SEM study. *Rivista Italiana di Paleontologia e Stratigrafia* 118, 131–141.

Preto, N., Agnini, C., Rigo, M., Sprovieri, M. & Westphal, H. 2013: The calcareous nannofossil Prinsiosphaera achieved rock-forming abundances in the latest Triassic of western Tethys: consequences for the $\delta^{13}C$ of bulk carbonate – *Biogeosciences* 10, 6053–6068.

Prins, B. 1969: Evolution and stratigraphy of coccolothinids from the lower and middle lias. International Conference Planktonic Microfossils, *Geneva* 2, 547–558.

Richoz, R., Krystyn, L., Von Hillebrandt, A. & Martindale, R. 2012: End-Triassic crisis events recorded in platform and basin of the Austrian Alps. The Triassic/Jurassic and Norian/Rhaetian GSSPs – *Journal of Alpine Geology* 55, 321–374.

Richoz, S. & Krystyn, L. 2015: The Upper Triassic events recorded in platform and basin of the Austrian Alps. The Triassic/Jurassic GSSP and Norian/Rhaetian GSSP candidate – *Berichte der Geologischen Bundesanstalt* 111.

Rivero-Calle, S., Gnanadesikan, A., Del Castillo, C.E., Balch, W.M. & Guikema, S.D. 2015: Multidecadal increase in North Atlantic coccolithophores and the potential role of rising CO_2. *Science* 350, 1533–1537.

Rutledge, D. C., Cole, S., Lawrence, T. & Gard, G.,2015:A new species of Late Triassic nannofossils, Botulus triassicus, and observations on Triassic assemblages from the NW Shelf of Australia. *INA15* 35, 71.

Schettino, A. & Turco, E. 2011: Tectonic history of the western Tethys since the late Triassic. Geological Society of America *Bulletin*, 123, 89–105.

Schoene, B., Guex, J., Bartolini, A., Schaltegger, U. & Blackburn, T.J. 2010: Correlating the end-Triassic mass extinction and flood basalt volcanism at the 100 ka level. *Geology* 35, 387–390.

Schorn, A. & Neubauer, F. 2014: The structure of the Hallstatt evaporite body (Northern Calcareous Alps, Austria): A compressive diapir superposed by strike-slip shear? *Journal of Structural Geology* 60, 70–84.

Scotese, C.R. 2004: A continental drift flipbook. *The Journal of Geology* 112, 729–741.

Suchéras-Marx, B., Giraud, F., Mattioli, E., Gally, Y., Barbarin, N. & Beaufort, L. 2014: Middle Jurassic coccolith fluxes: A novel approach by automated quantification. *Marine Micropaleontology* 111, 15–25.

Streng, M., Hildebrand-Habel, T., Willems, H., 2004: A proposed classification of archeopyle types in calcareous dinoflagellate cysts. Journal of Paleontology, 78 (3), 456 – 483.

Suchéras-Marx, B., Mattioli, E., Allemand, P., Giraud, F., Pittet, B., Plancq, J. & Escarguel, G. 2019: The colonization of the oceans by calcifying pelagic algae. *Biogeosciences* 16, 2501–2510.

Tangen, K., Brand, L.E., Blackwelder, P.L., Guillard, R.R.L., 1982: *Thoracosphaera heimii* (Lohman) Kamptner is a dinophyte: observations on its morphology and life cycle. Marine Micropaleontology, 7, 193 – 212.

Tollmann, K. 1995: Weitere beobachtungen an Rhätischen nannofossilien der Tethys. *Geolologisch Paläontologische Mitteilungen Innsbruck* 20, 1–10.

Wulff, L., Mutterlose, J. & Bornemann, A. 2020: Size variations and abundance patterns of calcareous nannofossils in mid Barremian black Shales of the Boreal Realm (lower Saxony Basin). *Marine Micropaleontology* 156, 101853.

Zeebe, R.E. & Caldeira, K. 2008: Close mass balance of long-term carbon fluxes from ice-core CO_2 and ocean chemitry records. *Nature Geoscience* 1, 12–315.

Zhang, S., Wang, X., Hammarlund, E. U., Wang, H., Mafalda Costa, M., Bjerrum, C.J., Connelly, J.N., Zhang, B., Bian, L. & Canfield, D.E. 2015: Orbital forcing of climate 1.4 billion

years ago. Proceedings of the National Academy of Sciences of the United States of America 112, 1406–1413.

CHAPTER 6 – THE CALCIUM ISOTOPE ($\delta^{44/40}$CA) RECORD THROUGH ENVIRONMENTAL CHANGES: INSIGHTS FROM THE LATE TRIASSIC

Zsófia Kovács[1,2], Isaline Demangel[1,2], Sylvain Richoz[1,2], Anne-Désirée Schmitt[3], Sophie Gangloff[3], Andre Baldermann[4], Dorothee Hippler[4], Leopold Krystyn[5]

1 Institute of Earth Sciences, University of Graz, NAWI Graz Geocenter, Graz, Austria

2 Department of Geology, University of Lund, Lund, Sweden

3 Laboratory of Hydrology and Geochemistry, University of Strasbourg, France

4 Institute of Applied Geosciences, Graz University of Technology, NAWI Graz Geocenter, Graz, Austria

5 Department of Palaeontology, University of Vienna, Vienna, Austria

Corresponding author: Zsófia Kovács, kov.zsofia0108@gmail.com, Institute of Earth Sciences, University of Graz, NAWI Graz Geocenter, Heinrichstrasse 26, 8010 Graz, Austria

Abstract

Calcium isotopes ($\delta^{44/40}$Ca) are particularly useful in palaeo-environmental studies due to the key role of carbonate minerals in continental weathering and marine precipitation. They can provide hints on changes in the calcium (palaeo)-fluxes, environmental shifts in terms of calcite vs. aragonite sea intervals and ecological factors through Earth history. The investigation of the Late Triassic calcium isotope record, which is not well-established yet, offers a great opportunity to evaluate such influencing factors in a time interval that witnessed important environmental and ecological turnovers, such as the first appearance of calcareous nannoplankton, ocean acidification and periods of elevated extinction rates.

In this study, we present a new $\delta^{44/40}$Ca dataset across the late Norian - Hettangian interval, established from carbonate successions in Austria and Turkey. The isotope records reveal two globally significant signals: a ~ 0.20 ‰ decrease through the early Rhaetian and a small, negative (~ 0.14 ‰) excursion corresponding to the emplacement of the Central Atlantic Magmatic Province. The possible explanations for these signals are changes in the isotopic ratio of the continental calcium influx due to the high chemical weathering rate of carbonates

and ocean acidification, respectively. The considerable (~ 0.15 – 0.30 ‰) offset in $\delta^{44/40}Ca$ between the study areas is likely the combined result of local differences in sedimentary mineralogy and early marine diagenesis. The major evolutionary step represented by the first occurrence of calcareous nannoplankton did not have a determining role on the calcium isotopic signature of the marine carbonates.

Key words: Isotope proxy, Rhaetian, nannofossils, carbonates, palaeo-environment, Triassic/Jurassic boundary.

1. Introduction

The stable calcium isotopic composition of marine carbonate archives ($\delta^{44/40}Ca$) was proposed to be an important palaeo-environmental and palaeo-oceanographic proxy, mainly because of the linkage between the Ca and C geochemical cycles. The continental weathering of Ca-bearing carbonates and silicates is the main source of Ca to the ocean, while authigenic and diagenetic carbonate precipitation in the marine realm is the main sink (DePaolo, 2004). The global Ca fluxes subsequently took a key control on the CO_2 level in the atmosphere and on the related oceanic-atmospheric system as well as on climate regulation throughout the geological record (Gussone et al., 2020; Fantle and Tipper, 2014). Due to fractionation processes of Ca during Ca-mineral weathering, carbonate precipitation and subsequent burial, variations in the calcium isotopic composition of marine carbonate archives through time have been used to trace Ca concentration flux changes between continents and the ocean (Sime et al., 2007). In turn, these flux imbalances can potentially reflect environmental changes (e.g.: Kasemann et al., 2005; Fantle and DePaolo, 2005; Silva-Tomayo et al., 2018; Wang et al., 2019).

The Late Triassic is an important interval regarding Earth´s climatic and tectonic evolution and is characterized by several processes, which could have impacted the global calcium cycle through changes in riverine Ca influx, marine Ca accumulation and burial or ocean chemistry. Sea-level fall at the Norian/Rhaetian boundary (Haq, 2018) and the break-up of the Pangea supercontinent (Golonka, 2007) could have impacted further the Ca cycle in the Triassic. Similarly, climate changes through the Rhaetian due to the N-ward drift of Pangea (Goddéris et al., 2008) and/or the emplacement of the Central Atlantic Magmatic Province at

the Triassic-Jurassic boundary (Davies et al., 2017) are other possible triggers of imbalances in the marine Ca isotope budget. Moreover, in this time interval fundamental biological changes have happened. In several steps, like in the early-middle Carnian, Carnian-Norian, Norian-Rhaetian and Triassic-Jurassic intervals, biodiversity went through a crisis (Lucas and Tanner, 2008). At the same time, other organisms originated or were particularly successful. For example, the emergence of coccolithophorids, the most productive calcifying organisms today, was recently dated back to the Alaunian (Norian) (Demangel et al., 2020). Changes in the dominant carbonate sink could therefore have influenced the global fractionation factor resulting in calcium isotopic shifts.

The increasing number of calcium isotopic studies indicate that several parameters may complicate the interpretation of Ca isotopic variations recorded in marine carbonates through time. Beyond the record of global Ca cycle variations, the $\delta^{44/40}$Ca ratio of marine carbonates seems to be sensitive to spatiotemporal changes in the carbonate precipitation rate (Tang et al., 2008), carbonate mineralogy (aragonite vs. (high-Mg) calcite) (Gussone et al. 2005), early-diagenesis (Lau et al., 2017; Higgins et al., 2018) and local Ca-(re)cycling (Holmden et al., 2012a,b; Shao et al., 2018).

In this study, we measured marine carbonate rocks from sections of today's Austria and Turkey of Late Triassic (Norian and Rhaetian) and earliest Jurassic (Hettangian) age for their calcium isotopic composition. The new records presented herein provide a better understanding of the individual influences of various global and regional factors, such as environmental, tectonic and biological changes on the carbonate $\delta^{44/40}$Ca ratios generally and in the Late Triassic in particular. This study interval is of particular interest, because the Mesozoic rock record is underrepresented regarding calcium isotopic studies in comparison to younger and older time intervals. For instance, Farkaš et al. (2007) established a long-term isotopic record of the Phanerozoic, with a few Carnian and Rhaetian data, but the Triassic $\delta^{44/40}$Ca isotopic development is not discussed in detail, while the study by Jost et al. (2017) focuses solely on the Triassic-Jurassic boundary (TJB). No Norian data have been published until recently.

2. Geological Setting and Stratigraphy

Two main study sites were investigated in the present study: the Oyuklu section (Taurides, Turkey) and several sections in the Northern Calcareous Alps (NCA, Austria). These

study sites were originally located at different palaeo-latitudes in the Late Triassic, i.e. Turkey at ~ 10˚N and the NCA at ~ 30˚N (Fig.6.1A).

2.1 *Turkey*

The Oyuklu section (36°50.07′ N, 32°55.81′ E) belongs to the Beysehir-Hoyran Nappes in the Central Taurides (Fig.6.1B). It covers the Carnian – Hettangian time interval, but in the present study only the uppermost Norian and the Rhaetian parts were investigated, which consist of white, fossil-poor hemipelagic limestone beds, chert nodules and red or gray chert layers (Gallet et al., 2007). The sedimentary succession represents a monotonous deep water sequence with condensed sedimentation (Gallet et al., 2007). The depositional record is complete, without breaks in sedimentation and therefore a continuous conodont zonation has been established for the section (Gallet et al., 2007). The covered biozones in the investigated interval are the following: *M. hernsteini* - *E. bidentata*, *M. posthernsteini* - *E. bidentata*, *M. hernsteini* - *M. posthernsteini*, *M. rhaetica* and *M. ultima* Zones.

2.2 *Austria*

The NCA belong to the uppermost tectonic unit of the Eastern Alps, in the Austroalpine Nappe complex (Fig.6.1C). This area was part of the passive margin of the Tethys between the late Permian and the lower Jurassic. More specifically, in the investigated time interval of the Late Triassic, gigantic carbonate platforms of several 100 kilometres width evolved (e.g. Dachstein Platform), which were bordered towards the global ocean by the Dachstein Reef. Further oceanward, a carbonate ramp with slope sedimentation (Zlambach Formation) evolved. The outer part of this carbonate ramp was affected by diapirism of Permian evaporites, which resulted in the formation of topographic highs, characterized with pelagic sedimentation (Hallstatt facies). From the upper Norian to the Hettangian, an intraplatform basin (Eiberg basin) opened on the Dachstein Platform, where limestone-marl alternations (Kössen Formation) were deposited (Richoz et al., 2012; Kovács et al., 2020) (Fig.6.2).

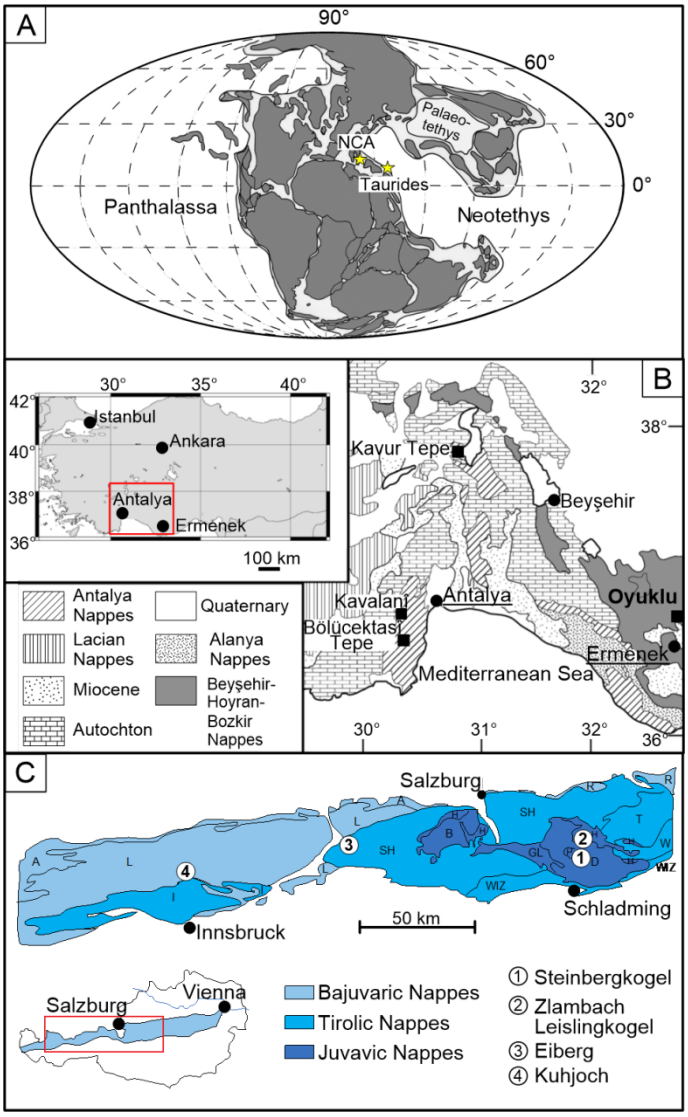

Fig.6.1 – Location of the studied sections (A): Palaeogeographic reconstruction of the Late Triassic world and the locations of the study sites, modified after Demangel et al. (2020) (B): Tectonostratigraphic map of SW-Turkey after Gallet et al. (2007) with the location of the Oyuklu section. (C): Simplified geological map of the nappe complex of the Northern Calcareous Alps (blue) (modified from Richoz et al., 2012) with the locations of the five studied sections from Austria, labelled by numbers.

The investigated sections represent three of the above-mentioned depositional environments. Leislingkogel (47°38’46,2’’N, 13°41’59,4’’E) and almost the entire Sommeraukogel-Steinbergkogel composite section (47°33’50’’N, 13°37’34"E) belong to the deep shelf environment (Hallstatt facies). As a result of the diapirism and uplift, this depositional environment did not receive allochthonous input e.g. via turbidites. The sedimentary succession in these sections is dominated by platy to nodular bioclastic

wackestones, which are usually red or grey in colour (Richoz et al., 2012). Both sections have a well-established stratigraphy, based on conodonts, ammonoids and calcareous nannoplankton (Richoz et al., 2012; Demangel et al., 2020). From the Leislingkogel section, middle Norian samples were investigated, while Sommeraukogel-Steinbergkogel covers the late Norian – early Rhaetian interval. In this latter section the last ~ 2 meters belong to the Zlambach Formation.

The stratigraphically following section, Kleiner Zlambach (47°38’32, 20"N, 13°39’33,36"E) represents a toe-of-slope – basin environment, with an estimated minimum depositional depth of 300 metres (Richoz et al., 2012). The section is mainly composed of an alternating succession of micritic limestone and marl, which is episodically interbedded by calciturbidites and mud/debris flows. The stratigraphic zonation is based on ammonoids, conodonts, foraminifers and calcareous nannoplankton (Richoz et al., 2012; Galbrun et al., 2020). The investigated samples cover approximately two thirds of the early Rhaetian *Paracochloceras suessi* ammonite Zone and the entire middle Rhaetian *Vandaites stuerzenbaumi* Zone, reaching the base of the *C. marshi* Zone (Kovács et al., 2020). Based on litho-, bio-, chemo- and cyclostratigraphy, the sections of Steinbergkogel and Zlambach may overlap over a short interval of one or two metres (Richoz et al., 2012; Galbrun et al., 2020; Kovács et al., 2020).

The following two sections, Eiberg (47°33"N, 12°10’07"E) and Kuhjoch (47°29′02″N, 11°31′50″E) represent an intraplatfrom basin setting. The Eiberg section consists of mixed siliciclastic-carbonate sediments with frequent organic-rich shale layers (Richoz et al., 2012). Several lines of evidence indicate the progressive deepening of the basin, such as occurrences of *Zoophycus* (trace fossil) and *Oxycolpella* (brachiopod), both specific for deep-water settings (Mette et al., 2012). The section covers the very top of the *V. stuerzenbaumi* Zone and the entire late Rhaetian *Choristoceras marshi* Zone (Mette et al., 2012; Richoz et al., 2012; Galbrun et al., 2020), therefore it can be easily correlated with the Zlambach section. In this study we sampled the interval, which belongs to the *C. marshi* Zone. The following Kuhjoch section is the Global Stratotype Section and Point (GSSP) for the base of the Jurassic system (e.g. von Hillebrandt et al., 2013). At Kuhjoch, our sampling focuses on the TJB interval, marked by the First Occurence Datum of the ammonite *Psiloceras spelae*. These latter two sections can be correlated through a characteristic marker bed of dark colour due to increased clay content,

representing the mass-extinction level (T-bed) (von Hillebrandt et al., 2013). The sampling of Eiberg section stops shortly before the T-bed, while the sampling of Kuhjoch start just below it, therefore, the dataset can be regarded as continuous.

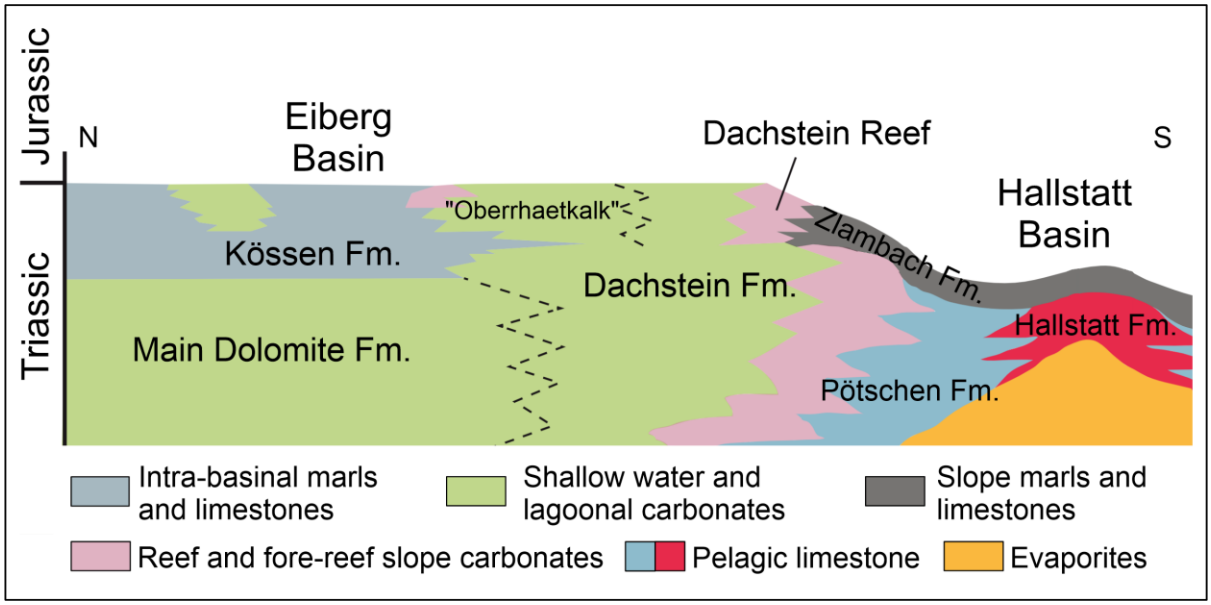

Fig.6.2 – Schematic Late Triassic stratigraphy of the Northern Calcareous Alps (after Mandl, 2000; Demangel et al., 2020).

3. Material and Methods

3.1 *Samples (and previous measurements)*

Bulk rock carbonate samples were collected from the investigated sections and were used for all analyses described below. The samples were either powdered with an electric agate mortar and pestle or drilled with a hand-held drill to avoid sampling of visible bioclasts, carbonate veins and other types of cement. In total, forty-two samples were investigated for their calcium isotopic composition ($\delta^{44/40}Ca$). Except for the two samples in Leislingkogel and one carbonate-lean sample in Kuhjoch, the samples were previously investigated for their elemental and strontium isotopic ($^{87}Sr/^{86}Sr$) composition (Kovács et al., 2020). The mineralogical composition of the samples (except Leislingkogel) was determined by Rietveld-based analysis of powder X-ray diffraction (XRD) patterns as described in Kovács et al. (2020). The mineralogical and geochemical data are presented in the Electronic Appendix 1. of this paper. For the stratigraphic position of the samples the reader is referred to Kovács et al. (2020).

3.2 *Calcium isotope ($\delta^{44/40}Ca$) measurements*

All isotopic work was performed at Laboratoire d'Hydrologie et de Geochemie de Strasbourg (LHyGeS), University of Strasbourg, France. Usually 150 mg (rarely 50 mg) of powder was leached with 5 mL 0.5 N HCl and stirred at 40 rpm for 10 min on an SB3 Stuart™ rotator. The mixtures were then centrifuged at 4000 rpm for 10 minutes using a Thermo Jouan B4-I™ multifunction centrifuge and the supernatants were recovered and filtered at 0.2 µm. The same procedure was applied three times and three more times with distilled water to recover all the carbonate and exchangeable fractions of Ca. After dilution and collecting the supernatants, an aliquot of each sample was analysed on a ThermoScientific iCAP 6000series™ ICP-AES with an accuracy of 5% to determine the Ca concentration of each sample.

For the $\delta^{44/40}Ca$ analyses, 0.14 µmol of Ca from each sample was mixed with 0.01 µmol of Ca from a ^{42}Ca-^{43}Ca double spike ($^{42}Ca/^{43}Ca$ spike ratio of ~5) and dried at 70°C on a hot plate. The evaporated sample-double spike mixtures were then re-dissolved in 2 N HNO_3 and chemical separations were performed on a normal DGA resin (TODGA, Triskem™). Eluted Ca (~100% of recovery) was dried a first time at 70°C and converted in nitric form with 7 N HNO_3 before a second phase of drying at 70°C on a hot plate. The total Ca blank for the chemical separation procedure represent less than 1.25 nmol. This represents an average contribution of less than 1% to the Ca of each sample and will therefore not be taken into further consideration.

The dried residues of the chemical separation were dissolved in 1 to 3 µL 1 N HNO_3 and deposited on single tantalum filaments (99.995% purity) previously outgassed and oxidized (under primary vacuum) for the $\delta^{44/40}Ca$ measurements. All the isotope measurements were performed on a Thermo Scientific Triton™ TIMS (thermal ionization mass spectrometer) at LHyGeS, Strasbourg, in static mode for Ca measurements. To avoid $\delta^{44/40}Ca_{SRM915a}$ inter-session drifts, the ^{42}Ca-^{43}Ca double spike was calibrated at each measurement session by measuring three standards composed of a NIST SRM 915a standard solution and a ^{42}Ca-^{43}Ca double spike following the protocol published by Lehn et al. (2013).

Measured values were expressed as $\delta^{44/40}Ca$ in per mil relative to the NIST SRM915a reference material (Hippler et al., 2003):

$$\delta^{44/40}Ca_{SRM915a}\ (‰) = \left\{ \frac{\left(\frac{^{44}Ca}{^{40}Ca}\right)_{sample}}{\left(\frac{^{44}Ca}{^{40}Ca}\right)_{SRM915a}} - 1 \right\} \times 1000$$

The average external reproducibility of the $\delta^{44/40}$Ca measurements was 0.07 ‰ based on repeated measurements of NIST SRMS 915a between November 2018 and October 2019 (2SD, N = 32) and 0.11 ‰ based on sample replicate measurements (2SD, N = 10). The highest value was chosen as the external reproducibility (i.e. 0.11‰) in this study. The accuracy of our measurements was explored through the measurements of an internal Atlantic seawater standard (1.90 ‰ ± 0.11, 2SD, N=12) during the same period of time, which matches the reported value of 1.88 ‰ by Hippler et al. (2003) and Heuser et al. (2016). The latter value was used to recalculate the values relative to seawater:

$$\delta^{44/40}Ca_{sample/sw} = \delta^{44/40}Ca_{sample/SRM915a} - 1.88$$

Throughout the text, $\delta^{44/40}$Ca values are expressed against seawater to ensure direct comparison with other published literature. In the figures, both expressions are reported.

4. Results

4.1 *Calcium isotopes ($\delta^{44/40}Ca$)*

For all sections, the isotopic results alongside the sedimentary log can be found in Appendix 2. The $\delta^{44/40}$Ca record of the Oyuklu section (Turkey) shows a decrease from the latest Norian until the base of the middle Rhaetian, from -0.92 ‰ to -1.11 ‰. Afterwards, in the middle Rhaetian and most of the late Rhaetian the $\delta^{44/40}$Ca curve remains stable within analytical uncertainty at -1.14 ± 0.086 (2SD, N=5), only the uppermost sample in the late Rhaetian displays a further decline to -1.29 ‰ (Fig.6.3).

Regarding the Austrian sections, the Norian $\delta^{44/40}$Ca isotopic record is constant with the average of -0.74 ± 0.07 ‰ (2SD, N=7) (Fig.6.3). Afterwards, a decrease of 0.22 ‰ is observed across the Norian-Rhaetian boundary (NRB) and at the base of the Rhaetian, within the Steinbergkogel section. The major part of this decline is due to the last data point measured in

this section, which represents the transition from Hallstatt to the Zlambach facies and contributes with 0.15 ‰ to this trend. In the stratigraphically following Zlambach section, the $\delta^{44/40}$Ca values are significantly more negative (average of -1.35 ‰ ± 0.10 ‰ (2SD, N=8)) than in the preceding sections. The $\delta^{44/40}$Ca values in this section show a decrease from -1.34 ‰ until -1.45 ‰ through the *P. suessi* and the very beginning of *V. stuerzenbaumi* Zones. In contrast, the $\delta^{44/40}$Ca values in the upper part of the section remain stable within analytical uncertainty at -1.4 ‰ ± 0.10 ‰ (2SD, N=4). The next section, Eiberg, starts in the *C. marshi* ammonite Zone with slightly more negative values (-1.57 ‰) than observed at the terminal Zlambach section. There is a 0.22 ‰ increase in $\delta^{44/40}$Ca until the penultimate data point in the upper half of the *C. marshi* Zone, up to -1.35 ‰. The last data point shows again a decrease, which continues also in the following Kuhjoch section. The lowest $\delta^{44/40}$Ca value (-1.60 ‰) of the entire investigated interval is reached in the T-bed, representing the end-Triassic extinction (ETE) level. In the lower Hettangian, a considerable increase in the $\delta^{44/40}$Ca record, up to a value of -1.23 ‰, is observed, however this time interval is represented by two samples only.

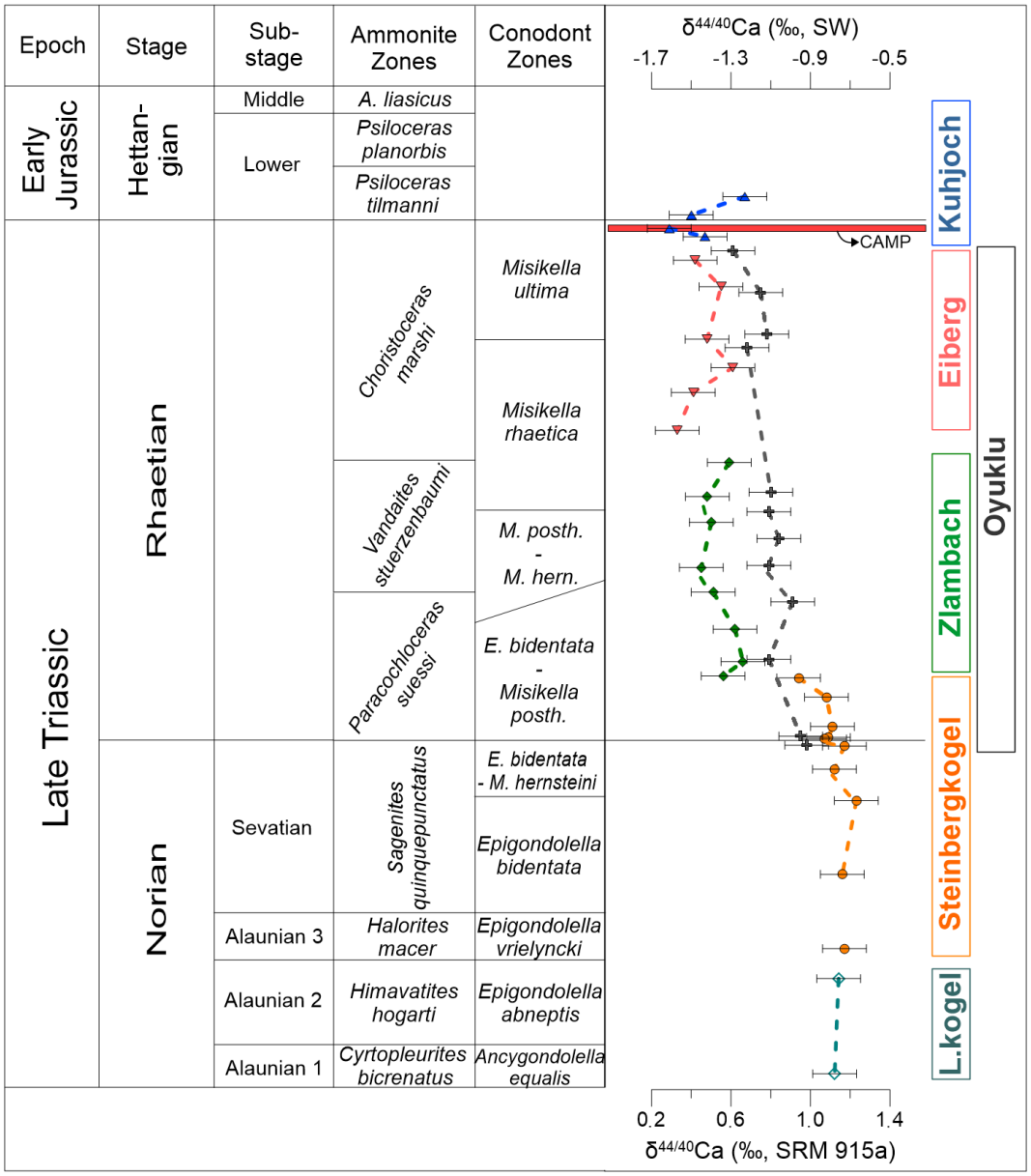

Fig.6.3 – Composite $\delta^{44/40}$Ca record through the Norian – lower Hettangian.

5. Discussion

Three key features of the Late Triassic $\delta^{44/40}$Ca isotopic record are highlighted in the present study: (i) a ~ 0.20 ‰ decrease in $\delta^{44/40}$Ca through the early Rhaetian after a stable Norian interval as seen best in Oyuklu (ii) a short, negative (0.14 ‰) excursion in $\delta^{44/40}$Ca across the ETE, and (iii) a significant (0.15–0.30 ‰) offset between contemporaneous $\delta^{44/40}$Ca isotopic records from sections in Austria and Turkey. The possible driving factors of these three key features are in the focus of the following discussion.

5.1 *Global changes in the carbonate sink*

Calcium isotopic shifts can be achieved by changing the global fractionation of the dominant carbonate sinks, which can be related to changes either in precipitation rate, in the mineralogy of the precipitating carbonate phase or to the process of biocalcification (Farkaš et al., 2007; Fantle, 2010; Blättler et al., 2012). According to Farkaš et al. (2007) the variation between calcite and aragonite sea intervals, i.e. the mineralogy of the main precipitating carbonate phase, was an important determining factor of the calcium isotope record in the Palaeozoic, early Mesozoic and in the Neogene. The effect of such a change on the carbonate and seawater $\delta^{44/40}$Ca ratios differs depending on the timescale of the fractionation factor change. If the fractionation factor changes on a similar timescale to the residence time of Ca in the ocean (~ 1 Ma), $\delta^{44/40}$Ca isotopic composition of the seawater ($\delta^{44/40}Ca_{sw}$) will adjust to the new fractionation factor. Meanwhile, after a certain time (couple of millions of years) of opposite change, the $\delta^{44/40}$Ca isotopic composition of the carbonates ($\delta^{44/40}Ca_{carb}$), will return to the initial values (Fantle, 2010; Fantle and Tipper, 2014).

Under such conditions, a switch to aragonite sea would result in a temporal negative $\delta^{44/40}Ca_{carb}$ excursion and positive shift of the $\delta^{44/40}Ca_{sw}$ values, while a rapid transition to calcite sea would result in (according to the smaller Ca isotope fractionation in calcite than in aragonite (Gussone et al., 2005)) a temporary positive excursion in the $\delta^{44/40}Ca_{carb}$, and lower $\delta^{44/40}Ca_{sw}$ values (Farkaš et al., 2007; Fantle and Tipper, 2014). These scenarios are not capable to explain the observed Rhaetian calcium isotopic pattern in the light of the geological context during this time interval. Ooid mineralogy and Mg/Ca ratios obtained from fluid inclusions suggest that an aragonite sea interval was established in the Triassic, just as in the Permian and part of the Carboniferous (Horita et al., 2002). Only later, between the Sinemurian and Pliensbachian in the Jurassic a change to a calcite sea occurred (Vulpius and Kiessling, 2018).

Calcareous nannofossils emerged in the Late Triassic; it was suggested that they reached rock-forming abundance in periplatform palaeo-environmental setting in the latest Triassic (Preto et al., 2013). A relatively rapid increase in calcite precipitation and carbon burial due to the increase of calcareous nannofossil abundance over aragonitic fossils could result in smaller fractionation of the carbonate flux and therefore a transient positive $\delta^{44/40}Ca_{carb}$ excursion if affecting the global fractionation factor (Blättler et al., 2012). Similarly, a positive $\delta^{44/40}Ca_{carb}$ excursion would be expected if carbonate output flux would exceed continental input flux due

to enhanced calcareous nannofossil bioproductivity (De La Rocha and DePaolo, 2000; Blättler et al., 2011). This is clearly not observed in the presented dataset. There are two possible hypotheses to explain the apparent lack of influence of the emerging planktonic calcification on the calcium isotopes. Either the increase happened gradually on a time-scale well exceeding the residence time of the calcium, which would mean the isotopic composition of the output flux remained unchanged (Fantle and Tipper, 2014), or the contribution of the calcareous nannofossils to the overall carbonate burial remained limited. During the Carnian, the first calcispheres from calcifying organisms appear but they remain rare in the sediments. From the Norian to the lower Rhaetian the increase of the calcareous nannoplankton is slow; the main calcifier *P. triassica* composes between 0.1 % and 20 % of the rock samples in different palaeo-environmental settings (Fig. 6.4) (Preto et al., 2013; Demangel et al., 2020). During the rest of the Rhaetian, the increase was significantly faster in the deep-water sediments of Sicily (Pizzo Mondello, Sicanian Basin); the abundance of *P. triassica* reached there as high as 60 % of the total rock mass (Preto et al., 2013). However, in the Southern Appennines (Pignola-Abriola, Lagonegro Basin, Italy) and in Northern Calcareous Alps (Hallstatt Basin, Austria) its abundance remained around 20 % (Fig. 6.4) (Preto et al., 2013; Demangel et al. 2020) and no Late Triassic calcareous nannofossils were documented in Turkey and Oman (personal observations of I. Demangel). Hence, the global contribution of the calcareous nannofossils to the overall carbonate burial has been still limited at this early stage of their evolution. Therefore, it exerted no influence neither on the in- vs. output ratio of calcium nor on the global fractionation factor of the global carbonate output.

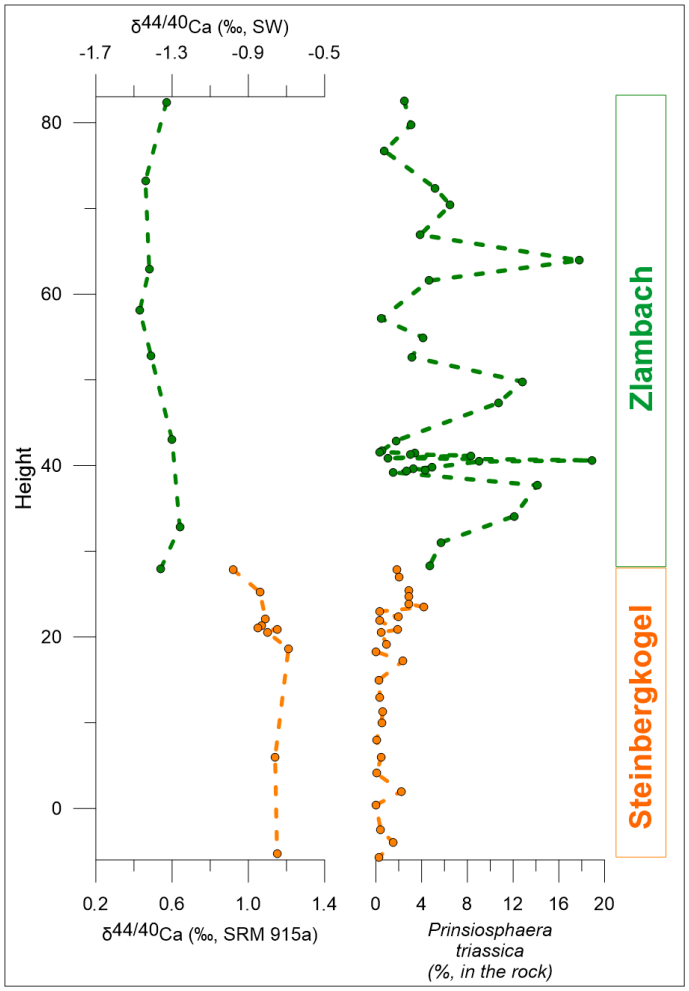

Fig.6.4 – $\delta^{44/40}$Ca record (this study) and the abundance of *Prinsiosphaera triassica* calcareous nannofossil in the Steinbergkogel (Demangel et al., 2020) and Zlambach sections (Demangel, submitted).

5.2 *Flux changes*

Several studies suggested that especially on time scales similar to or shorter than the residence time of Ca in the ocean, an increasing continental Ca input flux relative to marine carbonate sedimentation can cause a decrease in the $\delta^{44/40}$Ca isotopic composition of the seawater and of the associated carbonates, as the calcium isotopic composition of the calcareous sediments is fractionated relative to the calcium isotopic signature of seawater (De La Rocha and DePaolo, 2000; Blättler et al., 2011; Silva-Tamayo et al., 2018).

Previously, it was widely accepted that the $\delta^{44/40}$Ca isotopic values of both continental and hydrothermal fluxes are constant and close to each other, therefore the variation of the isotopic ratio of these two fluxes are not capable to change the $\delta^{44/40}Ca_{sw}$ (Schmitt et al., 2003).

Later, this view was partly challenged; it was suggested that especially on timescales longer than the residence time of Ca in the ocean (~ 1 Ma), the isotopic composition of the weathering flux becomes the determining factor (Fantle, 2010; Fantle and Tipper, 2014). There is an ~ 0.4 ‰ difference between the average $\delta^{44/40}$Ca isotopic value of river waters depending on the lithology of the source rocks (De La Rocha and DePaolo, 2000); carbonate-derived calcium being isotopically lighter than silicate-derived calcium (Fantle and Tipper, 2014). On timescales over several hundred years the variation of the isotopic composition of the riverine flux is probably smaller, but considerable changes are still expected due to changing proportions of the weathered rock types (De La Rocha and DePaolo, 2000; Sime et al., 2007).

Evaporites have been increasingly investigated to understand their role in the calcium cycle. Both natural evaporites and laboratory precipitates (mainly gypsum and anhydrite) can have a wide range of $\delta^{44/40}$Ca isotopic values, with the precipitates being ~1 ‰ lighter than the parenting fluid at isotopic equilibrium (Hensley, 2006). Under closed-system conditions, the $\delta^{44/40}$Ca values of the precipitates will get higher as the $\delta^{44/40}$Ca values of the parenting fluid increase due to Rayleigh-fractionation associated with continuous evaporation. However, in most natural evaporitic settings, basins recharge occurs, providing additional Ca that prevents the precipitation of evaporites with extremely high $\delta^{44/40}$Ca isotopic values (Hensley, 2006). The range of $\delta^{44/40}$Ca values of continental evaporites described so far is between -1.91 ‰ and -1.21 ‰ (Hensley, 2006; Chen et al., 2020). The investigation of marine evaporites is restricted to the Messinian, which yields similar or slightly heavier values than reported for the continental evaporites, ranging between -1.72 ‰ and -0.28 ‰ (Hensley, 2006). Despite the relatively low abundance of evaporites compared to silicates and carbonates in the rock record, they are thought to have a significant influence on seawater chemistry due to their high solubility and low weathering resistance (Chen et al., 2020).

A high-amplitude sea-level fall at the NRB emphasizes the relevance of both the imbalance between input versus removal of calcium and isotopic ratio changes of the input flux at the early Rhaetian in the Late Triassic. After a period of steady sea-level in the Lacian, Alaunian and most of the Sevatian, the sea-level dropped significantly at the NRB (e.g. Haq, 2018). As a result of this high-amplitude sea-level fall, large carbonate shelves and evaporite deposits could have been exposed to erosion. For instance, in the Central Tethyan area (Arabian Platform, Iran), Anisian, Ladian and Carnian carbonates are frequently missing from the

sedimentary record (e.g. Sharland et al., 2001). Furthermore, extensive evaporite deposits (gypsum, anhydrite, halite) of the Keuper facies were deposited on the western margin of the Neotethys in the Triassic Epicontinental European Seas (Ortí et al., 2017).

Carbonate and evaporite dissolution are expected to operate on a shorter time-scale as silicate weathering (Bufe et al., 2021). For example, the decreasing $\delta^{44/40}Ca$ trend at the end-Permian in less than 60 kyr was interpreted by Wang et al. (2019) in the light of sea-level changes. According to their hypothesis, the large marine regression at this time enhanced the weathering of the aragonitic shelf carbonates with low $\delta^{44/40}Ca$ values. The early Rhaetian $\delta^{44/40}Ca$ decreasing trend happened within approximately 200 kyr based on cyclostratigraphic analysis at Steinbergkogel (Galbrun et al., 2020). This short time interval supports the hypothesis, according to dissolution of carbonate and evaporites have probably influenced the $\delta^{44/40}Ca$ trend during the Late Triassic.

5.3 *Ocean acidification*

Ocean acidification was invoked to explain the preferably loss of organisms with aragonite or high-Mg calcite mineralogy and frequent carbonate preservation gaps in the sedimentary successions during the TJB interval (Greene et al., 2012). Ocean acidification was also proposed to have a possible effect on the $\delta^{44/40}Ca_{carb}$ signal (e.g.: Payne et al., 2010; Hinojosa et al., 2012; Jost et al., 2017; Silva-Tamayo et al., 2018), although it is still debated which mechanism impacts the calcium isotopic record and whether a negative or a positive $\delta^{44/40}Ca_{carb}$ excursion is expected. The majority of the studies focusing on time intervals where ocean acidification was previously identified (e.g., Permian-Triassic boundary, Triassic-Jurassic boundary, Toarcian OAE in the Early Jurassic, OAE1a and OAE2 in the Cretaceous, Cretaceous-Paleogene boundary) documented a negative calcium isotopic excursion between ~ 0.1 and 0.6 ‰ (Payne et al., 2010; Blättler et al., 2011; Hinojosa et al., 2012; Brazier et al., 2015; Komar and Zeebe, 2016; Jost et al., 2017; Silva-Tamayo et al., 2018; Linzmeier et al., 2020). At the Cretacaous-Paleogene boundary, the negative excursion was interpreted as the result of the changing molluscan fractionation factor due to changes in the carbonate chemistry of the seawater (Linzmeier et al., 2020). The negative excursions in case of all other pre-cited events were explained by two factors; both are the results of environmental changes caused by time-equivalent volcanic activity: (i) increased continental weathering and (ii) decreasing

carbonate saturation were proposed as driving factors (e.g. Brazier et al., 2015). These two consequences of the elevated CO_2 level in the atmosphere lead to Ca flux imbalances, and both the excess calcium delivery from the continents and reduced marine carbonate precipitation results in more negative $\delta^{44/40}Ca_{carb}$ values (Blättler et al., 2011; Gussone et al., 2005). Although in some cases excursions up to 0.6 ‰ were observed (Silva-Tamayo et al. 2018), modelling studies revealed that only ~ 0.14 ‰ can be caused by volcanism and Ca flux imbalances, meaning that additional factors have to be considered (Brazier et al., 2015; Jost et al., 2017; Silva-Tamayo et al., 2018).

Importantly, the above-described mechanisms would require a parallel and contemporaneous change in the $\delta^{44/40}Ca_{sw}$ value. In the case of the Permian-Triassic boundary, conodont measurements, which are thought to directly reflect the seawater changes, such a negative excursion has been observed (Hinojosa et al., 2012). Moreover, sedimentological features and other geochemical proxies also support the aforementioned changes in weathering fluxes and carbonate saturation (Payne et al., 2010; Blättler et al., 2011; Brazier et al., 2015; Silva-Tamayo et al., 2018).

Despite these arguments, Komar and Zeebe (2016) questioned the effect of flux imbalances and explained the negative excursion at the Permian-Triassic boundary (PTB) with variable mass-dependent fractionation. According to their model, the shutdown of the biological pump caused the saturation and $[CO_3^{2-}]$ level to drop, which in turn led to stronger fractionation and therefore to a negative excursion. This relation between carbonate saturation and Ca isotope fractionation is however not widely accepted. Indeed, several studies indicate that the fractionation between seawater and calcareous sediments gets smaller at lower precipitation rates (Du Vivier et al., 2015; Silva-Tamayo et al., 2018; Linzmeier et al., 2020; Wang et al., 2021). The latter relation was used to explain the rarely described positive excursions related to ocean acidification events at the OAE1a and OAE2 (Du Vivier et al., 2015; Wang et al., 2021). Fantle and Ridgwell (2020) also argues for a positive excursion related to ocean acidification due to authigenic carbonate formation.

In this study, we describe a short, negative excursion in $\delta^{44/40}Ca$ of ~0.14 ‰ across the ETE from the T-bed (Kuhjoch section). We note that this is a very small excursion, which is represented only by a single sample; therefore, this observation requires further studies. However, we attribute this excursion to ocean acidification, corroborating the modelling

outcomes on negative $\delta^{44/40}$Ca excursion of 0.14 ‰ at the TJB reported by Jost et al. (2017). The excursion observed in Italy by Jost et al. (2017) and in this study are probably time-equivalent, although the timing is biostratigraphically better constrained in this study. Besides, previous studies described $\delta^{13}C_{org}$, Hg/TOC and Ir excursions from the same bed (T-bed), which are related to the CAMP volcanic activity (Tanner et al., 2016; Percival et al., 2017; Lindström et al., 2021), while the $^{87}Sr/^{86}Sr$ ratios show an increasing trend through the TJB, due to the increasing continental weathering (Kovács et al., 2020).

We note that negative excursions at the PTB at the ETE are not in contradiction with positive excursions related to other acidification events. For instance, Du Vivier et al. (2015) discussed the possible reasons for a negative $\delta^{44/40}$Ca excursion at the PTB and a positive one at the Cenomanian/Turonian boundary and attributed these to (i) the emplacement of Siberian Trap at the PTB on land instead of in the ocean, which could have resulted in different path to cause ocean acidification and (ii) differences in the carbonate chemistry of the seawater in the Permian and in the Cretaceous due to the absence vs. presence of carbonate precipitating planktonic organisms. It seems reasonable that the $\delta^{44/40}$Ca trend at the TJB is similar to the PTB, because the CAMP was also emplaced on continent (Self et al., 2014) and calcareous nannofossils just started to evolve, but did not globally reach rock-forming abundance (Demangel et al., 2020).

5.4 *Local differences*

The main $\delta^{44/40}$Ca isotopic trends of the Late Triassic (Rhaetian $\delta^{44/40}$Ca isotope decline, negative $\delta^{44/40}$Ca excursion at the ETE horizon) can be explained by the factors discussed above. However, the offset (0.15 – 0.30 ‰) between the overlapping section intervals from Austria and Turkey calls for another explanation, which introduces local differences in the isotopic composition of the carbonates.

5.4.1 Submarine groundwater dischrages

An isotopic difference could be present between shallow vs. deeper marine settings due to the effect of submarine groundwater discharge (SGD). The SGD flux, which delivers isotopically light Ca to the ocean, is expected to be approximately equal to the combined flux from rivers and hydrothermal vents at mid-oceanic ridges and play an important role in areas

with restricted water cycling (Holmden et al., 2012b). In modern coastal, shallow environments it was shown that due to the enhanced subsurface weathering of carbonates and to the mixing of freshwater and seawater the Ca isotopic values in these environments can deviate from the oceanic signature (Holmden et al., 2012b; Shao et al., 2018). It was hypothesized that the nearshore areas of ancient epeiric seas, which covered vast areas in the geological past could be influenced by the same processes as the modern coastal bays (Holmden et al., 2012b). However, both Oyuklu and Steinbergkogel were deposited in basinal or deep ramp settings, therefore such an explanation is not relevant for this study.

5.4.2 Mineralogy

The $\delta^{44/40}$Ca vs. Sr (ppm) plot reveals an inverse correlation in all investigated sections except for Steinbergkogel (Fig. 6.5). It was suggested that the local mixing of aragonite and calcite mineralogies results in a linear inverse correlation between these two variables (Farkaš et al., 2017; Lau et al., 2017), while an inverse linear correlation with a slope of -0.00094 is characteristic for kinetic isotope effects due to changing precipitation rates during abiotic calcite precipitation (Tang et al., 2008). Among the investigated sections, Zlambach, Eiberg and Kuhjoch show a nearly linear, inverse correlation between $\delta^{44/40}$Ca and Sr (ppm) values with slopes significantly different from the above-mentioned kinetic one (Fig. 6.5). The observed linear inverse correlation thus excludes the precipitation rate as the determining factor of the calcium isotopic values.

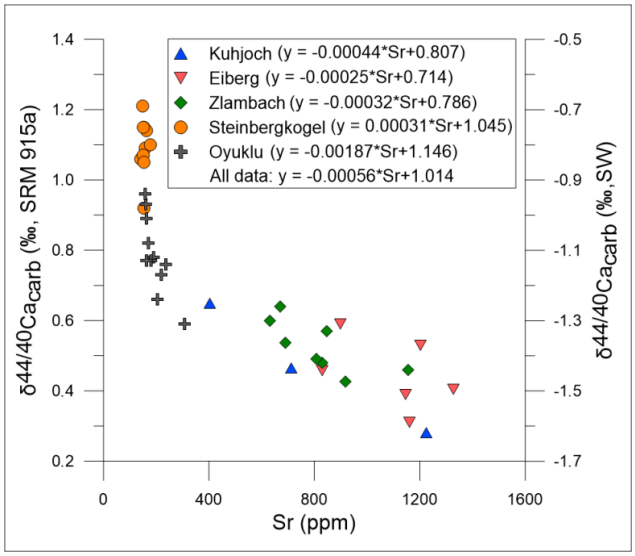

Fig.6.5 – Crossplot of $\delta^{44/40}$Ca values and Sr content in the investigated sections.

Different proportions of calcite and aragonite in the sediments can result in the described relation because aragonite has a much higher potential to incorporate Sr within its lattice due to its larger cation site and its orthorhombic system in comparison with calcite, and aragonite precipitation fractionates the Ca isotopes more than calcite does. These differences produce on average 0.60 ‰ lighter $\delta^{44/40}$Ca isotopic values in aragonite than in calcite precipitates (Gussone et al., 2005). The mixing of these two polymorphs in different relative proportions can be the result of shifts in the dominant carbonate facies due to eustasy or changes in the $CaCO_3$ mineralogy of the primary producers (Farkaš et al., 2016). In the light of the geological and palaeo-environmental settings of the investigated sections, the primary mixing of aragonite and calcite materials is a reasonable process to explain (I) the linear correlations observed at Zlambach, Eiberg and Kuhjoch, and (II) the fact that Steinbergkogel and Oyuklu are characterized by higher $\delta^{44/40}$Ca values and lower Sr content. The sections, Zlambach, Eiberg and Kuhjoch were located close to a giant carbonate platform and were therefore probably influenced by the recycling of aragonitic fossils from shallow shelf and reef environments. Oyuklu and Steinbergkogel, on the contrary, were located much further away from the carbonate platform and are mainly characterized by in-situ deep carbonate sedimentation, without significant input of allochthonous aragonitic material.

5.4.3 Early diagenesis

The fact that the Steinbergkogel and Oyuklu sections do not plot on the linear trendline indicates that the mixing of different $CaCO_3$ polymorphs is not the only local factor to account for the isotopic offsets between overlapping intervals. Due to the high Ca content in carbonate sediments, Ca isotopes are generally resistant to diagenesis. However, fluid flow with high Ca flux can alter the $\delta^{44/40}$Ca isotopic composition of the sediment at an early stage of burial (Gussone et al., 2020). The water-rock interaction model of Lau et al. (2017) offers the best explanation for the deviation of the trends seen in Steinbergkogel and Oyuklu. This model displays the increase of $\delta^{44/40}$Ca isotopic values and Sr loss as a function of the volume of water, which has passed through the sediment after deposition. It was proposed, that recrystallization of carbonate rocks in equilibrium with seawater-derived pore water would result in a non-linear relation between $\delta^{44/40}$Ca isotopic compositions and Sr concentrations, as the loss of Sr occurs more rapidly than the resetting of the $\delta^{44/40}$Ca isotopic values. Furthermore, the initial mineralogical composition of the carbonate rocks controls how these two variables are

changing over time (Lau et al., 2017). The equilibrium fractionation factor between $CaCO_3$ and pore fluid Ca is very close to 1.0000, consequently, early diagenetic recrystallization was suggested to account for a positive shift in $\delta^{44/40}Ca$, ~ 0.10 – 0.15 ‰ at maximum (Fantle and DePaolo, 2007). It is important to note that only the neomorphism and recrystallization under fluid-buffered conditions is capable to introduce significant changes in the carbonate $\delta^{44/40}Ca$, as in this case a big portion of the diagenetic fluid is unaltered seawater, which has the heaviest Ca isotopic signal (Higgins et al., 2018). On the contrary, in case of sediment-buffered conditions, the secondary changes in the $\delta^{44/40}Ca$ values tend to be far less as a big portion of the Ca is delivered from the sediment itself (Higgins et al., 2018). This effect is arguably to be the most significant at low sedimentation rates, which allows the sediments to remain near to the seafloor for a long time, and can be an important mechanism in platform systems with advective seawater flux (Lau et al., 2017; Higgins et al., 2018; Gussone et al., 2020). Among the investigated sections Steinbergkogel and Oyuklu were deposited in palaeo-environmental settings with low sedimentation rates, and in the case of Steinbergkogel probably with strong bottom currents as well, which could have resulted in calcitic sedimentation with low Sr contents (Kovács et al., 2020). Our results confirm the potential of this effect. Oyuklu had probably similar early diagenetic conditions all along. Steinbergkogel with low sedimentation rate but stronger bottom current is indeed more positive. However, Zlambach and Eiberg sections with their higher sedimentation rate show lower values than Oyuklu.

Similar non-linear, inverse correlation was documented in numerous sections throughout the Phanerozoic in shallow marine carbonates (Lau et al., 2017) and is most evident during aragonite sea intervals (Gussone et al., 2020). In summary, the combination of the sediment mineralogy and early-stage diagenesis with intensive fluid flow in certain settings can account for a significant $\delta^{44/40}Ca$ range in contemporaneous sections. This finding supports the potential of bulk $\delta^{44/40}Ca$ measurements as a tool to determine diagenetic processes and carbonate minerology in environments, where other proxies are lacking or facing difficulties (Gussone et al., 2020) and with that contributes to a better understanding of the applicability of this isotopic proxy.

Conclusion

The investigation of the Late Triassic and earliest Jurassic (Norian – Hettangian) $\delta^{44/40}Ca$ composition of bulk carbonates in two study areas, the Taurides (Turkey) and the Northern

Calcareous Alps (Austria), revealed three main features. First, a decreasing trend across the Rhaetian, with the major decline of ~ 0.20 ‰ in the early Rhaetian. This feature is particularly evident in the Turkish section, which is characterized by monotonous lithology across almost the entire Rhaetian. Several lines of evidence suggest that the ratio between Ca input to the ocean and removal from it and the isotopic ratio of the continental Ca flux were changed and drove this trend. A significant global sea-level fall occurred around the Norian-Rhaetian boundary, exposing widespread pre-Norian platform carbonates and evaporites to weathering and erosion. The chemical weathering of these lithologies (mainly of carbonate) is expected to shift the $\delta^{44/40}Ca_{sw}$ and $\delta^{44/40}Ca_{carb}$ signatures towards lighter values. The hypothesis is supported also by the relatively short duration; < 200 kyr, of the decreasing trend.

The second feature is a ~ 0.14 ‰ negative excursion, corresponding to the emplacement of the Central Atlantic Magmatic Province. This pattern is compatible with the widely accepted ocean acidification at that time and confirms the view that ocean acidification events result only in small $\delta^{44/40}Ca$ isotopic excursions. The third characteristics of the compiled $\delta^{44/40}Ca$ isotope record is the ~ 0.15 – 0.30 ‰ offset seen between the two main study sites in Austria and Turkey during the Rhaetian. In contrast to the previous global patterns, this shift is attributed to local mineralogical differences and early marine diagenesis as indicated by the relation between $\delta^{44/40}Ca$ isotopic ratios and Sr concentrations. This finding supports the emerging view that Ca isotopes can be successfully applied to constrain effects of diagenetic processes and original $CaCO_3$ minerology of calcareous rocks through time and space.

Acknowledgement

The Austrian Science Fund (FWF) (Project Number: P 29497-P29 to Sylvain Richoz) is greatly acknowledged for financial support of this research. We thank the help of Colin Fourtet with the ICP-AES measurements. We thank Bruno Galbrun, Silvia Gardin and Annachiara Bartolini for their help during the sampling at Zlambach. We gratefully acknowledge the technical assistance of Franz Tscherne during material preparation.

References

Blättler, C. L.; Henderson, G. M.; Jenkyns, H. C. (2012): Explaining the Phanerozoic Ca isotope history of seawater. *Geology* **40**(9), 843-846. DOI: 10.1130/G33191.1

Blättler, C. L.; Jenkyns, H. C.; Reynard, L. M.; Henderson, G. M. (2011): Significant increases in global weathering during Oceanic Anoxic Events 1a and 2 indicated by calcium isotopes. *Earth Planet. Sci. Lett.* **309**(1-2), 77-88. DOI: 10.1016/j.epsl.2011.06.029

Brazier, J. M.; Suan, G.; Tacail, T.; Simon, L.; Martin, J. E.; Mattioli, E.; Balter, V. (2015): Calcium isotope evidence for dramatic increase of continental weathering during the Toarcian oceanic anoxic event (Early Jurassic). *Earth Planet. Sci. Lett.* **411**, 164-176. DOI: 10.1016/j.epsl.2014.11.028

Bufe, A.; Hovius, N.; Emberson, R.; Rugenstein, J. K.; Galy, A.; Hassenruck-Gudipati, H. J.; Chang, J. M. (2021): Co-variation of silicate, carbonate and sulfide weathering drives CO 2 release with erosion. *Nat. Geosci.* **14**(4), 211-216. DOI: 10.1038/s41561-021-00714-3

Chen, B. B.; Li, S. L.; von Strandmann, P. A. P.; Sun, J.; Zhong, J.; Li, C., Ma, T. T.; Xu, S.; Liu, C. Q. (2020): Ca isotope constraints on chemical weathering processes: Evidence from headwater in the Changjiang River, China. *Chem. Geol.* **531**, 119341. DOI: 10.1016/j.chemgeo.2019.119341

Davies, J. H. F. L.; Marzoli, A.; Bertrand, H.; Youbi, N.; Ernesto, M.; Schaltegger, U. (2017): End-Triassic mass extinction started by intrusive CAMP activity. *Nat. Commun.* **8**, 15596. DOI: 10.1038/ncomms15596

De La Rocha, C. L.; DePaolo, D. J. (2000): Isotopic evidence for variations in the marine calcium cycle over the Cenozoic. *Science* **289**(5482), 1176-1178. DOI: 10.1126/science.289.5482.1176

Demangel, I.; Kovács, Z.; Richoz, S.; Gardin, S.; Krystyn, L.; Baldermann, A.; Piller, W. E. (2020): Development of early calcareous nannoplankton in the late Triassic (Northern Calcareous Alps, Austria). *Glob. Planet. Change* **193**, 103254. DOI: 10.1016/j.gloplacha.2020.103254.

Demangel, I.; Kovács, Z.; Richoz, S.; Gardin, S.; Krystyn, L.; Piller, W. E. (submitted): Fate of the calcareous nannofossils during the Rhaetian. Example from the Northern Calcareous Alps (Austria).

DePaolo, D. J. (2004): Calcium isotopic variations produced by biological, kinetic, radiogenic and nucleosynthetic processes. *Rev. Mineral. Geochem.* **55**(1), 255-288. DOI: 10.2138/gsrmg.55.1.255

Du Vivier, A. D.; Jacobson, A. D.; Lehn, G. O.; Selby, D.; Hurtgen, M. T.; Sageman, B. B. (2015): Ca isotope stratigraphy across the Cenomanian–Turonian OAE 2: Links between volcanism, seawater geochemistry, and the carbonate fractionation factor. *Earth Planet. Sci. Lett.* **416**, 121-131. DOI: 10.1016/j.epsl.2015.02.001

Fantle, M. S. (2010): Evaluating the Ca isotope proxy. *Am. J. Sci.* **310**(3), 194-230. DOI: 10.2475/03.2010.03

Fantle, M. S.; DePaolo, D. J. (2005): Variations in the marine Ca cycle over the past 20 million years. *Earth Planet. Sci. Lett.* **237**(1-2), 102-117. DOI: 10.1016/j.epsl.2005.06.024

Fantle, M. S.; DePaolo, D. J. (2007): Ca isotopes in carbonate sediment and pore fluid from ODP Site 807A: the Ca^{2+} (aq)–calcite equilibrium fractionation factor and calcite recrystallization rates in Pleistocene sediments. *Geochim. Cosmochim. Acta* **71**(10), 2524-2546. DOI: 10.1016/j.gca.2007.03.006

Fantle, M. S.; Ridgwell, A. (2020): Towards an understanding of the Ca isotopic signal related to ocean acidification and alkalinity overshoots in the rock record. *Chem. Geol.* **547**, 119672. DOI: 10.1016/j.chemgeo.2020.119672

Fantle, M. S.; Tipper, E. T. (2014): Calcium isotopes in the global biogeochemical Ca cycle: implications for development of a Ca isotope proxy. *Earth-Sci. Rev.* **129**, 148-177. DOI: 10.1016/j.earscirev.2013.10.004

Farkaš, J.; Böhm, F.; Wallmann, K.; Blenkinsop, J.; Eisenhauer, A.; Van Geldern, R.; Munnecke, A.; Voigt, S.; Veizer, J. (2007): Calcium isotope record of Phanerozoic oceans: Implications for chemical evolution of seawater and its causative mechanisms. *Geochim. Cosmochim. Acta* **71**(21), 5117-5134. DOI: 10.1016/j.gca.2007.09.004

Farkaš, J.; Frýda, J.; Holmden, C. (2016): Calcium isotope constraints on the marine carbon cycle and CaCO3 deposition during the late Silurian (Ludfordian) positive $\delta^{13}C$ excursion. *Earth Planet. Sci. Lett.* **451**, 31-40. DOI: 10.1016/j.epsl.2016.06.038

Farkaš, J.; Frýda, J.; Holmden, C. (2017): Corrigendum to "Calcium isotope constraints on the marine carbon cycle and $CaCO_3$deposition during the late Silurian (Ludfordian) positive $\delta^{13}C$excursion" [Earth Planet. Sci. Lett. 451 (2016) 31-40]. *Earth Planet. Sci. Lett.* **469**, 170-171. DOI: 10.1016/j.epsl.2017.04.013

Galbrun, B.; Boulila, S.; Krystyn, L.; Richoz, S.; Gardin, S.; Bartolini, A.; Maslo, M. (2020): Astronomical calibration of Austrian key sections. *Glob. Planet. Change* 103253. DOI: 10.1016/j.gloplacha.2020.103253

Gallet, Y.; Krystyn, L.; Marcoux, J.; Besse, J. (2007): New constraints on the End-Triassic (Upper Norian–Rhaetian) magnetostratigraphy. *Earth Planet. Sci. Lett.* **255**(3-4), 458-470. DOI: 10.1016/j.epsl.2007.01.004

Goddéris, Y.; Donnadieu, Y.; de Vargas, C.; Pierrehumbert, R. T.; Dromart, G.; van de Schootbrugge, B. (2008): Causal or casual link between the rise of nannoplankton calcification and a tectonically-driven massive decrease in Late Triassic atmospheric CO_2? *Earth Planet. Scie. Lett.* **267**(1- 2), 247-255. DOI: 10.1016/j.epsl.2007.11.051

Golonka, J. (2007): Late Triassic and Early Jurassic palaeogeography of the world. *Palaeogeogr. Palaeoclimatol. Palaeoecol.* **244**(1-4), 297-307. DOI: 10.1016/j.palaeo.2006.06.041

Greene, S. E.; Martindale, R. C.; Ritterbush, K. A.; Bottjer, D. J.; Corsetti, F. A.; Berelson, W. M. (2012): Recognising ocean acidification in deep time: An evaluation of the evidence for acidification across the Triassic-Jurassic boundary. *Earth-Sci. Rev.* **113**(1-2), 72-93. DOI: 10.1016/j.earscirev.2012.03.009

Gussone, N.; Ahm, A. S. C.; Lau, K. V.; Bradbury, H. J. (2020): Calcium isotopes in deep time: Potential and limitations. *Chem. Geol.* 119601. DOI: 10.1016/j.chemgeo.2020.119601

Gussone, N.; Böhm, F.; Eisenhauer, A.; Dietzel, M.; Heuser, A.; Teichert, B. M.; Reitner, J.; Wörheide, G.; Dullo, W. C. (2005): Calcium isotope fractionation in calcite and aragonite. *Geochim. Cosmochim. Acta* **69**(18), 4485-4494. DOI: 0.1016/j.gca.2005.06.003

Haq, B. U. (2018): Triassic Eustatic Variations Reexamined. *GSA Today* **28**(12), 4-9. DOI: 10.1130/GSATG381A.1

Hensley, T. M. (2006): Calcium isotopic variation in marine evaporites and carbonates: Applications to Late Miocene Mediterranean brine chemistry and Late Cenozoic calcium cycling in the oceans. (PhD dissertation) University of California.

Heuser A.; Schmitt A.-D.; Gussone N.; Wombacher F. (2016): Analytical methods. In *Calcium Stable Isotope Geochemistry*, Advances in Isotope Geochemistry. Springer, Berlin, Heidelberg, 23-73.

Higgins, J. A.; Blättler, C. L.; Lundstrom, E. A.; Santiago-Ramos, D. P.; Akhtar, A. A.; Ahm, A. C.; Bialik, O.; Holmden, C.; Bradbury, H.; Murray, S. T.; Swart, P. K. (2018): Mineralogy, early marine diagenesis, and the chemistry of shallow-water carbonate sediments. *Geochim. et Cosmochim. Acta*, **220**, 512-534. DOI: 10.1016/j.gca.2017.09.046

Hinojosa, J. L.; Brown, S. T.; Chen, J.; DePaolo, D. J.; Paytan, A.; Shen, S. Z.; Payne, J. L. (2012): Evidence for end-Permian ocean acidification from calcium isotopes in biogenic apatite. *Geology* **40**(8), 743-746. DOI: 10.1130/G33048.1

Hippler, D.; Schmitt, A. D.; Gussone, N.; Heuser, A.; Stille, P.; Eisenhauer, A.; Nägler, T. F. (2003): Calcium isotopic composition of various reference materials and seawater. *Geostandards Newsl.* **27**(1), 13-19. DOI: 10.1111/j.1751-908X.2003.tb00709.x

Holmden, C.; Panchuk, K.; Finney, S. C. (2012a): Tightly coupled records of Ca and C isotope changes during the Hirnantian glaciation event in an epeiric sea setting. *Geochim. Cosmochim. Acta*, **98**, 94-106. DOI: 10.1016/j.gca.2012.09.017

Holmden, C.; Papanastassiou, D. A.; Blanchon, P.; Evans, S. (2012b): $\delta^{44/40}$Ca variability in shallow water carbonates and the impact of submarine groundwater discharge on Ca-cycling in marine environments. *Geochim. Cosmochim. Acta*, **83**, 179-194. DOI: 10.1016/j.gca.2011.12.031

Horita, J.; Zimmermann, H.; Holland, H. D. (2002): Chemical evolution of seawater during the Phanerozoic: Implications from the record of marine evaporites. *Geochim. Cosmochim. Acta* **66**(21), 3733-3756. DOI: 10.1016/S0016-7037(01)00884-5

Jost, A. B.; Bachan, A.; van de Schootbrugge, B.; Brown, S. T.; DePaolo, D. J.; Payne, J. L. (2017): Additive effects of acidification and mineralogy on calcium isotopes in

Triassic/Jurassic boundary limestones. *Geochem. Geophys. Geosyst.* **18**(1), 113-124. DOI: 10.1002/2016GC006724

Kasemann, S. A.; Hawkesworth, C. J.; Prave, A. R.; Fallick, A. E.; Pearson, P. N. (2005): Boron and calcium isotope composition in Neoproterozoic carbonate rocks from Namibia: evidence for extreme environmental change. *Earth Planet. Sci. Lett.* **231**(1-2), 73-86. DOI: 10.1016/j.epsl.2004.12.006

Komar, N.; Zeebe, R. E. (2016): Calcium and calcium isotope changes during carbon cycle perturbations at the end-Permian. *Paleoceanography*, **31**(1), 115-130. DOI: 10.1002/2015PA002834

Kovács, Z.; Demangel, I.; Richoz, S.; Hippler, D.; Baldermann, A.; Krystyn, L. (2020): New constraints on the evolution of $^{87}Sr/^{86}Sr$ of seawater during the Upper Triassic. *Glob. Planet. Change* **192**, 103255. DOI: 10.1016/j.gloplacha.2020.103255

Lau, K. V.; Maher, K.; Brown, S. T.; Jost, A. B.; Altıner, D.; DePaolo, D. J.; Eisenhauer, A.; Kelley, B. M.; Lehrmann, D. J.; Paytan, A.; Yu, M.; Silva-Tamayo, J. C.; Payne, J. L. (2017): The influence of seawater carbonate chemistry, mineralogy, and diagenesis on calcium isotope variations in Lower-Middle Triassic carbonate rocks. *Chem. Geol.* **471**, 13-37. DOI: 10.1016/j.chemgeo.2017.09.006

Lehn, G. O.; Jacobson, A. D.; Holmden, C. (2013): Precise analysis of Ca isotope ratios (δ44/40Ca) using an optimized 43Ca–42Ca double-spike MC-TIMS method. *Int. J. Mass Spectrom.* **351**, 69-75. DOI: 10.1016/j.ijms.2013.06.013

Lindström, S.; Callegaro, S.; Davies, J.; Tegner, C.; van de Schootbrugge, B.; Pedersen, G. K.; Youbi, N.; Sanei, H.; Marzoli, A. (2021): Tracing volcanic emissions from the Central Atlantic Magmatic Province in the sedimentary record. Earth Sci. Rev. 103444. DOI: 10.1016/j.earscirev.2020.103444

Linzmeier, B. J.; Jacobson, A. D.; Sageman, B. B.; Hurtgen, M. T.; Ankney, M. E.; Petersen, S. V.; Tobin, T. S.; Kitch, G. D.; Wang, J. (2020): Calcium isotope evidence for environmental variability before and across the Cretaceous-Paleogene mass extinction. *Geology*, **48**(1), 34-38. DOI: 10.1130/G46431.1

Lucas, S. G., Tanner, L. H. (2008): Reexamination of the end-Triassic mass. In *Mass extinction*. 65-102. Springer, Berlin, Heidelberg. DOI: 10.1007/978-3-540-75916-4_8

Mandl, G. W. (2000): The Alpine sector of the Tethyan shelf—examples of Triassic to Jurassic sedimentation and deformation from the Northern Calcareous Alps. Mitteilungen der Österreichischen Geologischen Gesellschaft, 92 (1999), pp. 61–77.

Mette, W.; Elsler, A.; Korte, C. (2012): Palaeoenvironmental changes in the Late Triassic (Rhaetian) of the Northern Calcareous Alps. Clues from stable isotopes and microfossils. *Palaeogeogr. Palaeoclimatol. Palaeoecol.* **350-352**, 62-72. DOI: 10.1016/j.palaeo.2012.06.013

Ortí, F.; Pérez-López, A.; Salvany, J. M. (2017): Triassic evaporites of Iberia: Sedimentological and palaeogeographical implications for the western Neotethys evolution during the Middle Triassic–Earliest Jurassic. *Palaeogeogr. Palaeoclimatol. Palaeoecol.* **471**, 157-180. DOI: 10.1016/j.palaeo.2017.01.025

Payne, J. L.; Turchyn, A. V.; Paytan, A.; DePaolo, D. J.; Lehrmann, D. J.; Yu, M.; Wei, J. (2010): Calcium isotope constraints on the end-Permian mass extinction. *Proc. Natl. Acad. Sci. USA* **107**(19), 8543-8548. DOI: 10.1073/pnas.0914065107

Percival, L. M.; Ruhl, M.; Hesselbo, S. P.; Jenkyns, H. C.; Mather, T. A.; Whiteside, J. H. (2017): Mercury evidence for pulsed volcanism during the end-Triassic mass extinction. *Proc. Natl. Acad. Sci. USA* **114**(30), 7929-7934. DOI: 10.1073/pnas.1705378114

Preto, N.; Agnini, C.; Rigo, M.; Sprovieri, M.; Westphal, H. (2013): The calcareous nannofossil *Prinsiosphaera* achieved rock-forming abundances in the latest Triassic of western Tethys: consequences for the $\delta^{13}C$ of bulk carbonate. *Biogeosci. Discuss.* **10**(5), 7989-8025. DOI: 10.5194/bgd-10-7989-2013

Richoz, S.; Krystyn, L.; Hillebrandt, A. von; Martindale, R. (2012): End-Triassic crisis events recorded in platform and basin of the Austrian Alps. The Triassic/Jurassic and Norian/Rhaetian GSSPs. *Journal of Alpine Geology* **54**, 323-377

Schmitt, A. D.; Chabaux, F.; Stille, P. (2003): The calcium riverine and hydrothermal isotopic fluxes and the oceanic calcium mass balance. *Earth Planet. Sci. Lett.* **213**(3-4), 503-518. DOI: 10.1016/S0012-821X(03)00341-8

Self, S.; Schmidt, A.; Mather, T. A. (2014): Emplacement characteristic, time scales, and volcanic gas release rates of continental flood basalt eruption on Earth. Geological Society of America Special Papers, 505.

Shao, Y.; Farkaš, J.; Holmden, C.; Mosley, L.; Kell-Duivestein, I.; Izzo, C.; Reis-Santos, P.; Tyler, J.; Törber, P.; Frýda, J.; Taylor, H.; Haynes, D.; Tibby, J.; Gillanders, B. M. (2018): Calcium and strontium isotope systematics in the lagoon-estuarine environments of South Australia: Implications for water source mixing, carbonate fluxes and fish migration. *Geochim. Cosmochim. Acta*, **239**, 90-108. DOI: 10.1016/j.gca.2018.07.036

Sharland, P. R.; Archer, R.; Casey, D. M.; Davies, R. B.; Hall, S. H.; Heward, A. P.; Horbury, A. D.; Simmons, M. D. (2001): Sequence stratigraphy of the Arabian Plate. *GeoArabia* Special Publication 2, Gulf PetroLink, Bahrain, 371 p.

Silva-Tamayo, J. C.; Lau, K. V.; Jost, A. B.; Payne, J. L.; Wignall, P. B.; Newton, R. J.; Eisenhauser, A.; DePaolo, D. J.; Brown, S.; Maher, K.; Lehrmann, D. J.; Altiner, D.; Yu, M.; Richoz, S.; Paytan, A. (2018): Global perturbation of the marine calcium cycle during the Permian-Triassic transition. *Bulletin* **130**(7-8), 1323-1338. DOI: 10.1130/B31818.1

Sime, N. G.; Christina, L.; Tipper, E. T.; Tripati, A.; Galy, A.; Bickle, M. J. (2007): Interpreting the Ca isotope record of marine biogenic carbonates. *Geochim. Cosmochim. Acta* **71**(16), 3979-3989. DOI: 10.1016/j.gca.2007.06.009

Tang, J.; Dietzel, M.; Böhm, F.; Köhler, S. J.; Eisenhauer, A. (2008): Sr^{2+}/Ca^{2+} and $^{44}Ca/^{40}Ca$ fractionation during inorganic calcite formation: II. Ca isotopes. *Geochim. Cosmochim. Acta* **72**(15), 3733-3745. DOI: 10.1016/j.gca.2008.05.033

Tanner, L. H.; Kyte, F. T.; Richoz, S.; Krystyn, L. (2016): Distribution of iridium and associated geochemistry across the Triassic–Jurassic boundary in sections at Kuhjoch and Kendlbach, Northern Calcareous Alps, Austria. *Palaeogeogr. Palaeoclimatol.Palaeoecol.* **449**, 13-26. DOI: 10.1016/j.palaeo.2016.01.011

von Hillebrandt, A.; Krystyn, L.; Kurschner, W.M.; Bonis, N.R.; Ruhl, M.; Richoz, S.; Schobben, M.A.N.; Urlichs, M.; Bown, P.R.; Kment, K.; McRoberts, C.A.; Simms, M.; Tomasovych, A. (2013): The global stratotype sections and point (GSSP) for the base of the

Jurassic System at Kuhjoch (Karwendel Mountains, Northern Calcareous Alps, Tyrol, Austria). *Episodes* **36**(3), 162-198

Vulpius, S.; Kiessling, W. (2018): New constraints on the last aragonite–calcite sea transition from early Jurassic ooids. *Facies* **64**(1), 3. DOI: 10.1007/s10347-017-0516-x

Wang, J.; Jacobson, A. D.; Sageman, B. B.; Hurtgen, M. T. (2021): Stable Ca and Sr isotopes support volcanically triggered biocalcification crisis during Oceanic Anoxic Event 1a. *Geology*, **49**(5), 515-519. DOI: 10.1130/G47945.1

Wang, J.; Jacobson, A. D.; Zhang, H.; Ramezani, J.; Sageman, B. B.; Hurtgen, M. T.; Bowring, S. A.; Shen, S. Z. (2019): Coupled $\delta^{44/40}$Ca, $\delta^{88/86}$Sr, and $87^{Sr/86}$Sr geochemistry across the end-Permian mass extinction event. *Geochim. Cosmochim. Acta* **262**, 143-165. DOI: 10.1016/j.gca.2019.07.035

Supplementary material

Electronic appendix 1

SAMPLE ID	$\delta^{44/40}$Ca (‰, SRM915a) this study	$\delta^{44/40}$Ca (‰, SW) this study	$^{87}Sr/^{86}Sr$ Kovács et al., (2020)	Calcite % Kovács et al., (2020)	Sr ppm Kovács et al., (2020)	Sr/Ca (mmol/mol) Kovács et al., (2020)	Mn/Sr (mol/mol) Kovács et al., (2020)	Sr ppm exclude	Mn/Sr (mol/mol) exclude
KJB 2	0,65	-1,23	0,707802	94,5	404	0,49	1,766543525		
KN 90	0,38	-1,50		4,3				66	26,15478545
KN 14	0,28	-1,60	0,707790	73,2	1224	1,98	0,691886631		
KJ12_12	0,46	-1,42	0,707805	99,1	712	0,84	1,753307516		
EB 402	0,40	-1,48	0,707731	95,9	1327	1,61	0,090920338		
EB 426	0,53	-1,35	0,707704	92,9	1202	1,52	0,063464167		
EB 291	0,46	-1,42	0,707841	71,9	831	1,72	0,168387162		
EB 220	0,59	-1,29	0,707777	90,6	900	1,22	0,326629709		
EB 140	0,39	-1,49	0,707837	76,6	1145	1,93	0,117527087		
EB 78	0,31	-1,57	0,707764	89,7	1161	1,62	0,384241181		
ZL 54	0,57	-1,31	0,707829	95,9	847	1,14	0,805308511		
ZL 45	0,46	-1,42	0,707809	96,1	1156	1,35	0,60231349		
ZL 35	0,48	-1,40	0,707845	84,5	830	1,22	0,633544391		
ZL 30	0,43	-1,45	0,707780	95,7	919	1,12	0,528217366		
ZL 24 *	0,49	-1,39	0,707795	93,6	807	0,95	0,437261423		
ZL 15	0,60	-1,28	0,707871	97,6	630	0,84	0,763067921		
ZL 4.9	0,64	-1,24	0,707900	95,3	670	0,83	0,5951287		
ZL 0.06	0,54	-1,34	0,707865	100,0	690	0,83	0,647144764		
STK B 44	0,92	-0,96	0,707839	95,8	154	0,21	2,458886986		
STK B/27A	1,06	-0,82	0,707831	100,0	141	0,19	1,089909521		
STK A/114B	1,09	-0,79	0,707898	100,0	159	0,22	1,815625219		
STK A/112A	1,07	-0,81	0,707960	93,4	150	0,21	1,380927909		
STK A/111A	1,05	-0,83	0,707994	91,1	153	0,21	1,155558724		
STK A/109 *	1,15	-0,73	0,707977	100,0	154	0,20	1,01604772		
STK 4/40	1,10	-0,78	0,708016	100,0	178	0,23	0,398103973		
STK A/104	1,21	-0,67	0,708016	96,8	149	0,20	1,083223923		
STK 4 14*	1,14	-0,74	0,707974	100,0	162	0,21	0,219260368		
SO 3	1,15	-0,73	0,707932	98,1	150	0,21	1,385072263		
LK 40	1,12	-0,76							
LK 07	1,10	-0,78							
OY 59	0,59	-1,29	0,707709	100,0	307	0,39	1,250527059		
OY 96/158A	0,73	-1,15	0,707689	100,0	218	0,29	0,441069272		
OY 96/157C	0,76	-1,12	0,707700	100,0	238	0,28	0,416977632		
OY 96/157A	0,66	-1,22	0,707722	100,0	204	0,24	0,58952		
OY28 *	0,78	-1,10	0,707715	100,0	190	0,24	0,53844		
OY22 *	0,77	-1,11	0,707775	100,0	181	0,22	0,59294		
OY 19	0,82	-1,06	0,707738	100,0	171	0,21	0,64067338		
OY16	0,77	-1,11	0,707780	100,0	163	0,21	0,617044692		
OY 96/148	0,89	-0,99	0,707872	100,0	164	0,20	1,140453618		
OY9	0,77	-1,11	0,707864	100,0	164	0,20	1,218747687		
OY4	0,93	-0,95	0,707914	100,0	159	0,20	0,98953		
OY 03/176	0,96	-0,92	0,707911	100,0	157	0,19	0,950730267		

* number of replicates for these Ca-isotope measurements: 2 other samples were measured once

Steinberg - kogel	*P. triassica* (%) Demangel et al., (2020)	$\delta^{44/40}$Ca (‰, SW)	$^{87}Sr/^{86}Sr$		Zlambach	*P. triassica* (%) Demangel et al., submitted	$\delta^{44/40}$Ca (‰, SW)	$^{87}Sr/^{86}Sr$
STK B/45	1,8							
STK B/44		-0,96	0,707839		ZL 54,6826	2,5		
STK B/37B	2,0				ZL 54,4726	-1,31	0,707829	
STK B/33			0,707866		ZL 51,8669	3,1		
STK B/29A	2,9				ZL 49,9289		0,707844	
STK B/27B		-0,82	0,707831		ZL 48,8069	0,8		
STK B/25B	2,9				ZL 45,3393	-1,42	0,707809	
STK B/22A			0,707903		ZL 44,4778	5,2		
SKT B/19	2,9				ZL 42,4778	6,5		
STK B/16	4,2				ZL 40,3909		0,707833	
STK B/120	0,3				ZL 39,0211	3,9		
STK A/119A			0,707883		ZL 36,0341	17,8		
STK A/116	2,0				ZL 35,0041	-1,4	0,707845	
STK 114B		-0,79	0,707898		ZL 33,6651	4,7		
STK A/113	0,3				ZL 30,1895	-1,45	0,707780	
STK 4/112A		-0,81	0,707960		ZL 29,2395	0,5		
STK 4/111A		-0,83	0,707994		ZL 27,0319	4,2		
STK A/109A	1,9	-0,73	0,707977		ZL 24,8689	-1,39	0,707795	
STK 4/40	0,4	-0,78	0,708016		ZL 24,7659	3,1		
STK A/108A			0,708134		ZL 21,8819	12,8		
STK A/106B	0,9				ZL 19,4099	10,7		
STK A/104R		-0,67	0,708016		ZL 15,1040	-1,28	0,707871	
STK A/103	0,0				ZL 14,9960	1,8		
ST 4/36	2,4				ZL 13,8210	0,5		
ST 4/32	0,3				ZL 13,6820	0,3		
ST 4/31			0,707927		ZL 13,5430	3,4		
ST 4/29	0,4				ZL 13,4040	3,0		
ST 4/25	0,6		0,708061		ZL 13,2650	8,3		
ST 4/22	0,5				ZL 12,9870	1,1		
ST 4/18	0,0				ZL 12,7090	18,9		
ST 4/14	0,5	-0,74	0,707974		ZL 12,5700	9,0		
ST 4/10	0,0				ZL 11,8750	4,9		
ST4/6	2,2				ZL 11,7360	3,3		
ST 4/3			0,707991		ZL 11,5970	4,3		
ST 4/2	0,0				ZL 11,4580	2,7		
SO/17	0,4		0,708176		ZL 11,3190	1,5		
SO/11	1,5				ZL 10,0680		0,707926	
SO/3		-0,73	0,707932		ZL 9,7900	14,1		
SO/1	0,3				ZL 6,1944	12,1		
					ZL 4,9514		-1,24	0,707900
					ZL 3,1434	5,7		
					ZL 0,4078	4,7		
					ZL 0,0678		-1,34	0,707865

River	(Blättler et al., 2011)	**Hydrothermal**	(Blättler et al., 2011)	**Evaporite**	
Flux	Ratio "normal"	Flux	Ratio	Flux *	Ratio
2,3E+13	-1,08	2E+12	-0,98	3,00E+08	-1,5
Flux x 1.5				Flux x 1,5	
3,45E+13				4,50E+08	

Ca isotopic ratio of carbonates over geol. time — Fantle and Tipper, 2014

-1,3

GOAL — to result in ~0.2 decrease

*From Hensley, for the deposition of the evaporites during the Messinian salt crisis (mol/year)

I.) flux X1, ratio: "normal", hydro

-1,0720

II.) as I.) plus evaporite

-1,0720 No change

III.) River 1x, with carbonate mean values

-1,2744 -0,2024 change

IV.) River 1,5 X, flux "normal"

-1,0745 -0,0025 change

V.) River 1.5X, flux normal, evap. 1.5X

-1,0745 -0,0025 change

Appendix 2

Leislingkogel

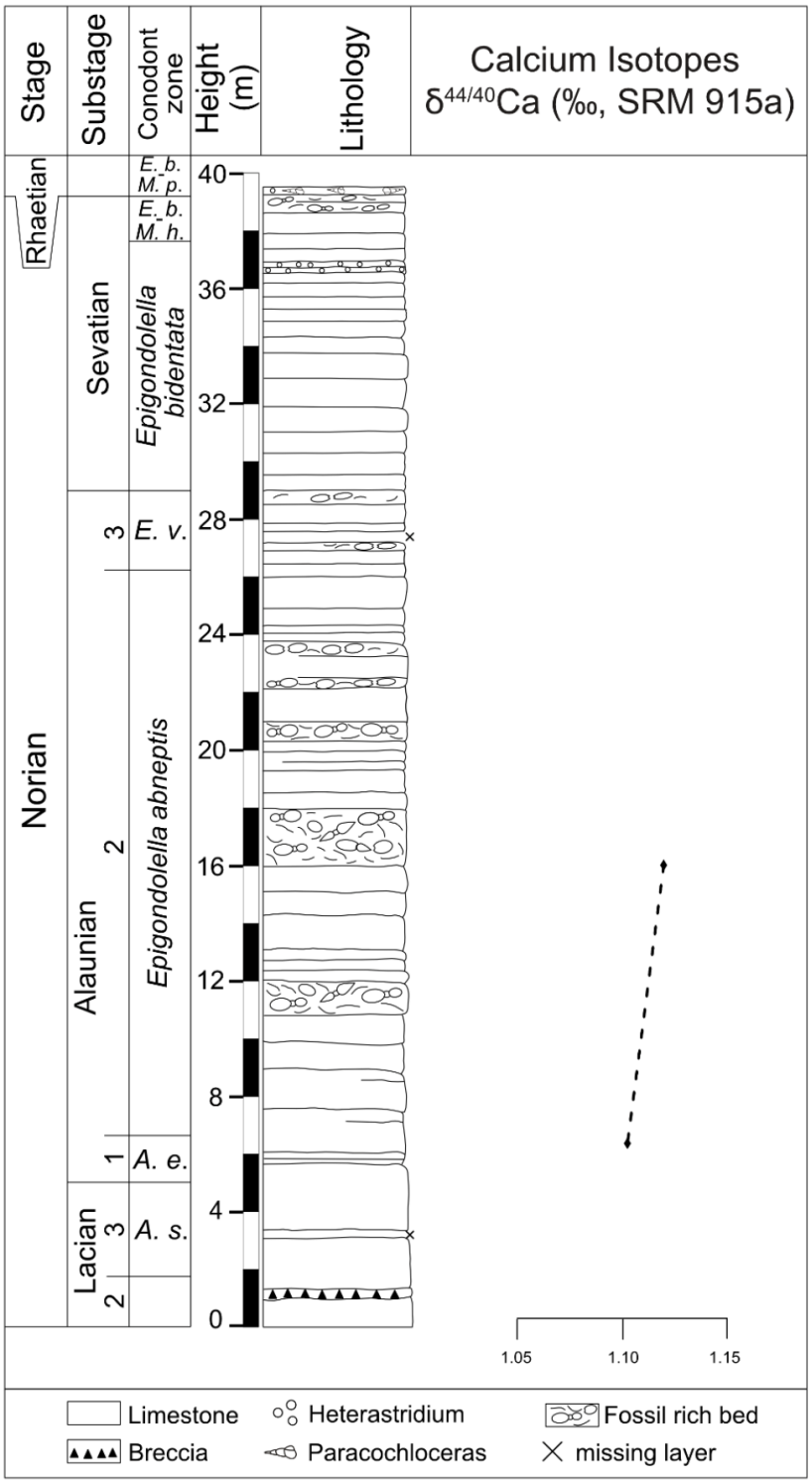

Steinbergkogel

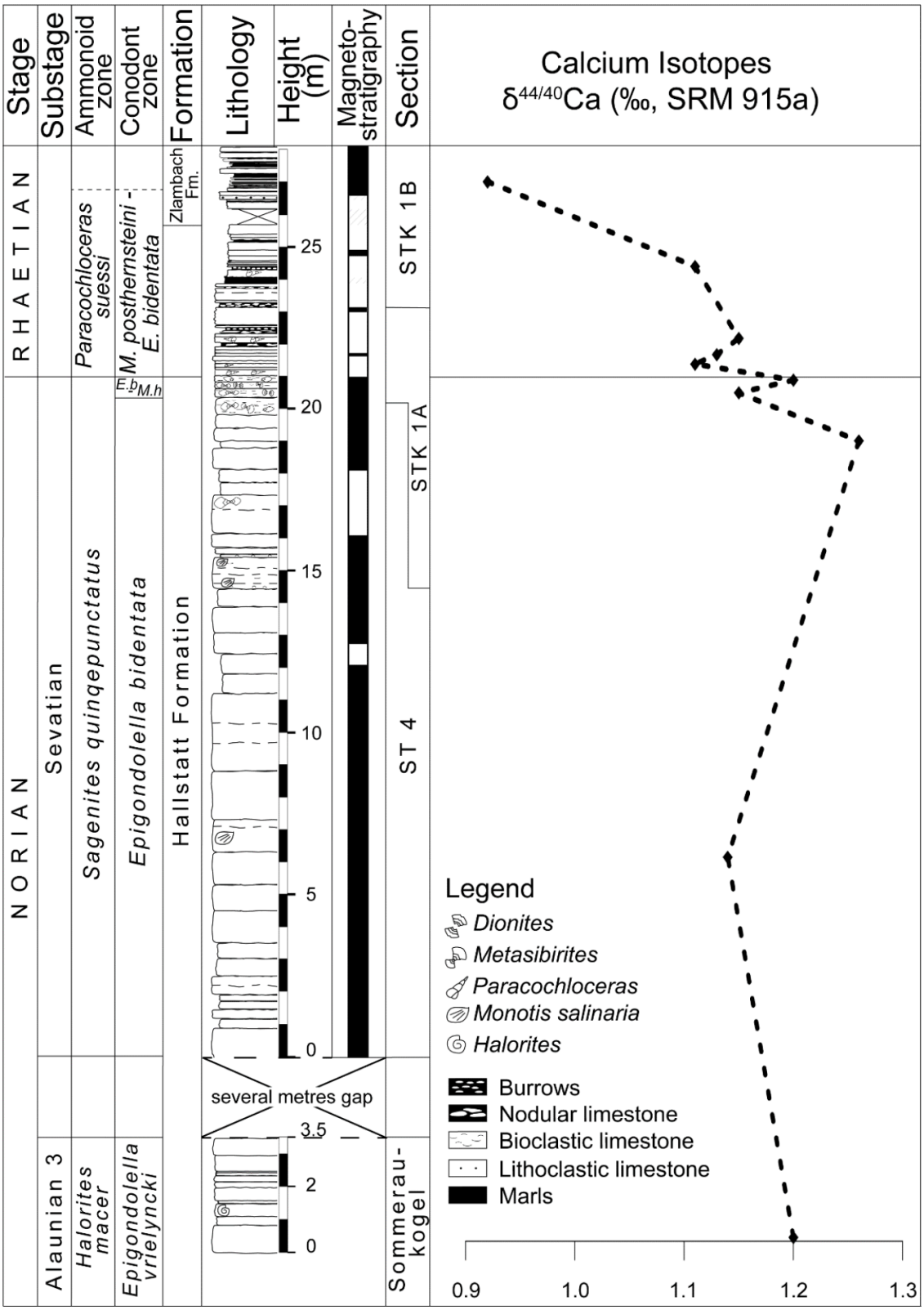
Stage
Substage
Ammonoid zone
Conodont zone
Formation
Lithology
Height (m)
Magneto-stratigraphy
Section
Calcium Isotopes
δ44/40Ca (‰, SRM 915a)
NORIAN
RHAETIAN
Sevatian
Alaunian 3
Sagenites quinquepunctatus
Paracochloceras suessi
Halorites macer
Epigondolella bidentata
M. posthernsteini - E. bidentata
Epigondolella vrielyncki
E.b M.h
Hallstatt Formation
Zlambach Fm.
several metres gap
STK 1B
STK 1A
ST 4
Sommerau-kogel
0
5
10
15
20
25
3.5
2
0
0.9
1.0
1.1
1.2
1.3
Legend
Dionites
Metasibirites
Paracochloceras
Monotis salinaria
Halorites
Burrows
Nodular limestone
Bioclastic limestone
Lithoclastic limestone
Marls

Zlambach

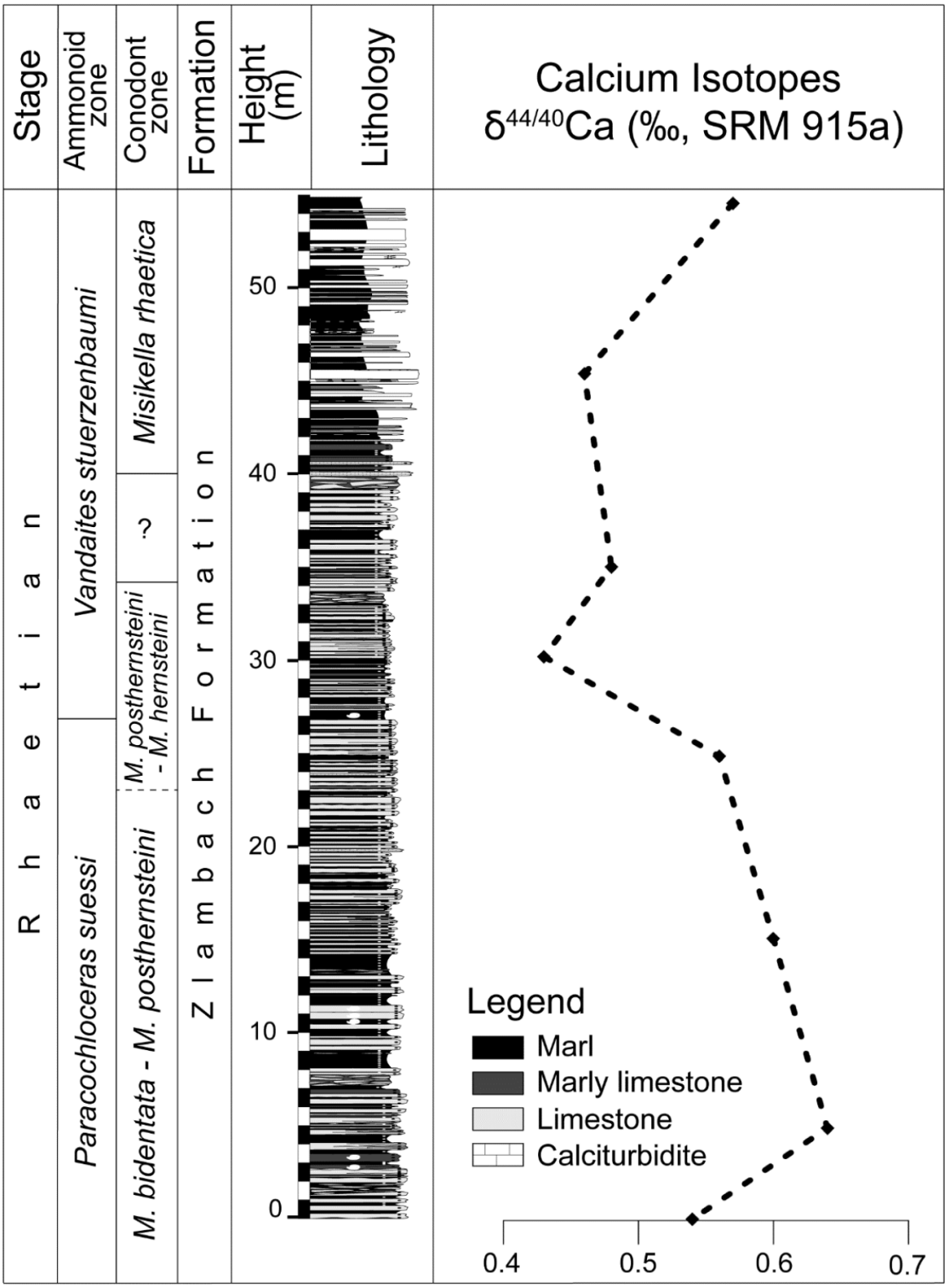
Stage
Ammonoid zone
Conodont zone
Formation
Height (m)
Lithology
Calcium Isotopes
δ44/40Ca (‰, SRM 915a)
Rhaetian
Vandaites stuerzenbaumi
Paracochloceras suessi
Misikella rhaetica
?
M. posthernsteini - M. hernsteini
M. bidentata - M. posthernsteini
Zlambach Formation
50
40
30
20
10
0
Legend
Marl
Marly limestone
Limestone
Calciturbidite
0.4
0.5
0.6
0.7

Eiberg

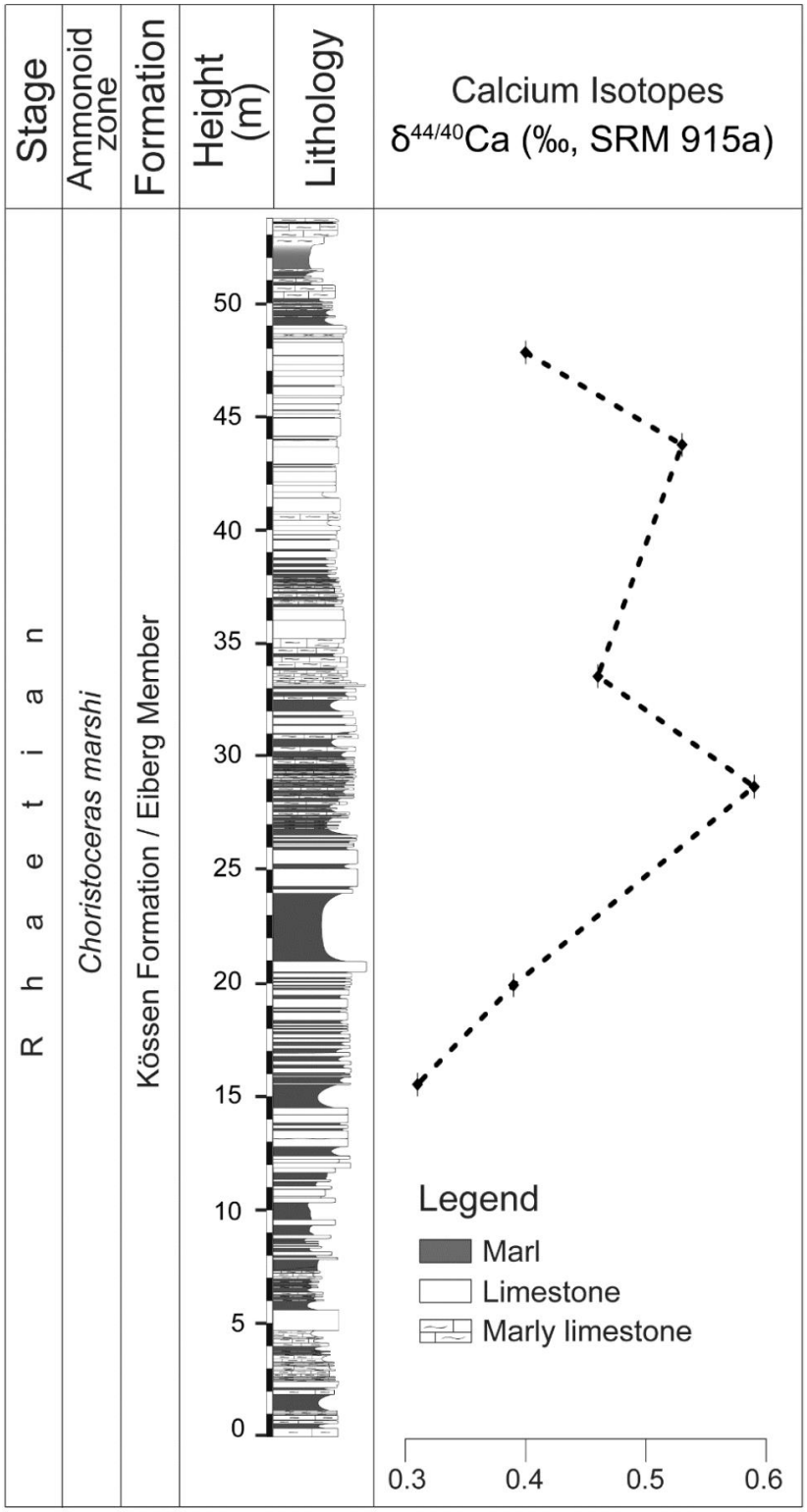
Stage
Ammonoid zone
Formation
Height (m)
Lithology
Calcium Isotopes
δ44/40Ca (‰, SRM 915a)
Rhaetian
Choristoceras marshi
Kössen Formation / Eiberg Member
50
45
40
35
30
25
20
15
10
5
0
Legend
Marl
Limestone
Marly limestone
0.3
0.4
0.5
0.6

Kuhjoch

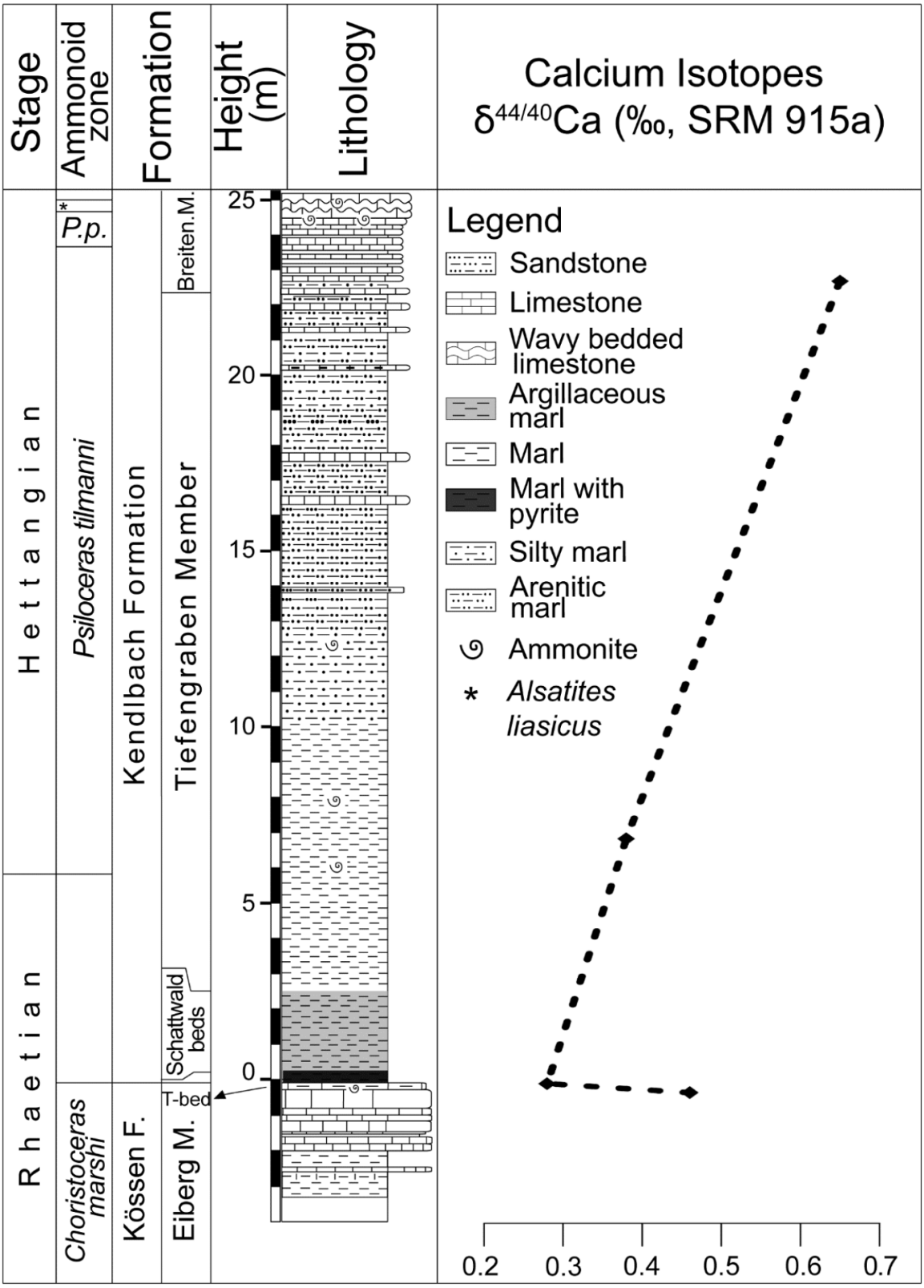
Stage
Ammonoid zone
Formation
Height (m)
Lithology
Calcium Isotopes
δ44/40Ca (‰, SRM 915a)
Hettangian
Rhaetian
*
P.p.
Psiloceras tilmanni
Choristoceras marshi
Kendlbach Formation
Kössen F.
Breiten.M.
Tiefengraben Member
Schattwald beds
Eiberg M.
T-bed
25
20
15
10
5
0
Legend
Sandstone
Limestone
Wavy bedded limestone
Argillaceous marl
Marl
Marl with pyrite
Silty marl
Arenitic marl
Ammonite
* Alsatites liasicus
0.2
0.3
0.4
0.5
0.6
0.7

Oyuklu

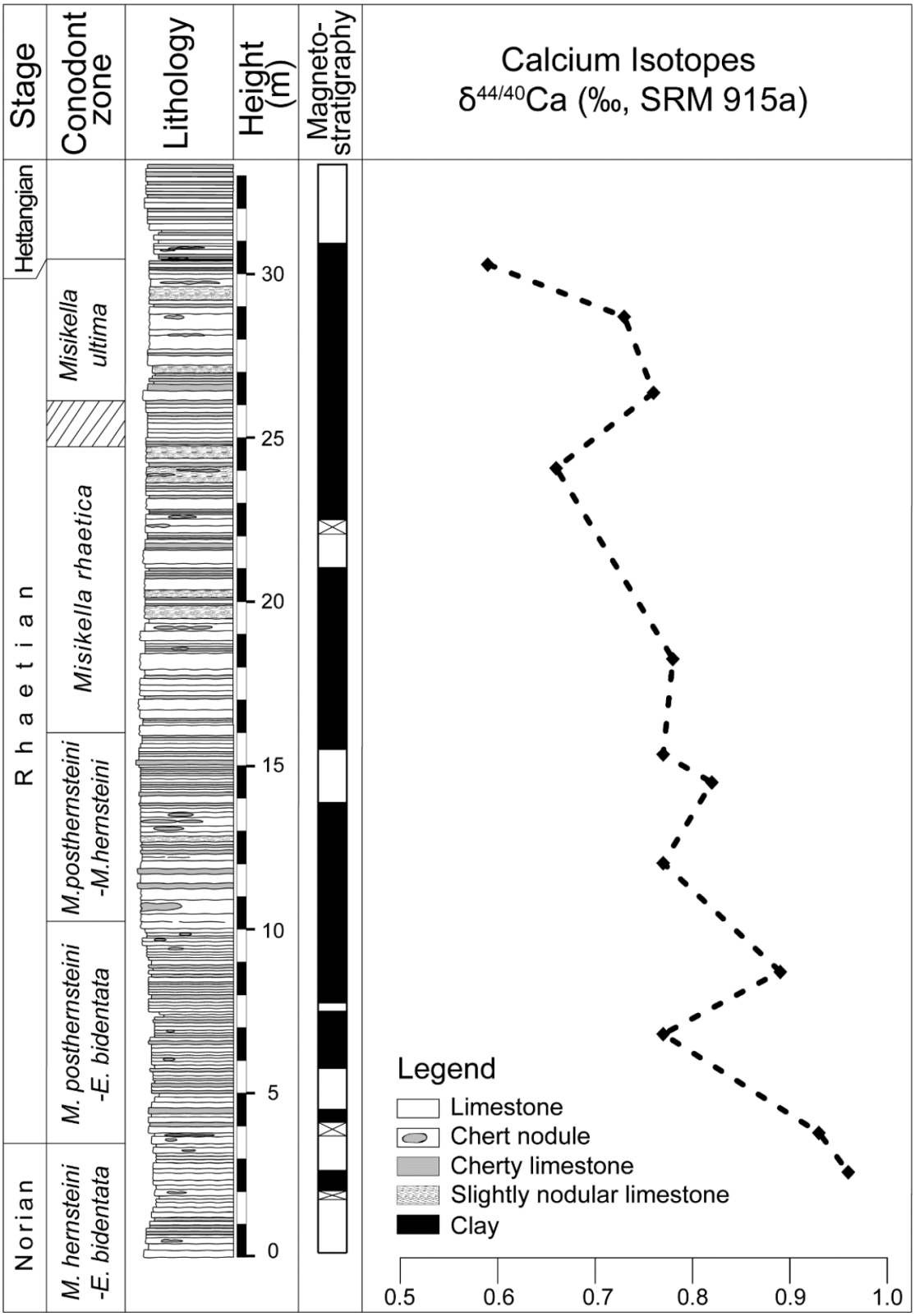
Stage
Conodont zone
Lithology
Height (m)
Magneto-stratigraphy
Calcium Isotopes
δ44/40Ca (‰, SRM 915a)
Hettangian
Rhaetian
Norian
Misikella ultima
Misikella rhaetica
M.posthernsteini -M.hernsteini
M. posthernsteini -E. bidentata
M. hernsteini -E. bidentata
0
5
10
15
20
25
30
Legend
Limestone
Chert nodule
Cherty limestone
Slightly nodular limestone
Clay
0.5
0.6
0.7
0.8
0.9
1.0

CHAPTER 7 – CONCLUSION AND PERSPECTIVES

1. Calcareous nannofossils assemblage and early evolution

This extent study on calcareous nannofossils compares differents palaeolatitude localities including the Paleo-Tethys with Romanian sections and Neo-Tethys Oceans with the Austrian sections in the western, Turkish section in the central and the Oman, Australian sections in the southern Neo-Tethys. This sampling associate with detailed observations and counting of the calcareous nannofossil under both light and scanning electron microscopy helped to better constrain their early evolution through the Upper Triassic.

1.1 *Calcispheres*

The Upper Triassic assemblages are dominated by numerous calcispheres. The most common, *Prinsiosphaera triassica,* appears in the mid-Norian (Alaunian 2; Fischer et al., 1967) and is present both in Northern and Southern Neo-Tethys Ocean as well as in the Paleo-Tethys Ocean (Moshkovitz, 1982; Jafar, 1983; Posch and Stradner, 1987; Janofske, 1987; Bralower et al., 1991; Bown, 1998; Gardin et al., 2012; Preto et al., 2013; Chapter 4 herein). *P. triassica* dominate the assemblage until the end-Rhaetian, but is affected from the lowermost Rhaetian by the appearance of the two nannolith, *E. hallstattensis* and *E. zlambachensis* (see below). The sub-species *P. triassica crenulata* was observed from the middle Rhaetian (*V. stuerzenbaumi* ammonoid Zone) in the Western Tethys Ocean sections, with characteristic parallelly organised lamellae appearing as striation (Demangel et al., 2020; 2021; submitted). *P. triassica crenulata* was described by Jafar (1983) among four other sub-species. They were all ruled out by Bralower et al. (1991) suggesting four diagenetic alterations of *P. triassica*. The SEM illustrations of the different stages are of good quality and the explanation of the alteration steps is convincing. However, the observation of *P. triassica crenulata* raise questions concerning the existence of the others sub-species described by Jafar (1983). Both possibilities are likely valid, i.e. different alteration stages of *P. triassica* can be observed and some sub-species described by Jafar (1983) exist but in very low abundance so difficult to observe. *P. triassica crenulata* presents a size-specific (i.e. 12 to 13 µm) and first occurs when *P. triassica* is affected by stressing conditions, i.e. cooler water and reduced availability of nutrients, visible with a size and abundance reduction. According to those observations, it can

be wondered if *P. triassica crenulata* is a species on its own or a sub-species of *P. triassica*. Additional observation on the morphological detail, size measurement, and preferential seawater conditions will bring more clues.

The other calcisphere present in the assemblage are *Thoracosphaera wombatensis*, first occurring in the mid-Norian (Bralower et al., 1991) followed by *Orthopithonella geometrica* and *Obliquipithonella rhombica* occurring in the Upper Norian in our studied sections. All those species were observed sporadically through the studied sections of the Neo-Tethys Ocean only. Those Upper Triassic calcispheres were first described as Dinophyceae. This classification is now debated due to a lack of archaeopyle and paratabulations (see fig. 1.4 Chapter 1, sub-chapter 2.2). However, the abundances of those three calcispheres are often in opposition to the abundance of the other calcareous nannofossils composing the assemblages. In the Zlambach section, the abundance of *O. geometrica*, *O. rhombica* and *T. wombatensis* increase along with an increase of (organic wall) dinoflagellates cyst (Kürschner et al., 2008). Furthermore, those three calcispheres shows a slight increase at the top of the section which is characterized by lower export of the platform. Cyst from modern calcifying dinoflagellates are found in high abundance in the more oligotrophic environment, so it seems interesting to follow the evolution of this increase in abundance and the export of the platform in a younger, continuous section. The Eiberg section located in the Austrian Northern Calcareous Alps covers the very top of the *V. stuerzenbaumi* Zone and the entire late Rhaetian *Choristoceras marshi* Zone allowing a good correlation with the Zlambach section. Eiberg section and Zlambach section are located in different basins, respectively Eiberg and Hallstatt Basin but relatively close so quantification of *O. geometrica*, *O. rhombica* and *T. wombatensis* in the Eiberg section would surely bring additional information to better assess their affinity.

1.2 *Eoconusphaera*

Two conical nannolith are also present in the Upper Triassic but three *Eoconusphaera* species have been described in past studies. The use of both SEM and LM in this study resolved the taxonomic confusion. A new species was described, i.e. *Eoconusphaera hallstattensis* occurring from the lower Rhaetian (*P. suessi* Zone) to the middle Rhaetian (middle of *V. stuerzenbaumi* Zone) in the Northern and Southern Neo-Tethys Ocean. Second, *E. zlambachensis* occurs from the middle Rhaetian (lower *V. stuerzenbaumi* Zone) until the

Triassic/Jurassic boundary in both Neo and Paleo-Tethys ocean. Those two last species have different arrangements of the inner lamellae, being vertical for *E. hallstattensis* and inclined (~145°) for *E. zlambachensis*. Additionally to the two *Eoconusphaera* species, the Mezosoic account three other genera with a conical form, all classified nowadays as coccoliths, i.e *Mitrolithus*, *Calcivascularis* (Lower Jurassic) and *Conusphaera* (uppermost Jurassic to Lower Cretaceous). All those coccoliths present an outer cycle of vertical, non-imbricating elements described as a protolithic rim and similar to the one observed in the *Eoconusphaera*. Also, the protolithic rim of those coccoliths show variation in height but can be as low as~ 2 µm, similar to the rim height of their Triassic ancestor, *Crucirhabdus* (Bown, 1987a). Both *Eoconusphaera hallstattensis* and *E. zlambachensis* show a broad range of sizes including low rims of ~ 2 µm. Those similarities argue in favour of relation to the protolith coccolith. In the Upper Triassic, *Crucirhabdus minutus* is the single coccolith species with a protolith rim present before *E. hallstattensis*, so the most possible ancestor of the Eoconusphaeraceae.

The two *Eoconusphaera* species and *P. triassica crenulata* can be used as biostratigraphic markers with short distinct stratigraphic ranges. Based on the Austrian data at Steinbergkogel and Zlambach three zones appear, i.e *E. hallstattensis*, *E. hallstattensis – E. zlambachensis* and *E. zlambachensis – P. triassica crenulata*. Those three calcareous nannofossils zones associated with conodonts and ammonoids zones would unable better time resolution of the Rhaetian. However, more observations on the first and last occurrence of those species in different localities are needed for the establishment of a solid zonation and stratigraphic comparison. In the southern Neo-Tethys, Bralower et al. (1991) only reported *E. hallstattensis* (named *E. zlambachensis* in their publication) because the studied section range until the lowermost Rhaetian just before the first occurrence of *E. zlambachensis* in the Western Tethys. However, *E. zlambachensis* is known in the southern Tethys thanks to its recent observation in the Northern Carnarvon Basin (Southern Tethys). Likely, the investigation of the entire Rhaetian at the ODP Leg 122 site (Bralower et al., 1991 studied site) could report *E. zlambachensis*. The estimation of the *E. hallstattensis* and *E. zlambachensis* occurrence interval in the southern Tethys would unable comparison with Western Tethys occurrence and helps to better constrain their spatial and temporal evolution. Additionally, Upper Triassic sediment in Italy at Pizzo Mondello and Pignola-Abriola have previously been analysed for the study of *P. triassica* (Preto et al., 2013). The other calcareous nannofossil were out of scope so

not reported but *E. zlambachensis* have been observed by Bottini et al. (2016) in another Italian section, Italcementi active quarry. It would be interesting to search for *Eoconusphaera* species in Pizzo Mondello and Pignola-Abriola for comparison within the Western Tethys.

1.3 *Coccolithophorids*

The Upper Triassic calcareous nannofossil assemblage account coccolithophorids observed so far only in the Neo-Tethys Ocean but our recent study of Romanian sections highlight the presence of form close to the coccoliths, increasing the confidence to observed coccolithophorids in the Paleo-Tethys Ocean. With the detailed investigation of mid-Norian sediment from the Western Tethys (Austria), the oldest coccolith not determined at the species level is reported from the mid-Norian (*Halorites macer* Zone) (Demangel et al., 2020). The oldest species, *Crucirhabdus minutus,* is recorded in the Upper Norian (Sevatian) and is suggested as the ancestor of *C. primulus* occurring in the lower Rhaetian (*P. suessi* Zone) (Demangel et al., 2020). *A. koessenensis* appears in between during the Upper Norian as a new lineage. This evolution is based on the structural evolution of the coccolithophorids during the Norian and Rhaetian. The coccolith evolves in size, from the minute *C. minutus* (1.6 to 2.4 µm) to middle size *A. koessenensis* (1.9 to 3.2 µm) and biggest size with *C. primulus* (3 to 5 µm). The rim structure also evolves from protolith toward loxolith rim with anticlockwise imbrication for *A. koessenensis* then clockwise imbrication for *C. primulus*. *Crucirhabdus primulus* has been considered as having a protolithic rim (Bown, 1987a; Bralower et al., 1991). For that reason, the phylogenetic relations of the early coccolithophorids reported by Bown (1987a) suggest *C. primulus* as the ancestor of the protolith species evolving from the Lower Jurassic and *A. koessenensis* as the possible ancestor of the loxolith (clockwise) species evolving from the Lower Jurassic. However, the anticlockwise imbrication of *A. koessenensis* loxolith rim seems very rare and not observed in other species (Bown, 1987b). *Crucirhabdus primulus* is the only species known in the Hettangian after the end-Triassic crisis (Fraguas et al., 2021). Considering *C. primulus* as a loxolith (clockwise), the evolutionary hypothesis proposed by Prins (1969) can be suggested with *C. primulus* as the ancestor of the Sinemurian (Lower Jurassic), loxolith genus, i.e. *Crepidolithus* and *Tubirhabdus* presenting also a clockwise orientation of the elements. This last hypothesis does not exclude the suggestion that protolith species from the Sinemurian evolve from the *Crucirhabdus* genus as proposed by Bown (1987a). Phylogeny of the early coccolithophorids must be revised in light of the new

observations brought by this study. Including the consideration of the *Eoconusphaera* species as possible coccolith descending from *C. minutus* and of *C. primulus* as a loxolith, giving the rise to the protolith and loxolith species occurring from the Lower Jurassic. The origin of *Archaeozygodiscus koessenensis* lineage remain unsolved, the characteristic anticlockwise loxolith rim appears as a default feature occurring only in this species during the early evolution of the coccolithophorids.

A possible coccolith specimen (See chapter 5, Fig. 5.9), was observed in the lower Rhaetian (*P. suessi* Zone) at the Zlambach section (Western Tethys) with a bigger size than *C. primulus*, i.e. width of 4 µm × length of 5 µm. The structure of the rim does not correspond to the common murolith of the Upper Triassic but seems closer to placolith with well developed R-unit (e.g. Watznaueriaceae) or holococcolith (e.g. *calculites*). The first placolith species appears only in the lower Jurassic followed slightly after by the first holococcoliths (Erba, 2006). As contamination can never be ruled out, a new set of smear slides and blocks of rocks must be prepared under extra clean and careful conditions. When the contamination risk is minimised, additional analyses are needed to observe several specimens under both LM and SEM to perfect the description and taxonomy of this form.

1.4 *Early calcareous nannofossil evolution*

The oldest calcareous nannofossils (Carnian, Norian) and most diverse assemblages were observed in Austrian sediments located in the Western Tethys Ocean around tropical latitude. During the Rhaetian, they spread to the subtropic and middle latitudes as suggested by observations of calcareous nannofossils in the Southern Tethys Ocean (Australia; see Bralower et al., 1991; Demangel et al., 2021) and toward the North in the Paleo-Tethys Ocean (Romania; See this thesis Chapter 4). However, pieces of information are missing regarding the global spread of the calcareous nannofossil as the analyse of samples from Turkey and Oman respectively located around the palaeo-equator and 20°S, did not report any calcareous nannofossil. The studied section in Turkey, i.e. Oyuklu is described as macroscopically unfossiliferous, probably due to the distal pelagic setting in greater, bathyal water depth (Gallet et al., 2007). This distal setting could explain the lack of calcareous nannofossil, as *P. triassica* was reported in higher abundance in a more proximal environment (Preto et al., 2013). The palaeo-latitude, i.e. equator, could also be unfavourable for those early species of

coccolithophorids as they seem to evolve first in subtropical areas (Bown, 1998; this study). However, the absence of calcareous nannofossils in samples from Oman is difficult to understand. Those studied sections show similar palaeoenvironments to the Austrian sections of Steinbergkogel and Zlambach. During the Triassic, all the exposed land are merged and centred around the equator (Ziegler et al., 1983). According to Parrish (1993), this palaeogeography would lead to mega-monsoon, affecting more the northern hemisphere while Oman was located in the southern hemisphere. This zone between the horse latitude was probably affected by dry climate thought the entire year (Preto et al., 2010). However, the climatic model from Sellwood and Valdes (2006) suggest tropical, humid summer conditions during the Upper Triassic in the Western Tethys and Oman. But the precipitation minus evaporation model show an excess of evaporation over precipitation for the Western Tethys, probably changing the trophic, salinity level leading to unfavourable conditions for the development of the calcareous nannoplankton around the palaeolatitude of Oman, i.e. 20°S. Moreover, the conditions during sinking and depositions of the calcareous nannofossils possibly did not allow their preservation.

Expanding data on Upper Triassic calcareous nannofossils will help stratigraphic comparison between worldwide localities. The recent investigation of the Northern Carnarvon Basin and the North Dobrogea showed ambitious results and those fewly studied areas need further attention. The Italian section, Italcementi active quarry shows a complete assemblage of calcareous nannofossils with coccoliths, *Eoconusphaera* and calcispheres so a deeper investigation of the all assemblage at Pizzo Mondello and Pignola-Abriola could be interesting for comparison between Italian sections and Western Tethys Basins. Additionally, it would be necessary to analyse Upper Triassic succession from the Panthalassa Ocean to estimate the real extent of the calcareous nannoplankton in this part of the globe rarely studied for its calcareous nannofossils content.

2. Calcareous nannofossil abundance and impact on seawater chemistry in the Upper Triassic

In addition to the investigation on the diversity of the different groups and the morphology of the species present, quantification was performed on all the species composing the assemblages. *Prinsiosphaera triassica* dominate the assemblage during most of the Upper

Triassic (Gardin et al., 2012; Preto et al., 2013; Demangel et al., 2020). The abundance of *P. triassica* increased from the late Norian with a maximum during the middle Rhaetian (in the studied sections). However, during the studied interval, i.e. mid-Norian to mid-Rhaetian, *P. triassica* does not reach rock-forming proportions as recorded in the Italian section during the late Rhaetian (Preto et al., 2013). The two *Eoconusphaera* species are the second most abundant, even dominating in the assemblage in few samples. *E. hallstattensis* occurs first with a low abundance in the lower Rhaetian (*P. suessi* Zone). Then *E. zlambachensis* occurs from the middle Rhaetian (*V. stuerzenbaumi* Zone) with a higher abundance compared to *E. hallstattensis*. The maximum abundance is reached just after the first occurrence of *E. zlambachensis* in the middle Rhaetian (*V. stuerzenbaumi* Zone). The three (possible) dinoflagellates spheres, *Obliquipithonella rhombica*, *Orthopithonella geometrica* and *Thoracosphaera wombatensis*, represent the third most abundant component and present a low abundance throughout the entire studied interval. The coccolithophorids are the minor part of the assemblage with very rare abundance after their first occurrence. They start to increase slightly in abundance from the lower Rhaetian reaching a maximum in the middle Rhaetian.

Prinsiosphaera triassica abundance was compared with $\delta^{44/40}$Ca isotopic values at Steinbergkogel and Zlambach sections, to better constrain the influence of the early calcification by the nannoplankton on the seawater chemistry. No significant relation was discerned between the variation of the $\delta^{44/40}$Ca isotopic and *P. triassica* abundance values. Additionally, expected positive excursions of the $\delta^{44/40}Ca_{carb}$ due to the contribution of the calcareous nannofossil to the calcite precipitation and carbon burial were not observed in the studied region. This suggests no influence of the early pelagic calcification by the calcareous nannoplankton of the seawater chemistry and especially the global carbon and calcium cycles during the Upper Triassic. Either the contribution of pelagic calcifiers in the Western Tethys is overly low to influence the global cycle during their early emergence in the Upper Triassic. Or the observed gradual increase in abundance of the calcareous nannofossils occurred on a longer time scale than the residence time of the calcium (~ 1 Myr) so a possible influence can not be detected. The question can now be addressed inversely, i.e. does the increasing availability of calcium in the Upper Triassic ocean could have influenced the emergence of pelagic calcifiers?

3. Rhaetian palaeoenvironmental changes

The Triassic Period is particular as framed by two mass extinction, the end-Permian (Clapham, 2021) and the end-Triassic event (Lucas, 2021). Before this last extinction, several crises occurs during the Late Triassic, such as the Carnian Pluvial Event (Simms and Ruffel, 1989), the vertebrate turnover at the Carnian/Norian boundary (Brusatte et al., 2008), the strong biodiversity loss (70%) of molluscs during the Norian (McRoberts and Newton, 1995) and the decline of ammonoids, conodonts and bivalve *Monotis* around the Norian/Rhaetian boundary (Richoz et al., 2012). The calcareous nannofossils are not affected by those previous events; they appear during the Carnian and slowly increase in diversity and abundance through the Late Triassic. However, smaller scale perturbations are recorded at the Zlambach section and seems to affect the calcareous nannofossil. Along the Zlambach section (*P. suessi – V. stuerzenbaumi* zones), *P. triassica* decreased in size from an average of 8 to 5.8 µm due mainly to the disappearance of very large size specimens (13 – 10 µm) (Demangel et al., 2020; Chapter 5). The minimum size is reached along with major events occurring between 35 and 45 m in the section (*V. stuerzenbaumi* Zone). This interval record the FO of *E. zlambachensis* and *P. triassica crenulata*, the last occurrence of *E. hallstattensis*, an increased abundance of calcareous nannofossils (Chapter 5) and dinocysts (Kürschner et al., 2008); a turnover in the miospore (Kürschner et al., 2008), benthic ammonoids and conodonts (Richoz and Krystyn, 2015; Galbrun et al., 2020). Especially, the occurrence of high latitude palynological assemblage suggests an inflow of cooler water from the North, which could also lead to a change in salinity influencing the calcification of *P. triassica*. Additionally, during this interval, the productivity of the platform dropped leading to reduced availability of nutrients and adding stressing conditions for *P. triassica* visible through the size decrease. To better constrain the palaeoenvironmental changes occurring during the middle Rhaetian, it seems necessary to observe the evolution of the pattern recorded at the top of the Zlambach section, i.e. the size fluctuation of *P. triassica (*affected by change in temperature or salinity) and the increase in abundance of the calcareous dinoflagellates cyst showing more adverse condition. The Eiberg section located in the NCA is successive to the Zlambach section, and thus represents good potential to access this information. The Val Taleggio section in the Bergamo Alps could be also interesting as representing a time-equivalent but more southern section with potentially less influence of the cold input of water from the north. Whatever the future results, it seems that the upper triassic calcareous nannofossils will not only be a new stratigraphic tool for this

time but could also contribute to reveal and understand palaeenvironmental changes during this fascinating period.

Reference

Bottini, C., Jadoul, F., Rigo, M., Zaffani, M., Artoni, C., Erba, E., 2016: Calcareous nannofossils at the Triassic/Jurassic boundary: Stratigraphic and paleoceanographic characterization. *Rivista Italiana di Paleontologia e Stratigrafia (Research in Paleontology and Stratigraphy)* 122, 141 – 164.

Bown, P.R., 1987a: The structural Development of Early Mesozoic Coccoliths and its Evolutionary and Taxonomic Significance. Abhandlungen der Geologischen Bundesanstalt. 39, 33 – 49.

Bown, P.R., 1987. Taxonomy, evolution, and biostratigraphy of Late Triassic-Early Jurassic Calcareous Nannofossils. Special paper in Paleontology, 38: 1 – 118.

Bown, P.R., 1998: Triassic. In: Bown, P.R., (Ed) Calcareous nannofossil biostratigraphy. Kluwer Academic Publishers, 29 – 33.

Bralower, T.J., Bown, P.R., Siesser, W.G., 1991. Significance of Upper Triassic nannofossils from the Southern Hemisphere (ODP Leg 122, Wombat Plateau, N.W. Australia) – Marine Micropaleontology. 17, 119 – 154. 10.1016/0377-8398(91)90025-2.

Brusatte, S.L., Benton, M.J., Ruta, M., Lloyd, G.T., 2008: Superiority, competition, and Opportunism in the Evolutionary Radiation of Dinosaurs. Science, 321, 1485 – 1488.

Clapham, M.E., 2021: The End-Permian Mass Extinction. In: Alderton, D., Elias, S.A. (Eds.), Encyclopedia of Geology (Second Edition), Academic Press. 645 – 652. 10.1016/B978-0-12-409548-9.12052-4.

Demangel, I.; Kovács, Z.; Richoz, S.; Gardin, S.; Krystyn, L.; Piller, W. E. (submitted): Fate of the calcareous nannofossils during the Rhaetian. Example from the Northern Calcareous Alps (Austria).

Demangel, I., Kovacs, Z., Richoz, S., Gardin, S., Krystyn, L., Baldermann, A., Piller, W. E., (2020): Development of early calcareous nannoplankton in the Northern Calcareous Alps (Austria) in the Late Triassic. Global and Planetary Change, 193, 103254.

Demangel, I., Howe, R., Gardin, S., Richoz, S. 2021: *Eoconusphaera hallstattensis* sp. nov. and review of the Rhaetian genus *Eoconusphaera*. *Journal of Nannoplankton Research*. 39 (1), 77 – 87.

Erba, E., 2006. The first 150 million years history of calcareous nannoplankton: Biosphere-geosphere interactions. Palaeogeography, Palaeoclimatology, Palaeoecology. 232, 237 – 250. 10.1016/j.palaeo.2005.09.013.

Fischer, A.G., Honjo, S., Garrison, R.A.E., 1967: Electron Micrographs of Limestones and their Nannofossils. Princeton University Press, Princeton.

Fraguas, A., Gómez, J.J., Comas-Rengifo, M.J., Goy, A., 2021: Pliensbachian calcareous nannofossils paleoecology in the E Rodiles section (Asturias, N Spain): A key location connecting the Boreal and Tethyan realms. Marine Micropaleontology, 163, 101962. 10.1016/j.marmicro.2021.101962.

Galbrun, B., Boulila, S., Krystyn, L., Richoz, S., Gardin, S., Bartolini, A., (2020): « Short » or « long » Rhaetian? Astronomical calibration of Austrian key sections. Global and Planetary Change. 192, 103253. 10.1016/j.gloplacha.2020.103253.

Gallet, Y.; Krystyn, L.; Marcoux, J.; Besse, J. (2007): New constraints on the End-Triassic (Upper Norian–Rhaetian) magnetostratigraphy. Earth and Planetary Science Letters, 255(3-4), 458-470. DOI: 10.1016/j.epsl.2007.01.004.

Gardin, S., Krystyn, L., Richoz, S., Bartolini, A., Galbrun, B., 2012. Where and when the earliest coccolithophores? Lethaia. 45, 507 – 523. 10.1111/j.1502-3931.2012.00311.x.

Jafar, S.A., (1983): Significance of Late Triassic calcareous Nannoplankton from Austria and Southern Germany. Neues Jahrbuch für Geologie und Paläeontologie, 166, 218 – 259.

Janofske, D., 1987. Kalkige Nannofossillien aus der Ober-Trias (Rhät) der Nördlichen Kalkalpen. Berliner Geowissenschaftlichen Abhandlungen. 86, 45 – 67.

Janofske, D., (1992). Calcareous nannofossils of the Alpine Upper Triassic. In: Hamrsmid, B., Young, J.R., (Eds), Nannoplankton Research (Proceedings INA Conference). Knihovnicka ZPN, Hodonin, Cz. 87 – 109.

Korte, C., Thibault, N., Ullmann, C.V., Clémence, M-E., Mette, W., Olsen, T.K., Rizzi, M., Ruhl, M., 2017: Brachiopod biogeochemistry and isotope stratigraphy rom the Rhaetian Eiberg section in Austria: potentials and limitations. Neues Jahrbuch für Geologie und Paläontologie, 284 (2), 117 – 138. 10.1127/njgpa/2017/0651.

Kürschner, W.M., Krystyn, L., Richoz, S. 2008: An integrated palaeontological, geochemical and palynological study of the Rhaetian Zlambach marls in the Northern Calcareous Alps (Austria). *Berichte geologischen Bundesanstalt*, 76, 13 – 14.

Lucas, S.G., 2021 End-Triassic Extinctions. In: Alderton, D., Elias, S.A. (Eds.), Encyclopedia of Geology (Second Edition), Academic Press. 653 – 664. 10.1016/B978-0-12-409548-9.12013-5.

McRoberts, C.A., Newton, C.R., 1995: Selective extinction among end-Triassic European bivalves. Geology, 23 (2), 102 – 104.

Mette, W.; Elsler, A.; Korte, C. (2012): Palaeoenvironmental changes in the Late Triassic (Rhaetian) of the Northern Calcareous Alps. Clues from stable isotopes and microfossil. Palaeogeography, Palaeoclimatology, Palaeoecology, 350 – 352, 62 – 72. 10.1016/j.palaeo.2012.06.013.

Moshkovitz, S., 1982. On the findings of a new calcareous nannofossil (*Conusphaera zlambachensis*) and other calcareous organisms in the Upper Triassic sediments of Austria. Eclogae Geologicae Helvetiae. 75, 611–619. 10.5169/seals-165245.

Parrish, J.T., 1993: Climate of the supercontinent Pangea: Journal of Geology, 101, 215 – 233.

Posch, F., Stradner, H., 1987. Report on Triassic Nannoliths from Austria. Abhandlungender Geologischen Bundesanstalt, 39: 231 – 237.

Preto, N., Kustatscher, E., Wignall, P.B., 2010: Triassic climates – State of the art and perspectives – Palaeogeography, Palaeoclimatology, Palaeoecology. 290, 1 – 10. 10.1016/j.palaeo.2010.03.015.

Preto, N., Agnini, C., Rigo, M., Sprovieri, M., Westphal, H., 2013. The calcareous nannofossil Prinsiosphaera achieved rock-forming abundances in the latest Triassic of western

Tethys: consequences for the $\delta^{13}C$ of bulk carbonate – Biogeosciences. 10, 6053 – 6068. 10.5194/bg-10-6053-2013.

Prins, B., 1969: Evolution and stratigraphy of coccolothinids from the lower and middle lias. International Conference Planktonic Microfossils, Geneva. 2, 547 – 558.

Richoz, S., Krystyn, L., Hillebrandt, A.V., Martindale, R., 2012: End Triassic crisis events recorded in platform and basin of the Austrian Alps. The Triassic/Jurassic and Norian/Rhaetian evolution. Journal of Alpine Geology, 54, 323 – 377.

Richoz, S., Krystyn, L., 2015: The Upper Triassic events recorded in platform and basin of the Austrian Alps. The Triassic/Jurassic GSSP and Norian/Rhaetian GSSP candidate. Berichte der geologischen bundesanstalt, 111.

Sellwood, B.W., Valdes, P.J., 2006: Mesozoic climates: General circulation models and the rock record. Sedimentary Geology, 190 (1 – 4), 269 – 287. 10.1016/j.sedgeo.2006.05.013.

Simms, M.J., Ruffell, A., 1989: Synchroneity of climate change and extinctions in the Late Triassic. Geology, 17 (3), 265 – 268. 10.1130/0091-7613(1989)017<0265:SOCCAE>2.3.CO;2.

Ziegler, A.M., Eshet, G., McAllister Rees, P., Rothfus, T.A., Rowley, D.B., Sunderlin, D., 2003: Tracing the tropics across land and sea: Permian to present. Lethaia, 36, 227 – 254.